

Interacting Fermions in External Fields, at Finite Temperature and Non-Zero Density



Dissertation

zur Erlangung des akademischen Grades
doctor rerum naturalium (Dr. rer. nat.)

vorgelegt dem Rat der
Physikalisch-Astronomischen Fakultät
der Friedrich-Schiller-Universität Jena

von M.Sc. Michael Mandl
geboren am 23. Oktober 1995 in Bruck an der Mur

Gutachter:

1. Prof. Dr. Andreas Wipf (*Friedrich-Schiller-Universität Jena*)
2. Prof. Dr. Gergely Endrődi (*Universität Bielefeld*)
3. Prof. Dr. Rajamani Narayanan (*Florida International University*)

Tag der Disputation: 30. August 2023

Abstract

In this thesis we investigate a certain class of low-dimensional fermionic quantum field theories with four-Fermi interactions. Such theories are commonly used as effective low-energy models for quantum chromodynamics, the theory of strong interactions, and have applications in the realm of condensed-matter physics as well. Four-Fermi theories are well suited for the study of non-trivial phenomena within strongly-interacting quantum field theories. For our purposes, their most important properties are the notion of chiral symmetry as well as its spontaneous breakdown, which is why a major part of this thesis is devoted to their study.

In our non-perturbative investigations, we mostly employ numerical lattice quantum field theory simulations, but we also present a brief analytical study performed in the mean-field limit. In particular, we are concerned with two major questions: On the one hand, we investigate a certain two-dimensional four-Fermi theory, the so-called chiral Gross-Neveu model, which has a continuous chiral symmetry group. We study the possibility of the model at finite temperature and density to exhibit inhomogeneous regions, where the order parameter for chiral symmetry breaking shows oscillatory behavior with the spatial coordinate. In the light of numerous no-go theorems, this is a non-trivial question. We find that remnant inhomogeneous structures can indeed be found even beyond the mean-field limit, albeit likely only on short scales.

On the other hand, we consider a related theory with a discrete chiral group, referred to as the Gross-Neveu model, in three space-time dimensions. There, we shall be concerned with the influence of an external magnetic field on chiral symmetry and its spontaneous breaking. While mean-field approaches predict a rich phase structure for non-zero magnetic field and chemical potential, our simulations suggest that this is not the case in the full quantum theory. For all parameter values within the region of spontaneously broken chiral symmetry, we find the magnetic field to enhance the symmetry breaking even further, a phenomenon referred to as magnetic catalysis. In fact, a major goal of this thesis is to contrast the findings of our lattice simulations with existing mean-field results in order to understand to which extent the latter are capable of representing the full theory.

Zusammenfassung

In dieser Doktorarbeit untersuchen wir eine gewisse Klasse von niedrig-dimensionalen fermionischen Quantentheorien mit vier-Fermi-Wechselwirkungen. Theorien dieser Art werden häufig als effektive Modelle für die Beschreibung der Quantenchromodynamik, der Theorie der starken Wechselwirkung, bei niedrigen Energien verwendet, haben aber auch Anwendungen in der Festkörperphysik. Vier-Fermi-Theorien sind hervorragend geeignet für das Studium nicht-trivialer Phänomene innerhalb stark wechselwirkender Quantenfeldtheorien. Deren für unsere Zwecke wichtigsten Eigenschaften sind der Begriff der chiralen Symmetrie, sowie deren spontane Brechung. Beide werden uns in einem Großteil dieser Arbeit begegnen.

Für unsere Untersuchungen jenseits der Störungstheorie verwenden wir hauptsächlich numerische Simulationen aus dem Bereich der Gitterquantenfeldtheorie, präsentieren aber auch eine kurze analytische Studie in der Molekularfeldnäherung. Im Speziellen beschäftigen wir uns mit zwei Fragestellungen: Einerseits betrachten wir eine bestimmte zweidimensionale vier-Fermi-Theorie, das sogenannte chirale Gross-Neveu-Modell, welches eine kontinuierliche Symmetriegruppe aufweist. Wir untersuchen, ob das Modell bei endlicher Temperatur und Dichte eine inhomogene Region aufweist, in welcher der Ordnungsparameter der chiralen Symmetriebrechung in der räumlichen Koordinate oszilliert. Angesichts einer Anzahl von No-go-Theoremen ist diese Fragestellung eine nicht-triviale. Wir finden, dass derartige inhomogene Strukturen tatsächlich auch jenseits der Molekularfeldnäherung beobachtet werden können, allerdings vermutlich nur auf kurzen Skalen.

Auf der anderen Seite untersuchen wir eine verwandte Theorie mit diskreter Symmetriegruppe, das sogenannte Gross-Neveu-Modell, in drei Raumzeitdimensionen. Hier sind wir an dem Einfluss eines äußeren Magnetfeldes auf die chirale Symmetrie und deren spontane Brechung interessiert. Während die Molekularfeldnäherung eine komplizierte Phasenstruktur bei endlichem Magnetfeld und chemischem Potential vorhersagt, lassen unsere Simulationen darauf schließen, dass die volle Quantentheorie ein anderes Verhalten zeigt. Innerhalb der Region mit spontan gebrochener chiraler Symmetrie, finden wir, dass das Magnetfeld die Symmetriebrechung nur noch verstärkt, ein Phänomen, welches üblicherweise als magnetische Katalyse bezeichnet wird. In der Tat ist es eines der Hauptziele dieser Doktorarbeit, die Erkenntnisse unserer Gittersimulationen mit existierenden Ergebnissen in der Molekularfeldnäherung zu vergleichen, um zu verstehen, zu welchem Grad letztere in der Lage ist, die volle Theorie zu beschreiben.

Table of Contents

1	Introduction	3
2	Four-Fermi Theories	9
2.1	Notation and conventions	9
2.2	Four-Fermi theories and their symmetries	10
2.2.1	Space-time symmetries	11
2.2.2	Internal symmetries	12
2.2.3	Prominent four-Fermi theories	13
2.2.4	Reducible representations	14
2.3	Partition function and bosonization	16
2.4	Spontaneous symmetry breaking	18
3	The Mean-Field Gross-Neveu Model	19
3.1	Landau levels	19
3.2	Effective potential of the Gross-Neveu model	22
3.3	Chiral condensate	24
3.4	Phase diagrams	28
3.5	Thermodynamic observables	29
3.6	Finite volume	30
4	Lattice Field Theory	33
4.1	Basic concepts	33
4.2	Lattice discretization of fermions	34
4.2.1	The problem of chiral lattice fermions	35
4.2.2	SLAC fermions	36
4.2.3	Ginsparg-Wilson fermions	37
4.3	Magnetic fields on the lattice	39
4.3.1	Formulations using link variables	40
4.3.2	Formulations based on minimal coupling	41
4.4	Numerical tests	41
4.4.1	Two dimensions	43
4.4.2	Three dimensions	46

5	Inhomogeneous Structures	49
5.1	Inhomogeneous phases in the mean-field limit	49
5.2	Inhomogeneities beyond the mean-field limit	51
5.3	Simulation setup	53
5.3.1	Observables	55
5.3.2	On thermalization and auto-correlations	58
5.4	Results	58
5.4.1	Spatial oscillations of correlation functions	59
5.4.2	Phase structure beyond the mean-field limit	61
5.4.3	Perfect long-range order vs. quasi-long-range order	64
6	Magnetic Catalysis	66
6.1	Strongly-interacting theories within magnetic fields	66
6.2	Spectral properties of the overlap operator	70
6.2.1	Landau levels on the lattice	70
6.2.2	Index theorem	72
6.2.3	Finite-size effects	74
6.3	Simulation setup	76
6.3.1	Observables	78
6.4	Tests and cross-checks	80
6.4.1	Dyson-Schwinger equation	80
6.4.2	Critical exponents	82
6.4.3	Saturation effects	83
6.5	Results for vanishing magnetic field	83
6.5.1	Vanishing chemical potential	84
6.5.2	Finite chemical potential	85
6.6	Results for finite magnetic field	89
6.6.1	Vanishing temperature and chemical potential	89
6.6.2	Finite temperature and vanishing chemical potential	90
6.6.3	Low temperature and non-vanishing chemical potential	92
6.6.4	Search for inhomogeneities	94
6.6.5	Comparison to the literature	96
7	Conclusions & Outlook	98
	Appendices	101
A	Derivation of Landau levels	101
B	The chiral condensate from the density of states	104
C	Zeta function regularization	106
D	Derivation of the effective potential	107
E	On the complex-action problem	113
	References	117
	Acronyms	142

1 Introduction

According to our current understanding, the universe is governed by four fundamental forces: the strong and weak interactions, the electromagnetic interaction and gravity. From a theoretical point of view, the strong interaction is particularly challenging since one cannot employ perturbation theory for its study at low energies but has to resort to non-perturbative methods instead. The latter, however, tend to be far from straightforward on a computational level, often involving large-scale simulations on the most powerful supercomputers the world has to offer. This and related difficulties make the strong interaction one of the most active topics of contemporary physics research to this day, with a plethora of thus far unanswered questions. The three remaining fundamental forces, while being equally important and interesting in their own right, are less relevant in the present context and shall not be in the focus of what follows.

The theoretical framework underlying the strong interaction is quantum chromodynamics (QCD), a highly non-trivial theory comprising fermionic fields, the so-called quarks, and non-Abelian gauge fields, which are referred to as gluons. It describes, for instance, how quarks interact with each other via the exchange of gluons to form bound states like the protons and neutrons that make up atomic nuclei. One particular field of research that is being studied intensely by present-day high-energy physicists is that of QCD in extreme conditions, such as high temperature, high particle density or strong magnetic fields. Its proper understanding would allow us to gain important insights into complicated physical processes like collisions of heavy ions within particle accelerators, the inner workings of compact stellar objects such as neutron stars and even the early history of our universe. In all of these processes the strong interaction is believed to play a dominant role [1, 2].

Of special importance for the context of this thesis is the study of QCD exposed to background (electro)magnetic fields, which has received an ample amount of interest in recent years for various reasons (see [3, 4] for reviews). For one, it has become clear that magnetic fields produced in non-central heavy-ion collisions [5], e.g., in the Large Hadron Collider (LHC) at CERN, can be of the order of several times the squared pion mass, thus reaching energy scales relevant for QCD [6–12]. Magnetic fields of this magnitude – should they persist for long enough during a collision – are thus expected to have a significant impact on the outcome of such an experiment, i.e., on physical observables. A prominent example for observable phenomena induced by strong magnetic fields is the so-called chiral magnetic effect [13, 14], for which possible experimental evidence was found in [15, 16]. In the chiral magnetic effect topological arguments predict the generation of an electric current along the direction of

the produced field, i.e., perpendicular to the reaction plane. Closely related phenomena are known as the chiral separation effect [17], generating an axial current along the direction of the field, and the chiral magnetic wave [18], arising due to the interplay between the chiral magnetic and chiral separation effects (see also [19–22]).

Beyond heavy-ion collisions strong magnetic fields are believed to play a role in a number of other strongly-interacting systems as well. For instance, it has been conjectured that a certain class of neutron stars – appropriately named magnetars [23] – can feature in their interiors magnetic fields comparable in strength to those produced at the LHC, as well as somewhat weaker ones on their surfaces [24, 25] (see [26–28] for reviews). In fact, strong magnetic fields are thought to be capable of changing the equation of state of neutron stars [24], lead to their deformation [29], and they have been theorized to be responsible for so-called pulsar kicks [30]. Furthermore, it is likely that extremely strong fields were produced during the cosmological phase transitions of the early universe, possibly resulting in the galactic magnetic fields one observes today [31–36]. We also mention the possibility for strong magnetic fields to turn the QCD vacuum into a superconductor [37]. For an extensive review on the role of magnetic fields in quantum field theory, covering all of the aforementioned phenomena and many more topics as well as giving a more complete list of references, we refer to [3].

Let us now discuss a more technical aspect of investigations of QCD in extreme conditions. The computational tool that has proven most successful in the study of quantum field theories beyond perturbation theory is lattice field theory, i.e., the idea of discretizing space and time to a finite lattice and computing physical observables from first principles via Monte-Carlo simulations. In fact, lattice simulations have contributed a major part of our current understanding of strongly-interacting matter at both zero and non-zero temperatures, see, e.g., [38]. However, conventional Monte-Carlo techniques based on importance sampling cannot be applied when attempting to study QCD at finite baryon density, i.e., at non-zero chemical potential. This is due to the infamous complex-action problem [39], which, despite countless attempts (see [40, 41] for reviews), has not yet been overcome for the case of finite-density QCD [42, 43]. Still, for the proper description of high-density phenomena, such as neutron stars and the physics of the early universe, one requires a working theory that allows to make accurate and testable predictions at finite chemical potential. Alternative approaches to the straightforward application of importance sampling in lattice QCD are thus much needed.

One such alternative that allows for insights into the low-energy regime of QCD is the use of effective theories. A prime example of an effective theory of QCD is chiral perturbation theory (see, e.g., [44]), in which the elementary degrees of freedom are no longer quarks and gluons, but instead hadrons such as pions. In this thesis, however, we shall be concerned with a different class of low-energy theories of QCD, namely so-called four-Fermi theories (4FTs). While originally postulated to describe the weak interaction [45], 4FTs have since been employed with great success for the study of QCD. In fact, a

large part of our knowledge about strongly-interacting matter at finite density is due to results from effective models [46, 47]. Moreover, it has been shown that 4FTs, albeit in a non-local form, arise more or less naturally from QCD after integrating out the gauge fields [48]. Quite obviously, 4FTs are not capable of capturing all relevant features of QCD faithfully, not even at low energies. An important example is the confinement of quarks within hadrons, which purely fermionic theories do not describe.

On the other hand, there is also a plethora of properties of utmost importance to QCD that certain 4FTs do have in common with their target theory [49]. Examples include, but are not restricted to, asymptotic freedom (in two dimensions) [50], renormalizability (in three dimensions or lower) [51], as well as dimensional transmutation [50]. We remark that, while being non-renormalizable in four space-time dimensions, the interpretation of 4FTs as effective theories makes possible the introduction of a finite momentum cutoff below which they are assumed to be valid. For our purposes, however, the most important parallels between 4FTs and QCD are the notion of chiral symmetry and its spontaneous breakdown, resulting in the dynamical generation of mass [52, 53]. These topics and some of the related subtleties shall be the main focus of this thesis.

It would be unfair to praise 4FTs only for their success in the context of high-energy physics without also mentioning their accomplishments in the realm of condensed matter. In fact, there exist a number of low-dimensional materials whose quasi-particle excitations are well described by the massless Dirac equation by virtue of their linear dispersion relation, the Fermi velocity thereby playing the role of the speed of light. Taking interactions between these quasi-particles into account, one often ends up with 4FTs as effective descriptions of their low-energy excitations. Indeed, employing a theory with four-Fermi interactions led, for instance, to the successful description [54, 55] of the phase transition between the solitonic and metallic phases in *trans*-polyacetylene, including a correct result for the critical doping concentration [56]. Similarly, the experimental observation of a magnetic-field-induced phase transition in a certain high-temperature superconductor [57] was explained by modeling the system with a 4FT [58–60]. It can hardly be overemphasized how remarkable it is to be able to compute observables in relativistic models that are in agreement with experiments of non-relativistic solids. Further examples of 4FTs in the context of solid-state physics include their use as low-energy theories for graphene [61–64]. In fact, there has been a remarkable cross-fertilization between the two seemingly unrelated fields of high-energy and condensed-matter physics over the years [65–71]. Parts of this development are summarized in [72].

While in earlier days effective fermionic models were predominantly studied in mean-field approaches [73–80], where quantum fluctuations are suppressed and computations are relatively straightforward, more recently there has been a surge of beyond-mean-field approaches, including lattice simulations [81–89]. The broad picture that appears to emerge is that, in general, the mean-field limit is capable of giving a reasonable intuition about the physics one can expect to find in the full theory. In many cases, accounting

for fluctuations then only changes the situation on a quantitative level and we shall see examples of this in later chapters of this thesis. Nonetheless, it is important to check whether this observation is generically true or if one may also encounter situations where mean-field approaches fail to give the correct picture even qualitatively. In fact, one such case will be discussed later on as well.

In this thesis we shall be concerned with two different scenarios, which can be thought of as first or intermediate steps in the direction of describing QCD from the point of view of 4FTs beyond the mean-field limit, but may have applications in condensed-matter physics as well. On the one hand, we consider one particular 4FT, the so-called chiral Gross-Neveu (χ GN) model, in $1 + 1$ space-time dimensions. We study its chiral condensate as an order parameter for the breakdown of chiral symmetry and the way in which it is affected by external conditions, i.e., non-zero temperature and density. In particular, we ask the question whether there exist regions (in the parameter space spanned by temperature and chemical potential) where the chiral condensate develops crystalline order, i.e., oscillates as a function of the spatial coordinate. Such behavior was predicted in mean-field studies [90, 91] and, as we shall see, can also be observed to some extent in our lattice simulations beyond the mean-field limit. Similar phenomena are quite abundant in the condensed-matter literature. For instance, in certain BCS superconductors [92] subjected to sufficiently strong magnetic fields, a novel inhomogeneous state, the so-called Fulde-Ferrell-Larkin-Ovchinnikov (FFLO) phase, was discovered [93, 94] (see [95] for a review). Moreover, computations using functional methods have found indications that inhomogeneous phases could also be of relevance for QCD at high densities [96, 97] and they have been predicted to be present in its color-superconducting phase as well [98]. Potential experimental signatures of inhomogeneous phases in so-called moat regimes were identified in [99]. For a review on inhomogeneous chiral condensates, including a more exhaustive list of examples, see [100].

On the other hand, motivated by the aforementioned implications that magnetic fields can have on strongly-interacting matter, we are interested in the question of how exactly they affect 4FTs as effective theories for both QCD and solid-state models. To this end, we employ the Gross-Neveu (GN) model, a somewhat simpler version of the χ GN model mentioned above, in $2 + 1$ space-time dimensions. We compute its phase structure, again determined by the behavior of the chiral condensate at finite temperature and density, and study how it is altered under the influence of a background magnetic field both in the mean-field limit and beyond. Earlier mean-field studies revealed that the model exhibits an extremely rich phase structure in the finite-density regime when the magnetic field is non-zero [101]. We investigate whether this observation is merely an artifact of the mean-field limit or still holds true when fluctuations are taken into account. To this end, we perform extensive lattice simulations, the main finding of which is that the phase diagram of the model looks much simpler in our study than it does in the mean-field limit.

This thesis is structured as follows: In Chapter 2 we give a brief introduction into 4FTs, highlighting the particular models that we shall be concerned with in the sequel, and discuss their symmetries, among which chiral symmetry is most important for our purposes. Furthermore, we show how to partially bosonize such theories in order to make them accessible for our later analytical and numerical treatments and address some peculiarities that arise in low space-time dimensions.

We proceed with Chapter 3, in which we first discuss the important concept of Landau levels and associated spectral properties of fermionic theories within magnetic fields. For instance, we shall derive how the chiral condensate in a theory of massive non-interacting fermions in a magnetic field is decomposed into contributions from low-lying and higher eigenmodes of the corresponding Dirac operator. We then discuss analytical findings in the mean-field limit of the $(2 + 1)$ -dimensional GN model at finite density, temperature and magnetic field. In particular, we compute phase diagrams in the space spanned by these control parameters, as well as a few thermodynamic observables. While most results of this chapter are obtained in an infinite volume, we also briefly discuss the implications of considering finite volumes instead.

In Chapter 4 we then depart from the analytical part of the thesis and enter the more numerically-oriented one. We introduce the idea behind lattice simulations of quantum field theories on a general level and put a particular emphasis on how to discretize chiral fermions, thereby discussing the so-called SLAC and overlap formalisms in more detail. Moreover, we outline how to implement magnetic fields on the lattice and compare different lattice discretizations of fermions to continuum computations in a simple setup of non-interacting fermions for the purpose of testing.

The next two chapters then contain the main findings of this thesis in the form of lattice simulation results. On the one hand, Chapter 5 deals with the search for inhomogeneous structures in 4FTs. After summarizing the most important historical developments in this field of research, both on the mean-field level and beyond, we present our lattice results for the χ GN model in $1+1$ dimensions. We discuss the influence of temperature and chemical potential on the observed inhomogeneities and investigate how they are affected by approaching larger volumes or smaller lattice spacings. We also address the problem of spontaneous symmetry breaking in low space-time dimensions in some detail, thereby carefully distinguishing between perfect long-range and quasi-long-range order.

On the other hand, Chapter 6 is concerned with strongly-interacting quantum field theories in background magnetic fields. We give a brief account on the relevant existing literature before performing a number of numerical tests on the overlap Dirac operator employed in our simulations. We thereby put a particular emphasis on its spectral properties, discussing the important index theorem as well as arising finite-size effects. Afterwards, we present our simulation results for the $(2 + 1)$ -dimensional GN model, both for zero and non-zero magnetic field, predominantly investigating the fate of the

results of Chapter 3 beyond the mean-field limit. We also spend some time searching for inhomogeneities in this three-dimensional model and compare our simulation results to the existing literature.

Since parts of our findings are – perhaps – somewhat unexpected, we devote Chapter 7 to a thorough discussion and critical analysis. We summarize our results and attempt to make possible conclusions regarding their applicability in QCD where possible. Furthermore, we present ideas on how to improve on the models considered and suggest directions for potential future research.

The compilation of this thesis is solely due to the author. However, a large part of the presented results is based on work in collaboration with Julian Lenz and Andreas Wipf. Parts of the content of Chapters 3, 5 and 6 were published as conference proceedings [102, 103]. The results of Chapter 5 were furthermore published in the journal article [104], while some of the work of Chapters 3, 4 and 6 appeared in [105, 106]. All simulations were performed using a codebase developed mainly by Björn Wellegehausen, albeit with significant contributions from Daniel Schmidt and Julian Lenz, among others. The major part of the simulations used computational resources provided by the University of Jena, mainly the cluster ARA. Additional simulations were performed on the GOETHE cluster of the University of Frankfurt and the SUNBIRD cluster of the University of Swansea. The results of Sections 4.4 and 6.2 were computed using code written in collaboration with Julian Lenz.

2 Four-Fermi Theories

We begin this chapter by briefly presenting the notation and conventions that shall be used throughout this thesis. Afterwards, we introduce 4FTs, discuss their symmetries and outline how to make them amenable for our studies in later chapters.

2.1 Notation and conventions

For the entirety of this thesis we shall work in space-times with Euclidean signature exclusively. This will be reflected by a few additional signs and imaginary units in places where they are not present in Minkowski space-time. It also entails that we do not distinguish between covariant and contravariant vector indices. Regardless, throughout all of this thesis Einstein's summation convention applies whenever an index occurs twice in an expression, unless specified otherwise.

In a slight abuse of notation we may nonetheless refer to, say, a three-dimensional Euclidean space-time as $(2 + 1)$ -dimensional. The reason for this is as follows: We are predominantly concerned with the study of fermionic fields, which obey periodic boundary conditions in all spatial directions and anti-periodic ones in the (Euclidean) time direction [107]. In our notation the “+1” simply indicates the presence of a direction with anti-periodic boundary conditions for fermions. Apart from two exceptions in Sections 4.4 and 6.2, where we consider $(2 + 0)$ -dimensional theories for testing purposes, we shall always assume that there is a Euclidean time direction in which fermions are anti-periodic.

We refer to the total number of space-time dimensions as d and we shall use Greek letters to label the components of d -vectors, e.g., x_μ for the components of a vector x . The zeroth component (e.g., x_0) is reserved for the time direction, while we indicate the spatial directions by Latin letters (e.g., x_i) as well as bold symbols (e.g., \mathbf{x}). For space-times with no anti-periodic direction there is no zeroth component.

For most of this thesis we work on finite space-time volumes. We denote the extent of the temporal direction as β and we always assume all spatial directions to have the same extent, which we refer to as L . A finite space-time volume entails the discretization of the corresponding momenta and we define

$$p_0 = \frac{2\pi}{\beta} \left(n_0 + \frac{1}{2} \right), \quad p_i = \frac{2\pi}{L} n_i, \quad (2.1)$$

where the n_μ are integers. We furthermore note that β plays the role of the inverse

temperature, $\beta = \frac{1}{T}$. Throughout this thesis we use natural units in which the speed of light, the reduced Planck constant and the Boltzmann constant are all set to unity, i.e., $c = 1$, $\hbar = 1$ and $k_B = 1$.

We write z^* to denote the complex conjugate of a complex number z . For a matrix or operator A we shall denote its transpose as A^T and its Hermitian conjugate as A^\dagger . The commutator of two matrices or operators A and B is denoted as $[A, B] := AB - BA$ and their anti-commutator as $\{A, B\} := AB + BA$.

2.2 Four-Fermi theories and their symmetries

Let us now introduce 4FTs, which we will be concerned with in the entirety of this thesis. The basic form of a 4FT is given by a Lagrangian of the following type:

$$\mathcal{L} = i\bar{\psi}(\not{\partial} + m)\psi + \sum_i \frac{g_i^2}{2N_f} (\bar{\psi}M_i\psi) (\bar{\psi}M_i\psi) . \quad (2.2)$$

Here, ψ is a short-hand notation for the Grassmann-valued fermion fields $\psi_\alpha(x)$, with a labeling fermionic flavors and α being a Dirac index, m is the bare fermion mass, which we assume to be identical for all flavors, the g_i^2 denote coupling constants and the M_i are matrices acting in flavor and Dirac space. Since we work in Euclidean space-time we define $\bar{\psi} = \psi^\dagger$ [108]. In (2.2) and in the remainder of this thesis we suppress the explicit summations over the internal indices a and α . The former runs from 1 to the number of fermion flavors, N_f , while the latter runs from 1 to the dimension of the Clifford algebra, d_c . As is discussed below, d_c is determined by the space-time dimension as well as the chosen Dirac algebra representation. Moreover, we have not indicated the space-time-dependence of ψ explicitly in (2.2) and we shall continue to do so in most of what follows. Lastly, we mention that the fermion fields could additionally be endowed with another index, corresponding to degrees of freedom in color space. This, however, shall not be of relevance for this thesis.

In Euclidean space-time the Dirac matrices γ_μ may be chosen Hermitian. There exists one irreducible representation of γ_μ for even d , while there are two inequivalent ones, γ_μ and $-\gamma_\mu$, when d is odd. For now, we only discuss irreducible representations of Dirac matrices, in which the number of spinor components is given by

$$d_c = 2^{\lfloor \frac{d}{2} \rfloor} , \quad (2.3)$$

with $\lfloor \cdot \rfloor$ denoting the floor function. The intricacies involved in using reducible representations will be discussed in more detail in Section 2.2.4.

In even dimensions one may – in addition to the γ_μ – introduce another gamma

matrix, denoted by γ_* and defined as

$$\gamma_* := -i \lfloor \frac{d}{2} \rfloor \gamma_0 \gamma_1 \dots \gamma_{d-1} , \quad (2.4)$$

which has the following properties:

$$\gamma_*^\dagger = \gamma_* , \quad \gamma_*^2 = \mathbb{1} , \quad \{\gamma_*, \gamma_\mu\} = 0 \quad \text{for all } \mu . \quad (2.5)$$

For $d = 4$ this definition coincides with the usual “fifth” gamma matrix γ_5 . On the other hand, in odd dimensions (2.4) is proportional to the identity. When there exists a non-trivial γ_* we shall usually – unless specified otherwise – choose a basis in which it is diagonal, such that spinors decompose into their right- and left-handed components:

$$\psi = \begin{pmatrix} \psi_R \\ \psi_L \end{pmatrix} . \quad (2.6)$$

As usual, one may define projection operators onto right- and left-handed spinor components by $\mathbb{P}_R := \frac{\mathbb{1} + \gamma_*}{2}$ and $\mathbb{P}_L := \frac{\mathbb{1} - \gamma_*}{2}$, respectively. In the following, we discuss the symmetries of 4FTs in some more detail (see also [108–110]).

2.2.1 Space-time symmetries

We begin by considering continuous transformations on Euclidean space-time. In a d -dimensional space-time with Euclidean metric the usual Lorentz symmetry is replaced by invariance under $\text{SO}(d)$ transformations $\Lambda_{\mu\nu}$,

$$x_\mu \mapsto x'_\mu = \Lambda_{\mu\nu} x_\nu , \quad (2.7)$$

which act on Dirac spinors as follows:

$$\psi(x) \mapsto e^{-\frac{i}{4} \omega_{\mu\nu} \sigma_{\mu\nu}} \psi(x') , \quad \bar{\psi}(x) \mapsto \bar{\psi}(x') e^{\frac{i}{4} \omega_{\mu\nu} \sigma_{\mu\nu}} . \quad (2.8)$$

Here, $\sigma_{\mu\nu} = \frac{i}{2} [\gamma_\mu, \gamma_\nu]$ represents the generators of $\text{SO}(d)$ and $\omega_{\mu\nu}$ is an anti-symmetric tensor characterizing the rotation axes and angles of $\Lambda_{\mu\nu}$. Similarly, space-time translations by a d -vector a_μ ,

$$x_\mu \mapsto x'_\mu = x_\mu + a_\mu , \quad (2.9)$$

are represented on spinors by

$$\psi(x) \mapsto e^{-ia_\mu P_\mu} \psi(x) , \quad \bar{\psi}(x) \mapsto \bar{\psi}(x) e^{ia_\mu P_\mu} , \quad (2.10)$$

with the momentum operators P_μ generating the translations.

In addition to continuous space-time symmetries, 4FTs also enjoy a number of discrete

symmetries, namely invariance under parity transformations, time reversal and charge conjugation, only the former of which we discuss here exemplarily. We define a parity transformation as the inversion of the last spatial coordinate,

$$x_\mu \mapsto x'_\mu = P_{\mu\nu}x_\nu, \quad \text{where } P = \text{diag}(1, \dots, -1), \quad (2.11)$$

which is implemented on the fermion fields as

$$\psi(x) \mapsto \mathcal{P}\psi(x), \quad \bar{\psi}(x) \mapsto \eta_p \bar{\psi}(x) \mathcal{P}^{-1}, \quad (2.12)$$

where we have introduced the parity matrix \mathcal{P} . In even dimensions the latter can be defined as $\mathcal{P} = i\gamma_*\gamma_{d-1}$ with $\eta_p = 1$, while in odd dimensions a valid definition is $\mathcal{P} = \gamma_{d-1}$ but one has $\eta_p = -1$. The latter fact causes certain fermion bilinear operators to transform differently in even and odd dimensions. We furthermore require

$$\mathcal{P}^{-1}\gamma_\mu\mathcal{P} = \eta_p P_{\mu\nu}\gamma_\nu \quad (2.13)$$

in order for the action of massless non-interacting fermions to be invariant under (2.12). More details about parity, as well as the other discrete symmetries, i.e., time reversal and charge conjugation, including the associated intricacies that arise in Euclidean space-time, can be found, e.g., in [109].

2.2.2 Internal symmetries

Having discussed the space-time symmetries of 4FTs, let us now turn to their internal symmetries, all of which are global. First of all, all 4FTs are trivially invariant under the $U(1)_V$ vector transformations

$$\psi(x) \mapsto e^{i\alpha}\psi(x), \quad \bar{\psi}(x) \mapsto \bar{\psi}(x)e^{-i\alpha}, \quad (2.14)$$

where α is a real parameter. Additionally, if for some model the matrices M_i in (2.2) are trivial in flavor space, then that model also enjoys a $SU(N_f)_V$ symmetry, i.e., it is invariant under

$$\psi(x) \mapsto e^{i\alpha_i T_i}\psi(x), \quad \bar{\psi}(x) \mapsto \bar{\psi}(x)e^{-i\alpha_i T_i}, \quad (2.15)$$

where the T_i ($i = 1, \dots, N_f^2 - 1$) denote the generators of $SU(N_f)$ and the α_i are, again, real parameters. That this can be a symmetry is due to the fact that we always assume all fermion flavors to be mass-degenerate. A non-trivial flavor structure in M_i breaks this symmetry in general. However, there are also examples of theories for which this is not the case, see, e.g., the NJL model (2.18) below. In this thesis we shall restrict ourselves to theories with an intact $SU(N_f)_V \times U(1)_V$ vector flavor symmetry.

The vector transformations discussed up to now do not distinguish between left- and

right-handed spinor components, as they act on both in the same way. However, when the space-time dimension or Dirac algebra representation allows for the introduction of γ_* , one may also consider axial rotations, under which the left- and right-handed components transform oppositely. We define the action of $U(1)_A$ axial rotations on Dirac spinors as

$$\psi(x) \mapsto e^{i\alpha\gamma_*}\psi(x), \quad \bar{\psi}(x) \mapsto \bar{\psi}(x)e^{i\alpha\gamma_*}, \quad (2.16)$$

while the corresponding $SU(N_f)_A$ transformations read (α and α_i are not related to the parameters of the vector transformations above)

$$\psi(x) \mapsto e^{i\alpha_i\gamma_*T_i}\psi(x), \quad \bar{\psi}(x) \mapsto \bar{\psi}(x)e^{i\alpha_i\gamma_*T_i}. \quad (2.17)$$

Invariance of a theory under both vector and axial transformations is referred to as chiral symmetry, which plays a major role in the context of this thesis.

A theory of N_f flavors of free massless fermions is invariant under the full symmetry group $SU(N_f)_V \times SU(N_f)_A \times U(1)_V \times U(1)_A$. However, a fermionic mass term breaks chiral symmetry explicitly, as it mixes left- and right-handed spinor components. For this reason, we shall set the mass m in (2.2) to zero in most of what follows. Moreover, the full chiral symmetry of free fermions is also commonly broken explicitly by four-Fermi interactions. Thus, we shall find it useful at this point to introduce a few common models and discuss their respective chiral symmetry groups.

2.2.3 Prominent four-Fermi theories

Perhaps the most famous 4FT is the Nambu–Jona-Lasinio (NJL) model [53], defined by

$$\mathcal{L} = \bar{\psi}i\cancel{\partial}\psi + \frac{g^2}{2N_f} \left[(\bar{\psi}\psi)^2 + (i\bar{\psi}\gamma_*\vec{\tau}\psi)^2 \right], \quad (2.18)$$

where $\vec{\tau}$ is a vector of Pauli matrices acting in two-dimensional flavor (or isospin) space, i.e., we assume $N_f = 2$ here. Similar to free fermions, this model is invariant under the full $SU(2)_V \times SU(2)_A \times U(1)_V \times U(1)_A$ group.

A related theory, which is referred to here as the chiral Gross-Neveu (χ GN) model [50], is defined as

$$\mathcal{L} = \bar{\psi}i\cancel{\partial}\psi + \frac{g^2}{2N_f} \left[(\bar{\psi}\psi)^2 + (i\bar{\psi}\gamma_*\psi)^2 \right]. \quad (2.19)$$

In contrast to the NJL model, we may study (2.19) for arbitrary flavor numbers. It breaks the $SU(N_f)_A$ symmetry (2.17), but is invariant under $U(1)_A$ rotations (2.16). Thus, its full symmetry group reads $SU(N_f)_V \times U(1)_V \times U(1)_A$. Notice that an equivalent model for $N_f = 1$ had already been introduced in [52]. Nonetheless, we shall refer to (2.19) as the chiral Gross-Neveu model. It is of great importance for this thesis and Chapter 5 is devoted to its study.

Another well-known 4FT and perhaps the simplest relativistic theory of interacting fermions is the Gross-Neveu (GN) model [50], defined by

$$\mathcal{L} = \bar{\psi}i\cancel{\partial}\psi + \frac{g^2}{2N_f} (\bar{\psi}\psi)^2 . \quad (2.20)$$

The absence of the $(\bar{\psi}\gamma_*\psi)^2$ term breaks the χ GN model's $U(1)_A$ symmetry down a discrete \mathbb{Z}_2 subgroup,

$$\psi(x) \rightarrow i\gamma_*\psi(x) , \quad \bar{\psi}(x) \rightarrow i\bar{\psi}(x)\gamma_* . \quad (2.21)$$

Thus, the chiral symmetry group of the GN model is $SU(N_f)_V \times U(1)_V \times \mathbb{Z}_2$. We shall study it in detail in Chapters 3 and 6. While we focus on the GN and χ GN models for the remainder of this thesis, we also mention the Thirring model [111], which has a vector-vector interaction channel, as another well-known example of a 4FT.

2.2.4 Reducible representations

In three space-time dimensions irreducible representations of the Dirac algebra are two-dimensional according to (2.3), i.e., irreducible spinors are two-component objects. However, there is no notion of chirality in this case due to the absence of a matrix γ_* that would anti-commute with all γ_μ and allow for the distinction between left- and right-handed spinor components as in (2.6). In order to nonetheless introduce such a γ_* , we shall instead work in a reducible representation [112] of gamma matrices for parts of this thesis, i.e., when we consider three-dimensional space-times. As is outlined below, this allows for the definition of γ_* and entails that spinors have four components instead of two. As a matter of fact, this is commonly done in the condensed-matter literature. For instance, in graphene the electronic modes near the two Dirac points, where the dispersion relation is approximately linear, are each described by two-component spinors, which one commonly combines into a single four-component object [113].

In order to outline the central idea behind the use of a reducible representation of gamma matrices, let us consider a theory of fermions in d dimensions, where d is odd, as well as one in $d' = d + 1$ dimensions. In what follows, primes indicate (irreducible) gamma matrices in the d' -dimensional theory. To define a reducible representation in d dimensions we may simply set $\gamma_\mu = \gamma'_\mu$, which doubles the number of spinor components by virtue of (2.3). However, this leaves us with two gamma matrices that anti-commute with all γ_μ instead of one, namely γ'_d and γ'_* , each of which is a viable candidate for γ_* . Indeed, they both generate $U(1)_A$ transformations of the form (2.16),

$$\psi(x) \mapsto e^{i\alpha\gamma'_d}\psi(x) , \quad \bar{\psi}(x) \mapsto \bar{\psi}(x)e^{i\alpha\gamma'_d} \quad (2.22)$$

and

$$\psi(x) \mapsto e^{i\alpha\gamma'_*} \psi(x) , \quad \bar{\psi}(x) \mapsto \bar{\psi}(x) e^{i\alpha\gamma'_*} , \quad (2.23)$$

and analogously for the axial flavor rotations (2.17). A theory of free massless fermions is invariant under both of these transformations. Moreover, the matrix $\gamma'_d \gamma'_*$ commutes with all other gamma matrices in the d -dimensional theory, giving rise to an additional $U(1)_V$ symmetry (as well as the corresponding vector flavor symmetry) that was not present before,

$$\psi(x) \mapsto e^{i\alpha\gamma'_d \gamma'_*} \psi(x) , \quad \bar{\psi}(x) \mapsto \bar{\psi}(x) e^{-i\alpha\gamma'_d \gamma'_*} . \quad (2.24)$$

A mass term breaks both (2.22) and (2.23), but leaves (2.24) intact. We see that it is indeed possible to introduce an analog of γ_* – in fact, two such analogs – in odd dimensions as well by working in a reducible representation of the Dirac algebra. For more details, see, e.g., [114].

The ambiguity in the choice of γ_* is not relevant for the GN model, however. The reason for this is that the scalar-scalar interaction term in (2.20) breaks both axial symmetries, (2.22) and (2.23), down to respective \mathbb{Z}_2 subgroups as in (2.21). These resulting \mathbb{Z}_2 transformations can then be shown to be related to each other via (2.24). This means that the GN model in a reducible representation is invariant under two different $SU(N_f)_V \times U(1)_V$ groups, but only under one \mathbb{Z}_2 group, with a mass term only breaking the latter. We remark that N_f denotes the number of reducible flavors here. Despite the notion of chiral symmetry not being defined in odd space-time dimensions, we shall nonetheless make use of that terminology throughout this thesis for reasons of convenience. We also mention that the use of a reducible representation allows for a parity transformation (2.12) with $\eta_p = 1$ and the definition of χ GN and NJL models in odd dimensions.

To demonstrate the concept, let us consider a $(2 + 1)$ -dimensional theory as an example. An explicit expression for the gamma matrices in a reducible representation is given by

$$\gamma_\mu = \begin{pmatrix} \tau_\mu & 0 \\ 0 & -\tau_\mu \end{pmatrix} , \quad (2.25)$$

where the τ_μ can be chosen as the conventional Pauli matrices, e.g.,

$$\tau_0 = \sigma_3 , \quad \tau_1 = \sigma_1 , \quad \tau_2 = \sigma_2 . \quad (2.26)$$

The block structure of (2.25) makes clear the fact that the reducible representation consists of both of the two inequivalent irreducible representations (τ_μ and $-\tau_\mu$), which we shall find useful in later chapters. Notice, however, that γ_* is not diagonal in this basis.

2.3 Partition function and bosonization

Having discussed the symmetries of 4FTs we now define their partition functions and outline how their computation can simplify due to the introduction of auxiliary fields. With the (Euclidean) action of a theory specified by a Lagrangian \mathcal{L} ,

$$S = \int d^d x \mathcal{L} , \quad (2.27)$$

the partition function of a 4FT is given by the fermionic path integral

$$Z = \int \mathcal{D}\bar{\psi} \mathcal{D}\psi e^{-S} . \quad (2.28)$$

Expectation values of observables \mathcal{O} may then be computed via

$$\langle \mathcal{O} \rangle = \frac{1}{Z} \int \mathcal{D}\bar{\psi} \mathcal{D}\psi e^{-S} \mathcal{O} , \quad (2.29)$$

where we suppress the explicit functional dependence of S and \mathcal{O} on the fermion fields.

For the particular case of the GN model (2.20), the partition function reads

$$Z_{\text{GN}} = \int \mathcal{D}\bar{\psi} \mathcal{D}\psi e^{-\int d^d x \left[\bar{\psi} i \not{\partial} \psi + \frac{g^2}{2N_f} (\bar{\psi} \psi)^2 \right]} . \quad (2.30)$$

Now, consider the identity

$$\int \mathcal{D}\sigma e^{-\int d^d x \left[\frac{N_f}{2g^2} \sigma^2 + i\sigma \bar{\psi} \psi \right]} = e^{-\int d^d x \frac{g^2}{2N_f} (\bar{\psi} \psi)^2} , \quad (2.31)$$

where σ denotes a scalar field and we have absorbed an irrelevant prefactor into the integral measure $\mathcal{D}\sigma$. Using (2.31), we can rewrite the partition function (2.30) as

$$Z_{\text{GN}} = \int \mathcal{D}\bar{\psi} \mathcal{D}\psi \mathcal{D}\sigma e^{-\int d^d x \left[i\bar{\psi} (\not{\partial} + \sigma) \psi + \frac{N_f}{2g^2} \sigma^2 \right]} . \quad (2.32)$$

With this so-called Hubbard-Stratonovich transformation [115, 116], we have thus related the Lagrangian (2.20) to the following, partially bosonized, one:

$$\mathcal{L}_\sigma = i\bar{\psi} (\not{\partial} + \sigma) \psi + \frac{N_f}{2g^2} \sigma^2 . \quad (2.33)$$

Since the integral (2.31) is Gaussian, the equivalence of (2.20) and (2.33) holds not only on the classical level, but also in the full quantum theory. Notice, however, that in order for (2.33) to retain its \mathbb{Z}_2 symmetry (2.21), we require σ to flip its sign under such

a transformation. This means that the model (2.33) is invariant under

$$\psi \rightarrow i\gamma_*\psi, \quad \bar{\psi} \rightarrow i\bar{\psi}\gamma_*, \quad \sigma \rightarrow -\sigma. \quad (2.34)$$

Analogous Hubbard-Stratonovich transformations can be applied to other four-Fermi terms as well. As an example, the partially bosonized version of the χ GN model (2.19) reads

$$\mathcal{L}_{\sigma,\pi} = i\bar{\psi}(\not{\partial} + \sigma + i\gamma_*\pi)\psi + \frac{N_f}{2g^2}(\sigma^2 + \pi^2), \quad (2.35)$$

where π denotes another auxiliary field, which transforms as a pseudo-scalar. The $U(1)_A$ symmetry of (2.35) then reads

$$\psi \rightarrow e^{i\alpha\gamma_*}\psi, \quad \bar{\psi} \rightarrow \bar{\psi}e^{i\alpha\gamma_*}, \quad \begin{pmatrix} \sigma \\ \pi \end{pmatrix} \rightarrow \begin{pmatrix} \cos(2\alpha) & \sin(2\alpha) \\ -\sin(2\alpha) & \cos(2\alpha) \end{pmatrix} \begin{pmatrix} \sigma \\ \pi \end{pmatrix}. \quad (2.36)$$

The Lagrangians (2.33) and (2.35) no longer contain the four-Fermi interaction terms, as we have traded them off in exchange for the auxiliary fields. These Lagrangians are particularly convenient to work with, since the fermion fields only enter them bilinearly and can thus be integrated out entirely, as we shall discuss next.

As we have seen, a generic partially bosonized 4FT can be written in the form

$$\mathcal{L} = i\bar{\psi}D_{N_f}\psi + \mathcal{L}_B, \quad (2.37)$$

where D_{N_f} , which is referred to as the Dirac operator, describes the fermionic part of the action including the interactions with the auxiliary fields and \mathcal{L}_B denotes the purely bosonic contributions. One may now integrate out the fermions by using a well-known result of Gaussian integration over Grassmann numbers,

$$Z = \int \mathcal{D}\bar{\psi}\mathcal{D}\psi\mathcal{D}\sigma e^{-\int d^d x [i\bar{\psi}D_{N_f}\psi + \mathcal{L}_B]} = \int \mathcal{D}\sigma \det(D_{N_f}) e^{-S_B}, \quad (2.38)$$

where $S_B = \int d^d x \mathcal{L}_B$. If we assume the Dirac operator to have a trivial structure in flavor space, which shall always be the case throughout this thesis, its determinant factorizes into a product of N_f one-flavor Dirac operators D , i.e., $\det(D_{N_f}) = \det(D)^{N_f}$. In other words, one ends up with a purely bosonic theory,

$$Z = \int \mathcal{D}\sigma e^{-N_f S_{\text{eff}}}, \quad (2.39)$$

with an effective action

$$S_{\text{eff}} = S_B - \ln \det D, \quad (2.40)$$

in which the scalar fields become dynamical via fermion loops, as dictated by the fermion determinant. The convenient form (2.39) is the starting point for both the analytical and

the numerical approaches to studying 4FTs that we pursue in this thesis. From now on, we shall use the same symbol D for the one- and N_f -flavor Dirac operators for notational convenience.

2.4 Spontaneous symmetry breaking

Let us now introduce a concept that shall be of central importance for this thesis, namely that of the spontaneous breakdown of a symmetry. By that, we refer to a symmetry of the classical theory, i.e., of its Lagrangian, which is broken by the vacuum or thermal equilibrium state. It is in particular the spontaneous breakdown of chiral symmetry that is of relevance for us. For its study, let us consider the expectation value of the scalar fermion bilinear, $\langle \bar{\psi}\psi \rangle$. This quantity, which we shall henceforth refer to as the fermion or chiral condensate, behaves like a mass term under chiral transformations. Thus, if a theory that is chirally invariant on the classical level develops a non-zero value of $\langle \bar{\psi}\psi \rangle$, one may conclude that chiral symmetry is spontaneously broken. We mention that the spontaneous breakdown of chiral symmetry and the associated dynamical mass generation plays a major role in QCD, where it is responsible, e.g., for the fact that the masses of nucleons by far exceed the combined bare masses of their quark constituents.

The computation of fermionic expectation values, such as $\langle \bar{\psi}\psi \rangle$, drastically simplifies with the introduction of auxiliary scalar fields in Lagrangians of the form (2.37). To see this, let us consider as an example the GN model (2.33), where the following identity holds:

$$\int \mathcal{D}\bar{\psi}\mathcal{D}\psi\mathcal{D}\sigma \frac{\delta}{\delta\sigma} e^{-\int d^d x [i\bar{\psi}(\not{\partial}+\sigma)\psi + \frac{N_f}{2g^2}\sigma^2]} = 0 . \quad (2.41)$$

Using (2.29), we thus find that

$$\langle \bar{\psi}\psi \rangle = i \frac{N_f}{g^2} \langle \sigma \rangle , \quad (2.42)$$

i.e., the chiral condensate is determined exactly by the expectation value of σ , the latter usually being much more straightforward to compute. The same trick can also be applied in the χ GN model, where one may additionally perform an analogous variation with respect to π to obtain

$$\langle \bar{\psi}\gamma_*\psi \rangle = \frac{N_f}{g^2} \langle \pi \rangle . \quad (2.43)$$

These and similar Ward identities (or Dyson-Schwinger equations (DSEs)) facilitate the computation of expectation values of fermionic bilinears considerably and we shall make heavy use of them in the remainder of this thesis.

3 The Mean-Field Gross-Neveu Model

We devote this chapter to an analytical study of fermionic theories exposed to background magnetic fields. We shall first introduce the important concept of Landau levels, which govern the physics of magnetized particles. In particular, we emphasize the effect a magnetic field has on the density of fermionic energy states. Afterwards, as the main focus of this chapter we investigate the $(2 + 1)$ -dimensional GN model in the mean-field limit. We provide a detailed discussion of its phase structure in the three-dimensional parameter space spanned by temperature, chemical potential and magnetic field and discuss thermodynamic observables. Finally, we outline the qualitative differences that arise when considering the model in a finite spatial volume.

3.1 Landau levels

The energy levels of charged particles within a homogeneous magnetic field are quantized in terms of so-called Landau levels [117]. In the following, we consider a theory of non-interacting fermions in three space-time dimensions exposed to an external magnetic field B perpendicular to the spatial plane. For simplicity, we consider an irreducible representation of the Dirac algebra here, comprising two-component spinors. Using a four-component representation instead only changes the results by a trivial factor of 2.

Denoting the fermion mass by m , the squared one-particle energies of non-interacting fermions in a magnetic field are derived in Appendix A and read

$$E_l^2 = m^2 + 2|eB|l, \quad (3.1)$$

where $e > 0$ denotes the elementary electric charge and l is a non-negative integer labeling the energy levels, which we refer to as Landau levels. The expression (3.1) should be compared with the usual energy-momentum relation that holds when $B = 0$,

$$E_p^2 = m^2 + \mathbf{p}^2, \quad (3.2)$$

with \mathbf{p} denoting the vector of spatial momenta.

The momentum-independence of (3.1) gives rise to a degeneracy d_l of the Landau levels that is proportional to the magnetic flux through the spatial plane. Namely, as is shown in Appendix A, if we assume space-time to have a finite volume $V = L^2\beta$ and

impose the usual fermionic boundary conditions, then

$$d_l = \begin{cases} \frac{|eB|}{2\pi} L^2 & \text{if } l = 0 \\ \frac{|eB|}{\pi} L^2 & \text{if } l > 0 \end{cases}, \quad (3.3)$$

i.e., the degeneracy of the lowest Landau level (LLL) is half of that of the higher levels. This stems from the fact that only one of the two possible spin orientations is allowed in the LLL, being energetically favored by the magnetic field. In comparison, all energies in (3.2) have a two-fold degeneracy. It is quite obvious that the magnetic field has a significant impact on the fermionic energy spectrum and in the following we shall work out the consequences of this in more detail.

It is known that the magnetic flux through a two-dimensional torus is necessarily quantized [118] (see also Appendix A), in order to ensure gauge-invariance and the smoothness of the magnetic field across the boundary [119]. This means that one can only have

$$eB = \frac{2\pi}{L^2} b, \quad (3.4)$$

where b is an integer that we shall refer to as the magnetic flux quantum number. From this quantization condition one may already infer that the limit $B \rightarrow 0$ cannot be taken in a continuous manner without simultaneously approaching the limit $L \rightarrow \infty$.

Let us now consider the density of states that have an energy below some value $\varepsilon \geq 0$. In Appendix B we show that for $B = 0$ this integrated density of states is given by

$$\rho_0(\varepsilon) = \frac{2}{L^2} \sum_{n=0}^{\infty} r_2(n) \Theta \left(\varepsilon - \sqrt{m^2 + \frac{4\pi^2}{L^2} n} \right), \quad (3.5)$$

where r_2 is the sum-of-squares function defined in (B.19). For non-vanishing B (i.e., non-vanishing b , which we use as a label for ρ) the density reads

$$\rho_b(\varepsilon) = \frac{|b|}{L^2} \left[\Theta(\varepsilon - m) + 2 \sum_{l=1}^{\infty} \Theta \left(\varepsilon - \sqrt{m^2 + \frac{4\pi|b|}{L^2} l} \right) \right]. \quad (3.6)$$

We show a comparison between these two functions for two different spatial volumes L^2 in Fig. 3.1. One observes that, while the densities for different b approach each other asymptotically for large ε , they differ substantially for low energies on small volumes. In particular, the contribution of the lowest-lying modes at $\varepsilon = m$ is different for $B = 0$ and $B \neq 0$. When increasing the volume, this difference becomes negligible if one keeps the magnetic flux (i.e., b) fixed in the process, but is still sizable if one instead fixes the magnetic field (i.e., b/L^2). This fact has important implications for observables, as we shall demonstrate in the following, using the fermion condensate $\langle \bar{\psi} \psi \rangle$ as an example.

In Appendix B we derive the following relation for the change in the condensate

3. The Mean-Field Gross-Neveu Model

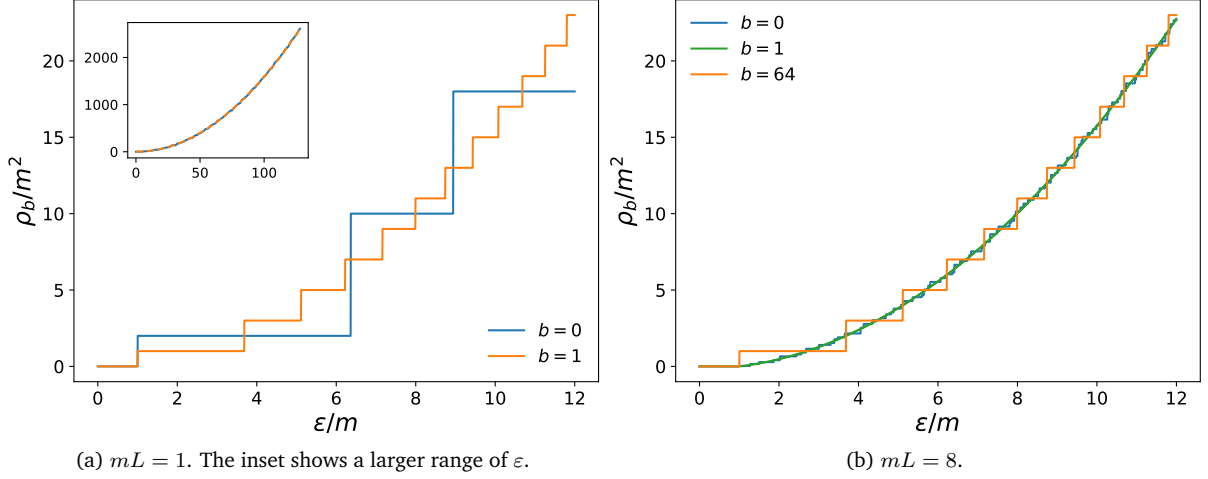


Figure 3.1: Densities of states from (3.5) and (3.6) two different volumes. Equal magnetic field strengths are indicated by equal colors.

induced by the magnetic field:

$$\Delta\langle\bar{\psi}\psi\rangle := \langle\bar{\psi}\psi\rangle(B) - \langle\bar{\psi}\psi\rangle(0) = -\frac{m}{\beta} \sum_{n=-\infty}^{\infty} \int_0^{\infty} d\varepsilon \frac{1}{\omega_n^2 + \varepsilon^2} [g_b(\varepsilon) - g_0(\varepsilon)] , \quad (3.7)$$

where

$$\omega_n = \frac{2\pi}{\beta} \left(n + \frac{1}{2} \right) , \quad n \in \mathbb{Z} \quad (3.8)$$

are the usual Matsubara frequencies, $\beta = \frac{1}{T}$ is the inverse temperature and $g(\varepsilon) = \frac{\partial}{\partial\varepsilon}\rho(\varepsilon)$ denotes the density of states with energy ε , given by a sum of delta distributions. Here and in the following we require that $B \neq 0$. The sum over n can be found in sum tables (see, e.g., [120]) and it gives

$$\sum_{n=-\infty}^{\infty} \frac{1}{\omega_n^2 + \varepsilon^2} = \frac{\beta}{2\varepsilon} \tanh\left(\frac{\varepsilon\beta}{2}\right) . \quad (3.9)$$

We now perform the integral over ε in (3.7) in order to split $\Delta\langle\bar{\psi}\psi\rangle$ into contributions from the lowest-lying modes ($\varepsilon = m$) and those from higher modes ($\varepsilon > m$),

$$\Delta\langle\bar{\psi}\psi\rangle = \Delta\langle\bar{\psi}\psi\rangle_{\varepsilon=m} + \Delta\langle\bar{\psi}\psi\rangle_{\varepsilon>m} , \quad (3.10)$$

where the former is given by

$$\Delta\langle\bar{\psi}\psi\rangle_{\varepsilon=m} = -\frac{1}{2L^2} \tanh\left(\frac{m\beta}{2}\right) (|b| - 2) , \quad (3.11)$$

while the latter reads

$$\Delta\langle\bar{\psi}\psi\rangle_{\varepsilon>m} = -\frac{m}{L^2} \left[\sum_{l=1}^{\infty} \frac{|b|}{\sqrt{m^2 + \frac{4\pi|b|}{L^2}l}} \tanh\left(\frac{\beta}{2}\sqrt{m^2 + \frac{4\pi|b|}{L^2}l}\right) - \sum_{n=1}^{\infty} \frac{r_2(n)}{\sqrt{m^2 + \frac{4\pi^2}{L^2}n}} \tanh\left(\frac{\beta}{2}\sqrt{m^2 + \frac{4\pi^2}{L^2}n}\right) \right]. \quad (3.12)$$

We see that on finite volumes $\Delta\langle\bar{\psi}\psi\rangle_{\varepsilon=m}$ changes its sign going from $b = 1$ to $b > 2$. In the limit $L \rightarrow \infty$, keeping B fixed, on the other hand, there is no such sign change as the low-lying modes of g_0 do not contribute in that limit. More concretely, one finds

$$\Delta\langle\bar{\psi}\psi\rangle_{\varepsilon=m} \xrightarrow[\substack{L \rightarrow \infty \\ \frac{b}{L^2} = \text{const.}}]{} -\frac{|eB|}{4\pi} \tanh\left(\frac{m\beta}{2}\right), \quad (3.13)$$

where we have used (3.4). This means that on small volumes one may expect a change in the fermion condensate's monotonicity for the weakest magnetic fields allowed by the geometry, while on large volumes this effect vanishes. For strong enough magnetic fields the magnitude of $\Delta\langle\bar{\psi}\psi\rangle$ should increase with B . Notice that we have ignored the higher-lying modes ($\varepsilon > m$) in this discussion. However, while their contribution to the fermion condensate may also change its monotonicity as b increases, this effect is likely sub-dominant, which is further substantiated in Section 6.2.3 below, where we encounter the same phenomenon in the discretized free theory.

3.2 Effective potential of the Gross-Neveu model

Having discussed non-interacting fermions in a magnetic field, we now turn towards non-trivial theories. In the following – and in a large part of the remainder of this thesis – we are concerned with the GN model (2.20) in $2+1$ dimensions. In the next few sections we shall derive its phase structure in the parameter space spanned by the temperature T , the chemical potential μ and the external magnetic field B in the mean-field limit.

The massless GN model in its partially bosonized form reads

$$\mathcal{L}_\sigma = \bar{\psi}iD\psi + \frac{N_f}{2g^2}\sigma^2, \quad (3.14)$$

where the Dirac operator D is (up to an identity matrix in flavor space) defined as

$$D = \not{\partial} + ie\not{A} + \mu\gamma_0 + \sigma. \quad (3.15)$$

Here, A_μ is a three-dimensional vector potential describing a constant and homogeneous magnetic field, which we again assume to be perpendicular to the spatial plane and

denote by B . More precisely, using the conventional definition of the field strength tensor $F_{\mu\nu}$ (A.3), the magnetic field in three dimensions is defined by $B = F_{12} := \partial_1 A_2 - \partial_2 A_1$. Furthermore, we have introduced the chemical potential in (3.15) in the usual way, coupling to the fermion number density operator $\bar{\psi}\gamma_0\psi$ in the action.

In the following, we restrict the auxiliary scalar field σ to be homogeneous in both space and time, which *a priori* is a simplifying assumption. In fact, this choice would even lead to incorrect results in certain 4FTs, as they are known to exhibit inhomogeneous phases where σ develops a non-trivial space-dependence [72, 90, 91, 121]. However, for vanishing magnetic field such inhomogeneous phases are believed not to play a role in $2 + 1$ dimensions once the regulator is removed [122–124]. The presence of a magnetic field \mathbf{B} , on the other hand, is capable of inducing spatial inhomogeneities in principle [125–128], but they can likely only form along the direction of \mathbf{B} . Since in our $(2 + 1)$ -dimensional setup we only allow for propagation perpendicular to \mathbf{B} , we think it unlikely that there could be any inhomogeneities present, thus justifying the above choice. In Chapter 5 we shall come back to the discussion of inhomogeneities in 4FTs with more rigor.

Now, with the assumption $\sigma(x) = \sigma = \text{const.}$, the effective action (2.40) takes the following form for the GN model:

$$S_{\text{eff}}(\sigma) = \frac{V}{2g^2}\sigma^2 - \ln \det(D) , \quad (3.16)$$

where V denotes the space-time volume $V = L^2\beta$, as before. As can be seen from (2.39), in the limit $N_f \rightarrow \infty$, henceforth referred to as the large- N_f limit [129], only the global minimum of S_{eff} contributes to the path integral by means of a saddle-point approximation. One could then – in principle – compute corrections to this picture order by order in $\frac{1}{N_f}$. These, however, shall not be of major importance for this thesis. In fact, our non-perturbative approach discussed in later chapters includes all such corrections automatically.

Denoting the minimum position of S_{eff} as σ_{min} , the field expectation value of σ in the large- N_f limit is simply given by

$$\langle \sigma \rangle = \sigma_{\text{min}} . \quad (3.17)$$

In this sense the mean-field approximation, commonly used in the context of solid-state physics, becomes exact in the limit of infinite flavor number. For convenience, we introduce the effective potential

$$V_{\text{eff}} = \frac{S_{\text{eff}}}{V} , \quad (3.18)$$

which is an intensive quantity in contrast to S_{eff} , but shares the same σ_{min} .

Due to the identity (2.42), relating $\langle \sigma \rangle$ to the chiral condensate, i.e., the order parameter for chiral symmetry breaking, we can determine the phase structure of the GN

model by minimizing V_{eff} in (T, μ, B) space, which amounts to solving the gap equation

$$\left. \frac{\partial}{\partial \sigma} V_{\text{eff}}(\sigma) \right|_{\sigma=\sigma_{\text{min}}} = 0. \quad (3.19)$$

The main computational difficulty is the calculation of the fermion determinant $\det(D)$, which is divergent and needs to be regularized. One way to compute it is the zeta-function regularization and renormalization technique [130] summarized in Appendix C.

Using this method, we compute V_{eff} in Appendix D. For $eB > 0$, we find the result (D.82):

$$\begin{aligned} V_{\text{eff}}^{(B)} = & -\frac{\sigma_0}{2\pi}\sigma^2 + \frac{eB}{2\pi}|\sigma| - \frac{(2eB)^{3/2}}{2\pi}\zeta_H\left(-\frac{1}{2}, \frac{\sigma^2}{2eB}\right) \\ & - \frac{eB}{2\pi\beta} \sum_{l=0}^{\infty} (2 - \delta_{l0}) \left[\ln\left(1 + e^{-\beta(\sqrt{\sigma^2+2eBl}+\mu)}\right) + \ln\left(1 + e^{-\beta(\sqrt{\sigma^2+2eBl}-\mu)}\right) \right], \end{aligned} \quad (3.20)$$

where ζ_H is the Hurwitz zeta function (D.79) and l was introduced in (3.1). Moreover, $\sigma_0 > 0$ denotes the minimum position of the effective potential for vanishing T , μ , and B given in (D.50). For the solution $\sigma_0 > 0$ to exist, we work in the strong-coupling regime, where g^2 is larger than some critical value g_c^2 (see Appendix D), throughout.

Notice that (3.20) is equally valid on finite and infinite volumes. The volume-dependence only enters via the discretization of eB on a torus (3.4), restricting the allowed values that the magnetic field can assume. If one is interested in taking the limit $B \rightarrow 0$ on a finite volume, a separate calculation is required, as was to be expected based on the discussion in Section 3.1, and we discuss finite-volume effects in Section 3.6. In the infinite-volume limit, the effective potential for $B = 0$ is given by (D.72):

$$\begin{aligned} \lim_{L \rightarrow \infty} V_{\text{eff}}^{(0)} = & -\frac{\sigma^2}{2\pi}\sigma_0 + \frac{|\sigma|^3}{3\pi} + \frac{|\sigma|}{\pi\beta^2} \left[\text{Li}_2\left(-e^{-\beta(|\sigma|+\mu)}\right) + \text{Li}_2\left(-e^{-\beta(|\sigma|-\mu)}\right) \right] \\ & + \frac{1}{\pi\beta^3} \left[\text{Li}_3\left(-e^{-\beta(|\sigma|+\mu)}\right) + \text{Li}_3\left(-e^{-\beta(|\sigma|-\mu)}\right) \right], \end{aligned} \quad (3.21)$$

where $\text{Li}_\nu(z)$ denotes the polylogarithm of order ν (D.71).

3.3 Chiral condensate

With the mean-field effective potential (3.18) discussed in the previous section, we may now study the combined influence of the external control parameters B , T , and μ on chiral symmetry and its spontaneous breakdown as well as – in later sections – on thermodynamic observables. The latter is possible due to the fact that in the large- N_f

3. The Mean-Field Gross-Neveu Model

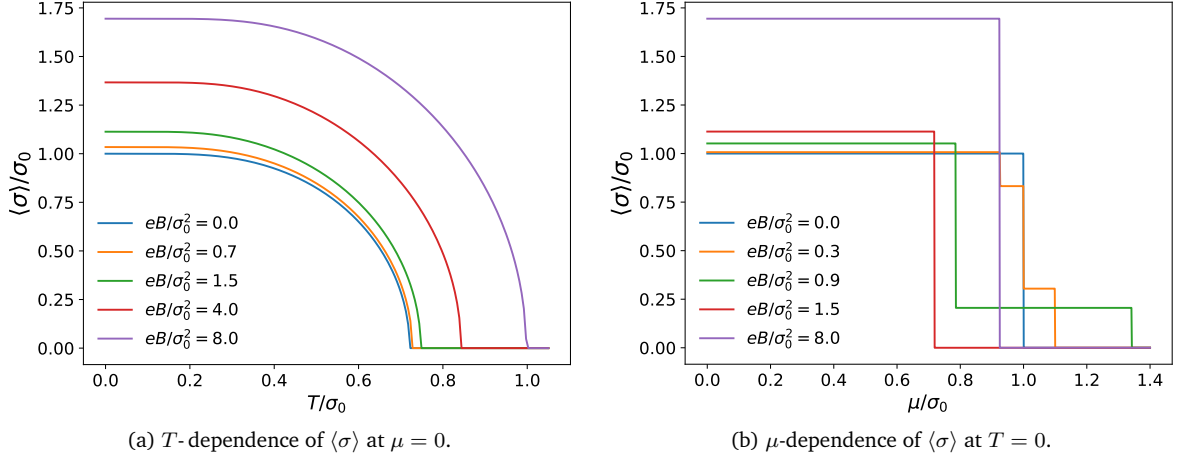


Figure 3.2: Order parameter $\langle\sigma\rangle$ for different magnetic field strengths.

limit the minimum of V_{eff} is related to the relevant thermodynamic potential Φ via

$$V_{\text{eff}}(\sigma_{\min}) = -\frac{1}{V} \ln Z = \frac{\Phi}{L^2}. \quad (3.22)$$

The first – and for our purposes the most important – quantity we compute is the minimum position σ_{\min} of V_{eff} , i.e., the expectation value of σ , as an order parameter for chiral symmetry breaking. Let us first study the dependence of $\langle\sigma\rangle$ on the temperature for $\mu = 0$ and how this dependence changes when switching on a magnetic field B . The corresponding result, obtained via numerically solving the gap equation (3.19), is shown in Fig. 3.2a. At $T = 0$, $\mu = 0$ and $B = 0$ chiral symmetry is spontaneously broken in the strong-coupling regime we consider here. As the temperature increases, the condensate decreases until it vanishes at $T = T_c = \frac{\sigma_0}{2 \ln 2}$, indicating a phase transition to a phase with intact chiral symmetry, $\langle\sigma\rangle = 0$. This phase transition is of second order. The magnetic field then leads to an increase of the order parameter for all $T < T_c$, therefore enhancing the breakdown of chiral symmetry, while at the same time increasing T_c itself. This is the so-called *magnetic catalysis* scenario [131–134], the physical origins of which we shall discuss in more detail in Section 6.1

Next, we consider the finite-density region of the GN phase diagram at $\mu \neq 0$ and vanishing temperature, which is interesting from the point of view of QCD, where it is inaccessible via conventional methods. In Fig. 3.2b, we show the μ -dependence of $\langle\sigma\rangle$ for various magnetic field strengths. For $B = 0$, one observes a sharp phase transition from $\langle\sigma\rangle = \sigma_0$ to $\langle\sigma\rangle = 0$ at a critical chemical potential $\mu_c = \sigma_0$. In fact, the behavior of σ resembles what one would expect from a first-order phase transition. However, since the effective potential is completely flat at the point $(T = 0, \mu = \sigma_0)$ for $|\sigma| \leq \sigma_0$, one finds at the same time phenomena associated with second-order transitions and should thus be careful with the terminology. Hence, we rather refer to the transition as a degenerate one.

What appears unusual is the behavior of the μ -dependence of $\langle\sigma\rangle$ once B is switched

3. The Mean-Field Gross-Neveu Model

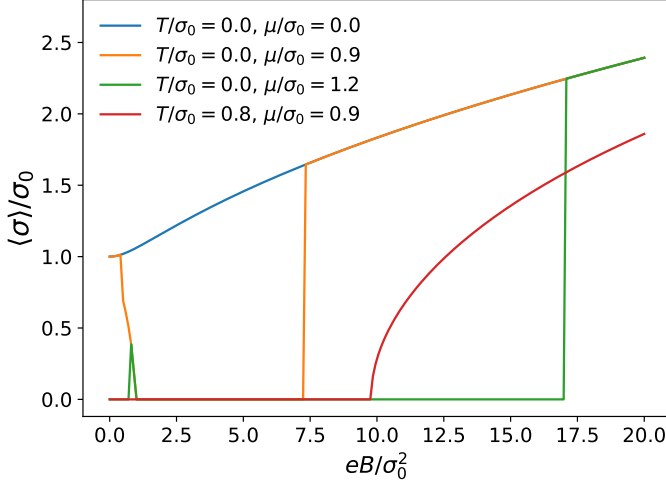


Figure 3.3: B -dependence of $\langle \sigma \rangle$ for various T and μ .

on, as for weak magnetic fields one observes a pattern of multiple discontinuous jumps of $\langle \sigma \rangle$ as μ is increased. A closer inspection of the effective potential reveals that these transitions are actually of first order. The physical reason for this discontinuous behavior is the Landau level structure, since a transition may occur whenever the Fermi level, given by the chemical potential, crosses a Landau level and similar results have been found in related model theories as well [135–144]. This highlights the fact that for weak magnetic fields higher Landau levels play an important role in the correct description of the phase structure. In particular, it means that the LLL approximation (corresponding to the omission of all $l > 0$ in (3.20)) is – in general – not reliable in this region.

The effect the magnetic field has on the order parameter (and hence on chiral symmetry) thus depends heavily on both temperature and chemical potential, as is visualized in Fig. 3.3, where we show $\langle \sigma \rangle$ as a function of B for different combinations of T and μ . While at $\mu = 0$ magnetic catalysis takes place for arbitrary magnetic field strengths and the critical temperature T_c grows monotonically as a function of B , the situation is very different at finite density. Both $\langle \sigma \rangle$ and μ_c (with μ_c we refer to the critical chemical potential of the *chiral* phase transition, i.e., the transition from some $\langle \sigma \rangle \neq 0$ to $\langle \sigma \rangle = 0$) are non-monotonic in B for weak enough magnetic fields. What is particularly curious is that within a certain parameter region $\langle \sigma \rangle$ may decrease as a function of B , as this is in contrast to the magnetic catalysis scenario found at $\mu = 0$. However, this *inverse magnetic catalysis* phenomenon [145] can be understood as follows (see [146] for an analogous argument in the context of the (3 + 1)–dimensional NJL model):

For the discussion we consider $T = 0$, where inverse magnetic catalysis is most prominent. In this limit, (3.20) takes the form

$$\begin{aligned} \lim_{T \rightarrow 0} V_{\text{eff}}^{(B)} = & -\frac{\sigma_0}{2\pi} \sigma^2 + \frac{eB}{2\pi} |\sigma| - \frac{(2eB)^{2/3}}{2\pi} \zeta_H \left(-\frac{1}{2}, \frac{\sigma^2}{2eB} \right) \\ & - \frac{eB}{2\pi} \sum_{l=0}^{l_{\text{max}}} (2 - \delta_{l0}) \left(\mu - \sqrt{\sigma^2 + 2eBl} \right), \end{aligned} \quad (3.23)$$

where the sum runs until $l_{\max} = \left\lfloor \frac{\mu^2 - \sigma^2}{2eB} \right\rfloor$ and thus only contributes when $\mu > |\sigma|$. We compute the difference in the thermodynamic potential between the symmetric phase, where $\langle \sigma \rangle = 0$, and the broken phase, where $\langle \sigma \rangle = M \neq 0$, M denoting a non-trivial solution of the gap equation (3.19). Furthermore, we assume $M > 0$ without loss of generality and focus on weak magnetic fields, $eB \ll M^2$.

Working at finite chemical potential in equilibrium, the appropriate thermodynamic potential Φ in (3.22) is the grand potential, which we shall denote as Ω . In the symmetric phase, we find

$$\frac{\Omega}{L^2} \Big|_{\langle \sigma \rangle = 0} = \frac{(2eB)^{3/2}}{2\pi} c - \frac{eB}{2\pi} \mu, \quad (3.24)$$

where $c = |\zeta(-\frac{1}{2})| \approx 0.21$, ζ denoting the Riemann zeta function. We have ignored the contribution from the higher Landau levels $l > 0$, which might appear counter-intuitive at first glance, since we are concerned with the low- B regime. However, we shall see that inverse magnetic catalysis is, in fact, an LLL effect, such that this approximation is justified and sufficient to capture the relevant physics [145]. We remark that the higher Landau levels give a negative contribution to Ω . In the broken phase, the solution of the gap equation for small eB is given by [132]

$$M \approx \sigma_0 \left(1 + \frac{(eB)^2}{12\sigma_0^4} \right) \quad (3.25)$$

plus terms of higher order in $\frac{eB}{\sigma_0^2}$ for all $\mu < M$. To this order the grand potential density in the broken phase thus reads

$$\frac{\Omega}{L^2} \Big|_{\langle \sigma \rangle = M} \approx -\frac{\sigma_0^3}{6\pi} + \frac{(eB)^2}{12\pi\sigma_0}. \quad (3.26)$$

Which phase is energetically favored can be determined by investigating the difference between the thermodynamic potentials of the two respective phases,

$$\Delta\Omega = \Omega|_{\langle \sigma \rangle = M} - \Omega|_{\langle \sigma \rangle = 0}. \quad (3.27)$$

A negative value of $\Delta\Omega$ indicates that the broken phase is energetically favored while for $\Delta\Omega > 0$ chiral symmetry is restored. We find

$$\frac{2\pi}{L^2} \Delta\Omega = -\frac{\sigma_0^3}{3} - (eB)^{3/2} \left(2^{3/2} c - \frac{\sqrt{eB}}{6\sigma_0} \right) + eB\mu. \quad (3.28)$$

The first term on the right-hand side represents the energy gain due to the formation of a condensate. The second term, which is negative for the weak magnetic fields for which our approximation is valid, is the additional energy gain due to the magnetic field favoring the spin misalignment between the particles and anti-particles that make up the

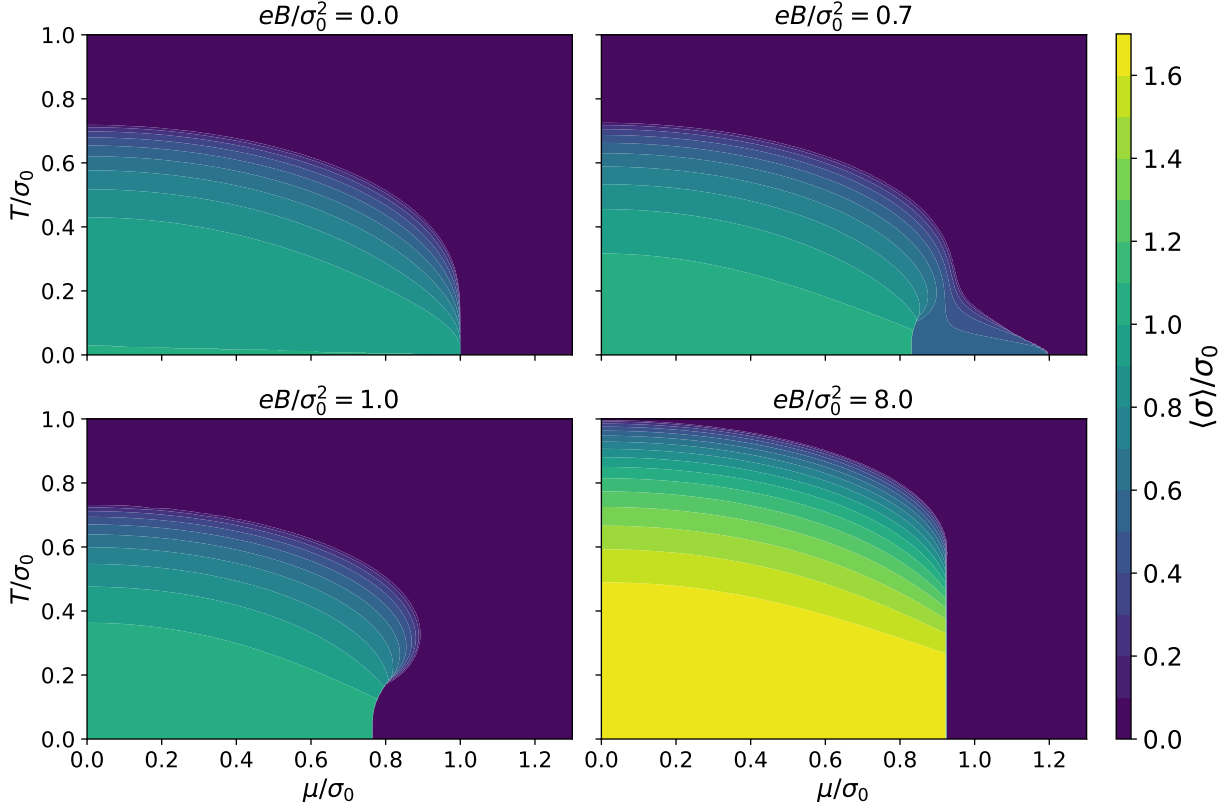


Figure 3.4: Phase diagrams in the (μ, T) plane for various magnetic field strengths.

condensate. This term is responsible for magnetic catalysis. The last term, on the other hand, is the energy cost of forming a condensate at finite μ , i.e., when the Fermi surfaces of particles and anti-particles are mismatched. This mismatch is enhanced even further by the magnetic field. One may convince oneself that there exists a region in (B, μ) space where this last term dominates, leading to a sign change of $\Delta\Omega$, such that the symmetric phase becomes favored over the broken one as the magnetic field strength increases. Thus, we have not only found a physical explanation for inverse magnetic catalysis, but also that the latter is already present in the LLL approximation. The contributions of higher Landau levels would then favor the symmetric phase even more.

3.4 Phase diagrams

Having minimized the effective potential (3.18) in (T, μ, B) space we are now in a position to map out phase diagrams in planes given by various cuts of this three-dimensional parameter space. To begin with, we show in Fig. 3.4 phase diagrams in the (μ, T) plane for increasing magnetic field strengths. One observes how the phase structure is deformed by the combined effects of magnetic catalysis and inverse magnetic catalysis that are at play for finite μ and B . In particular, one can see the multiple phase transition pattern at $eB/\sigma_0^2 = 0.7$ and that it disappears at $eB/\sigma_0^2 = 1$. For the latter, one finds the curious situation where, starting in the symmetric phase, increasing the temperature

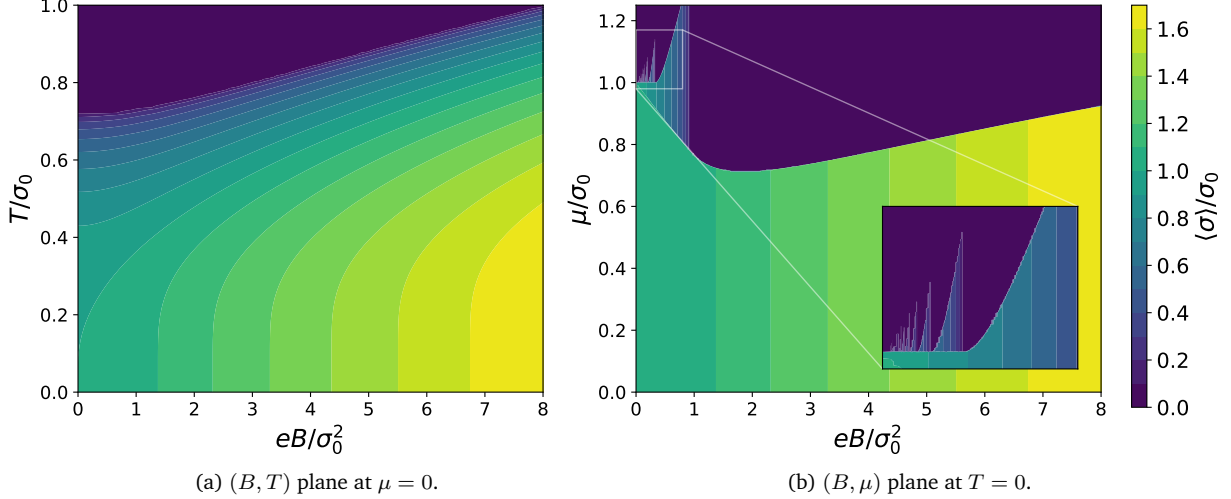


Figure 3.5: Phase diagrams in the (B, T) and (B, μ) planes at $\mu = 0$ and $T = 0$, respectively. The inset shows a close-up view of the intermediate phases – see the main text for details.

can actually break chiral symmetry. This phenomenon, however, also disappears for asymptotically large magnetic fields.

In Figs. 3.5a and 3.5b, we show the phase structure along the coordinate axes $\mu = 0$ and $T = 0$, respectively. It is apparent that the phase transition pattern is much simpler in the first case, where $\langle \sigma \rangle$ and T_c both increase monotonically with B . For $T = 0$, on the other hand, one observes the presence of intermediate phases, where the chiral condensate is smaller in value than for vanishing μ , but still non-zero. Despite these phases growing in size with increasing B , they disappear entirely at $eB = \sigma_0^2$, where the physics is governed by the LLL. We also mention that the multiple phase transitions present in (B, μ) space become washed out when increasing the temperature but can still be observed for low enough $T \neq 0$. In Chapter 6, we investigate whether this complicated structure is merely an artifact of the large- N_f limit or can be observed for finite flavors number as well.

3.5 Thermodynamic observables

The interpretation of the GN effective potential (3.18) as a thermodynamic potential via (3.22) allows for the study of various thermodynamic observables, such as the particle number and magnetization, but also various others not considered here. In the context of the grand-canonical ensemble in statistical mechanics, the average particle number is defined as

$$\langle N \rangle = -\frac{\partial}{\partial \mu} \Omega, \quad (3.29)$$

where Ω once more denotes the grand potential. To compute the particle density $\frac{\langle N \rangle}{L^2}$, we thus have take the μ -derivative of V_{eff} and evaluate the result at $\sigma = \sigma_{\text{min}}$. The result is shown as a function of μ for zero temperature and various magnetic field strengths

3. The Mean-Field Gross-Neveu Model

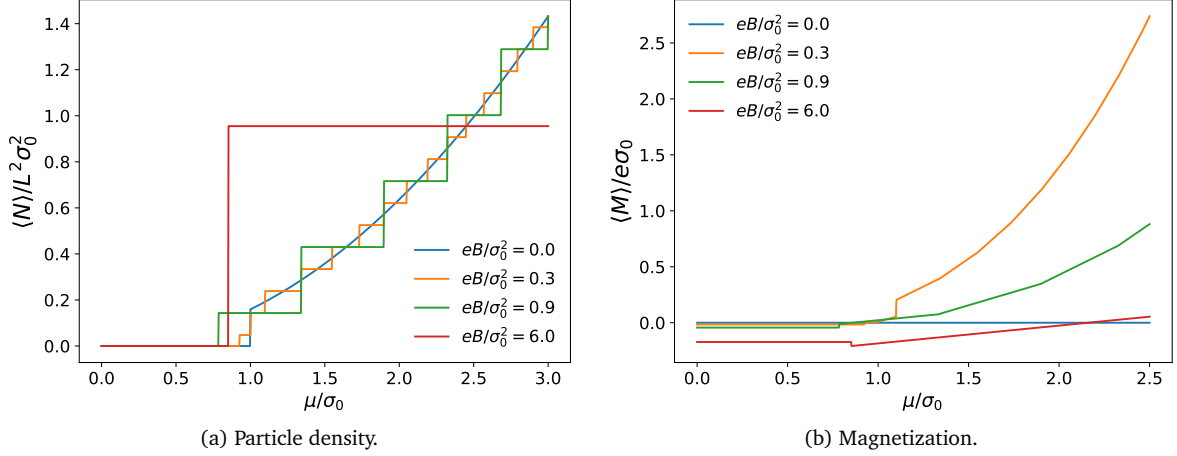


Figure 3.6: Thermodynamic observables as functions of μ for $T = 0$ and different B .

in Fig. 3.6a. While for $B = 0$ the density vanishes up to the critical chemical potential $\mu_c = \sigma_0$, a behavior commonly referred to as the Silver Blaze phenomenon [147], and has a smooth μ -dependence beyond, it shows step-like behavior once the magnetic field is switched on. This can once more be explained by the successive filling of Landau levels, whose degeneracy (and thus, by extension, the step size) increases with B .

Similarly, the average magnetization can be defined as

$$\langle M \rangle = -\frac{1}{L^2} \frac{\partial}{\partial B} \Omega, \quad (3.30)$$

with an equally straightforward computation. We show its μ -dependence at vanishing T in Fig. 3.6b. For small chemical potential the magnetic field has the expected effect of increasing the magnetization (in magnitude), but this picture changes for larger μ , as the B -dependence of $\langle M \rangle$ becomes non-monotonic and even exhibits oscillatory behavior. These oscillations with the magnetic field are tightly related to the well-known de Haas – van Alphen oscillations of the magnetic susceptibility of diamagnetic metals [148], as well as the Shubnikov – de Haas oscillations observed in the electric conductivity of certain materials [149]. For more details about magnetic oscillations in 4FTs, see, e.g., [150]. We find it remarkable to which extent footprints of the discrete Landau levels can be found even in an interacting theory.

3.6 Finite volume

After the discussions in Sections 3.3 to 3.5, which implicitly assumed the spatial extent of space-time to be infinite, $L = \infty$, we shall now briefly investigate the mean-field GN model in a finite $(2 + 1)$ -dimensional box. As was discussed in Section 3.2, for non-vanishing magnetic field the effective potential has an identical form irrespective of the volume and one only has to take into account the quantization condition (3.4) for finite L . For $B = 0$, on the other hand, this is no longer true, as one has to replace the

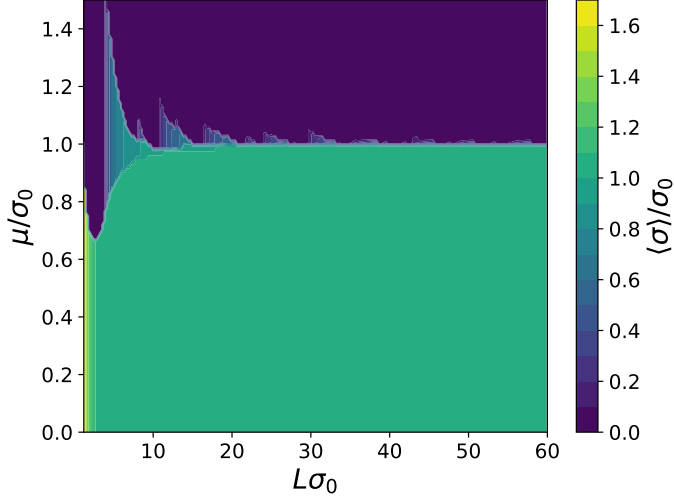


Figure 3.7: Phase diagram in the (L, μ) plane at $T = 0$ and $B = 0$. The reason that some lines appear wiggly is the poor resolution. Notice that σ_0 was computed in the limit $L \rightarrow \infty$.

integrals over spatial momenta \mathbf{p} in the derivation of V_{eff} by discrete sums, resulting in the finite-volume effective action (D.66),

$$V_{\text{eff}}^{(V)} = -\frac{\sigma^2}{2\pi}\sigma_0 + \frac{|\sigma|^3}{3\pi} + \frac{|\sigma|}{L^2\pi} \sum'_{\mathbf{k} \in \mathbb{Z}^2} e^{-L|\sigma||\mathbf{k}|} \frac{1}{\mathbf{k}^2} \left(1 + \frac{1}{L|\sigma||\mathbf{k}|} \right) - \frac{2}{V} \sum_{\mathbf{p}} \left[\ln \left(1 + e^{-\beta(\sqrt{\sigma^2 + \mathbf{p}^2} + \mu)} \right) + \ln \left(1 + e^{-\beta(\sqrt{\sigma^2 + \mathbf{p}^2} - \mu)} \right) \right], \quad (3.31)$$

where the prime in the sum over \mathbf{k} indicates the omission of the term for $k_1 = k_2 = 0$. Here and in the remainder of this section, σ_0 denotes the minimum position of the effective potential at $T = 0$, $\mu = 0$ and $B = 0$ in the infinite-volume limit, (D.50), and not its finite- L counterpart. The first sum in $V_{\text{eff}}^{(V)}$ is a finite-size correction, vanishing as $L \rightarrow \infty$, while the second sum is the analog of the last term in (3.20) for $B = 0$. The striking similarity between these two sums for $B = 0$ and $B \neq 0$ can be best appreciated when inserting the quantization laws for the magnetic field and the spatial momenta, (3.4) and (2.1), respectively.

In particular, it should be noted that the discretized momenta play a role similar to that of the Landau levels in that both give rise to a fully discrete energy spectrum, see (3.1) and (3.2). One can thus conjecture that similar physical effects will be at play in a theory at $B = 0$ on a finite volume as in a theory in a weak magnetic field. That this is indeed the case can be seen in Fig. 3.7, where we show the phase diagram in (L, μ) space at zero temperature and magnetic field, obtained via numerical minimization of (3.31). We observe that, similar to the $B \neq 0$ case, there are multiple phase transitions between the phase of spontaneously broken chiral symmetry at $\mu = 0$ and the symmetric phase at large μ . Depending on the spatial extent the emerging intermediate phases differ in size, generically shrinking on larger volumes. Notice the resemblance between Fig. 3.7 and Fig. 3.5b. We emphasize that the phase transitions observed in (L, μ) space at $T = 0$ can be of genuine first order, in contrast to the degenerate phase transition present in the infinite-volume limit.

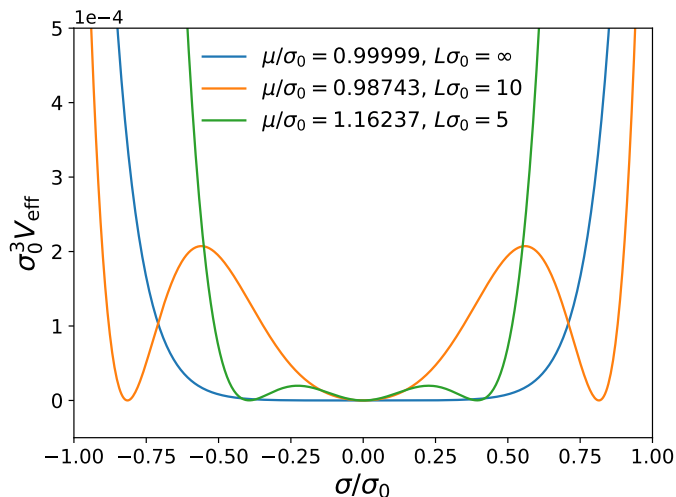


Figure 3.8: Effective potential $V_{\text{eff}}^{(V)}$ from (3.31) at $T/\sigma_0 = 0.1$ for two finite volumes and the $L \rightarrow \infty$ limit. Notice that σ_0 was computed in the limit $L \rightarrow \infty$.

Interestingly, this can even happen at finite temperature. To see this, we show in Fig. 3.8 the effective potential (3.31) at the critical chemical potential of the chiral phase transition, $\mu = \mu_c$, for $T/\sigma_0 = 0.1$ and three different spatial extents. We clearly observe the presence of three different minima for the finite volumes, whereas the potential is almost flat in the infinite-volume limit. Thus, while the phase transition for $L \rightarrow \infty$ is of second order at finite temperature, on a finite volume one finds first-order transitions as well. Notice that the notion of proper phase transitions on finite volumes only makes sense due to large- N_f limit, since N_f plays a role similar to that of the volume in the path integral. It shall be interesting in later chapters to study to which extent – if at all – this observation holds beyond the mean-field limit. We mention that finite-size effects in 4FTs have also been investigated in [151].

4 Lattice Field Theory

In this chapter we briefly introduce the concept of lattice quantum field theory as a whole to lay the foundation for the two extensive lattice studies presented in Chapters 5 and 6, respectively. We put a particular emphasis on the problem of finding a suitable lattice discretization for chiral fermions and discuss two solutions, the [SLAC](#) derivative and the overlap operator, in more detail. Besides outlining how they are employed in Chapters 5 and 6, we also compare how they perform in comparison with other discretizations.

4.1 Basic concepts

The powerful method of lattice quantum field theory allows – in principle – for a direct computation of the path integrals defining the observables of a quantum field theory. A generic path integral of a theory describing a quantum field Φ is given by an integral over all classical field configurations of Φ , which can formally be understood as the product of integrals over $\Phi(x)$ at every space-time point x ,

$$\int \mathcal{D}\Phi = \prod_x \int d\Phi(x) . \quad (4.1)$$

This product over continuous space-time, however, is not mathematically well defined as it stands. In order to arrive at a well-defined expression, one typically discretizes (Euclidean) space-time to a lattice with finite lattice spacing a . Then, the path integral (4.1) reduces to the product of integrals on a countable number of lattice points and the original expression is recovered by taking the continuum limit $a \rightarrow 0$.

In this thesis, however, we shall use lattice field theory rather as a computational tool. The central idea is to approximate the expectation value of an observable $\mathcal{O}[\Phi]$,

$$\langle \mathcal{O} \rangle = \frac{1}{Z} \int \mathcal{D}\Phi \mathcal{O}[\Phi] e^{-S} , \quad Z = \int \mathcal{D}\Phi e^{-S} , \quad (4.2)$$

via a Monte-Carlo simulation, i.e., the generation of randomly distributed lattice configurations of Φ . Since these configurations contribute to the path integral according to the Boltzmann weight e^{-S} , only configurations with low actions will give significant contributions. One thus commonly employs the technique of importance sampling, where the configurations are drawn from a probability distribution given by $\frac{e^{-S}}{Z}$ instead of, e.g., a uniform distribution. For an ensemble $\{\Phi\}$ comprising N configurations generated

in this way, an estimator for the expectation value of \mathcal{O} is then simply given by the ensemble average,

$$\langle \mathcal{O} \rangle \approx \frac{1}{N} \sum_{\Phi \in \{\Phi\}} \mathcal{O}[\Phi]. \quad (4.3)$$

A necessary requirement for this procedure to work is that the Boltzmann factor e^{-S} can be properly interpreted as a probabilistic weight, meaning that it has to be real and non-negative. If the Euclidean action S has a non-vanishing imaginary part, however, this is no longer true. In this case one is confronted with a so-called complex-action or sign problem, which renders conventional simulation algorithms based on importance sampling inapplicable, see, e.g., [39]. A prominent example of a theory with a sign problem is QCD at finite density, i.e., non-vanishing chemical potential [43].

The theories that are of predominant interest to us throughout this thesis are 4FTs. For this particular class of theories the dynamical degrees of freedom that one generates configurations of in lattice simulations are the auxiliary scalar fields that arise in the bosonized theories after performing Hubbard-Stratonovich transformations and integrating out the fermions, see (2.39). As one might expect, the bottleneck of a lattice simulation of a 4FT is the computation of the fermionic determinant in the lattice equivalent of (2.40). For this purpose, we use a standard rational hybrid Monte-Carlo (rHMC) algorithm [152] in all simulations discussed in this thesis. For details on the precise implementation we refer to [153].

Let us now introduce some notation and conventions that we shall use throughout, thereby staying as close as possible to the continuum notation established in previous sections. We denote by N_t the number of lattice points in the temporal direction, in which we again impose anti-periodic boundary conditions for fermions and periodic ones for the scalar fields. The inverse temperature is then given by the temporal lattice extent in physical units, $\beta = aN_t$. Similarly, N_s denotes the number of sites in each spatial direction, which we assume to have equal extents $L = aN_s$. All fields considered obey periodic boundary conditions in the spatial directions. We denote the lattice itself by Λ and its volume is given by $V = \beta L^{d-1}$. The lattice spacing a is always assumed isotropic, i.e., equal in each direction. In our simulations of the GN and χ GN models we control a by varying the four-Fermi couplings g^2 in (2.33) and (2.35), respectively. Lastly, unless stated otherwise, the lattice points in each direction shall be counted starting from zero, i.e., $x_0 \in \{0, a, \dots, \beta - a\}$ and $x_i \in \{0, a, \dots, L - a\}$.

4.2 Lattice discretization of fermions

In this section we discuss different ways of discretizing fermions on a lattice, putting a particular emphasis on the preservation of chiral symmetry in the discretized theory.

4.2.1 The problem of chiral lattice fermions

The lattice discretization of fermions, represented by the Dirac operator D in (2.40), is a non-trivial issue, as there is no single discretization of D that one may reliably use for every possible application. In practice, one chooses a lattice Dirac operator based on how suitable it is for addressing a particular problem while at the same time being computationally affordable. In our case, we are predominantly interested in studying chiral symmetry and so we would like to employ a lattice Dirac operator that preserves chiral symmetry in the best possible way. In the following we shall briefly discuss a few fermion discretizations that are commonly used in the literature and outline some of their advantages and disadvantages.

The most intuitive discretization giving rise to an anti-symmetric covariant derivative operator is the – appropriately named – naive discretization. The resulting naive Dirac operator is defined as

$$\mathbb{D}_{\text{naive}} := \frac{1}{2} \gamma_{\mu} (\nabla_{\mu}^* + \nabla_{\mu}) , \quad (4.4)$$

where the action of the forward and backward covariant difference operators ∇_{μ} and ∇_{μ}^* on some function $\psi(x)$ with support on the lattice is given by

$$\begin{aligned} \nabla_{\mu} \psi(x) &= \frac{1}{a} [U_{\mu}(x) \psi(x + a\hat{\mu}) - \psi(x)] , \\ \nabla_{\mu}^* \psi(x) &= \frac{1}{a} [\psi(x) - U_{\mu}^{\dagger}(x - a\hat{\mu}) \psi(x - a\hat{\mu})] . \end{aligned} \quad (4.5)$$

In these definitions $\hat{\mu}$ denotes the unit vector in the direction of x_{μ} and we have furthermore introduced the gauge link variables

$$U_{\mu}(x) = e^{ieaA_{\mu}(x)} , \quad (4.6)$$

with e and A_{μ} defined as in Section 3.2, albeit the generalization to non-Abelian gauge fields is straightforward. The use of group-valued gauge degrees of freedom ensures the gauge invariance of the fermionic action [154, 155]. Note the – perhaps counter-intuitive but nonetheless common – definition of $U_{\mu}(x)$ as the parallel transporter from the point $x + a\hat{\mu}$ to the point x instead of the other way around.

The naive discretization (4.4) gives rise to chiral lattice fermions but comes with a major drawback. Namely, it suffers from the infamous fermion-doubling problem, as it gives rise to $2^d - 1$ unphysical poles of the fermion propagator on the edges of the first Brillouin zone, the so-called fermion doublers. Needless to say, there are countless attempts to get rid of these spurious degrees of freedom to be found in the literature. For instance, the fact that for vanishing gauge field $\frac{1}{2} (\nabla_{\mu}^* + \nabla_{\mu})$ reduces to the usual symmetric difference operator might raise the question as to why one does not simply employ a one-sided difference instead, since this would cure the problem of

doublers [156]. The reason is that a one-sided difference operator violates reflection positivity [156] (see [157] for a definition) and could even lead to the theory losing renormalizability [158]. It is thus usually discarded.

Another idea, dating back to Wilson [159], is to introduce an irrelevant (i.e., vanishing in the limit $a \rightarrow 0$) term proportional to the discretized Laplacian operator into $\mathbb{D}_{\text{naive}}$, which results in the removal of the doublers due to their mass diverging with the inverse lattice spacing. The ensuing Wilson operator reads

$$\mathbb{D}_W := \frac{1}{2} [\gamma_\mu (\nabla_\mu^* + \nabla_\mu) - a \nabla_\mu^* \nabla_\mu] . \quad (4.7)$$

While the naive action arising from (4.4) is invariant under chiral transformations (2.16), the extra term added in (4.7) explicitly breaks chiral symmetry, and thus Wilson fermions cannot be used for our purposes in a straightforward way (i.e., without fine-tuning the bare masses, see, e.g., [160], or [161] for the context of 4FTs).

These observations are, in fact, consequences of a general theorem formulated by Nielsen and Ninomiya [162–164] (see also [165]), stating – in essence – that it is impossible to construct a chiral fermionic lattice derivative that is local (in the sense that it is continuous in momentum space) and free of doublers. This no-go theorem is at the root of most difficulties in choosing appropriate discretizations for chiral fermions. Nonetheless, there are ways to circumvent it, two of which we shall outline in the remainder of this section.

4.2.2 SLAC fermions

The first such method is the so-called **SLAC** derivative [166, 167], the underlying idea of which is to apply the derivative in momentum space. To illustrate this, let us consider a function $\psi(x)$ that is defined on the lattice and obeys fermionic boundary conditions. The Fourier decomposition of $\psi(x)$ reads

$$\psi(x) = \frac{1}{V} \sum_{p \in \tilde{\Lambda}} \tilde{\psi}(p) e^{ipx} , \quad \tilde{\psi}(p) = a^d \sum_{x \in \Lambda} \psi(x) e^{-ipx} , \quad (4.8)$$

where $\tilde{\psi}(p)$ is the Fourier transform of $\psi(x)$ and the elements of the reciprocal lattice $\tilde{\Lambda}$ are the discrete momenta (2.1) with the integers n_μ restricted to $n_0 \in \{-\frac{N_t}{2}, \dots, \frac{N_t}{2} - 1\}$ and $n_i \in \{-\frac{N_s-1}{2}, \dots, \frac{N_s-1}{2}\}$, respectively. Here, we have chosen N_t to be even and N_s to be odd for reasons that will become clear below.

The **SLAC** derivative of $\psi(x)$ with respect to x_μ is now defined in analogy to the continuum as the multiplication with ip_μ :

$$\partial_\mu^{(SLAC)} \psi(x) := \frac{1}{V} \sum_{p \in \tilde{\Lambda}} ip_\mu \tilde{\psi}(p) e^{ipx} = \sum_{x' \in \Lambda} \psi(x') \delta_\mu^{(SLAC)}(x - x') , \quad (4.9)$$

where we have introduced

$$\delta_\mu^{(SLAC)}(x - x') := \frac{1}{N} \sum_{p \in \tilde{\Lambda}} i p_\mu e^{ip(x-x')} \quad (4.10)$$

and $N = \frac{V}{a^d}$ denotes the total number of lattice points. Our earlier choice of even N_t and odd N_s ensures that the **SLAC** derivative is a real and anti-symmetric operator like the continuum derivative. We also note that $\delta_\mu^{(SLAC)}(x - x')$ vanishes if either $x_\mu = x'_\mu$ or $x_\nu \neq x'_\nu$ for any $\nu \neq \mu$. The crucial observation, however, is that the **SLAC** derivative is non-local, as it includes contributions from every lattice point in x_μ -direction. This becomes especially clear after evaluating the sum in (4.10), yielding [168, 169]

$$\delta_\mu^{(SLAC)}(x - x') = \begin{cases} 0 & \text{if } x_\mu = x'_\mu \text{ or } x_\nu \neq x'_\nu \text{ for any } \nu \neq \mu \\ \frac{\pi}{L_\mu} \frac{(-1)^{(x_\mu - x'_\mu)/a}}{\sin(\pi(x_\mu - x'_\mu)/L_\mu)} & \text{else} \end{cases}, \quad (4.11)$$

where $L_0 = \beta$ and $L_i = L$. **SLAC** fermions avoid the Nielsen-Ninomiya theorem due to this non-locality. Indeed, the **SLAC** Dirac operator, defined as

$$\not{D}_{\text{SLAC}} := \gamma_\mu \partial_\mu^{(SLAC)}, \quad (4.12)$$

gives rise to chiral lattice fermions that are free of doublers. A mass (or Yukawa-like) term or a chemical potential can then be added just like in the continuum.

In many ways \not{D}_{SLAC} resembles the continuum Dirac operator as closely as possible, as it, e.g., reproduces the continuum dispersion relation of a free fermion correctly by construction [167], which naive and Wilson fermions are not capable of. The important difference is that the discretized theory gives rise to Brillouin zones, i.e., a momentum cutoff $|p_\mu| < \frac{\pi}{a}$, across which the **SLAC** dispersion relation is discontinuous due to the non-locality. This implies that **SLAC** fermions are bound to be problematic for theories that probe the Brillouin zone edges. Indeed, it has been shown that their use can lead to violations of Lorentz symmetry in gauge theories [170, 171]. However, for theories without local symmetries, such as supersymmetric Yukawa models [172, 173] or **4FTs** [174, 175], **SLAC** fermions have repeatedly proven to be competitive with – if not better than – their alternatives.

4.2.3 Ginsparg-Wilson fermions

Another approach entirely was initiated by Ginsparg and Wilson [176], who departed from the continuum-inspired idea that any valid discretized derivative operator obeying chiral symmetry must necessarily anti-commute with γ_* and instead proposed that a

suitable Dirac operator D_{GW} should be a solution of

$$\{D_{\text{GW}}, \gamma_*\} = aD_{\text{GW}}\gamma_*D_{\text{GW}} , \quad (4.13)$$

using renormalization group transformations for its derivation. The reason why Ginsparg-Wilson fermions can evade the Nielsen-Ninomiya theorem is that they make use of an alternative definition of chiral symmetry, replacing the continuum chiral transformation (2.16) by the non-local expression [177]

$$\psi \rightarrow e^{i\alpha\gamma_*(\mathbb{1} - \frac{a}{2}D_{\text{GW}})}\psi , \quad \bar{\psi} \rightarrow \bar{\psi}e^{i\alpha(\mathbb{1} - \frac{a}{2}D_{\text{GW}})\gamma_*} . \quad (4.14)$$

As in the continuum, this symmetry should be explicitly broken by a mass term. While for naive, Wilson, and SLAC fermions one may simply add a mass term of the form $m\bar{\psi}\psi$ to the lattice action, in the Ginsparg-Wilson formalism massive fermions are less trivial, because such a naive mass term transforms incorrectly under (4.14). Instead, the mass term with the correct transformation behavior contains yet another irrelevant term and reads $m\bar{\psi}(\mathbb{1} - \frac{a}{2}D_{\text{GW}})\psi$ [178]. One may thus define a Dirac operator describing massive Ginsparg-Wilson fermions by

$$D_m = D_{\text{GW}} + m\left(\mathbb{1} - \frac{a}{2}D_{\text{GW}}\right) . \quad (4.15)$$

As a consequence, the definition of the chiral condensate is altered as well in the Ginsparg-Wilson formalism. It reads

$$\langle\bar{\psi}\psi\rangle_{\text{GW}} := -\left\langle\bar{\psi}\left(\mathbb{1} - \frac{a}{2}D_{\text{GW}}\right)\psi\right\rangle , \quad (4.16)$$

where the negative sign is purely conventional. Notice that Eqs. (4.13) to (4.16) each approach their respective continuum counterparts in the limit $a \rightarrow 0$, as they should.

While over the years a number of solutions to (4.13) have been found (see, e.g., [179]), we shall focus here on one in particular, namely the so-called overlap operator devised by Narayanan and Neuberger [180–184]. The overlap Dirac operator in the form we shall use throughout was introduced in [185] and can be written as

$$D_{\text{ov}}^{(0)} := \frac{1}{a}\left[\mathbb{1} + A_{\text{W}}\left(A_{\text{W}}^\dagger A_{\text{W}}\right)^{-1/2}\right] , \quad (4.17)$$

where A_{W} is just the Wilson operator (4.7), but with a negative mass,

$$A_{\text{W}} = a\mathcal{D}_{\text{W}} - \mathbb{1}am_{\text{W}} , \quad am_{\text{W}} \in (0, 2) . \quad (4.18)$$

Unless specified otherwise, we shall always set $am_{\text{W}} = 1$ in the sequel. Notice that the definition (4.17) does not make use of γ_* , which means that there is no obstruction

against employing the overlap operator in odd dimensions [186, 187], where there is no γ_* if one works in an irreducible representation of the Dirac algebra, see Section 2.2.

Overlap fermions are free of doublers, a property that they share with SLAC fermions. However, in contrast to the SLAC derivative the overlap operator is local, falling off exponentially at large distances [188]. It is not ultra-local, though, which means that it connects all possible pairs of lattice sites. In fact, this is a generic property of doubler-free solutions of (4.13) [189], rendering them much more expensive numerically than ultra-local formulations. We see that the modified symmetry transformations (4.14) indeed allow for a lattice discretization of fermions that is chiral, local, and free of doublers.

Next, we discuss how to introduce a chemical potential μ in the overlap formalism. One way to do so is by adapting the usual assignment [190] of factors e^μ ($e^{-\mu}$) to the forward (backward) temporal hopping terms of the Wilson operator (4.7) and then using the resulting \mathbb{D}_W in the definition of the kernel (4.18) entering (4.17) [191]. Despite this overlap operator obeying the Ginsparg-Wilson relation (4.13), however, the ensuing action is not invariant under (4.14) [192]. The same holds true as well when attempting to introduce μ as for SLAC fermions via a – more intuitive – linear coupling to the number density operator in analogy to the continuum [193]. In order to preserve lattice chiral symmetry, we instead employ another prescription that was introduced by Gavai and Sharma [194]. The overlap operator in this setup, including the symmetry-breaking mass term, reads

$$D_{\text{ov}}(\mu) := D_{\text{ov}} + \mu\gamma_0 \left(\mathbb{1} - \frac{a}{2} D_{\text{ov}}^{(0)} \right), \quad (4.19)$$

where

$$D_{\text{ov}} = D_{\text{ov}}^{(0)} + m \left(\mathbb{1} - \frac{a}{2} D_{\text{ov}}^{(0)} \right), \quad (4.20)$$

see (4.15). We note that the quadratic divergence of the fermion number susceptibility that ensues with this choice once the cutoff is removed is not considered to be a problem as it also arises for free fermions in the continuum and may simply be subtracted [195]. We compare the definition (4.20) with the other aforementioned possible implementations of μ within the overlap formalism in Section 4.4.

4.3 Magnetic fields on the lattice

Let us now briefly discuss how to implement an external magnetic field on the lattice. From (3.4) we know that a constant and homogeneous magnetic field perpendicular to a torus is quantized in terms of an integer b and we have to take this fact into account in our simulations. With the application in Chapter 6 in mind we only consider a $(2 + 1)$ –dimensional space-time in this section.

4.3.1 Formulations using link variables

For lattice formulations using compact gauge degrees of freedom, such as naive, Wilson, and overlap fermions the inclusion of a magnetic field appears to be a straightforward task. One might be tempted to simply employ the gauge

$$A_0(x) = 0, \quad A_1(x) = 0, \quad A_2(x) = Bx_1 \quad (4.21)$$

in the definition of the link variables (4.6). After all, in the continuum this definition of A_μ gives rise to a constant and homogeneous magnetic field, perpendicular to the spatial plane and with a magnitude B , as desired. On the lattice, however, this naive procedure would give rise to a vanishing total magnetic flux.

One may overcome this problem by introducing suitable correction terms for A_μ on the lattice boundary [196], i.e., by defining (see also [105] for a discussion)

$$A_0(x) = 0, \quad A_1(x) = -Bx_2 N_s \delta_{x_1, L-a}, \quad A_2(x) = Bx_1. \quad (4.22)$$

The resulting $U(1)$ link variables then take the modified form

$$\begin{aligned} U_0(x) &= 1, \\ U_1(x) &= \begin{cases} e^{2\pi i b x_2 / L} & \text{if } x_1 = L - a \\ 1 & \text{else} \end{cases}, \\ U_2(x) &= e^{2\pi i a b x_1 / L^2}. \end{aligned} \quad (4.23)$$

This prescription indeed leads to a lattice theory which is physically equivalent to one with a non-zero magnetic flux of $\frac{2\pi}{e}b$, as desired. It is furthermore necessary in order to ensure gauge invariance, as otherwise the physical magnetic field at the lattice boundary would have different magnitudes for different gauges.

Notice that the use of compact link variables entails that the lattice formulation and thus all physical observables are periodic in b with a period of N_s^2 . This introduces an effective upper bound for the magnetic field strengths we can simulate on the lattice, $|eB| < \frac{2\pi}{a^2}$. In practice, this bound is reduced even further due to discretization effects [197, 198]. In order to study continuum physics one thus conventionally introduces by hand a suitable upper bound for b .

While **SLAC** fermions are not commonly used in combination with gauge links due to the problems discussed in Section 4.2.2, a straightforward generalization of the **SLAC** derivative (4.9), now including link variables U_μ is given by [170]

$$\nabla_\mu^{(SLAC)} \psi(x) := \sum_{x' \in \Lambda} \psi(x') \delta_\mu^{(SLAC)}(x - x') \prod_{y=x}^{x'} U_\mu(y), \quad (4.24)$$

where the product is to be understood in such a way that

$$\prod_{y=x}^{x'} U_\mu(y) := \begin{cases} \prod_{y_\mu=x_\mu}^{x'_\mu-a} U_\mu(y) & \text{if } \frac{L}{2} \geq x'_\mu - x_\mu > 0 \text{ or } x_\mu - x'_\mu > \frac{L}{2} \\ \prod_{y_\mu=x'_\mu}^{x_\mu-a} U_\mu^\dagger(y) & \text{if } \frac{L}{2} \geq x_\mu - x'_\mu > 0 \text{ or } x'_\mu - x_\mu > \frac{L}{2} \end{cases}, \quad (4.25)$$

while we require that $y_\nu = x_\nu = x'_\nu$ for all $\nu \neq \mu$. In the case where $x_\mu = x'_\mu$ or $x_\nu \neq x'_\nu$, the covariant **SLAC** derivative vanishes due to the properties of $\delta_\mu^{(SLAC)}$, see (4.11). The definition (4.25) ensures that the product of gauge links is taken along the shortest possible path on the lattice, taking into account (anti-)periodic boundary conditions. This choice is by no means unambiguous, however. In fact, in the definition given in [170] the lattice boundary is never crossed, such that the boundary terms introduced in (4.23) would not have any effect. The expression (4.24) is gauge invariant by construction. However, the idea of taking the product of link variables, which amounts to exponentiating the vector potential summed up along a straight line by virtue of (4.6), in the definition of the Dirac operator might appear somewhat unnatural.

4.3.2 Formulations based on minimal coupling

As an alternative, one may consider employing the following continuum-inspired minimal coupling prescription for the covariant **SLAC** derivative:

$$\nabla_\mu^{(SLAC)} = \partial_\mu^{(SLAC)} + ieA_\mu. \quad (4.26)$$

Since this formulation does not make use of compact link variables, there is no periodicity in b . This also entails, however, that the total magnetic flux through the lattice can no longer be kept finite by introducing appropriate boundary terms. Moreover, gauge invariance is lost as well. One could only hope for (4.26) to give reasonable results for very weak magnetic fields such that ieA_μ could be viewed as a perturbation. Since the vector potential is x -dependent, however, it is questionable how justified such an assumption really is. In particular, large values of eA_μ will give rise to momenta close to the Brillouin zone edge, where the **SLAC** derivative is known to be problematic. In order to investigate this issue in more detail, we shall compare the definition (4.26) and variations thereof to the one given in (4.24) in the next section.

4.4 Numerical tests

Having introduced a number of different lattice discretizations for the Dirac operator in Sections 4.2 and 4.3, we shall now study some of their properties in more detail. In particular, we are concerned with their applicability in fermionic theories in two and three space-time dimensions, as these are the situations we shall be confronted with in

Chapters 5 and 6. To this end, we compute in this section the fermion condensate $\langle \bar{\psi}\psi \rangle$ in a simplified setup, namely a theory of massive non-interacting fermions. We compare results for $\langle \bar{\psi}\psi \rangle$ obtained using naive, Wilson, SLAC and overlap fermions, respectively, with corresponding finite-volume continuum results. In particular, we investigate how well the dependence of the condensate on the external control parameters μ and B is reproduced by the various lattice discretizations.

To this end, let us introduce the massive naive, Wilson and SLAC Dirac operators,

$$D_{\text{naive}} = \not{D}_{\text{naive}} + \mathbb{1}m, \quad D_{\text{W}} = \not{D}_{\text{W}} + \mathbb{1}m, \quad D_{\text{SLAC}} = \not{D}_{\text{SLAC}} + \mathbb{1}m, \quad (4.27)$$

with the massless operators defined in (4.4), (4.7) and (4.12), respectively. We compute the lattice condensate as the trace of a suitable lattice propagator,

$$\langle \bar{\psi}\psi \rangle_{\text{latt}} = \frac{1}{V} \frac{1}{n_{\text{dof}}} \text{tr} \left[\tilde{D}^{-1} \right], \quad (4.28)$$

where we have defined

$$\tilde{D} = \begin{cases} D_{\text{naive}} & \text{for naive fermions} \\ D_{\text{W}} & \text{for Wilson fermions} \\ D_{\text{SLAC}} & \text{for SLAC fermions} \\ D_{\text{ov}} \left(\mathbb{1} - \frac{a}{2} D_{\text{ov}}^{(0)} \right)^{-1} & \text{for overlap fermions} \end{cases}. \quad (4.29)$$

The massless and massive overlap operators $D_{\text{ov}}^{(0)}$ and D_{ov} were introduced in (4.17) and (4.20), respectively. Note that the modification of the overlap propagator is necessary to conform with the definition (4.16) of the condensate for Ginsparg-Wilson fermions. Moreover, n_{dof} in (4.28) denotes the total number of fermion degrees of freedom including doublers, i.e., $n_{\text{dof}} = 2^d$ for naive fermions and $n_{\text{dof}} = 1$ otherwise. Notice that simply dividing by n_{dof} gives the correct result here since we work in a free-theory setup, but would not work in a simulation of an interacting theory.

In order to compare the different discretizations among each other as well as with the continuum, we define for the following investigations the difference

$$\Delta \langle \bar{\psi}\psi \rangle(X) := \langle \bar{\psi}\psi \rangle(X) - \langle \bar{\psi}\psi \rangle(0), \quad (4.30)$$

where X stands for either μ or B . Moreover, we also study the relative deviation between $\langle \bar{\psi}\psi \rangle_{\text{latt}}$ and the condensate in the continuum $\langle \bar{\psi}\psi \rangle_{\text{cont}}$ (with the absence of a minus sign in (4.28) appropriately taken into account),

$$\Delta \langle \bar{\psi}\psi \rangle_{\text{rel}}(X) := \left| \frac{\Delta \langle \bar{\psi}\psi \rangle_{\text{latt}}(X) - \Delta \langle \bar{\psi}\psi \rangle_{\text{cont}}(X)}{\Delta \langle \bar{\psi}\psi \rangle_{\text{cont}}(X)} \right|. \quad (4.31)$$

The computation of the continuum condensate proceeds as follows: Since we consider a non-interacting theory, the condensate is defined as (see (B.25))

$$\langle \bar{\psi}\psi \rangle_{cont} = -\frac{1}{V} \frac{\partial}{\partial m} \ln \det D , \quad (4.32)$$

with D denoting the appropriate continuum Dirac operator. We may now compute $\ln \det D$ using the zeta function formalism of Appendix C – in fact, we have already done so for the three-dimensional case in Appendix D. Taking the derivative with respect to m is then straightforward. The calculations in two dimensions proceed along the same lines as in Appendix D and we shall not repeat them here.

4.4.1 Two dimensions

We start by considering a $(1 + 1)$ –dimensional theory for vanishing magnetic field but non-zero chemical potential. On the lattice side, we do not only consider the respective most obvious choices implementation of the chemical potential, but instead compare a number of alternatives for the sake of completeness.

First of all, we employ a linear coupling as in the continuum, i.e., we define

$$D_{\text{latt}}(\mu) = D_{\text{latt}} + \mu\gamma_0 , \quad (4.33)$$

where D_{latt} can be D_{naive} , D_{W} , D_{SLAC} or D_{ov} as defined above. Secondly, we employ the more conventional exponential coupling [190], which is commonly used to avoid certain divergences that appear with the definition (4.33). To this end, we replace

$$U_0(x) \rightarrow e^\mu U_0(x) , \quad U_0^\dagger(x) \rightarrow e^{-\mu} U_0^\dagger(x) \quad (4.34)$$

in the definition of the covariant difference operators (4.5). However, we only consider this prescription for naive and Wilson fermions. For the overlap operator we instead employ the chirally symmetric prescription (4.19) due to Gavai and Sharma (GS), while for SLAC fermions we only use (4.33). The resulting μ -dependent operators are then used within (4.29) to compute the lattice condensate (4.28).

We show the μ -dependence of $\Delta\langle \bar{\psi}\psi \rangle$ and $\Delta\langle \bar{\psi}\psi \rangle_{\text{rel}}$ for the different formulations in Fig. 4.1. One observes that, generically, the agreement between lattice and continuum results becomes worse for larger μ , which is expected due to discretization artifacts. Moreover, we see that the continuum-inspired linear μ -coupling gives rise to substantial deviations from the continuum result for Wilson and overlap fermions, while it works much better for the other discretizations. The overall best agreement is achieved with overlap fermions and the GS prescription. Naive fermions lead to reasonable results, independent of the way the chemical potential is introduced, while Wilson fermions with an exponential coupling as well as SLAC fermions yield acceptable agreement as well.

4. Lattice Field Theory

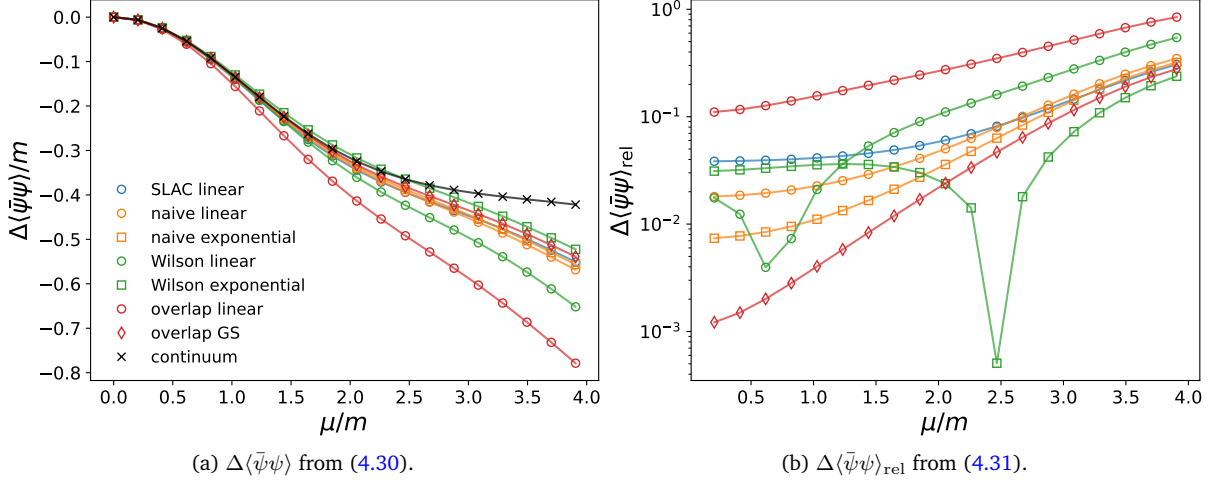


Figure 4.1: μ -dependence of $\langle\bar{\psi}\psi\rangle$ for SLAC (blue), naive (orange), Wilson (green) and overlap (red) fermions, employing linear (circles), exponential (squares) and GS (diamonds) couplings, as well as a comparison with the continuum result (black crosses) in $1 + 1$ dimensions – see the main text for details. $N_s = N_t = 32$ ($N_s = 31$ for SLAC fermions), $am = 0.0512$.

Although we do not show it here, we have also performed continuum extrapolations (amounting to increasing N_s while keeping m fixed) of these results, confirming that the relative deviation decreases with smaller a , albeit at a different rate for each formulation.

Next, we investigate the B -dependence of the chiral condensate. To this end, we stay in two dimensions but impose periodic boundary conditions in both directions and refer to the ensuing space-time as $(2 + 0)$ -dimensional. In particular, we wish to elucidate the complications arising for SLAC fermions in a magnetic field more carefully. For this, we employ both the compact formulation based on link variables (4.24) as well as the minimal-coupling prescription (4.26) for comparison. For both formulations we investigate the effects of the boundary terms in A_μ leading to the definition (4.23). Moreover, since the minimal coupling prescription is not gauge invariant, we consider two different gauges, (4.21) (without A_0), henceforth referred to as the Landau gauge, and the symmetric gauge

$$A_1(x) = -\frac{Bx_2}{2}, \quad A_2(x) = \frac{Bx_1}{2}. \quad (4.35)$$

The goal of this investigation is to see for which of the aforementioned prescriptions – if for any at all – the idea of treating ieA_μ in (4.26) as a perturbation is justified. The introduction of boundary terms ensuring a non-vanishing magnetic flux works similarly for (4.35) as for (4.21) (see (4.22)) and we simply omit A_0 and U_0 in our $(2 + 0)$ -dimensional setup.

Lastly, we consider the option of making the components of A_μ symmetric with respect to the spatial origin by assuming $x_i \in \{-\frac{L-a}{2}, \dots, \frac{L-a}{2}\}$ instead of starting to count the x_i from zero. While this choice makes no difference for gauge-invariant formulations, in the cases where it does one might, in fact, expect it to give better results since the absolute

4. Lattice Field Theory

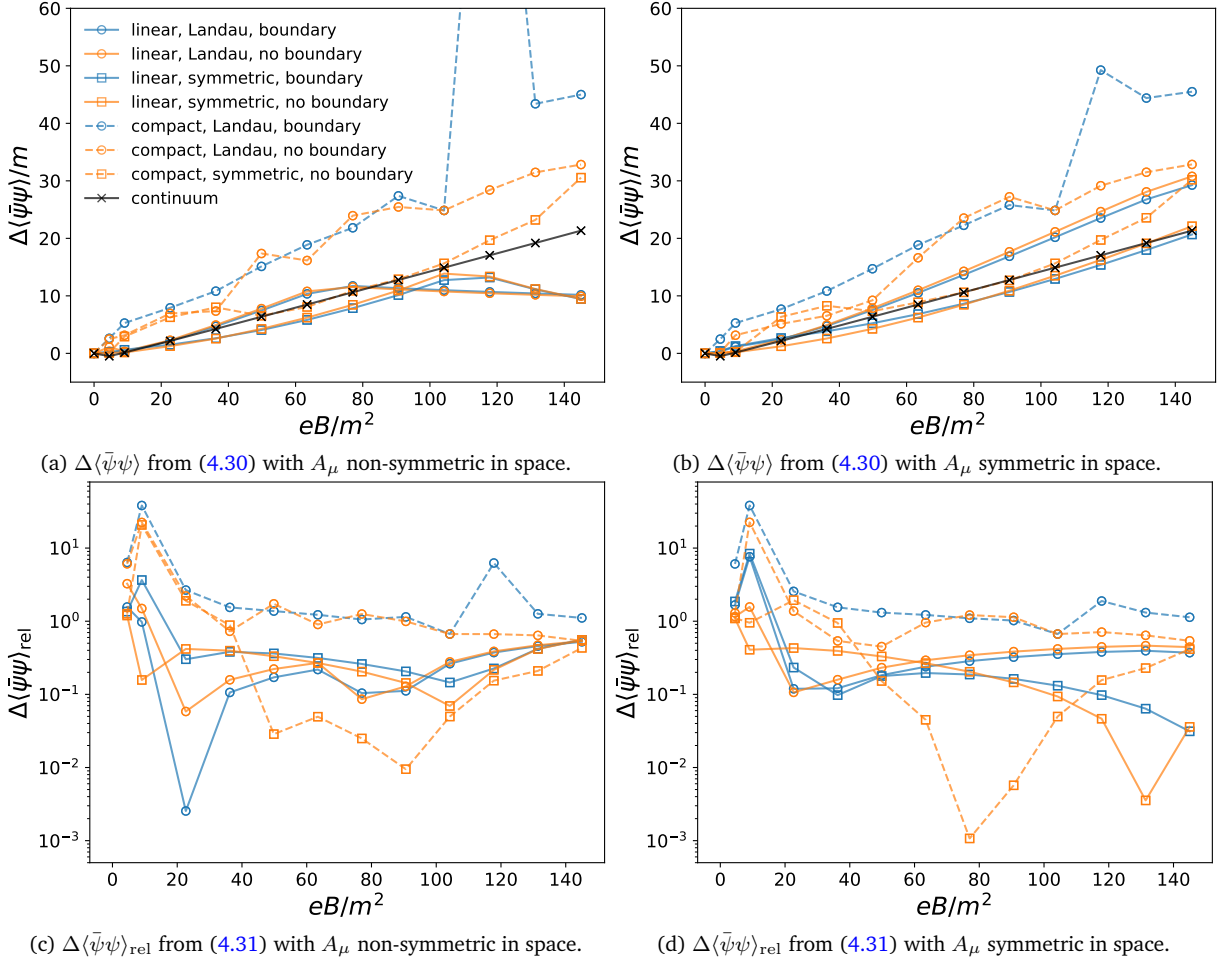


Figure 4.2: B -dependence of $\langle\bar{\psi}\psi\rangle$ for SLAC fermions in 2 + 0 dimensions. The left (right) column shows results for A_μ chosen (non-)symmetric in space. We employ the minimal coupling (4.26) (solid lines) and the compact formulation (4.24) (dashed lines), both in the Landau gauge (4.21) (circles) and the symmetric gauge (4.35) (squares) and we consider the inclusion (blue) and non-inclusion (orange) of boundary terms such as in (4.22). The black crosses indicate the continuum result. See the main text for details. $N_s = 23$, $N_t = 24$, $am = 0.0512$.

values of A_μ are smaller in magnitude. As the reader will notice, the construction has become rather artificial at this point. Moreover, since we do not employ SLAC fermions in simulations with a non-zero magnetic field in this thesis, the investigation at hand is predominantly of academic interest for the time being. However, it would certainly be desirable for future studies to find a working formulation of SLAC fermions in a magnetic field. We show a comparison between the different ways of introducing a magnetic field for SLAC fermions discussed above in Fig. 4.2. Recall that the compact formulation including boundary terms is gauge-invariant.

We observe that – perhaps surprisingly – the link formulations overall seem to give worse agreement than those based on minimal coupling. Also note that no implementation gives particularly convincing results for weak magnetic fields. It is difficult to estimate which formulation performs best overall – after all, the B -dependence of $\Delta\langle\bar{\psi}\psi\rangle_{\text{rel}}$ is very non-monotonic across the board. We are inclined to believe that for

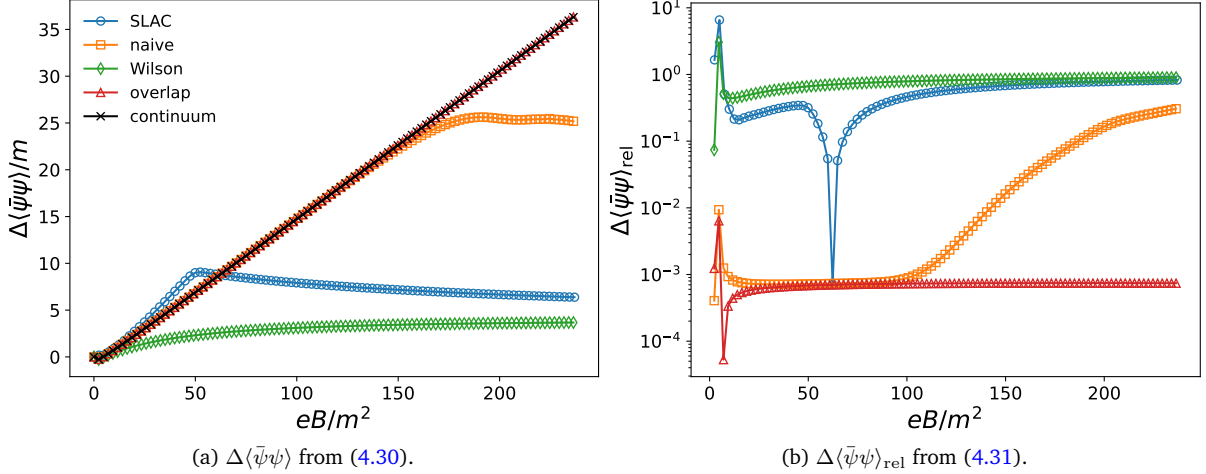


Figure 4.3: B -dependence of $\langle\bar{\psi}\psi\rangle$ for **SLAC** fermions (blue), naive (orange), Wilson (green) and overlap (red) fermions, as well as a comparison with the continuum result (black) in $2 + 0$ dimensions. For **SLAC** fermions we use the minimal coupling (4.26), while for the other discretizations we implement their usual link-based gauge-invariant formulations. In all cases we employ the vector potential given in (4.22) (but without A_0) – see the main text for details. $N_s = N_t = 32$ ($N_s = 31$ for **SLAC** fermions), $am = 0.0512$.

small B the minimal coupling prescription in the Landau gauge, i.e., the definition (4.23), has a slight edge in comparison to the others. However, due to the fact that the relative deviation seems to follow no predictable pattern, one is left wondering if this might not be merely a coincidence. Moreover, for different masses and/or volumes other **SLAC** variants might be favorable instead. For naive, Wilson and overlap fermions there is no ambiguity in the implementation, and a comparison between different possible variations indeed shows that the usual link formulation gives the best results.

Let us now examine how the best-performing **SLAC** implementation fares against the gauge-invariant formulations for naive, Wilson and overlap fermions. A comparison is shown in Fig. 4.3. While Wilson fermions are completely off, **SLAC** fermions actually agree with the continuum results reasonably well for intermediate B , but – as was mentioned before – the deviation does not seem to be systematic. We conclude that **SLAC** fermions are not reliable for their use in the present context with the implementations suggested here. On the other hand, the agreement for both naive and overlap fermions is very good, in particular for the latter. While the overlap result also starts to deviate from the continuum one at some point, this happens only for much stronger magnetic fields than it is the case for naive fermions. In their range of validity the naive and overlap results lie essentially on top of the continuum curve.

4.4.2 Three dimensions

Since in Chapter 6 we shall be concerned with a $(2 + 1)$ –dimensional theory, we check whether the results of the previous sub-section still hold when adding another dimension, in which fermions are assumed to obey anti-periodic boundary conditions. For the sake

4. Lattice Field Theory

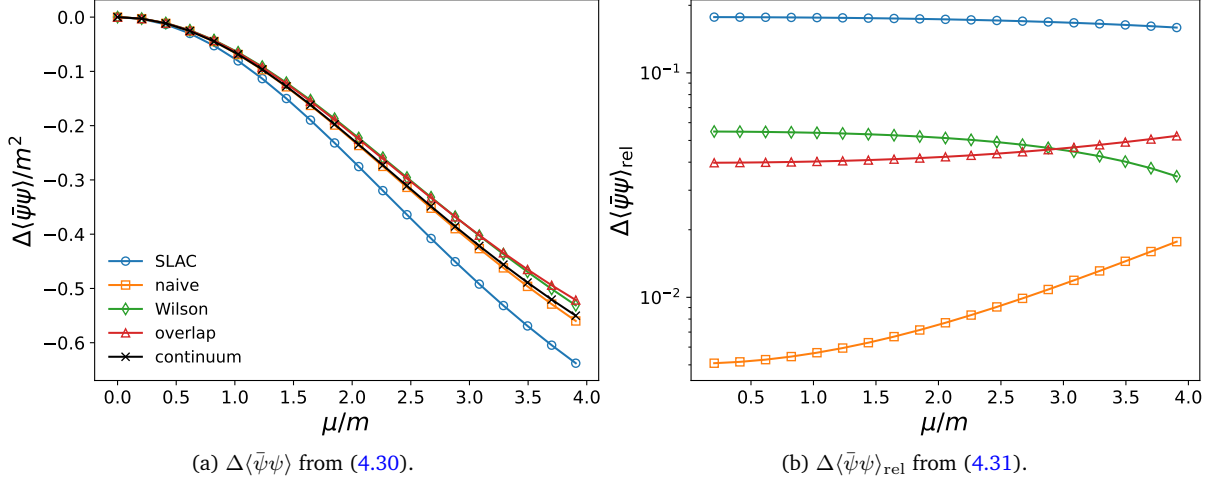


Figure 4.4: μ -dependence of $\langle\bar{\psi}\psi\rangle$ for **SLAC** (blue), naive (orange), Wilson (green) and overlap (red) fermions, as well as a comparison with the continuum result (black) in $2 + 1$ dimensions. We employ a linear coupling of μ for **SLAC** fermions, an exponential coupling for naive and Wilson fermions and the **GS** prescription for overlap fermions – see the main text for details. $N_s = N_t = 12$ ($N_s = 11$ for **SLAC** fermions), $am = 0.0512$.

of simplicity, however, we shall henceforth restrict ourselves only to the implementations that yielded the best results in two dimensions.

In Fig. 4.4 we compare the μ -dependence of the condensate for the different lattice discretizations with the continuum. Similar as in $1 + 1$ dimensions, **SLAC** fermions seem to perform worst, at least for this particular lattice spacing. The respective deviations for Wilson and overlap fermions are comparable with each other, with the relative deviation for the former (as well as for **SLAC** fermions) actually decreasing for large μ , which appears to be counter-intuitive. By far the best agreement is found for naive fermions. As far as the relative deviation can be compared between Figs. 4.1 and 4.4 it is smaller in $1 + 1$ dimensions for all discretizations apart from the naive one. The largest deviation between $1 + 1$ and $2 + 1$ dimensions can be seen for **SLAC** and overlap fermions.

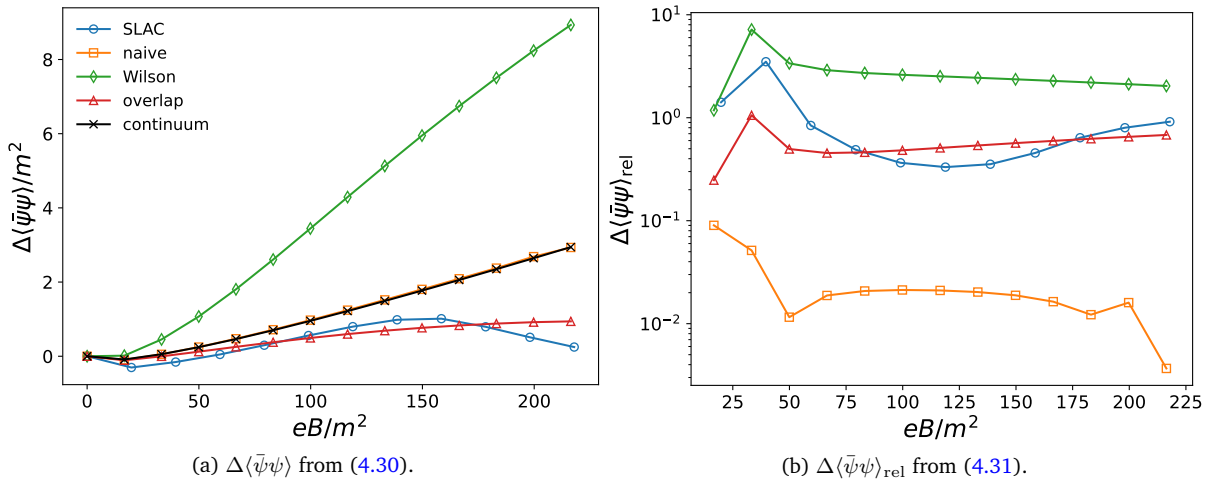


Figure 4.5: As in Fig. 4.3 but in $2 + 1$ dimensions. $N_s = N_t = 12$ ($N_s = 11$ for **SLAC** fermions), $am = 0.0512$.

Finally, the B -dependence of $\Delta\langle\bar{\psi}\psi\rangle$ is shown in Fig. 4.5. While the disagreement with the continuum results is not surprising for SLAC and Wilson fermions, one thing that clearly stands out when comparing to the $(2+0)$ -dimensional analog of Fig. 4.3 is that overlap fermions no longer lie on top of the continuum curve as naive fermions do. On the contrary, the disagreement for the overlap case is quite substantial. However, since the overlap condensate seems to systematically underestimate the continuum result, one may still be able to make qualitative statements with this discretization. In fact, we accredit the discrepancy to discretization effects. After all, while the massless overlap operator is $\mathcal{O}(a)$ improved automatically, this is no longer true when introducing a mass term as in (4.20), while the massive naive operator remains valid up to $\mathcal{O}(a^2)$. To some extent, this might be cured by employing an improved version of the overlap operator [199, 200]. Either way, when investigating an interacting theory, a particular focus should be put on the continuum limit and whether or not it is really under control.

5 Inhomogeneous Structures

In the discussion of the $(2 + 1)$ -dimensional GN model in the mean-field limit in Sections 3.2 to 3.6 we were always assuming translational invariance, i.e., that the effective action (2.40) is minimized by a homogeneous configuration, $\sigma(x) = \sigma = \text{const.}$, and thus reduces to (3.16). While we argued that in $2 + 1$ space-time dimensions such an assumption is indeed justified, this is not true in general and we shall devote this chapter to a more detailed discussion on this subject. After summarizing previous insights into the (non-)existence of inhomogeneous phases in low-dimensional 4FTs, both on the mean-field level and beyond, we present new simulation results for the χ GN model in $1 + 1$ dimensions. Most importantly, we find clear evidence for inhomogeneous structures for flavor numbers as low as $N_f = 2$.

5.1 Inhomogeneous phases in the mean-field limit

In light of the invariance of four-Fermi Lagrangians such as (2.18), (2.19), or (2.20) under translations (2.9) in both space and time, it is only reasonable to assume that the respective vacuum or thermal expectation values of 4FTs should respect this symmetry as well. This would entail, for instance, that in the GN model (2.20) the chiral condensate $\langle \bar{\psi}\psi \rangle$ and, by virtue of (2.42), the expectation value of the auxiliary field σ are homogeneous throughout all of space-time.

Indeed, this was the working assumption in early works on the model in $1 + 1$ dimensions such as [201], where its large- N_f phase structure in the (μ, T) plane was calculated. It was found that chiral symmetry is spontaneously broken at low T and μ . For $\mu = 0$ chiral symmetry is restored via a second-order phase transition at a critical temperature $T_c/\sigma_0 = \frac{e^\gamma}{\pi}$. Here, $\gamma \approx 0.577$ denotes the Euler-Mascheroni constant and, as usual, σ_0 denotes the (positive) minimum position of the effective potential (3.18) at vanishing T and μ . In contrast, the symmetry-restoring phase transition at zero temperature and a critical chemical potential of $\mu_c/\sigma_0 = \frac{1}{\sqrt{2}}$ is of first order and the two respective transition lines of first and second order meet at a tri-critical point at non-vanishing values of both T and μ . We mention in passing that in the large- N_f limit and under the assumption of homogeneous condensates the phase structures of the GN and χ GN models, in fact, exactly coincide. This is because the effective potential of the latter only depends on the combination $\rho^2 = \sigma^2 + \pi^2$, with π denoting the pseudo-scalar field introduced in (2.35), due to chiral symmetry. The calculation then proceeds in an identical fashion for both models [202].

However, it was realized in [90, 91] that the assumption of translational invariance leads to incorrect values for the masses of baryons within the models. Abandoning this assumption subsequently led to a number of novel insights, the most relevant for our purposes being that the phase diagram computed in [201] needed to be revisited. It turns out that, as a consequence of allowing for spatial modulations of σ (and π), the correct mean-field (μ, T) phase diagrams of the GN and χ GN models are, in fact, different, as we shall discuss in the following.

We invert the chronological order in which these results were found and begin with a discussion of the (massless) GN model with allowance for an inhomogeneous chiral condensate. The situation for low T and μ changes very little, as chiral symmetry is still spontaneously broken by a homogeneous order parameter. In addition, the second-order transition line between the phase of (homogeneously) broken chiral symmetry and the symmetric phase remains unchanged as well. However, it became clear that the first-order transition line at low T is no longer present [121, 203]. Instead, one finds two second-order transition lines delimiting an entirely new phase at high density, where – in addition to chiral symmetry – translation symmetry is spontaneously broken, as the order parameter develops a non-trivial dependence on the spatial coordinate. In fact, the space-dependence of the chiral condensate in this inhomogeneous phase can be described by a combination of Jacobi’s elliptic functions commonly referred to as a real kink crystal [204, 205]. We remark, however, that a discrete combination of translational and chiral symmetry remains intact. The large- N_f lattice studies [206, 207] lent further numerical support to the existence of an inhomogeneous phase and similar results were also found in the massive GN model [208]. For a comprehensive review of these developments we refer to [72].

Next, we turn to the χ GN model. Already in the seminal works [90, 91] it was found that the correct phase diagram of the χ GN model looks qualitatively different when the assumption of translational invariance is relaxed. In contrast to the GN model, however, the phase structure becomes much simpler in this case. Chiral symmetry is restored for temperatures higher than T_c (the value of T_c is carried over from the homogeneous case discussed above) independently of μ , while below T_c the system develops an inhomogeneous phase for every $\mu > 0$. The scalar and pseudo-scalar condensates form a so-called *chiral spiral*, which is the thermodynamically preferred realization of a more general solution to the inhomogeneous gap equation termed the twisted kink crystal [209–211]. In the chiral spiral phase, the space-dependence of the complex condensate is described by a plane wave, i.e., $\langle \bar{\psi}\psi \rangle - i\langle \bar{\psi}\gamma_*\psi \rangle = A e^{2i\mu x}$, whose wave number is proportional to μ and whose amplitude A only depends on the temperature. These results were confirmed and further elaborated upon in [212–214] and extended to the massive case in [215]. As for the GN model, a certain combination of translations and chiral rotations remains a symmetry of the inhomogeneous phase of the χ GN model as well. For the latter, however, this residual symmetry is continuous and one could thus

argue that – heuristically speaking – the effective “amount of symmetry breaking” is actually the same in both models.

The emergence of inhomogeneous condensates at non-zero μ can be explained as follows (see, e.g., [216]): Generically, a chiral condensate $\langle \bar{\psi}\psi \rangle = \langle \bar{\psi}_R\psi_L \rangle + \langle \bar{\psi}_L\psi_R \rangle$ is formed by the pairing of a left-handed fermion with a right-handed anti-fermion and vice-versa. At $\mu = 0$ the energetically favored way in which this can happen is by pairing fermions and anti-fermions with a vanishing total momentum, resulting in a homogeneous condensate. While this is also true for non-zero μ , the latter opens up the possibility for breaking chiral symmetry via a pairing between fermions and fermion holes. The excitation of such a fermion-hole pair costs very little energy if it occurs close to the Fermi surface. Importantly, whenever the pairing leads to a non-zero total momentum p , the resulting condensate is inhomogeneous in space, with a wave vector proportional to p . The latter is of the order of 2μ , which is, for instance, reflected in the space-dependence of the chiral spiral discussed above. This mechanism is very similar in spirit to the Peierls instability of one-dimensional electron chains [217].

5.2 Inhomogeneities beyond the mean-field limit

The central question that we aim to address in this chapter is whether the inhomogeneities discussed in Section 5.1 are merely an artifact of the mean-field limit or if they persist even for finite flavor numbers, where quantum fluctuations are not suppressed. The influence of the latter on the phase structure of a theory is generically expected to be non-trivial. In this section we discuss the intricacies that arise in low-dimensional theories beyond the mean-field limit and summarize the results of previous works dealing with similar questions.

The spontaneous breakdown of translational invariance, which is a continuous symmetry, is a highly delicate issue in low dimensions due to the Coleman-Hohenberg-Mermin-Wagner (CHMW) theorem [218–221]. In essence, this famous no-go theorem forbids the spontaneous breakdown of continuous symmetries in two or fewer (spatial) dimensions at finite temperature. We emphasize that this should affect the GN and χ GN models equally, despite the chiral symmetry of the former being discrete and that of the latter being continuous. After all, as we have argued before, the remnant combination of translations and chiral rotations left intact in an inhomogeneous phase is discrete for the GN and continuous for the χ GN model. This entails that in both models a continuous symmetry is broken spontaneously, such that the CHMW theorem does not distinguish between them. While it was argued that a conflict with the CHMW theorem can be avoided provided that one takes the limit $N_f \rightarrow \infty$ before the thermodynamic limit [202], this cannot be expected to be the case anymore when working with finite flavor numbers.

At this point we should introduce some terminology regarding (dis-)ordered systems

described by some field Φ , where $\langle \Phi \rangle$ is the relevant order parameter. We define as perfect *long-range order* the situation where

$$\lim_{|x-y| \rightarrow \infty} \langle \Phi(x)\Phi(y) \rangle = C(|x-y|) \neq 0, \quad (5.1)$$

i.e., the correlations of Φ at infinitely distant points do not decay to zero. They could, e.g., approach a constant or a non-trivial function of $|x-y|$. This asymptotic behavior is typically approached exponentially fast. On the contrary, we define as *quasi-long-range order* the case in which these correlations decay according to a power law,

$$\lim_{x \rightarrow \infty} \langle \Phi(x)\Phi(y) \rangle \propto \frac{1}{|x-y|^\alpha}, \quad \alpha > 0. \quad (5.2)$$

Such a power-law behavior is usually associated with the appearance of a phase of the Berezinskii-Kosterlitz-Thouless (**BKT**) type [222–224]. We shall henceforth refer to spontaneous symmetry breaking, as well as to the existence of proper phases, only in situations when there is perfect long-range order. Under certain conditions a **BKT** phase can showcase almost perfect ordering even on macroscopic scales [225], while at the same time avoiding the **CHMW** theorem, which rules out the existence of perfect long-range order.

That a **BKT** phase might be present in the $(1+1)$ –dimensional χ **GN** model was argued in [226], where it was also explained how perfect long-range order is re-established in the large- N_f limit. Despite the model only showing polynomially decaying correlations, one observes physical consequences usually associated with perfect long-range order, such as a non-vanishing fermion mass. That this is possible is due to the fact that the physical fermion does not appear as a pole in the two-point function of the elementary fermion, but as a branch cut instead, i.e., their quantum numbers are different [226]. Moreover, while there exists a massless scalar field in the theory, it is not a Nambu-Goldstone boson [227–229] and it fully decouples from the rest of the theory, thus avoiding the **CHMW** theorem [226]. The **BKT** phase in the $(1+1)$ –dimensional χ **GN** model is expected to exist only at $T = 0$, while at finite temperature chiral symmetry should be restored via exponentially decaying correlations [230]. In the $(2+1)$ –dimensional model, on the other hand, it was realized that a **BKT** phase should be present at $T > 0$, while at zero temperature one finds proper spontaneous symmetry breaking [230, 231].

All of the above references assume spatial homogeneity in their argumentation and, since they are only concerned with the study of chiral symmetry, they only consider the χ **GN** model due to its continuous symmetry group. However, as we have mentioned before, when allowing for the breakdown of translational symmetry, the **GN** and χ **GN** models should be treated on equal footing, such that similar effects might be taking place in the discrete **GN** model as well.

First signs for inhomogeneities at finite N_f had already been found in early simulations

of the $(1 + 1)$ -dimensional GN model [232]. However, dedicated simulations with the aim of finding inhomogeneous field configurations were only performed much later [233, 234]. These investigations revealed clear evidence for the existence of spatial inhomogeneities in the order parameter for flavor numbers as low as $N_f = 4$. While it is plausible that the discrete GN model also exhibits a BKT-type phase, other attempts at resolving the apparent clash with the CHMW theorem were presented in [233] as well.

5.3 Simulation setup

Here, we extend the work of [233, 234] to the χ GN model (2.35), which is invariant under the continuous $U(1)_A$ chiral transformations (2.36). In particular, we perform extensive lattice studies of the model in $1 + 1$ dimensions, studying its phase structure at finite temperature and density, for a small number of fermionic flavors and in the chiral limit. Since it became clear in [233] that SLAC fermions, when compared to other discretizations of 4FTs, have superior convergence properties towards the continuum limit, we employ them for the present study as well. More precisely, we use the SLAC Dirac operator introduced in Section 4.2.2 and couple the auxiliary fields σ and π , as well as the chemical potential μ , in the following straightforward way:

$$D = \gamma_\mu \partial_\mu^{(SLAC)} + \sigma + i\gamma_* \pi + \mu\gamma_0 , \quad (5.3)$$

where $\partial_\mu^{(SLAC)}$ is the SLAC derivative defined in (4.9). The lattice action in our simulations then reads

$$S = \frac{N_f}{2g^2} a^2 \sum_{x \in \Lambda} (\sigma^2(x) + \pi^2(x)) - \ln \det(aD) . \quad (5.4)$$

As is shown, e.g., in [108], the fermion determinant in this model is real even for non-zero μ . This means that there is no complex-action problem, provided that we simulate an even number of flavors, since $\det(aD)$ factorizes into a product of one-flavor determinants. The subsequent presentation closely follows the corresponding publication [104].

In order to study how bosonic quantum fluctuations alter the mean-field phase structure of the χ GN model, we perform simulations for $N_f = 2$ and $N_f = 8$ flavors, respectively, employing a standard rHMC algorithm [152]. Needless to say, one expects the results to approach their large- N_f counterparts for increasing flavor number. In our large-scale study we simulate a sizable number of different values for both μ and T in order to map out the parameter space as precisely as possible. Moreover, for $N_f = 2$ we consider three different volumes at fixed lattice spacing in order to estimate finite-size effects, as well as three different lattice spacings at fixed physical volume to approach the continuum limit. A detailed list of the various parameter values we consider can be found in [104].

5. Inhomogeneous Structures

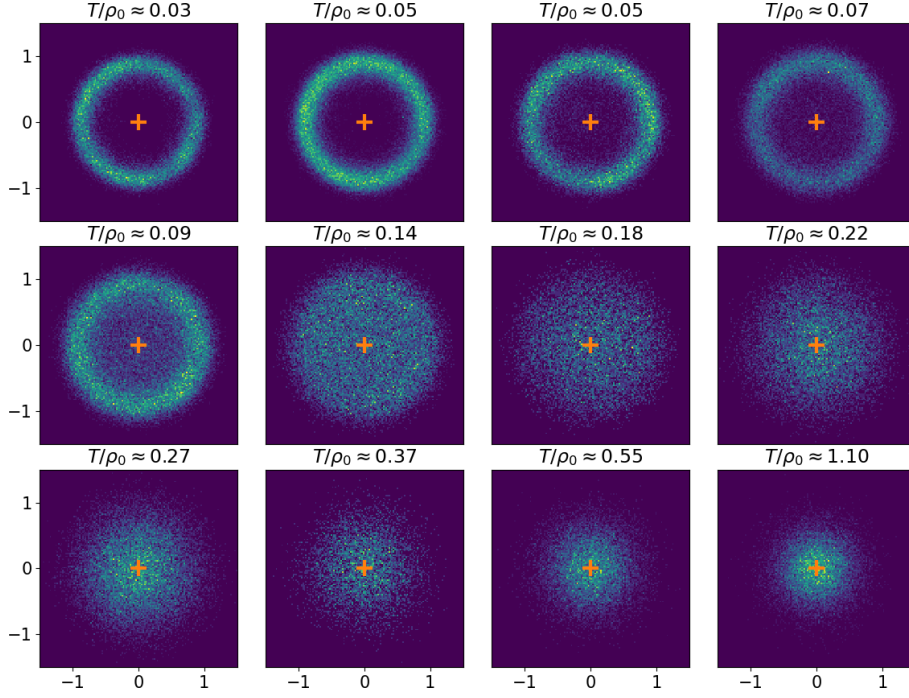


Figure 5.1: Distribution of $\bar{\Delta}/\rho_0$ in the complex plane for various temperatures. The crosses mark the origin for visual clarity. $N_s = 63$, $\mu = 0$, $a\rho_0 \approx 0.46$.

For subsequent discussions it shall be convenient to introduce the complex auxiliary field Δ , comprised by σ and π as its real and imaginary parts, respectively,

$$\Delta := \sigma + i\pi = \rho e^{i\theta}, \quad (5.5)$$

where we have furthermore defined the absolute value ρ and the phase θ of Δ . Notice that the chiral rotation (2.36) acts on these fields as

$$\Delta(x) \rightarrow e^{-2i\alpha} \Delta(x) \quad \text{or} \quad \rho(x) \rightarrow \rho(x), \quad \theta(x) \rightarrow \theta(x) - 2\alpha. \quad (5.6)$$

In particular, we see that ρ is invariant under chiral transformations and thus a non-vanishing expectation value of ρ does not entail the breakdown of chiral symmetry.

We may demonstrate the $U(1)$ -invariance of the action (5.4) by plotting histograms of the spatial average $\bar{\Delta} := \frac{a^2}{V} \sum_{x \in \Lambda} \Delta(x)$ in the complex plane, which reflect its probability distribution. This is done for different temperatures and at vanishing chemical potential in Fig. 5.1. We see that for low temperatures the distribution takes its maximum at a non-vanishing value of ρ , which moves to $\rho = 0$ at some critical temperature $T_c/\rho_0 \approx 0.1$, where the scale ρ_0 is defined in (5.14) below. For all temperatures the distribution is symmetric with respect to rotations in the complex plane, highlighting the ergodicity properties of our simulations.

5.3.1 Observables

The main observables of interest are the scalar and pseudo-scalar fermionic condensates $\langle \bar{\psi}\psi \rangle$ and $\langle \bar{\psi}\gamma_*\psi \rangle$, related to the expectation values of σ and π via (2.42) and (2.43), respectively. In the mean-field limit an inhomogeneous phase is characterized by an oscillatory behavior of the condensates as a function of the spatial coordinate. However, in order to search for inhomogeneous structures in our lattice theory, the computation of $\langle \sigma \rangle$ and $\langle \pi \rangle$ is of little help. This is because any sort of inhomogeneity present on the level of individual configurations of the auxiliary fields would be invisible in their expectation values due to translational invariance – after all, inhomogeneous configurations shifted by an arbitrary amount of lattice points are equally likely to be sampled in the path integral and will thus cancel each other in ensemble averages. Two such configurations of σ and π are shown exemplarily in Fig. 5.2.

In order to avoid this cancellation we follow [233] by introducing the spatial correlation functions

$$\begin{aligned} C_{\sigma\sigma}(x_1) &:= \frac{a^2}{V} \left\langle \sum_{x' \in \Lambda} \sigma(x'_0, x_1 + x'_1) \sigma(x'_0, x'_1) \right\rangle, \\ C_{\sigma\pi}(x_1) &:= \frac{a^2}{V} \left\langle \sum_{x' \in \Lambda} \sigma(x'_0, x_1 + x'_1) \pi(x'_0, x'_1) \right\rangle, \end{aligned} \quad (5.7)$$

as well as $C_{\pi\sigma}$ and $C_{\pi\pi}$, defined analogously. If the path integral is dominated by inhomogeneous configurations of σ and π , these correlators exhibit oscillatory behavior as well. Due to the $U(1)_A$ symmetry, they are related to each other via

$$C_{\sigma\sigma} = C_{\pi\pi}, \quad C_{\sigma\pi} = -C_{\pi\sigma}, \quad (5.8)$$

which implies that

$$C_{\Delta^*\Delta}(x_1) := \frac{a^2}{V} \sum_{x' \in \Lambda} \langle \Delta^*(x'_0, x_1 + x'_1) \Delta(x'_0, x'_1) \rangle = 2(C_{\sigma\sigma}(x_1) + i C_{\sigma\pi}(x_1)). \quad (5.9)$$

In (5.7) and (5.9), $\langle \cdot \rangle$ denotes the ensemble average (4.3), but does not imply averaging over lattice sites by itself and we shall retain that convention in what follows.

Useful information about oscillating correlation functions can be obtained by studying their Fourier spectrum. In particular, if the Fourier transform of a correlator takes its maximum at a non-vanishing momentum, this is a clear sign for oscillations. To this end, we define the dominant wave-number of $C_{\sigma\sigma}$ on a single configuration of σ as

$$k_{\max} := \operatorname{argmax}_k \left| \mathcal{F} \left[\frac{a^2}{V} \sum_{x' \in \Lambda} \sigma(x'_0, x_1 + x'_1) \sigma(x'_0, x'_1) \right] (k) \right|, \quad (5.10)$$

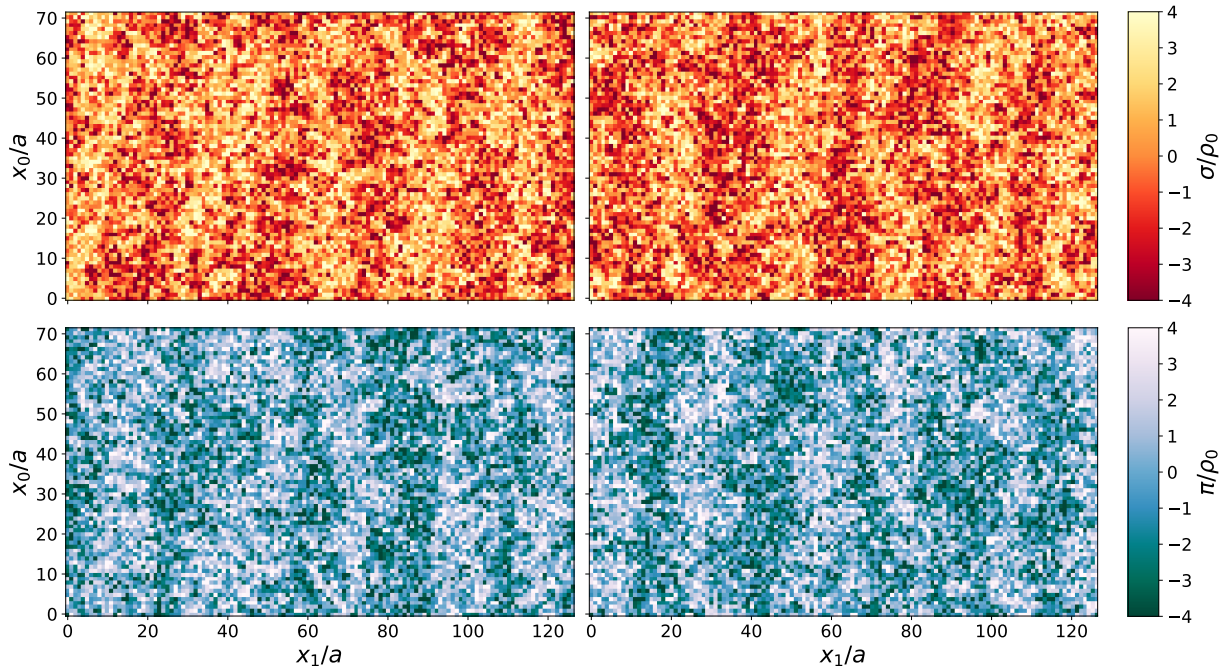


Figure 5.2: Two typical inhomogeneous configurations of σ (top) and π (bottom), respectively. $N_s = 127$, $N_t = 72$, $\mu/\rho_0 \approx 0.44$, $a\rho_0 \approx 0.46$.

where $\mathcal{F}[\cdot](k)$ denotes the one-dimensional discrete Fourier transform. Similarly, we introduce the winding number of $C_{\sigma\sigma}$ as

$$\nu_{\max} := \frac{L}{2\pi} \operatorname{argmax}_k |\mathcal{F}[C_{\sigma\sigma}(x_1)](k)|. \quad (5.11)$$

These two quantities have similar names only for notational convenience – notice that k_{\max} is defined configuration-wise, while ν_{\max} is related to an expectation value, such that, in general, $\nu_{\max} \neq \frac{L}{2\pi} \langle k_{\max} \rangle$. We also remark that it is sufficient for our purposes to compute the dominant wave-number and the winding number with respect to $C_{\sigma\sigma}$ only.

In order to scan the parameter space for inhomogeneities we require some quantity that allows us to distinguish between oscillating and non-oscillating correlation functions. To appreciate that this is not a trivial issue, first recall from Section 5.2 that some care is due with respect to terminology. After all, one is led to expect a **BKT**-type phase, where correlations decay algebraically, to be present in the model for temperatures equal or close to zero. In such a phase it would be incorrect to speak of perfect long-range order and the term quasi-long-range order is more appropriate. Despite resembling spontaneous symmetry breaking in some qualitative aspects, the actual physical situation in a **BKT** phase is different in detail.

It is thus important to investigate the spatial correlation functions both on small and on large scales. A quantity that enables us to study the presence of short-range oscillations was introduced in [104, 233] and is defined as

$$C_{\text{short}} := \min_x C_{\sigma\sigma(x)}. \quad (5.12)$$

As was explained in [233], if this quantity becomes negative one can conclude that inhomogeneities of some sort are present in σ . On the other hand, a positive value of C_{short} indicates a type of long-range ordering. However, it does not allow to distinguish between the aforementioned quasi-long-range order, with algebraically decaying correlations, and perfect long-range order, where correlations decay exponentially. Finally, if C_{short} vanishes there is no long-range order in the system at all.

We have remarked in [102] that a negative value of C_{short} , while being a clear sign for inhomogeneities, does not provide any insights on the behavior of $C_{\sigma\sigma}$ on large scales. This is because fluctuations in the spatial correlation functions are most prominent on short scales, as we shall see below. In order to probe larger scales we thus follow [102] by introducing

$$C_{\text{long}} := \min_x |C_{\Delta^*\Delta}(x)|, \quad (5.13)$$

where $C_{\Delta^*\Delta}$ was defined in (5.9). This quantity is insensitive to inhomogeneities, as any respective oscillations in $C_{\sigma\sigma}$ and $C_{\sigma\pi}$ cancel each other by definition. However, it allows us to make statements about the long-range behavior of the system. To be precise, if $C_{\text{long}} > 0$ there is an ordering on scales at least comparable to the system size, which hints at (quasi-)long-range order, whereas there is none if C_{long} vanishes. To obtain a complete picture, we thus study C_{short} and C_{long} in a complementary way. Notice, however, that C_{long} only yields additional information when oscillations are present, i.e., when $C_{\text{short}} < 0$. We remark that, despite the fact that we compute C_{short} and C_{long} in (μ, T) space in the next section, yielding what resembles phase diagrams, one should be aware that neither of these quantities is a genuine order parameter, as both are non-local observables.

Finally, let us discuss how we renormalize our observables. Ideally, we would like to use the expectation value of ρ , being non-negative and invariant under $U(1)_A$ transformations, as a scale. A direct comparison to mean-field results would then be straightforward. Thus, the most intuitive and conventional definition of a scale is the expectation value $\langle |\bar{\Delta}| \rangle$ at vanishing temperature and chemical potential, with $\bar{\Delta}$ again denoting the lattice average of Δ . However, as was discussed at length in [104], this quantity is severely spoiled by inhomogeneous configurations, which – perhaps surprisingly – can give a significant contribution to the path integral even at $\mu = 0$, especially on large volumes. For such configurations $\bar{\Delta}$ is close to zero, such that the naive definition above is biased towards smaller values. After considering a number of alternatives we came to the conclusion in [104] that a reasonable compromise is provided by the – admittedly unusual – definition of the scale as

$$\rho_0 := \frac{a^2}{V} \left\langle \sum_{x_1=0}^{N_s} \left| \sum_{x_0=0}^{N_t} \Delta(x) \right| \right\rangle \Big|_{T \approx 0, \mu=0}, \quad (5.14)$$

i.e., the absolute value is taken after the temporal average but before the spatial average.

We emphasize that configurations with an oscillating space-dependence nonetheless tend to be roughly homogeneous in time direction (see Fig. 5.2), such that taking the temporal average first results in a smaller variance of ρ_0 . However, as has become clear in [104], the definition (5.14) is still far from ideal, which should be kept in mind in the following.

5.3.2 On thermalization and auto-correlations

Drawing from previous experience with the simulation of fermionic systems exhibiting inhomogeneous structures on large scales, which typically suffer from long thermalization times, we employ the following strategy to counteract this problem. For high temperatures, where thermalization is not so much of an issue, we generate configurations until equilibrium is reached. We then “cool down” such an equilibrium configuration to a lower temperature by simply repeating the data in the temporal direction in an appropriate way. By iterating this procedure we reach lower and lower temperatures, thereby successfully reducing thermalization times. As was shown in [104], this cooling-down is free from hysteresis effects, i.e., if we first cooled the system down, then evolved it in Monte-Carlo time and at a later point heated it up again we would find results equivalent to such obtained without any cooling at all. We remark that we have only applied the cooling procedure in our simulations at $N_f = 2$.

We have analyzed the auto-correlations present in our simulations in great detail in [104] and only summarize the most important conclusions here. While for moderate temperatures the long auto-correlation times are under control due to sufficient statistics, the situation at low temperatures is more difficult, as auto-correlations become even more severe. This is expected from a physical point of view, but complicates the quantitative interpretation of our results. To be clear, we are confident that our findings capture the qualitative picture correctly, but the precise values of, say, winding numbers, might be somewhat off for temperatures close to zero. Lastly, our error analysis is performed via binned jackknife resamplings.

5.4 Results

Let us now present our simulation results for the $(1 + 1)$ -dimensional χ GN model with $N_f = 2$ and $N_f = 8$ fermion flavors, respectively. We first discuss oscillations in the spatial correlation functions (5.7), indicating the presence of inhomogeneities of some sort. Afterwards we shall map out the quantities C_{short} and C_{long} , defined in (5.12) and (5.13), respectively, in the parameter space spanned by the chemical potential and the temperature, in order to study for which parameter values one finds such inhomogeneities. Finally, we study the decay properties of correlation functions in an attempt to distinguish between perfect and quasi-long-range order.

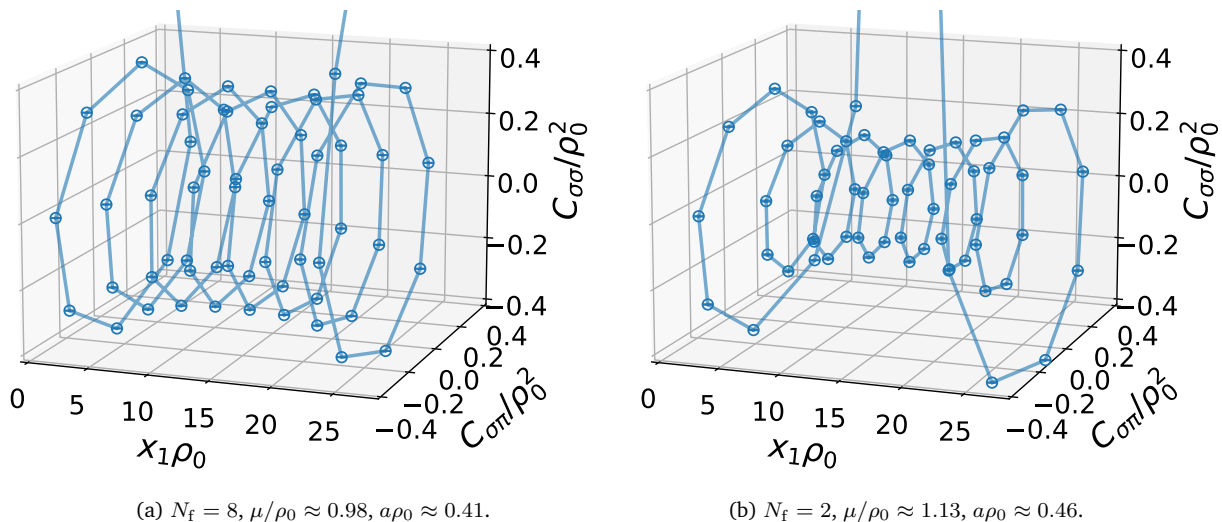


Figure 5.3: Spatial correlation functions $C_{\sigma\sigma}$ and $C_{\sigma\pi}$ from (5.7) for two different N_f , at equal temperature $T/\rho_0 \approx 0.03$ and with μ chosen such that the winding numbers match. $N_s = 63$.

5.4.1 Spatial oscillations of correlation functions

In order to search for possible inhomogeneities, we scan the (μ, T) plane for traces of oscillatory behavior in the spatial correlation function $C_{\Delta^*\Delta}$ defined in (5.9), or, equivalently, in the correlators $C_{\sigma\sigma}$ and $C_{\sigma\pi}$ of (5.7). Guided by the mean-field observations, we expect to find such inhomogeneities only for non-zero μ and low temperatures. In Fig. 5.3 we show exemplary plots of $C_{\sigma\sigma}$ and $C_{\sigma\pi}$ for $N_f = 2$ and $N_f = 8$, respectively. The most important observation is that the correlation functions indeed show oscillating behavior, indicative of the presence of inhomogeneities in the system. In fact, the space-dependence of $C_{\Delta^*\Delta}$ resembles that of the chiral spiral discussed in Section 5.1 and we shall thus henceforth use that terminology to refer to our results as well. Note that indications for inhomogeneities in the considered model have also been found using naive fermions [235].

An immediate conclusion is that inhomogeneous structures are not an artifact of the mean-field limit but are left intact to some extent by bosonic fluctuations. However, as the comparison between Figs. 5.3a and 5.3b shows, the amplitude of the chiral spiral decreases faster with the distance for $N_f = 2$ than for $N_f = 8$. This behavior is consistent with the expectation that in a BKT phase correlations decay more rapidly for smaller flavor numbers [226]. In fact, the decay properties of correlation functions at finite flavor number and zero temperature have recently been computed exactly by relating the χ GN model to a deformed conformal field theory [236], in qualitative agreement with our results.

It is instructive to investigate how the oscillatory behavior is affected when increasing the temperature. The expectation drawn from the mean-field results dictates that the chiral spiral amplitude should decrease with higher temperatures, whereas the oscillation frequency should remain unaffected. In Fig. 5.4 we show $C_{\sigma\sigma}$ and $C_{\sigma\pi}$ for two different

5. Inhomogeneous Structures

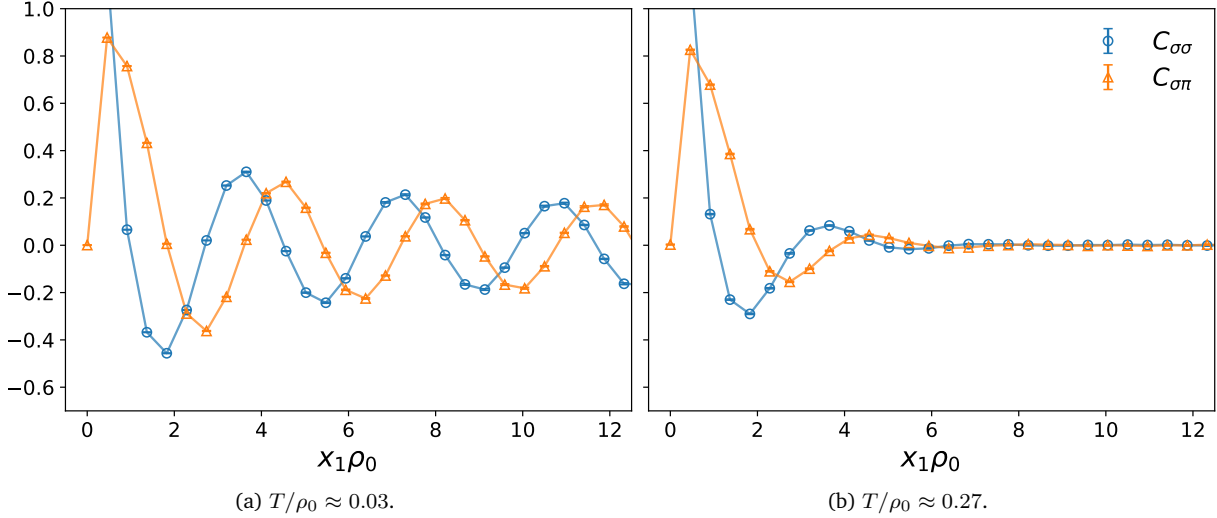


Figure 5.4: Spatial correlation functions $C_{\sigma\sigma}$ and $C_{\sigma\pi}$ from (5.7) for $N_f = 2$ and two different temperatures. $N_s = 63$, $\mu/\rho_0 \approx 1.14$, $a\rho_0 \approx 0.46$.

temperatures and constant μ . We observe that, while the correlators go to zero with x_1 more rapidly at the higher temperature, one can still clearly make out oscillatory behavior at small distances. This fact makes clear why it is necessary to distinguish between the short-range and long-range behavior of correlation functions and will become important when we study the “phase structure” of the model in the next section.

Based on the mean-field analysis, we are led to expect the frequency of oscillations and, thus, the winding number of the chiral spiral to be predominantly determined by the chemical potential. In order to see to which extent this holds beyond the mean-field limit, we show ν_{\max} as a function of μ for $N_f = 2$ and $N_f = 8$, with equal volumes and temperatures, in Fig. 5.5. We see that for both flavor numbers ν_{\max} grows with the chemical potential in a roughly linear way. Of course, an exact linear behavior as in the large- N_f limit is unlikely to occur on finite volumes due to ν_{\max} being a discrete number depending on the continuous variable μ . We furthermore show a comparison with the large- N_f expectation $\nu_{\max} = \frac{L}{\pi}\mu$ [211] in Fig. 5.5. The physical volumes for the two

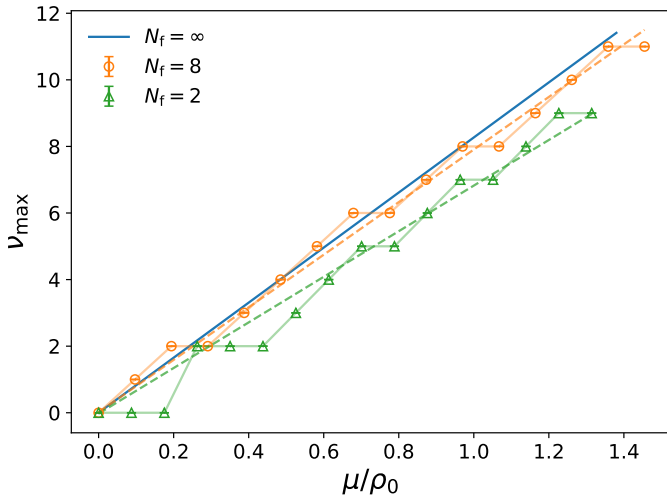


Figure 5.5: Winding number ν_{\max} from (5.11) for $N_f = 2$ ($a\rho_0 \approx 0.46$) and $N_f = 8$ ($a\rho_0 \approx 0.41$), as well as a comparison with the large- N_f result. For the latter, the physical volume was chosen to agree with the one for $N_f = 8$. See the main text for details. $N_s = 63$, $T/\rho_0 \approx 0.03$.

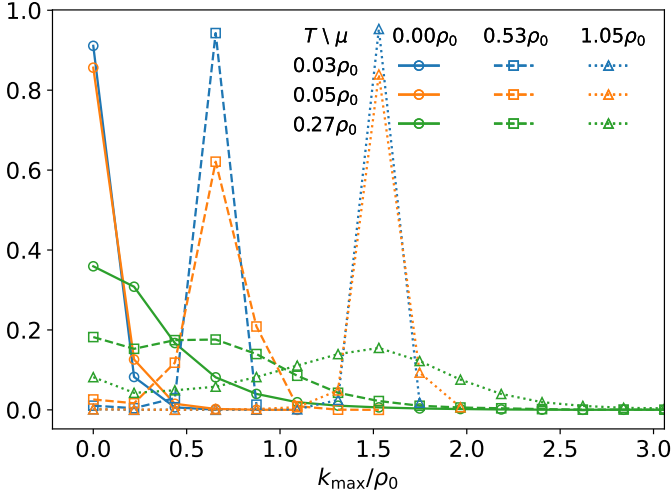


Figure 5.6: Normalized histograms of k_{\max} from (5.10) for various values of T and μ . $N_f = 2$, $N_s = 63$, $a\rho \approx 0.46$.

different flavor numbers do not match precisely and we only show the mean-field result for the smaller of the two, corresponding to $N_f = 8$. One observes that our result for $N_f = 8$ agrees very well with this expectation, while the deviations are larger for $N_f = 2$. This is, of course, precisely the kind of deviation one would expect when going beyond the large- N_f limit.

An important observation to be made is that the chiral condensate is not governed solely by its dominant wave-number but instead receives significant contributions from sub-dominant k as well. That this is especially true for high temperatures can be seen in Fig. 5.6, where we show exemplary histograms of k_{\max} for different T and μ . While, expectedly, the peak of the distribution of k_{\max} moves to larger values for larger μ , we also see that it decreases and broadens with increasing temperature. The fact that multiple oscillation frequencies contribute to the correlator is caused by a combination of quantum and thermal fluctuations and is also ultimately responsible for the avoidance of the CHMW theorem.

5.4.2 Phase structure beyond the mean-field limit

Let us now investigate the phase structure of the χ GN model for low flavor numbers. What we mean by that is that we are interested in where exactly in (μ, T) space one can find inhomogeneities of the form shown in Figs. 5.3 and 5.4. Inhomogeneities in our setup likely do not exhibit perfect long-range order, as this would imply a conflict with the CHMW theorem. To obtain a more complete picture, we thus probe short and long scales alike by investigating both C_{short} and C_{long} , introduced in (5.12) and (5.13), respectively. As was mentioned previously, referring to regions where some sort of structural order can be found as “phases” and to C_{short} and C_{long} as “order parameters” is technically incorrect, but we shall still do so for reasons of convenience and brevity.

We begin by showing the order parameters in (μ, T) space for $N_f = 8$ in Fig. 5.7. One sees in Fig. 5.7a that a large part of the (μ, T) plane is governed by negative values of C_{short} , indicating the presence of inhomogeneities on some scale. For small chemical

5. Inhomogeneous Structures

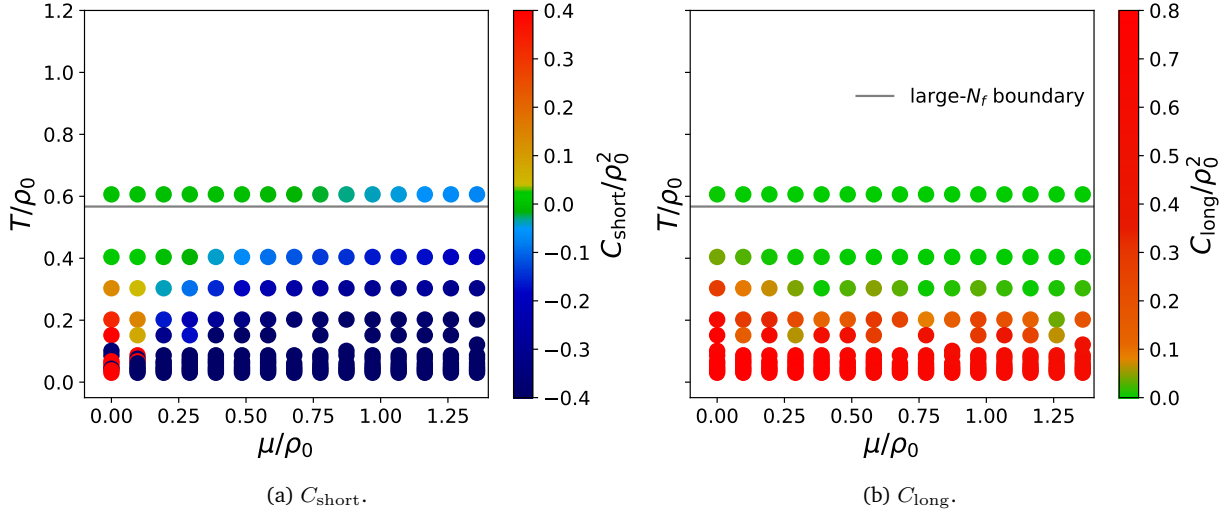


Figure 5.7: Order parameters C_{short} from (5.12) and C_{long} from (5.13) in the (μ, T) plane for $N_f = 8$. $N_s = 63$, $a\rho_0 \approx 0.41$.

potentials we observe that the dominant contributions to the path integral are homogeneous, as expected. Notice, however, that even at $\mu = 0$ one observes inhomogeneities for some temperatures. Since we have not applied the cooling procedure outlined in Section 5.3.2 for $N_f = 8$, we cannot rule out that these might be thermalization effects. On the other hand, in Fig. 5.7b we see that the phase structure as determined by C_{long} is quite similar to the one found in the mean-field limit, as the boundary between the respective regions where $C_{\text{long}} > 0$ and $C_{\text{long}} \approx 0$ is almost horizontal, albeit at a lower T_c . Other peculiarities to be found in Fig. 5.7 shall be discussed in more detail in the context of the $N_f = 2$ case below, where they play an even more prominent role.

For the two-flavor case we have performed simulations on increasing physical volumes at fixed lattice spacing as well as for decreasing a on a roughly constant volume. The phase diagrams resulting from C_{short} and C_{long} for the former case are shown in the top and bottom rows of Fig. 5.8, respectively. We see that the phase structure looks rather different from Fig. 5.7, confirming once more that bosonic fluctuations play an important role in the context of inhomogeneous structures. While many qualitative features remain the same in that there exist inhomogeneities for most $\mu > 0$ and low enough temperatures, the green region in the top row of Fig. 5.8 is much larger than the corresponding region in Fig. 5.7b. In this region the correlators show no oscillations and decay to zero, such that there is no (quasi-)long-range order to be found. As was outlined in [104], the phase structure can be understood by a comparison of the two relevant scales in the system, namely the correlation length, determined by the temperature, and the oscillation wavelength, determined by the chemical potential. In simple words, one expects to find inhomogeneities whenever the chiral spiral wavelength is shorter than the correlation length.

In the large- N_f limit one observes inhomogeneities for every non-vanishing μ below T_c . In our case, however, we see that the region of small $\mu \neq 0$ is dominated by

5. Inhomogeneous Structures

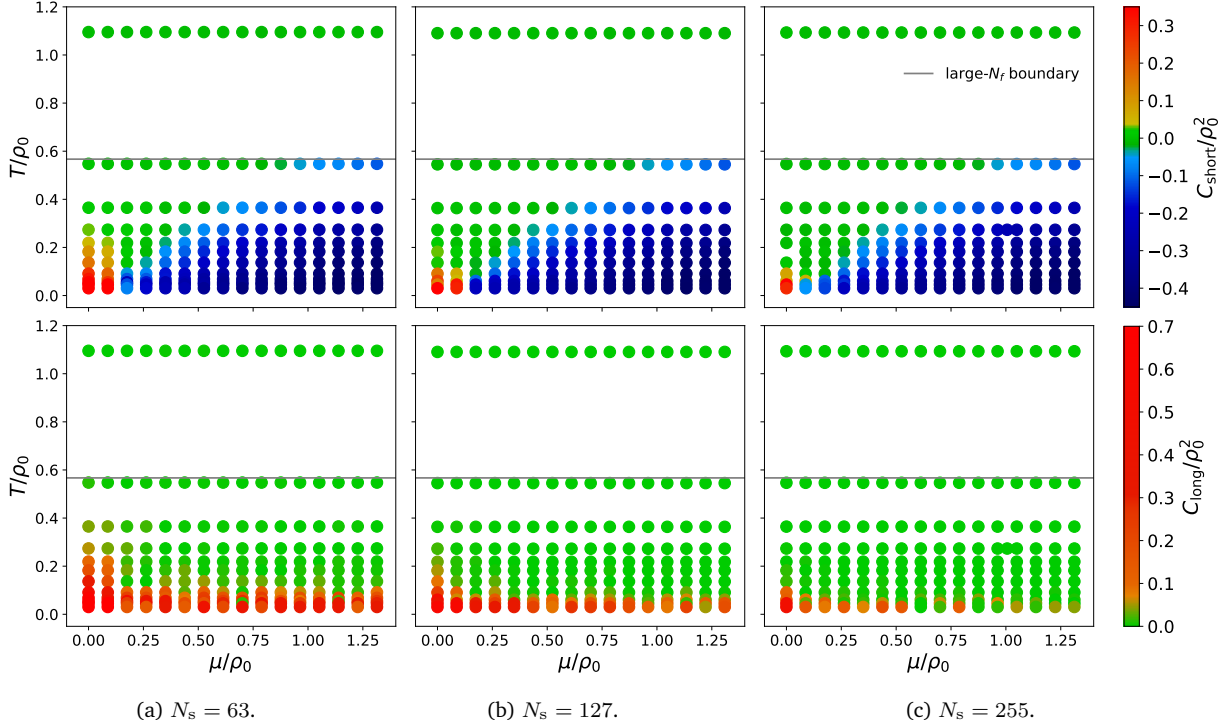


Figure 5.8: Order parameters C_{short} from (5.12) (top row) and C_{long} from (5.13) (bottom row) in the (μ, T) plane for $N_f = 2$ and different volumes at a constant lattice spacing $a\rho_0 \approx 0.46$. The gray line indicates the critical temperature in the large- N_f limit.

homogeneous configurations on small volumes. This is due to the fact that the chiral spiral wavelength is inversely proportional to the chemical potential, such that for small enough μ the wavelengths simply do not fit inside our finite lattice. As expected, this effect disappears, i.e., the red region in the top row of Fig. 5.8 shrinks, in the thermodynamic limit.

Regarding the existence of (quasi-)long-range order we study C_{long} in the bottom row of Fig. 5.8. We see that the two regions of $C_{\text{long}} > 0$ and $C_{\text{long}} \approx 0$, respectively, are separated roughly by a horizontal line as in the $N_f = 8$ case, at least when μ is sufficiently large to allow for inhomogeneities to develop. Despite happening at a much lower temperature, these results, as compared to those for C_{short} , are thus comparable to their mean-field counterparts on a qualitative level. Notice, however, that C_{long} approaches zero everywhere for larger volumes. This is consistent with the expectation that correlations should decay to zero for large distances, be it exponentially or algebraically. One thus concludes that no spontaneous symmetry breaking takes place, despite the presence of inhomogeneities.

Let us now turn to the continuum extrapolations of C_{short} and C_{long} , shown in the top and bottom rows of Fig. 5.9, respectively. Even for the smallest lattice spacing considered our results still suggest the presence of inhomogeneities on some scale, as is indicated by negative values of C_{short} . The behavior of C_{long} , on the other hand, appears to remain roughly unchanged as we decrease a , which is not surprising as we keep the physical volume roughly constant in the process. What we observe is, thus, that the correlations

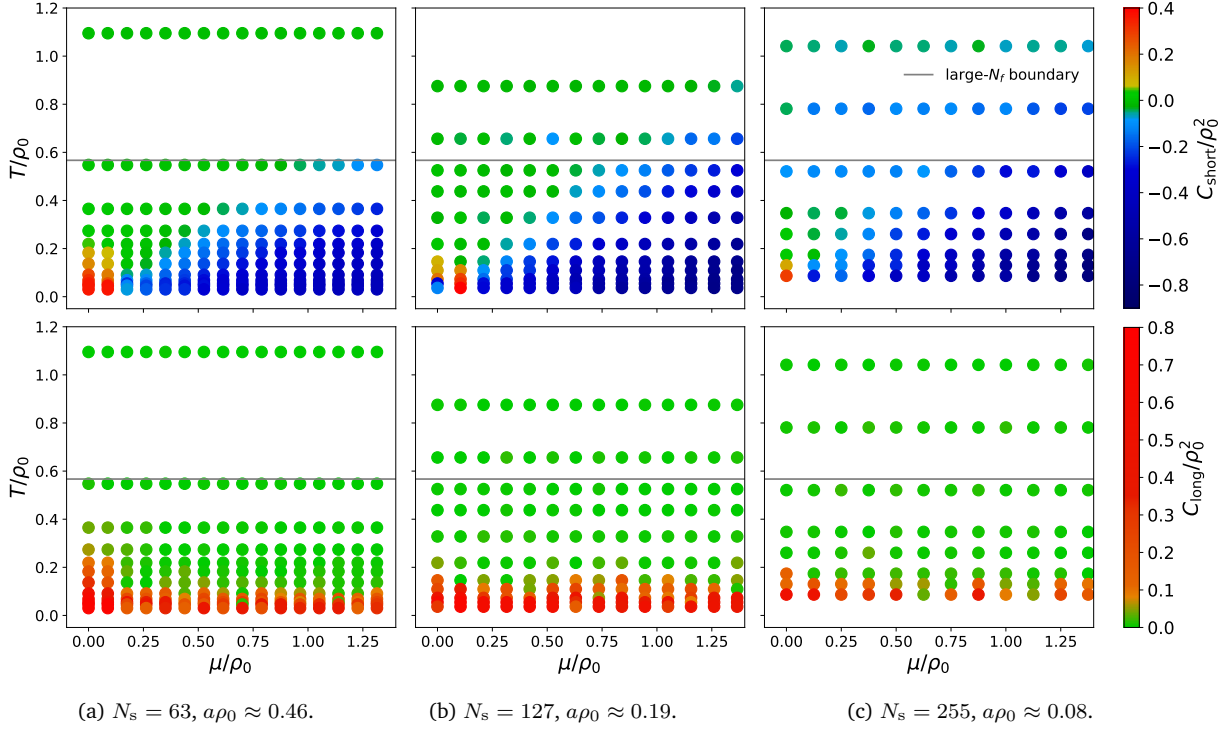


Figure 5.9: Order parameters C_{short} from (5.12) (top row) and C_{long} from (5.13) (bottom row) in the (μ, T) plane for $N_f = 2$ and different lattice spacings at constant physical volume. The gray line indicates the critical temperature in the large- N_f limit.

do not decay to zero on the small volumes considered here, which is not surprising. We should emphasize, however, that a precise statement about the existence or non-existence of inhomogeneities in the continuum limit is complicated by our scale-setting procedure discussed in Section 5.3.1. While our data suggest that short-scale inhomogeneities are present even in the continuum limit with the current scale-setting, an improved procedure might come to a different conclusion.

5.4.3 Perfect long-range order vs. quasi-long-range order

In [230] the correlation functions of our system were predicted to decay algebraically at $T = 0$ and exponentially for every non-zero temperature. Since we cannot simulate at exactly vanishing temperature, we are led to expect exponentially decaying correlations everywhere, approaching an algebraic decay as we lower the temperature. In order to put this assertion onto more solid ground we now study the decay properties of the correlator $C_{\Delta^*\Delta}$, which is related to the fermionic four-point function [104], in more detail. We show its absolute value at a low temperature for both flavor numbers considered in Fig. 5.10. Additionally, we attempt to fit the data using three different functions, each of which is chosen to be symmetric about $x_1 = \frac{L}{2}$ to account for the lattice periodicity. First of all, we consider an algebraic fit,

$$C_{\Delta^*\Delta}(x_1) = \frac{\kappa}{x_1^\alpha} + \frac{\kappa}{(L - x_1)^\alpha}, \quad (5.15)$$

5. Inhomogeneous Structures

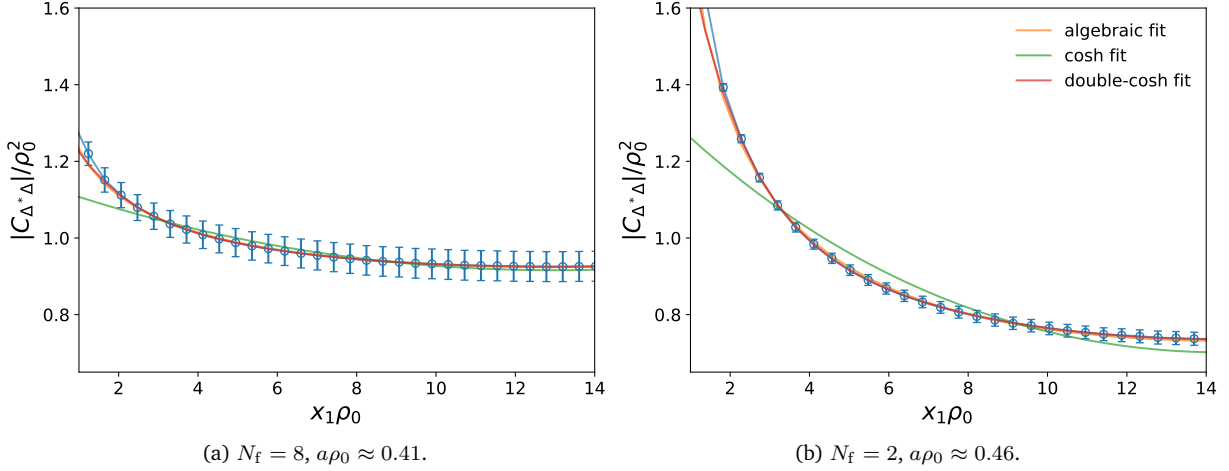


Figure 5.10: Correlation function $C_{\Delta^* \Delta}$ from (5.9) as a function of the spatial coordinate, as well as algebraic, cosh and double-cosh fits to the data – see the main text for details. The fit uncertainties are not shown. $N_s = 63$, $\mu = 0$, $T/\rho_0 \approx 0.03$.

which is expected to describe the long-distance behavior of the correlator in a **BKT** phase. Here, α and κ are fit parameters. In addition, we compute single- and double-cosh fits, obtained by setting $N = 1$ and $N = 2$ in

$$C_{\Delta^* \Delta}(x_1) = \sum_{i=1}^N a_i \cosh \left[m_i \left(x_1 - \frac{L}{2} \right) \right], \quad (5.16)$$

respectively, the fit parameters being denoted as a_i and m_i .

For both flavor numbers we observe that the algebraic and double-cosh fits lie practically on top of each other and describe the data almost perfectly, while the single-cosh fit performs much worse, therefore being discarded in what follows. The relevant parameters for the algebraic and double-cosh fits are α and m_i , respectively, but, since the exact values of the fit parameters depend on the chosen fit interval, we only give rough estimates here. We find $\alpha \approx 0.2$ for $N_f = 8$ and $\alpha \approx 0.5$ for $N_f = 2$, while $m_1/\rho_0 \approx 10^{-4}$ and $m_2/\rho_0 \approx 0.6$ for both flavor numbers. These values do not change much when increasing the volume.

As expected, at such a low temperature one cannot properly distinguish between algebraic and exponential decays. However, our data is consistent with the expectation that the exponential behavior should approach the algebraic one as the temperature is decreased. Indeed, we have verified that at higher temperatures the decay behavior rather resembles an exponential function. That one behavior turns into the other can be appreciated by observing that m_1 approaches zero. Moreover, our values for α are in qualitative agreement with the results of [236].

6 Magnetic Catalysis

We have seen in Chapter 3 that fermionic theories in background magnetic fields experience an enhancement of chiral symmetry breaking in the large- N_f limit at zero density and for all temperatures below the chiral phase transition. While it was argued in [237] that this *magnetic catalysis* is a model-independent feature, it might still be an artifact of the mean-field limit. Moreover, it is not clear to which extent bosonic fluctuations, present at finite N_f , affect the complicated phase structure found in mean-field fermionic theories at finite density, comprising inverse magnetic catalysis as well as patterns of multiple phase transitions. It shall be part of the investigation presented in this chapter to shed light on these and related questions by studying the fate of chiral symmetry in magnetized fermionic theories beyond the mean-field limit. We begin this chapter by giving a brief historic account of the study of magnetic catalysis, also covering QCD, where it has become clear that the behavior of the chiral condensate in a magnetic field is not as trivial as predicted by model approaches. After outlining some convenient spectral properties of our lattice discretization based on the overlap formalism, the main part of this chapter is then devoted to the presentation of results obtained in extensive lattice simulations of the GN model in $2 + 1$ dimensions.

6.1 Strongly-interacting theories within magnetic fields

In this section we shall summarize the most important historical developments in the study of strongly-interacting matter within (electro-)magnetic background fields. We put a particular emphasis on the investigation of chiral symmetry and its spontaneous breakdown and how it is affected by magnetic fields.

First studies of model theories in electromagnetic fields can be found, e.g., in [131, 132, 238–240]. In the context of the $(2 + 1)$ -dimensional GN model in the mean-field limit it was realized that the magnetic field leads to the spontaneous breakdown of chiral symmetry for arbitrarily weak couplings [132]. Recall from Appendix D that the GN model can be divided into a strong-coupling regime, where the bare four-Fermi coupling is larger than some critical value, $g^2 > g_c^2$ (or the renormalized coupling g_R^2 becomes negative), and a weak-coupling regime, where $g^2 < g_c^2$ (or $g_R^2 > 0$). In the strong-coupling regime chiral symmetry is spontaneously broken at vanishing temperature, chemical potential and magnetic field, and we again denote the corresponding value of $\langle \sigma \rangle$ by $\sigma_0 > 0$. As before, we only consider the branch of non-negative solutions of the gap equation (3.19) without loss of generality. On the other hand, for weak couplings σ_0

vanishes.

For weak but non-zero magnetic fields one then finds the following B -dependence of the order parameter [132]:

$$\langle \sigma \rangle(B) \propto \begin{cases} 1 + \frac{(eB)^2}{12\sigma_0^4} & \text{if } g^2 > g_c^2 \\ |eB| & \text{if } g^2 < g_c^2 \end{cases}, \quad (6.1)$$

where we have omitted higher-order terms as well as unimportant (but dimensionful) proportionality constants. We see that the chiral condensate increases in magnitude with the magnetic field in both regimes, corresponding to magnetic catalysis, albeit with different powers. Analogous results were also found at finite temperature [133, 134], provided that one stays below the transition temperature T_c , beyond which chiral symmetry is restored. This T_c was furthermore predicted to increase monotonically with B .

In [237, 241–243] a proper physical explanation for magnetic catalysis was given based on the fact that the magnetic field reduces the effective number of space-time dimensions by two, $d \rightarrow d - 2$; see [244] for a review. This has also been observed in the theory of superconductivity before [245] and can best be seen by investigating the fermion propagator and expanding it in terms of Landau-level poles [241]. In particular, the contribution of the LLL to the bare momentum-space propagator in $2 + 1$ dimensions reads (see also [246])

$$S_0(p) \propto e^{-\frac{p_{\parallel}^2}{|eB|}} \frac{m - p_0 \gamma_0}{p_0^2 + m^2} (1 - i\gamma_1 \gamma_2 \text{sign}(eB)), \quad (6.2)$$

where $p_{\parallel}^2 = p_1^2 + p_2^2$ and we have once again assumed the magnetic field to be perpendicular to the spatial plane. Since for strong magnetic fields the physics is governed by the LLL, one concludes that the motion perpendicular to the magnetic field, i.e., in the spatial plane, is indeed suppressed. Analogous conclusions can be drawn in dimensions higher than three as well [243]. Since low-dimensional theories are more prone to suffer from infrared divergences, an interpretation of magnetic catalysis is that the system responds to the dimensional reduction via the creation of a mass gap, which happens for arbitrarily weak fermionic interactions – see also [247–249] for accounts on magnetic catalysis from the point of view of the functional renormalization group.

Importantly, the dimensional reduction only affects electrically charged degrees of freedom, such as the elementary fermions, but leaves electrically neutral ones unaffected. In this way magnetic catalysis can, e.g., avoid the CHMW theorem mentioned in Chapter 5. For instance, in the NJL model, where chiral symmetry is continuous and its spontaneous breaking thus entails the presence of Nambu-Goldstone modes, it can be shown that the propagators of the latter have a genuine d -dimensional structure. This means that they do not suffer from the dimensional reduction and the associated infrared

divergences, which is accredited to their electric neutrality [241]. While there are no Nambu-Goldstone bosons in the GN model (2.20) due to its discrete chiral symmetry, there also exist different no-go theorems preventing the existence of phases in low dimensions, see, e.g., [250]. Nevertheless, we believe that, due to the electric neutrality of the chiral condensate $\langle \bar{\psi}\psi \rangle$, similar arguments should hold, such that magnetic catalysis in the GN model is not in conflict with any no-go theorems, both in the mean-field limit and beyond.

After the aforementioned seminal works it was long believed that magnetic catalysis at zero density was a universal, model-independent feature, as it was confirmed by countless model investigations [251–257] (see also [258–264] for accounts of the relevance of magnetic catalysis for condensed-matter physics). A notable exception is the study [265], employing the MIT bag model [266], where it was found that the critical temperature of the phase transition should decrease with the magnetic field. For a review of these developments, we refer to [267]. That the situation at $\mu \neq 0$ is more complicated was made clear in [146], as we have already discussed in detail in Section 3.3. Moreover, it was realized that the inclusion of gauge degrees of freedom might also spoil the argument of universality of magnetic catalysis [268].

The study of QCD in external magnetic fields has an even longer history than the aforementioned mean-field model studies, as, for instance, the magnetic moments of a number of baryons had already been computed in [269, 270]. The first dedicated studies of the QCD phase transition at finite temperature in a magnetic field, however, were only performed much later in [197, 271]. There, indeed, the picture of magnetic catalysis was confirmed, as the chiral condensate as well as the critical temperatures of the chiral and deconfinement cross-overs were all found to increase with B – see also [272] for a review of early results. However, these studies were performed on coarse lattices and for larger-than-physical pion masses. In later investigations at the physical point and with a proper continuum extrapolation it then became clear that the real physical situation is drastically different [273, 274]. While for low temperatures magnetic catalysis persists, close to the QCD cross-over this is no longer true. There, the order parameter exhibits non-monotonic behavior as a function of B . In particular, in an intermediate region the magnetic field actually lowers the chiral condensate, i.e., one observes inverse magnetic catalysis. For higher temperatures the condensate then again increases with B . Interestingly, one observes a monotonic decrease of the QCD critical temperature with B , even for extremely strong magnetic fields [275–278], at which the QCD cross-over might turn into a real first-order transition [278].

With these results at hand, it became clear that the model results one took for granted for years before [273, 274] do not give correct descriptions of finite-temperature QCD and an explanation for this discrepancy was much needed. One such explanation was provided in [279], where it was found that there are two competing effects governing the phenomenology of QCD in an external magnetic field, called the valence and sea quark

effects, respectively. While the former is caused by a direct enhancement of low-lying Dirac eigenmodes due to the magnetic field, thus contributing to magnetic catalysis via the Banks-Casher effect [280], the latter incorporates the influence of the magnetic field on the gluonic distribution in the path integral via the fermion determinant. Close to the QCD cross-over temperature the sea quark mechanism has the effect of decreasing the chiral condensate and dominates over the valence quark contribution, thus overall leading to inverse magnetic catalysis [279]. This dominance is possible since near the cross-over the Polyakov loop effective potential is practically flat, making the Polyakov loop susceptible to small changes induced by the magnetic field, which can suppress low-lying Dirac eigenmodes [279].

If this picture is indeed the correct one, purely fermionic model theories cannot be expected to reproduce the decrease of the chiral condensate with B at non-zero temperatures, as the latter is caused by interactions with gluons. In fact, a large number of alternative explanations for inverse magnetic catalysis (see, e.g., [281]), as well as various extensions to existing model theories were developed in the years following the original works [273, 274]. Perhaps unsurprisingly, the central idea that emerged from these investigations is that one should incorporate gluonic interactions into the picture somehow, for instance by coupling the models to the Polyakov loop. In particular, the Polyakov-loop-extended NJL (PNJL) model [282] as well as the Polyakov-loop-extended quark-meson (PQM) model under the influence of magnetic fields have been studied extensively [283–288] (see [289] for a review).

The crucial ingredient that the straightforward PNJL and PQM models miss, however, is the back-reaction of magnetized quarks onto the gluon distribution, encoded by the sea quark effect in QCD. In order to incorporate this back-reaction, one could let the fermionic coupling run with the magnetic field [290], as so does the QCD coupling [268]. The idea behind this is motivated by the fact that the effective interactions between quarks, obtained by integrating out gluons in a suitable way, are encoded in, say, the four-Fermi coupling g^2 . Thus, if gluons are somehow affected by the magnetic field, this should be reflected by the coupling. Indeed, the inclusion of such B -dependent couplings in model theories led to the reproduction of QCD phenomenology, such as inverse magnetic catalysis [291–297]. One particular approach that appears to be especially natural is the following [298]: One uses lattice QCD to compute magnetized baryon masses, from which constituent quark masses are extracted by using a simple quark model. This then gives magnetic-field-dependent input for a mean-field PNJL model, in which one indeed observes inverse magnetic catalysis and a decrease of the critical temperature. For reviews on the efforts to reproduce inverse magnetic catalysis in model theories, see [299–302]

We mention at this point two important aspects that remain to be addressed. On the one hand, most model studies dealing with the search for QCD phenomenology to be found in the literature were performed in the mean-field limit, which clearly does

not allow for the complete description of a quantum theory. On the other hand, despite tremendous progress in our understanding of magnetized QCD at finite temperature, the finite-density part of the QCD phase diagram [303] remains very much elusive to this day, both for zero and non-zero background magnetic fields [304].

The present chapter is a step into the direction of filling both of these gaps. To this end, we investigate the $(2 + 1)$ -dimensional GN model, as a very simplistic toy model for QCD, at finite temperature, density and magnetic field beyond the mean-field limit. Conceivably, allowing for (bosonic) quantum fluctuations might alter the mean-field picture of magnetic catalysis at finite temperatures. If this were indeed the case, the idea that gluonic degrees of freedom are capable of inducing inverse magnetic catalysis might have to be re-visited. As it shall turn out, however, there is no evidence for inverse magnetic catalysis in our results and – on the contrary – we believe that our work gives further support to the importance of gluonic degrees of freedom. Another important question concerns the fate of the phase structure of the GN model at finite density, where the mean-field limit predicts a plethora of interesting phenomena. As we shall see, however, they are not reproduced by our simulation results. Since QCD at intermediate chemical potentials is still – for the most part – uncharted territory, we nonetheless hope to provide some insight into the physics of magnetized strongly-interacting matter at finite density.

6.2 Spectral properties of the overlap operator

Before discussing our lattice simulations using overlap fermions in detail in the subsequent sections, we devote the present section to a spectral analysis of the overlap operator itself. We restrict ourselves to the study of non-interacting fermions in $2 + 0$ dimensions (i.e., with periodic boundary conditions only) for now. This is because the use of anti-periodic boundary conditions would introduce fermionic Matsubara frequencies, which would spoil the zero modes the overlap operator otherwise exhibits. We later comment on the applicability of the results presented here for our studies in $2 + 1$ dimensions.

6.2.1 Landau levels on the lattice

One of the most salient features of the (massless) overlap operator (4.17) is that it can have exact zero modes, just as the continuum Dirac operator. In fact, this is true for every solution of the Ginsparg-Wilson relation (4.13). This is especially convenient for the study of fermions exposed to background magnetic fields, as with the overlap formalism the Landau levels (3.1) have a particularly clear representation in the discretized theory. To see this, we show in Fig. 6.1a the (absolute-squared) eigenvalues of $D_{ov}^{(0)}$ as a function of the magnetic field. The color coding is chosen in analogy to the continuum degeneracy

6. Magnetic Catalysis

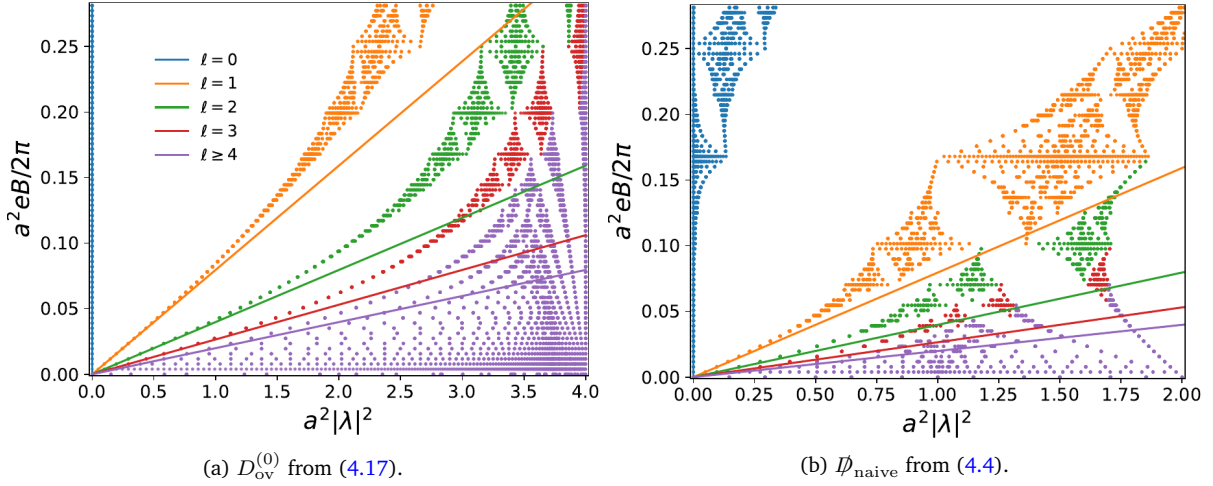


Figure 6.1: Spectra of the massless overlap and naive Dirac operators (horizontal axes), respectively, in $2 + 0$ dimensions as a function of the magnetic field (vertical axes). The solid lines correspond to the continuum eigenvalues and the points are colored according to their degeneracy. Notice the different scales on the x -axes. $N_s = 16$.

of Landau levels (3.3), i.e., using (3.4) and assuming $eB \geq 0$,

$$d_l = \begin{cases} b & \text{if } l = 0 \\ 2b & \text{if } l > 0 \end{cases}. \quad (6.3)$$

The continuum eigenvalues $|\lambda|^2 = 2|eB|l$ are shown as solid lines for comparison. For stronger magnetic fields than those shown in Fig. 6.1a one runs into numerical difficulties in the evaluation of the inverse square root in (4.17) due to the Wilson kernel A_W developing eigenvalues close to zero, see the discussion in Section 6.2.2 below.

We see in Fig. 6.1a that for weak magnetic field the spectrum of the overlap operator lies almost exactly on top of its continuum counterpart. Given the importance of Landau levels for continuum physics (see Chapter 3), this fact makes D_{ov} a very promising discretization for the study of fermions within magnetic fields. In particular, for all magnetic fields shown the zero modes of the Dirac operator, corresponding to the LLL, are represented exactly in the lattice theory. This remarkable fact can be better appreciated when comparing the overlap spectrum of Fig. 6.1a to Fig. 6.1b, where we show an analogous plot of the spectrum of the naive Dirac operator (4.4) in a magnetic field, taking into account the doubler modes in the degeneracies (6.3). While for weak magnetic field the agreement with the continuum eigenvalues is still remarkable, a deviation sets in at smaller eB than in the overlap case, in particular regarding the LLL.

We mention in passing that the fractal structure that emerges in the magnetized spectra due to a competition between the two relevant length scales, i.e., the magnetic length $\frac{1}{\sqrt{eB}}$ and the lattice spacing a , is commonly referred to as Hofstadter's butterfly [305], which can perhaps be better appreciated by looking at Fig. 6.1b. A detailed investigation of the role of Landau levels within lattice QCD can be found in [306,

[307]. There, it became evident that the LLL can clearly be distinguished from the higher Landau levels even when QCD interactions are taken into account. The reason for this is a topological argument, the so-called index theorem, which we shall discuss in the next subsection. On the other hand, in the GN model studied in this thesis there is no index theorem that would facilitate the interpretation and thus it is less clear what happens to the spectrum of $D_{\text{ov}}^{(0)}$ once interactions are considered. This question is part of an ongoing investigation.

6.2.2 Index theorem

Let us now discuss the celebrated index theorem [308] in some detail. From the Ginsparg-Wilson relation (4.13) it follows that the zero modes, or, more precisely, all real eigenmodes of $D_{\text{ov}}^{(0)}$, have definite chirality. Denoting the numbers of right- and left-handed zero modes of a Dirac operator D as n_+ and n_- , respectively, the index theorem in our two-dimensional setup can be formulated as (see, e.g., [309] and Appendix A)

$$\text{ind}(D) := n_+ - n_- = b, \quad (6.4)$$

This means that the difference between the numbers of left- and right-handed zero modes, i.e., the index of D , is entirely determined by the magnetic flux, represented by its quantum number b defined in (3.4). More generally, the index theorem relates the index of an operator to some topological quantum number, whose definition may not be as straightforward as that of b . A formulation of the index theorem on the lattice can be found in [310].

The spectrum of $D_{\text{ov}}^{(0)}$ at $b = 0$ can be computed in closed form (see, e.g., [311]) and one finds that there are two zero modes with opposite chirality, i.e., $n_+ = n_- = 1$. For any $b > 0$, on the other hand, one expects that either $n_+ = 0$ or $n_- = 0$. This assertion that the zero modes are either all left-handed or all right-handed is known as the vanishing theorem, see Appendix A. Thus, using (6.4), the total number of zero modes of the free massless overlap operator in a magnetic field in $2 + 0$ dimensions should be given by

$$n := n_+ + n_- = b + 2\delta_{b,0}. \quad (6.5)$$

Let us now test the validity of the vanishing theorem, as well as of (6.4). The index theorem in lattice QCD and related theories has been studied intensely in the literature [312–317], with the conclusion that for strong couplings it breaks down due to discretization effects. Similarly, we expect (6.4) not to hold anymore for large enough eB , i.e., when the lattice can no longer properly resolve the magnetic field. To this end, we show in the upper panel of Fig. 6.2 a comparison between the magnetic flux quantum number b , the number of zero modes n and the index of the overlap operator $\text{ind}(D_{\text{ov}}^{(0)})$ as a function of B . While the vanishing theorem is valid for all $B > 0$, we see that the

6. Magnetic Catalysis

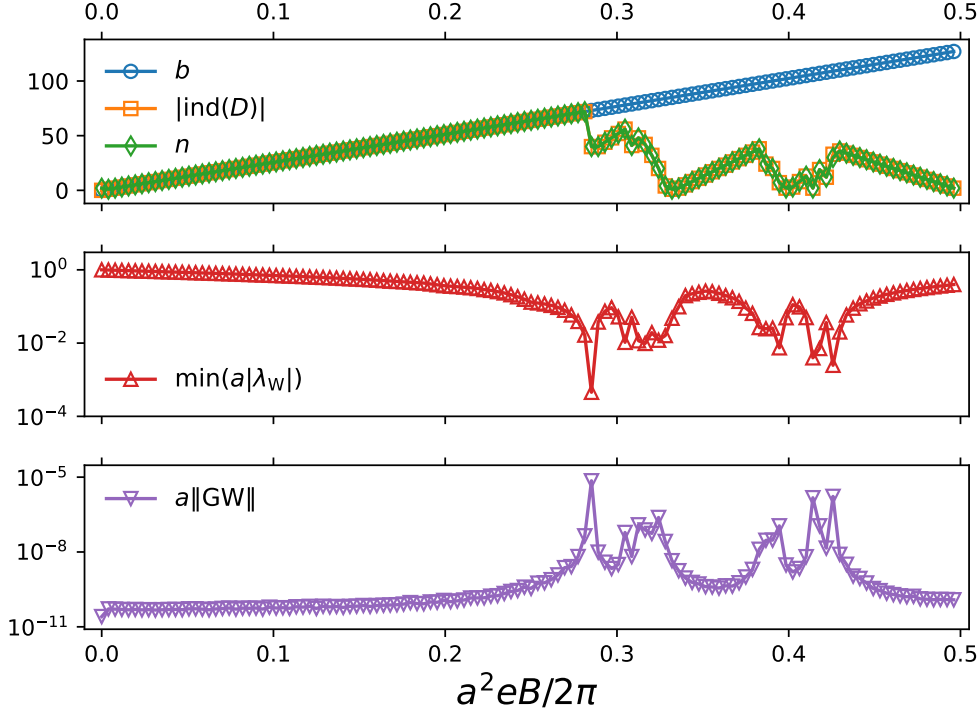


Figure 6.2: Various quantities related to the index theorem in $2 + 0$ dimensions as a function of B . (upper panel): magnetic flux quantum number b , modulus of the index of the overlap operator, $|\text{ind}(D)|$, and total number of zero modes of D , n (with $D = D_{\text{ov}}^{(0)}$ from (4.17)). (middle panel): lowest eigenvalue of the Wilson kernel A_W from (4.18). (lower panel): validity of the Ginsparg-Wilson relation (4.13). See the main text for details. $N_s = 16$.

index theorem holds exactly for a broad range of weak magnetic fields but breaks down above $\frac{a^2 e B}{2\pi} \approx 0.28$. There are two effects at play here, which we shall now discuss in turn.

On the one hand, as was mentioned in Section 6.2.1, the Wilson kernel A_W in (4.17) may acquire small eigenmodes for certain magnetic field strengths, resulting in numerical problems in the evaluation of the overlap operator. To see for which values of B this is the case, we show in the middle panel of Fig. 6.2 how the magnitude of the smallest eigenvalue of A_W changes with the magnetic field. We indeed observe a correspondence between the lowest eigenvalue of A_W being close to zero and the index theorem breaking down. These numerical difficulties are also reflected in the validity of the Ginsparg-Wilson relation (4.13), as can be seen in the lower panel of Fig. 6.2, where we show the matrix norm of (4.13),

$$\|GW\| := \left\| \{D_{\text{ov}}^{(0)}, \gamma_*\} - a D_{\text{ov}}^{(0)} \gamma_* D_{\text{ov}}^{(0)} \right\|. \quad (6.6)$$

On the other hand, we also find violations of the index theorem in regions where there are no small eigenvalues of A_W . To understand them, recall that for $b = 0$ the real eigenvalues λ of $D_{\text{ov}}^{(0)}$ come in two branches, the physical modes at $a\lambda = 0$ and the unphysical doubler modes at $a\lambda = 2$, both of which are affected by a magnetic field. For strong enough magnetic fields these two branches eventually intersect, resulting in a

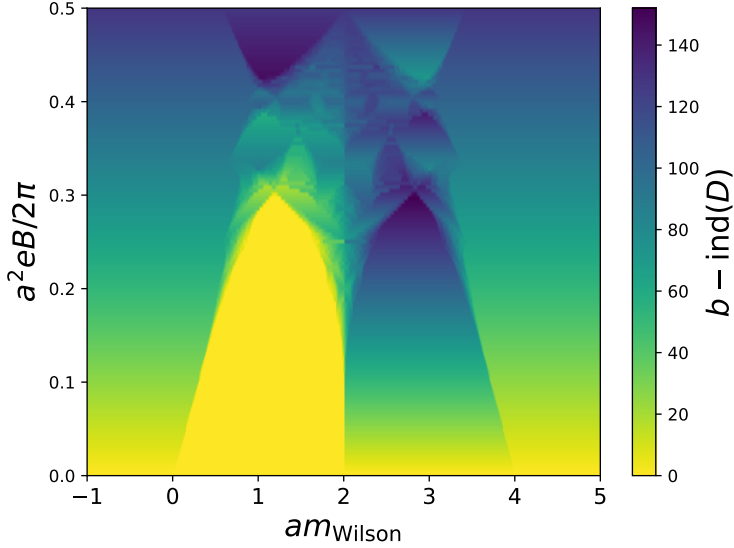


Figure 6.3: Violation of the index theorem in $2 + 0$ dimensions as measured by $b - \text{ind}(D)$, where $D = D_{\text{ov}}^{(0)}$ from (4.17), in the (m_W, B) plane. $N_s = 16$.

spurious counting of the unphysical modes in the index of $D_{\text{ov}}^{(0)}$. The index theorem (6.4) is thus no longer valid for strong magnetic fields without taking the doubler modes into account explicitly. Obviously, this is a discretization artifact.

It is interesting to study how one may influence the range of validity of the index theorem. To this end we follow [311] by tuning the Wilson mass parameter m_W in (4.18). As the choice of m_W controls the location of the eigenvalues of A_W in the complex plane, it should allow us to manipulate the distinction between the aforementioned physical and unphysical modes to some degree. One usually prefers to avoid this by restricting am_W to values between 0 and 2 as in (4.18) – recall that in our simulations we set $am_W = 1$ throughout. Here, however, we allow for arbitrary values. Plotting the violation of the index theorem (6.4), i.e., $b - \text{ind}(D_{\text{ov}}^{(0)})$, in the plane spanned by m_W and B , we obtain the topological phase diagram shown in Fig. 6.3. We see that the choice $am_W = 1$ is indeed not far from the optimal value, yielding a sizable range of magnetic fields where (6.4) is valid. On the contrary, for $am_W < 0$ or $am_W > 4$ we find that $D_{\text{ov}}^{(0)}$ has no zero modes at all, while in the range $2 < am_W < 4$ left- and right-handed zero modes are interchanged [318].

6.2.3 Finite-size effects

Finally, we shall discuss a peculiarity in the behavior of the chiral condensate as a function of B on finite volumes. Namely, we investigate how the finite-size effects studied in Section 3.1 in the context of (3.10) are reflected in our lattice formulation. To this end, we follow [319] by writing the chiral condensate for Ginsparg-Wilson fermions, (4.16), as

$$\langle \bar{\psi} \psi \rangle_{\text{ov}} = - \left\langle \bar{\psi} \left(1 - \frac{a}{2} D_{\text{ov}}^{(0)} \right) \psi \right\rangle = \frac{1}{\omega L^2} \text{tr} \left[D_{\text{ov}}^{-1} - \frac{a}{2} \mathbb{1} \right], \quad (6.7)$$

where $\omega := 1 - \frac{am}{2}$ and the massive overlap operator $D_{\text{ov}} = \omega D_{\text{ov}}^{(0)} + m \mathbb{1}$ was defined in (4.20). Notice that we consider a non-vanishing fermion mass m for this discussion. We

furthermore mention that (6.7) is equivalent to the definition given in (4.28) and (4.29). Expressing the trace in (6.7) as a sum over the eigenvalues of $D_{\text{ov}}^{(0)}$ one finds that the unphysical modes $a\lambda = 2$ do not contribute to the condensate and that the latter can be written as [319]

$$m\langle\bar{\psi}\psi\rangle_{\text{ov}} = \frac{n}{L^2} + q, \quad (6.8)$$

where n was defined in (6.5) and

$$q = \frac{1}{\omega L^2} \sum_{\substack{\lambda \\ \text{Im}(\lambda) \neq 0}} \left(\frac{1}{\omega\lambda + m} - \frac{a}{2} \right) \quad (6.9)$$

encodes the contributions from all eigenvalues with non-vanishing imaginary parts; see [320] for a similar argument.

Up to now, our calculation matches common derivations of the Banks-Casher theorem [280]. The point of deviation, however, is that one usually concludes that exact zero modes do not contribute to the condensate in the thermodynamic limit due to the factor $\frac{1}{L^2}$ in (6.8) and that $\langle\bar{\psi}\psi\rangle_{\text{ov}}$ is instead governed by near-zero modes. Here, we shall argue that this is not the case if one keeps magnetic field strength fixed in the limit $L^2 \rightarrow \infty$. Indeed, inserting (6.5) and (3.4) into (6.8), we find

$$m\langle\bar{\psi}\psi\rangle_{\text{ov}} = \frac{eB}{2\pi} + \frac{2\delta_{b,0}}{L^2} + q. \quad (6.10)$$

We emphasize that the first term, which is linear in B and arises due to exact zero modes, does not vanish in the infinite-volume limit. On the other hand, if we fixed b (i.e., the magnetic flux) and thus, by virtue of the index and vanishing theorems, n instead of B (i.e., the magnetic field strength), we would indeed find that exact zero modes do not contribute to $\langle\bar{\psi}\psi\rangle_{\text{ov}}$ as $L^2 \rightarrow \infty$, see (6.8). The second term in (6.10) arises since the vanishing theorem does not hold for $b = 0$. On finite volumes it gives an offset, resulting in a non-monotonicity of the condensate with B in the same way as n is non-monotonic in b . This is how the finite-volume effect discussed below (3.10) is represented in the lattice theory. Albeit not a desired feature for applications in high-energy physics, where one would like to approach infinite volumes in simulations, this still provides a non-trivial test for fermion discretizations in a magnetic field, see Section 4.4.

In order to visualize this finite-size effect we show in Fig. 6.4 the individual contributions to $\langle\bar{\psi}\psi\rangle_{\text{ov}}$ as a function of B for different volumes and fermion masses. One clearly observes how the non-monotonicity of the condensate becomes irrelevant as $L^2 \rightarrow \infty$. In the infinite-volume limit, the condensate then merely contains a contribution linear in B plus sub-leading contributions originating from non-zero eigenmodes of $D_{\text{ov}}^{(0)}$. For smaller masses we observe that the condensate is governed almost entirely by zero modes.

We have seen in this section that the overlap operator faithfully reproduces a plethora of important features of the continuum theory in the discretized setup. Although we

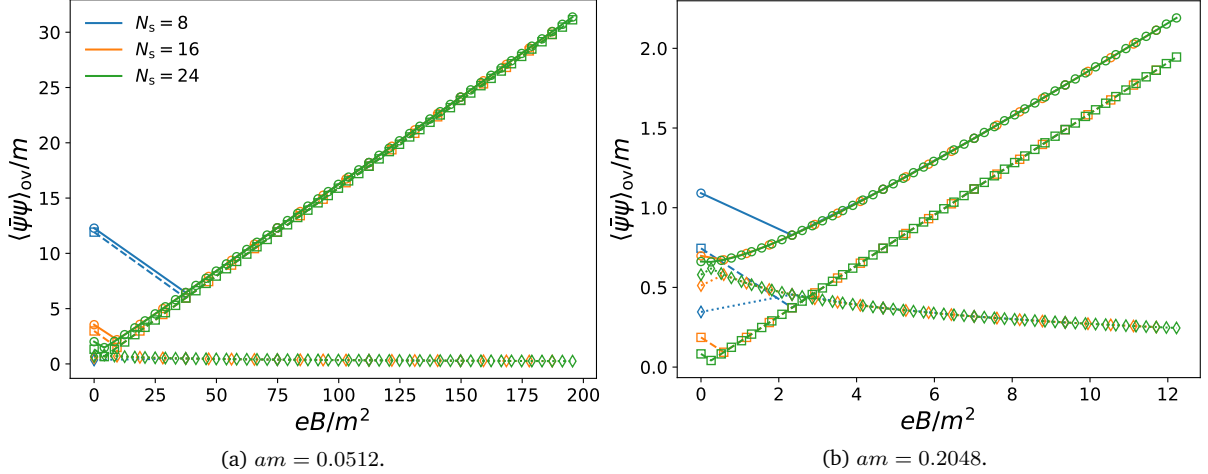


Figure 6.4: Chiral condensate $\langle \bar{\psi}\psi \rangle_{\text{ov}}$ from (6.7) in $2+0$ dimensions as a function of B for various spatial extents N_s and different masses am . We show the full condensate (circles, solid lines), as well as the individual contributions from zero modes (squares, dashed lines) and non-zero modes (diamonds, dotted lines), respectively. See the main text for details.

have only considered non-interacting fermions in a two-dimensional space-time here for simplicity, we believe that these features should – at least to some extent – be observable in the $(2+1)$ -dimensional interacting theory we consider in the remainder of this chapter as well. Of course, there are subtleties in three dimensions that do not play a role here. For instance, the index theorem is not defined in three dimensions and there are no exact zero modes of $D_{\text{ov}}^{(0)}$ anymore due to fermionic Matsubara frequencies. This raises the question of what remains of the finite-size effects shown in Fig. 6.4. Moreover, as we have seen in Section 4.4, there appear to be more severe discretization artifacts when anti-periodic boundary conditions are introduced in $2+1$ dimensions, which need to be studied properly. Nonetheless, we believe that the conclusions drawn from Section 4.4 and the present section imply that the overlap operator is well-suited for the study of fermionic theories within magnetic fields.

6.3 Simulation setup

We intend to simulate the GN model (2.20) within an external magnetic field in $2+1$ dimensions, using the overlap Dirac operator in the fermionic action. As we have seen in Sections 4.4 and 6.2, this discretization features a number of remarkable properties implying that it is well suited for that purpose. To this end, we need to couple the auxiliary field σ in (2.33) to the overlap fermions in a suitable manner. The most straightforward way to do so is by using the fact that the term $\sigma \bar{\psi}\psi$ in (2.33) would reduce to a fermionic mass term if σ were constant. We are thus guided by (4.20) in defining the overlap operator for the GN model in the chiral limit as

$$D = D_{\text{ov}}^{(0)} + (\sigma + \mu\gamma_0) \left(\mathbb{1} - \frac{a}{2} D_{\text{ov}}^{(0)} \right), \quad (6.11)$$

where the massless overlap operator $D_{\text{ov}}^{(0)}$ was given in (4.17) and we have coupled the chemical potential μ using the GS prescription (4.19). While a similar argument [321] has been used previously in the domain wall formalism [322], we also mention that an alternative prescription was proposed in [323], both for vanishing μ , however. To the best of our knowledge, there is no prior account of lattice simulations employing (6.11) to be found in the literature, even though an analogous expression has been devised for $\mu = 0$ in [324].

A remarkable property of (6.11) from a numerical point of view is that the dynamical degree of freedom in our simulations, i.e., the scalar field σ , does not enter the expensive computation of the operator sign function in the definition of $D_{\text{ov}}^{(0)}$ (4.17). In particular, this means that we do not have to re-compute $D_{\text{ov}}^{(0)}$ for every update step and may simply calculate it once (which can be done exactly, i.e., without approximation [325]) and store it for later use, which is a tremendous advantage as compared to, say, overlap simulations of gauge theories. Nonetheless, the non-ultralocality of the overlap operator comes with an extensive numerical cost, such that we are forced to restrict to rather small volumes in our investigations.

Here and in the remainder of this chapter we again consider a reducible representation of the Dirac algebra, allowing for the introduction of γ_* , see Section 2.2.4. Recall that the GN model in the continuum only has the discrete \mathbb{Z}_2 chiral symmetry (2.34). Indeed, the lattice action arising from (6.11) is not invariant under the full $U(1)$ group of lattice transformations (4.14) either. Rather, one finds the following \mathbb{Z}_2 symmetry:

$$\psi \rightarrow i\hat{\gamma}_*\psi, \quad \bar{\psi} \rightarrow i\bar{\psi}\gamma_*, \quad \sigma \rightarrow -\sigma, \quad (6.12)$$

where we have defined $\hat{\gamma}_* = \gamma_*(1 - aD_{\text{ov}}^{(0)})$. We remark that the use of lattice chiral transformations that do not act symmetrically on ψ and $\bar{\psi}$ as in (6.12) is not uncommon in the Ginsparg-Wilson literature, see, e.g., [187, 194]. After all, the difference between the transformations on ψ and $\bar{\psi}$ vanishes in the limit $a \rightarrow 0$ and one is again led back to (2.34). We remark that the ambiguity of choosing γ_* in the reducible representation, leading to the respective axial transformations (2.22) and (2.23), is respected exactly in the Ginsparg-Wilson formalism as well, and one also finds a correspondence of the vector symmetry (2.24) [114]. In our lattice GN model (6.14) below, the axial symmetries are both broken down to discrete symmetries like (6.12), which are related by the lattice version of (2.24). Hence, our lattice theory reproduces the continuum chiral symmetry group faithfully, which is another remarkable property of the Ginsparg-Wilson formalism.

Moreover, the discretization (6.11) was designed so as to carry over the continuum DSE (2.42) onto the lattice. Indeed, using (6.7), one finds

$$\langle \bar{\psi}\psi \rangle_{\text{ov}} = \frac{N_{\text{f}}}{g^2} \langle \sigma \rangle. \quad (6.13)$$

That there is a factor of i missing as compared to (2.42) has to do with the fact that we define the fermionic part of the lattice theory as $\bar{\psi}D\psi$ instead of $\bar{\psi}iD\psi$ like in the continuum (2.37), but bears no physical consequences, as $\langle\sigma\rangle$ serves as an order parameter for chiral symmetry breaking all the same.

With the Dirac operator D from (6.11), our full lattice action, which we use to simulate the GN model for one reducible fermion flavor, $N_f = 1$, reads

$$S = \frac{N_f}{2g^2} a^3 \sum_{x \in \Lambda} \sigma^2(x) - \ln \det(aD) . \quad (6.14)$$

As before, our simulations are performed using a standard rHMC algorithm. We have generated data for three different lattice sizes at fixed a in order to extrapolate to the thermodynamic limit and we have considered three different lattice spacings at fixed volume to approach the continuum theory. In our investigations we are mainly interested in the effects of a magnetic field at finite temperature and zero density, as well as on the non-zero density regime at low temperatures, i.e., we do not probe the combined case of high T and large μ . For lists of the parameter values we have simulated, we refer to the corresponding publications [105, 106].

For each data point in (B, T, μ) space we have generated between $\mathcal{O}(10^2)$ and $\mathcal{O}(10^4)$ independent trajectories. Regarding the error analysis we have once again performed binned jackknife resamplings, making sure that the bins are at least as large as the integrated auto-correlation time, but in most cases they are significantly larger than that. Indeed, we have made sure that auto-correlations, which become more severe with increasing system size, are under control in our simulations.

6.3.1 Observables

Let us now outline the lattice observables that we study in this chapter. The observable of predominant interest is the chiral condensate $\langle\bar{\psi}\psi\rangle$, as it serves as an order parameter for chiral symmetry breaking and allows us to determine the phase structure of the model. As in previous chapters, we instead consider the expectation value of the auxiliary scalar field σ , using the DSE (2.42) (or, rather, its lattice version for Ginsparg-Wilson fermions (6.13)), since its computation is a much simpler task numerically.

In order to avoid cancellations by the two competing minima of the effective action in the phase of broken chiral symmetry, we do not measure $\langle\sigma\rangle$ directly, as it would average to zero in an ergodic simulation. Instead, we compute the quantity

$$\langle|\bar{\sigma}|\rangle = \frac{a^3}{V} \left\langle \left| \sum_{x \in \Lambda} \sigma(x) \right| \right\rangle , \quad (6.15)$$

where we denote by $\bar{\sigma}$ the space-time average of σ , $\bar{\sigma} := \frac{a^3}{V} \sum_{x \in \Lambda} \sigma(x)$. While in the

thermodynamic limit $\langle |\bar{\sigma}| \rangle$ approaches the desired order parameter,

$$\lim_{V \rightarrow \infty} \langle |\bar{\sigma}| \rangle = |\langle \sigma \rangle| , \quad (6.16)$$

one should keep in mind that $\langle |\bar{\sigma}| \rangle$ will never vanish exactly on finite volumes, even when chiral symmetry is intact, which complicates the study of phase transitions. We also mention that the definition (6.15) assumes translational invariance, i.e., the absence of inhomogeneities in σ beyond random fluctuations. Below, we shall see that this assumption is indeed justified.

In order to study phase transitions and, in particular, determine their locations, we study the chiral susceptibility, which we define as

$$\chi := V (\langle \bar{\sigma}^2 \rangle - \langle |\bar{\sigma}| \rangle^2) . \quad (6.17)$$

Notice that we have explicitly included a factor of V in the definition of χ in order to compensate for the space-time average performed in the definition of $\langle |\bar{\sigma}| \rangle$. The resulting susceptibility is an intensive quantity. On a finite volume the chiral susceptibility exhibits a peak at a phase transition, which diverges rationally in the infinite-volume limit with a behavior governed by critical exponents.

Another method for pinning down the position of a phase transition is the study of the finite-size scaling of the Binder cumulant [326]

$$U_L := 1 - \frac{\langle \bar{\sigma}^4 \rangle}{3 \langle \bar{\sigma}^2 \rangle^2} . \quad (6.18)$$

At a phase transition the curves of Binder cumulants for different system sizes should intersect each other, providing us with a second, independent, estimate of the transition's location. We remark that the Binder cumulant is likely less reliable in this study due to the small volumes we consider. Nonetheless, we compute it alongside the chiral susceptibility for the sake of comparison.

The final observable we shall consider in this chapter is the spatial correlation function of σ , taken over from (5.7) and generalized to three dimensions,

$$C_{\sigma\sigma}(x_1, x_2) = \frac{a^3}{V} \sum_{x' \in \Lambda} \langle \sigma(x'_0, x_1, x_2) \sigma(x'_0, x_1 + x'_1, x_2 + x'_2) \rangle . \quad (6.19)$$

This correlator now depends on both spatial directions and we compute it, as before, in order to search for potential inhomogeneities. As in Chapter 5, oscillations present on the level of individual configurations would cancel each other in the naive expectation value $\langle \sigma(x) \rangle$, but should be captured by $C_{\sigma\sigma}$.

In order to set the scale in our computations we use the definition

$$\sigma_0 := \langle |\bar{\sigma}| \rangle \Big|_{B=0, \mu=0, T=T_0}, \quad (6.20)$$

i.e., the value of the chiral condensate for vanishing magnetic field and chemical potential and for the lowest temperature considered, $T_0 \approx 0$. As was outlined in [105], we use two different scale-setting temperatures for our infinite-volume and continuum extrapolations, respectively. The reason for this is that we would like to set the scale at as low a temperature as possible, while at the same time keeping T_0 constant in the two respective limits $V \rightarrow \infty$ and $a \rightarrow 0$. As before, since we can express the lattice spacing in units of σ_0 (and vice-versa) via the dimensionless combination $a\sigma_0$, we approach the continuum limit by tuning the coupling g^2 in (6.14) to smaller values of $a\sigma_0$ and control the temperature by changing N_t at a fixed lattice spacing.

We mention that there is no complex-action problem in our simulations provided that either $B = 0$ or $\mu = 0$, which we show in Appendix E. In the case where both B and μ are non-vanishing, a complex-action problem is present but under control for the order parameter $\langle |\bar{\sigma}| \rangle$, as is also discussed in Appendix E.

6.4 Tests and cross-checks

Having tested the applicability of the overlap operator and its limits in the context of non-interacting fermions in Section 4.4 and having studied its spectral properties in Section 6.2, we present here a number of additional numerical tests, performed in the full interacting theory of interest, i.e., the GN model in $2 + 1$ dimensions, governed by the lattice action (6.14)

6.4.1 Dyson-Schwinger equation

First and foremost, it is important to verify that the DSE (6.13) is indeed fulfilled, such that we can reliably use $\langle |\bar{\sigma}| \rangle$ as an order parameter for chiral symmetry breaking in the discretized theory. To this end we compare $\langle |\bar{\sigma}| \rangle$ with the corresponding fermionic observable, i.e., the absolute value of (4.28),

$$\langle |\langle \bar{\psi}\psi \rangle| \rangle_{\text{ov}} := \frac{1}{V} \left| \text{tr} \left[\left(\mathbb{1} - \frac{a}{2} D_{\text{ov}}^{(0)} \right) D^{-1} \right] \right|, \quad (6.21)$$

with D given in (6.11). Since the computation of $\langle |\langle \bar{\psi}\psi \rangle| \rangle_{\text{ov}}$ is much more expensive numerically, we only consider small lattices with $N_s = 8$ for this discussion. In Fig. 6.5 we show $\langle |\bar{\sigma}| \rangle$ and $\langle |\langle \bar{\psi}\psi \rangle| \rangle_{\text{ov}}$ for different values of the coupling g^2 and the control parameters T , B and μ .

We make the following observations: On cubic lattices, i.e., when $N_t = N_s$, the DSE

6. Magnetic Catalysis

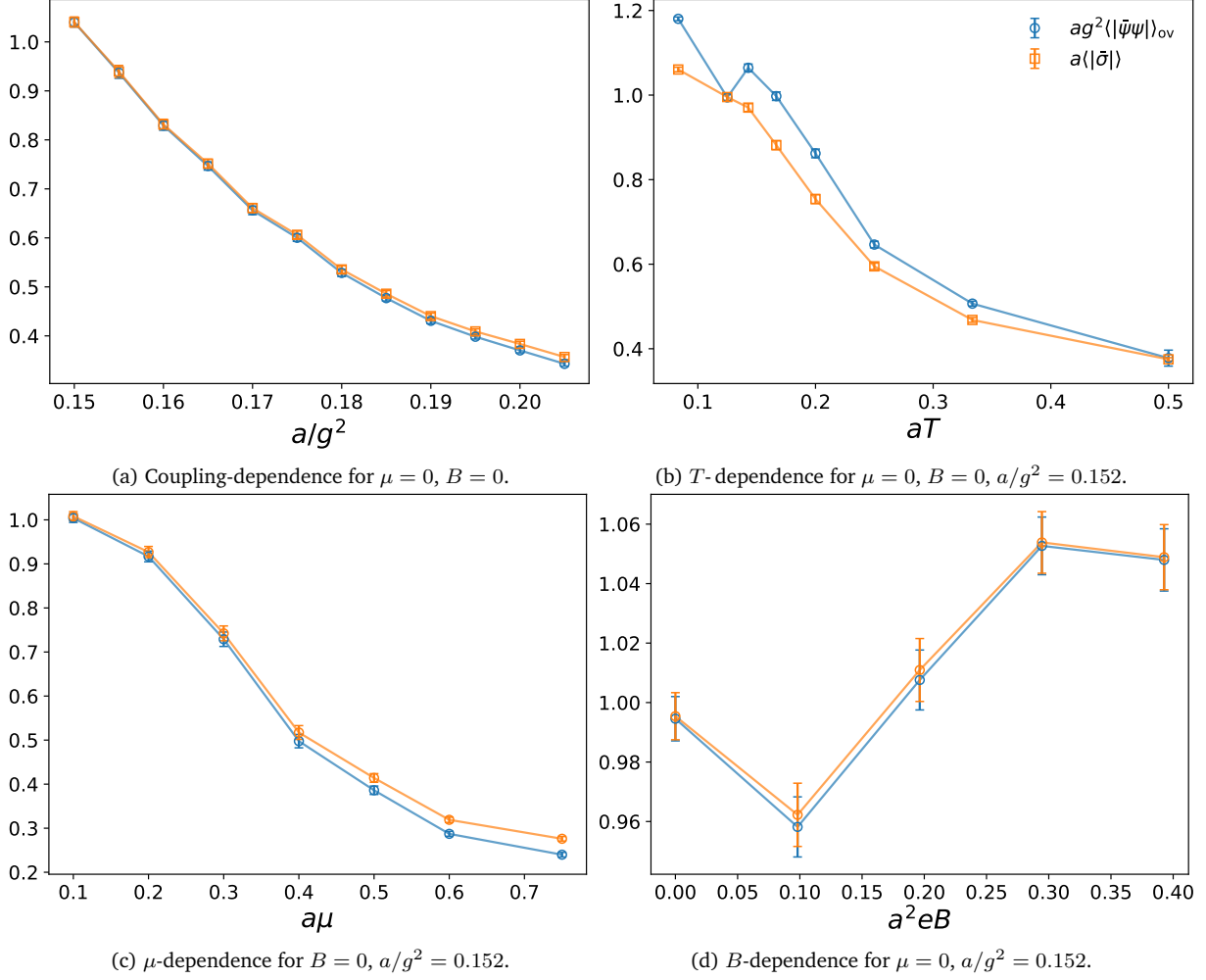


Figure 6.5: Comparison between the left-hand (blue) and right-hand (orange) sides of the DSE $g^2\langle|\bar{\psi}\psi|\rangle_{\text{ov}} = \langle|\bar{\sigma}|\rangle$ as a function of different control parameters and for $N_s = 8$. Except for Fig. 6.5b, we always consider cubic lattices, i.e., $N_t = N_s$.

is fulfilled very well for all values of g^2 , μ and B considered, the deviations growing somewhat larger for weak couplings and large μ . When N_t and N_s do not agree, however, i.e., when we investigate the T -dependence of the observables in Fig. 6.5b, the disparity is more severe. Curiously, $\langle|\bar{\psi}\psi|\rangle_{\text{ov}}$ and $\langle|\bar{\sigma}|\rangle$ appear to agree only for the second-to-lowest and the highest temperature considered, corresponding to the cubic lattice ($N_t = 8$) and $N_t = 2$, respectively. The non-monotonic behavior of the fermionic observable with T appears particularly odd, while $\langle|\bar{\sigma}|\rangle$ behaves as one would expect. While we do not have an explanation for the T -dependence of $\langle|\bar{\psi}\psi|\rangle_{\text{ov}}$, we remark that its overall behavior is nonetheless comparable to that of the bosonic observable. Since the latter is also more plausible from a physical point of view, we conclude from Fig. 6.5 that $\langle|\bar{\sigma}|\rangle$ is a reasonable order parameter for our purposes overall. We note that in the remainder of this section all results at low temperature are obtained on cubic lattices, in which case the disparity is of no concern either way.

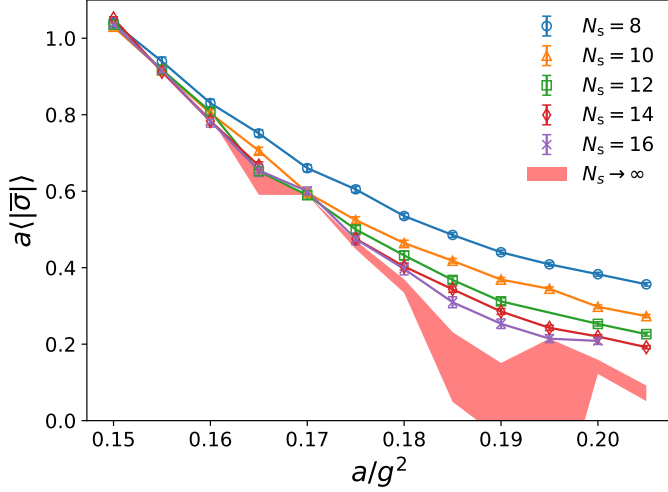


Figure 6.6: Coupling-dependence of the order parameter for different lattice volumes, as well as an infinite-volume extrapolation.

6.4.2 Critical exponents

As a further non-trivial test of the lattice action (6.14), we once again investigate the dependence of the order parameter on the coupling g^2 . It is well known that, while at low temperatures chiral symmetry is spontaneously broken in the strong-coupling regime, the system undergoes a phase transition to a chirally symmetric phase when the coupling is weakened below a critical value g_c^2 . As we have remarked before, on a finite volume this will not be a phase transition in the strict thermodynamical sense, but it should approach a real transition in the infinite-volume limit. In the vicinity of this transition the physical properties of the system are governed by its critical exponents. In particular, one expects a finite-size scaling law of the following form for the chiral condensate:

$$\langle |\bar{\sigma}| \rangle = \alpha + \gamma L^{-\kappa}, \quad (6.22)$$

where the parameters α , γ and κ in general depend on the coupling. Near the phase transition α vanishes and κ is related to the critical exponents β and ν of the order parameter and the correlation length, respectively, via

$$\kappa|_{g^2=g_c^2} = \frac{\beta}{\nu}. \quad (6.23)$$

In order to compare with the existing literature on the GN critical exponents, an extrapolation to the thermodynamic limit of the coupling-dependence of the chiral condensate is shown in Fig. 6.6. We find that the critical coupling of the phase transition likely lies somewhere between $a/g^2 = 0.188$ and $a/g^2 = 0.198$, giving rise to a very rough weighted estimate for the ratio of the critical exponents, $\frac{\beta}{\nu} = 0.9(3)$. While this measurement is certainly not competitive with state-of-the-art investigations, it is nonetheless compatible with estimates from dedicated methods, summarized, e.g., in [327], which also contains a list of relevant references. The various estimates for $\frac{\beta}{\nu}$ range from about 0.74 to roughly 1.01. This agreement is a strong indication that our overlap

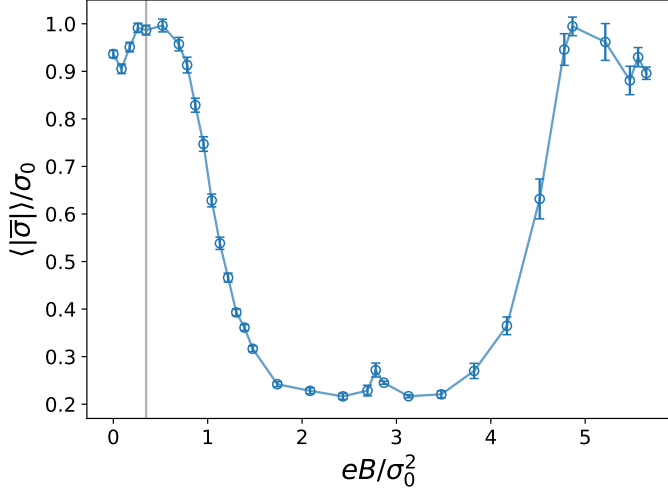


Figure 6.7: Chiral condensate for values of b between 0 and N_s^2 . The vertical line corresponds to $b = \frac{N_s^2}{16}$. $N_s = N_t = 8$, $a\sigma_0 \approx 1.063$.

formalism is capable of capturing the correct physics.

6.4.3 Saturation effects

Finally, we aim at obtaining a better understanding of the limits of the magnetic fields we can simulate in our lattice setup. As we have remarked in Section 4.3, our formulation is periodic in the flux quantum b with a periodicity given by N_s^2 , but one should expect saturation effects to set in and reduce the effective range of b that gives rise to physically sensible results [197, 198]. In order to estimate this range we show in Fig. 6.7 the B -dependence of the chiral condensate for values of b between 0 and N_s^2 on a lattice with $N_s = N_t = 8$. Indeed, the expected periodicity in B , as well as the resulting reflection symmetry $b \rightarrow N_s^2 - b$ [197] is observed. However, the largest part of Fig. 6.7 is governed by unphysical saturation effects. In order to avoid them we shall thus impose by hand the restriction $b \leq \frac{N_s^2}{16}$, indicated by the vertical line in Fig. 6.7, on the magnetic flux quantum number in all of our subsequent investigations, allowing us to study continuum physics.

With the findings presented in this section we are confident in our choice of lattice action for a broad range of values of B , T and μ , respectively, and we shall now turn towards the discussion of our main results.

6.5 Results for vanishing magnetic field

In the remainder of this chapter we present the results of extensive lattice simulations of the $(2+1)$ -dimensional GN model using $N_f = 1$ flavor of four-component overlap fermions. In this section we investigate the influence of finite temperature and chemical potential on the order parameter at vanishing magnetic field, providing estimates for the critical temperature T_c and the chemical potential μ_c of the chiral phase transition. Afterwards, we turn to the study of finite magnetic fields in the subsequent sections.

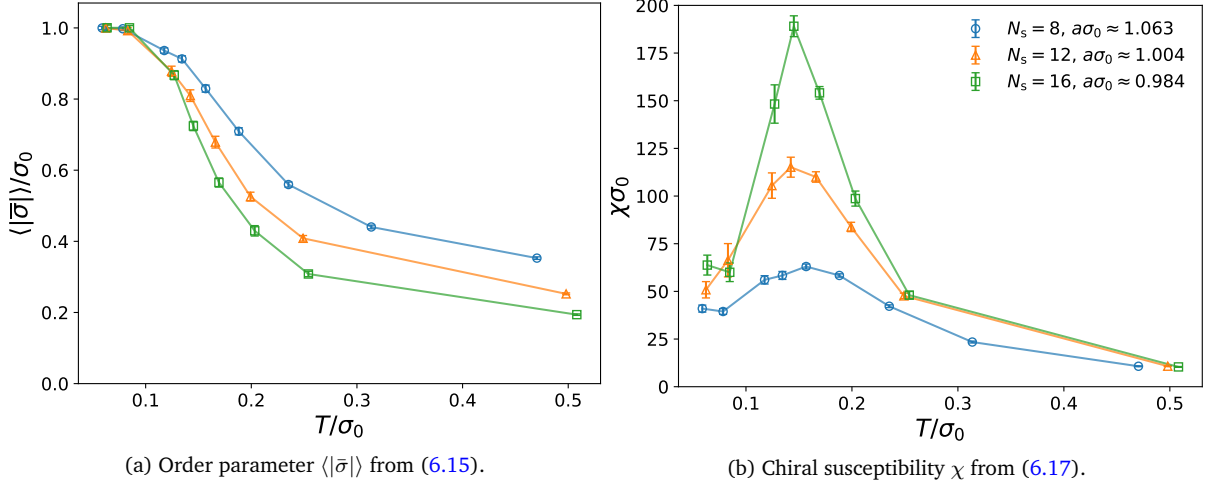


Figure 6.8: T -dependence of the chiral condensate and the chiral susceptibility for different physical volumes and constant lattice spacing.

While the main interest in this chapter shall be the determination of the phase structure of the one-flavor model, we also investigate whether a combination of finite flavor number, volume, temperature, chemical potential and magnetic field may induce spatial inhomogeneities in $2 + 1$ dimensions.

6.5.1 Vanishing chemical potential

We begin by studying the T -dependence of the chiral condensate at vanishing B and μ for different physical volumes. The corresponding results are shown in Fig. 6.8a. First of all, one observes that the chiral condensate decreases monotonically with the temperature, albeit to a non-zero value, due to the definition of the order parameter as $\langle |\bar{\sigma}| \rangle$. As expected, the transition in T becomes more pronounced for larger volumes, while the non-vanishing tails at high temperatures decrease in value. These observations are thus consistent with the presence of a phase transition in the thermodynamic limit. From the mean-field analysis of Section 3.3 one expects this transition to be of second order and our data suggest that this is indeed the case.

Let us now estimate the critical temperature T_c of this transition. Since we work with $N_f = 1$, we expect strong quantum fluctuations to be present in the system, which should generically reduce or even destroy any sort of long-range order. One thus conjectures that the extent of the phase of spontaneously broken chiral symmetry should shrink considerably when compared to the mean-field limit, where $T_c/\sigma_0 = \frac{1}{2 \ln 2} \approx 0.72$. In Fig. 6.8b we show the chiral susceptibility (6.17) as a function of T for different physical volumes. We observe a peak in χ , which becomes sharper as N_s increases while moving slightly to lower temperatures. For the largest volume considered we estimate $T_c/\sigma_0 \approx 0.145$. Compared to the mean-field result, this value is smaller by roughly a factor of 5.

For comparison, we compute another estimate for T_c , obtained by studying the finite-

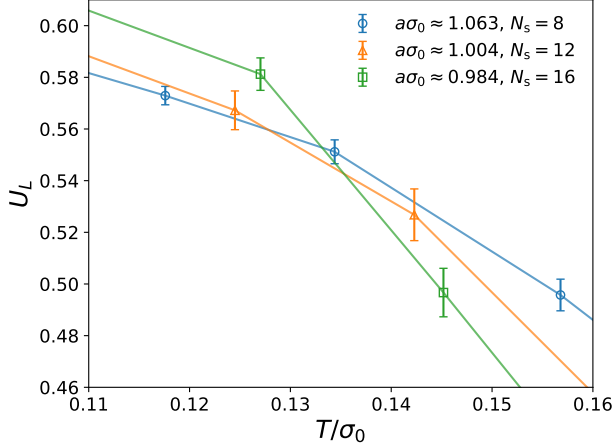


Figure 6.9: T -dependence of the Binder cumulant U_L from (6.18) for different physical volumes and constant lattice spacing.

size scaling of the Binder cumulant (6.18), whose T -dependence is shown in Fig. 6.9. Since we can only consider rather small volumes in our simulations, the finite-size analysis of U_L is not very reliable on its own. Indeed, it can be seen that the curves for different N_s in Fig. 6.9 do not yet intersect each other in a single point. We extract a rough estimate of $T_c/\sigma_0 \approx 0.135$ but note that the true result is likely larger than that, which is also consistent with the above estimate obtained from χ . We thus conclude that the critical temperature, extrapolated to the thermodynamic limit, likely lies between these two values, i.e., $T_c/\sigma_0 = 0.140(5)$.

We now study the continuum limit of these results. To this end, we show $\langle |\bar{\sigma}| \rangle$ and χ as functions of T for decreasing lattice spacing at (approximately) fixed physical volume in Figs. 6.10a and 6.10b, respectively. One observes that the behavior of the order parameter shows little change in this limit, indicating that we are already quite close to simulating continuum physics. The fact that the green curve in Fig. 6.10a, corresponding to the smallest lattice spacing considered, deviates from the other ones is likely due to the scale-setting being slightly off in this case, resulting in different physical volumes for the different lattice spacings. To be more specific, while we double the number of lattice sites in each spatial direction when going from $N_s = 8$ to $N_s = 16$, the corresponding lattice spacings differ from each other by slightly more than a factor of 2 and thus the physical volumes are not the same. On the other hand, within error margins the critical temperature determined from Fig. 6.10b remains constant for all lattice spacings considered. We remark that the physical volume considered in Fig. 6.10 corresponds to the smallest volume shown in Fig. 6.8.

6.5.2 Finite chemical potential

Having studied the effects of non-zero temperature on the order parameter, we now turn to the finite-density case. In particular, we study the μ -dependence of $\langle |\bar{\sigma}| \rangle$ at low temperatures. Phenomenologically, high enough densities can be expected to have the same disordering effect as high temperatures, i.e., restore chiral symmetry. We show the

6. Magnetic Catalysis

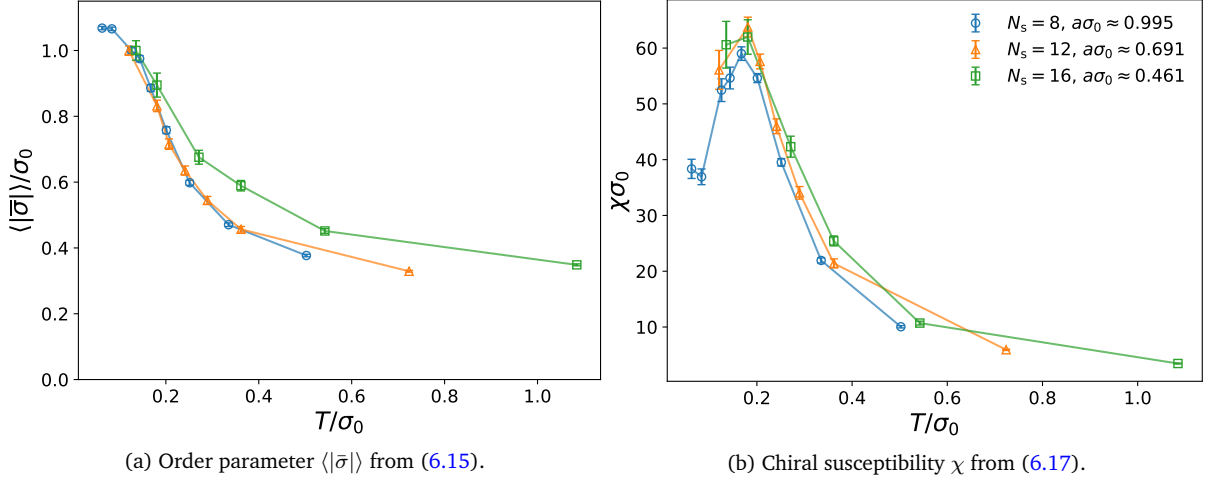


Figure 6.10: T -dependence of the chiral condensate and the chiral susceptibility for different lattice spacings and constant physical volume.

chiral condensate as a function of the chemical potential for different physical volumes in Fig. 6.11a. We see that, as before, the phase transition becomes sharper with larger volumes. Notice, however, that we work on cubic lattices here, i.e., $N_s = N_t$, such that the temperature decreases as we approach the thermodynamic limit. Based on the infinite-volume mean-field results of Section 3.3, one expects a strong-second order transition since we work at low but non-vanishing temperatures. However, as we have outlined in Section 3.6, the restriction of the model to finite volumes might cause the transition to be discontinuous even at non-zero T .

Before discussing this issue in more detail in subsequent paragraphs, we mention that the susceptibility (6.17), shown in Fig. 6.11b, also exhibits a peak as a function of μ , growing with N_s . For the largest volume considered we can read off a value for the critical chemical potential of $\mu_c / \sigma_0 \approx 0.3$. Compared to its mean-field value of $\mu_c = \sigma_0$, it is smaller by about a factor of 3. Thus, the phase of spontaneously broken chiral symmetry shrinks in both the T - and the μ -direction when comparing $N_f = \infty$ with $N_f = 1$. However, it is worth noting that T_c and μ_c at $N_f = 1$ deviate from their respective large $-N_f$ counterparts by different factors, contrary to what one could have naively anticipated. This makes it harder to draw quantitative conclusions from the large $-N_f$ limit.

In order to distinguish between a first- and a second-order transition in our system it is not sufficient to investigate the behavior of the order parameter as shown in Fig. 6.11a. The reason for this is as follows: In an ergodic simulation two (almost-)degenerate minima of the effective action are sampled with an (almost) equal probability. If one first simulates the system in a phase of broken symmetry, where the global minimum is non-trivial, and then subsequently approaches the symmetric phase by appropriately tuning the control parameters, a third minimum, namely the trivial one, will become relevant at some point if the transition is of first order. This emergence of a mixed phase

6. Magnetic Catalysis

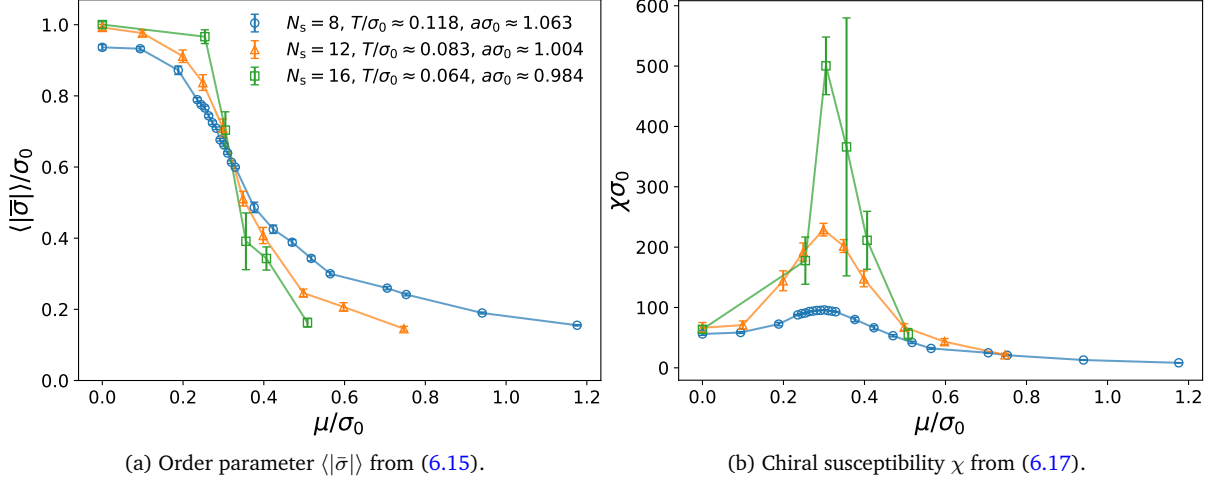


Figure 6.11: μ -dependence of the chiral condensate and the chiral susceptibility for different physical volumes of cubic lattices ($N_s = N_t$) and constant lattice spacing.

then leads to an overall decrease of the order parameter, which is, however, smooth on small volumes, complicating the determination of the order of the transition. On larger volumes, on the other hand, the minima become deeper and tunneling between them is generically less likely. A realistic simulation will thus be less prone to sampling a sub-dominant minimum, which leads to the transition in Fig. 6.11a becoming sharper for larger N_s .

The above discussion makes clear that one should rather investigate the action itself, as the presence of two or more degenerate non-trivial minima, separated by a barrier, is a clear indication for a first-order transition in the thermodynamic limit. To this end, we have computed histograms of time-series of $\bar{\sigma}$, which reflect the probability distributions $\frac{e^{-S_{\text{eff}}}}{Z}$ for various chemical potentials. We show the logarithm of the distributions obtained in this way (divided by the lattice volume and normalized to 0 at $\bar{\sigma} = 0$) on our smallest lattice in Fig. 6.12. The error estimates are obtained by computing the effective action on every jackknife ensemble and performing the usual jackknife analysis on the result. In passing we note that the results shown in Fig. 6.12 correspond to the so-called *constraint effective potential* [328].

Clearly, there are two non-trivial minima and no trivial minimum present for $\mu/\sigma_0 \approx 0.282$, which indicates the spontaneous breakdown of the \mathbb{Z}_2 chiral symmetry. For $\mu/\sigma_0 \approx 0.301$, on the other hand, the additionally emerging trivial minimum becomes degenerate with the non-trivial ones. Lastly, for $\mu/\sigma_0 \approx 0.376$ only the minimum at $\bar{\sigma} = 0$ is left, i.e., the system is in the symmetric phase. The described behavior is striking evidence for a first-order phase transition in μ , as one would have predicted based on the discussion in Section 3.6. Curiously, this can be observed already on our smallest lattice, while conventionally one first extrapolates to the thermodynamic limit in order to study phase transitions. Due to limited statistics an equally detailed analysis was not possible for our larger lattices, but our data indicate that the nature of the transition

6. Magnetic Catalysis

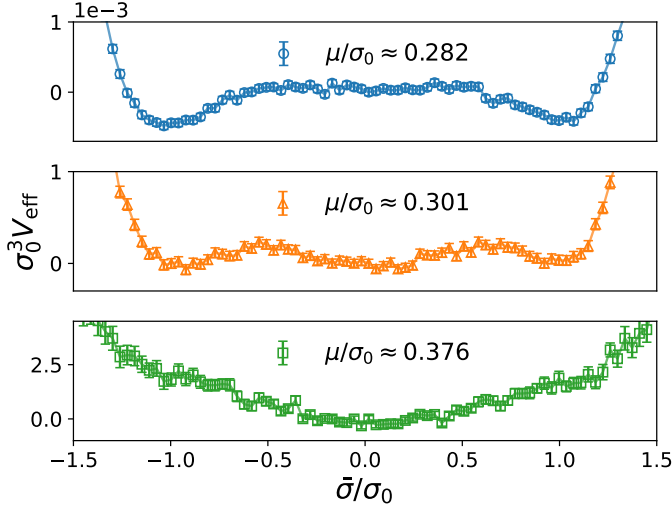
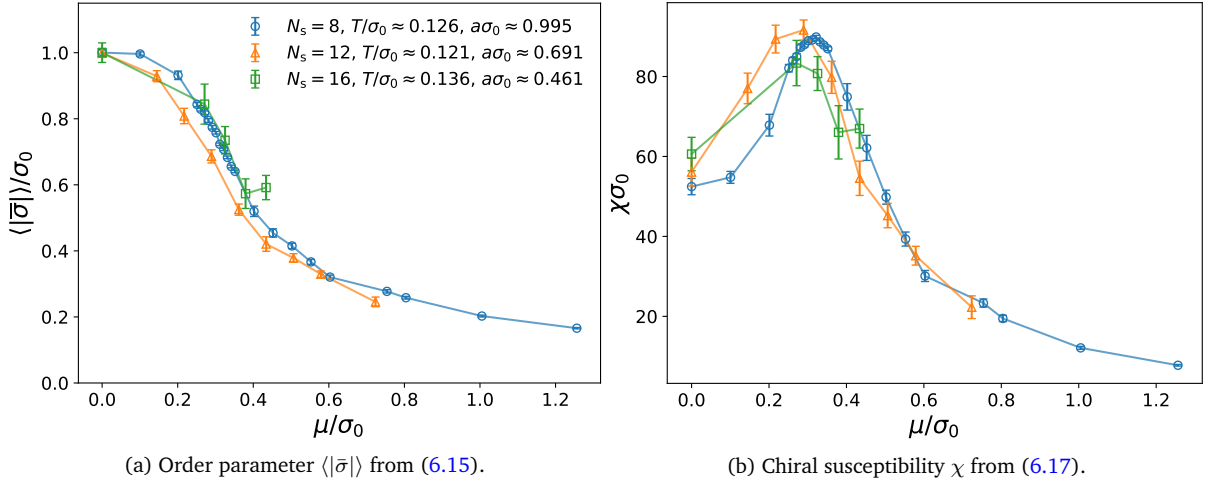


Figure 6.12: (Constraint) effective potential, normalized to zero at $\bar{\sigma} = 0$, for different chemical potentials. See the main text for details. $N_s = N_t = 8$, $a\sigma_0 \approx 1.063$, i.e., $T/\sigma_0 \approx 0.118$.

does not change as we approach the thermodynamic limit. We mention that indications for a first-order transition in the model were also found in the lattice study [329]. This behavior was later explained by studies employing the optimized perturbation theory (OPT) technique [330] to be a result of going beyond the mean-field limit [331, 332]. As we have seen in Section 3.6, however, a first-order transition can even be observed in the mean-field limit, provided that one considers a finite volume. In the next section we study how this behavior is affected by non-zero magnetic fields.

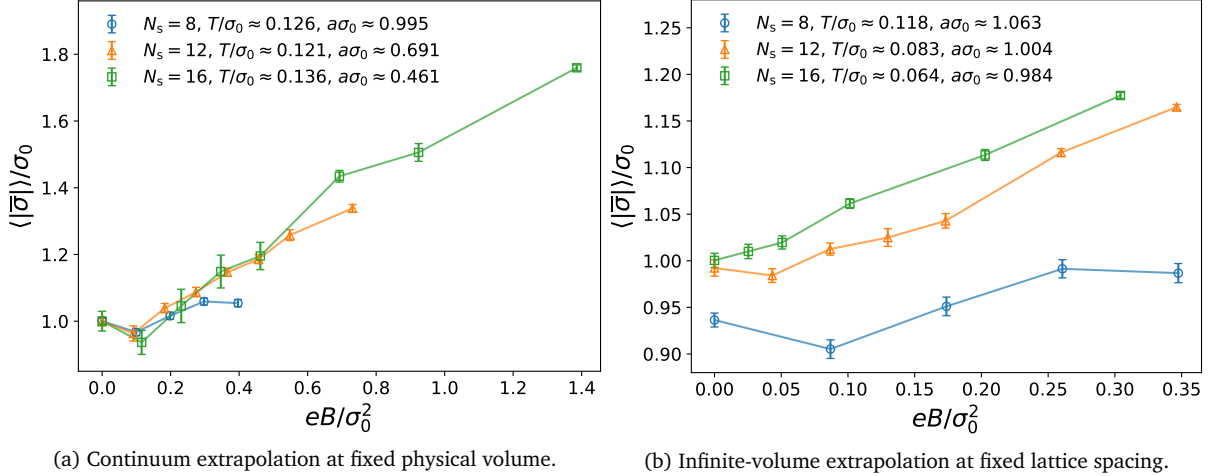
Before that, however, we provide for completeness a continuum extrapolation at fixed volume of the μ -dependence of $\langle |\bar{\sigma}| \rangle$ and χ in Figs. 6.13a and 6.13b, respectively. As above, we observe little change as the lattice constant is altered, providing further evidence that the system under consideration is not too far from the continuum limit.



(a) Order parameter $\langle |\bar{\sigma}| \rangle$ from (6.15).

(b) Chiral susceptibility χ from (6.17).

Figure 6.13: μ -dependence of the chiral condensate and the chiral susceptibility for different lattice spacings and constant physical volume on cubic lattices ($N_s = N_t$).


 Figure 6.14: B -dependence of the chiral condensate on cubic lattices ($N_s = N_t$).

6.6 Results for finite magnetic field

Let us now incorporate a non-zero background magnetic field B into our study. In light of the mean-field discussion of Chapter 3 we are led to expect a rich phase structure in (B, T, μ) space and we discuss in this chapter whether this is indeed true beyond the mean-field limit. We are predominantly interested in the dependence of the order parameter on the magnetic field, but we also study how the critical temperature and the critical chemical potential are affected and we search for remnants of multiple phase transitions due to the emergence of Landau levels.

6.6.1 Vanishing temperature and chemical potential

To begin with, we show a continuum extrapolation of the chiral condensate as a function of the background magnetic field for low temperatures and vanishing chemical potential in Fig. 6.14a. What is perhaps most striking is the non-monotonicity of the order parameter in B , as $\langle |\bar{\sigma}| \rangle$ exhibits a dip for the weakest non-vanishing magnetic field, i.e., the one corresponding to $b = 1$ in (3.4). We have previously discussed this feature in the context of a non-interacting theory in Sections 3.1 and 6.2 and we see here that it can still be observed when interactions are taken into account. We emphasize once more that this is not a discretization artifact, as it occurs in the continuum theory as well. Thus, it should be regarded as a physical feature that is present on finite volumes.

Apart from this dip the behavior of the condensate with B is as expected in that the magnetic field induces a monotonic increase of $\langle |\bar{\sigma}| \rangle$, which amounts to the phenomenon of magnetic catalysis. It is interesting to observe that the condensate for $b > 1$ seems to have a roughly linear dependence on the magnetic field, much like it does in the two-dimensional free theory setup discussed in Sections 3.1 and 6.2. This is in contrast to the mean-field expectation (6.1), predicting a quadratic increase in B in the strong-

coupling regime we investigate here. Only for the case of weak couplings does the order parameter grow linearly with B in the large $-N_f$ limit.

In Fig. 6.14b we show the B -dependence of the order parameter for different physical volumes and fixed lattice spacing. The aforementioned non-monotonicity clearly disappears on larger volumes and for $N_s = 16$ we observe pure magnetic catalysis for every value of B . This proves that the contributions to $\langle |\bar{\sigma}| \rangle$ that cause the dip are suppressed in the thermodynamic limit, just as in the non-interacting case. As we have discussed earlier, these contributions are likely due to low eigenmodes of the Dirac operator.

6.6.2 Finite temperature and vanishing chemical potential

Let us now investigate the influence of a non-zero magnetic field on the finite-temperature behavior of the chiral condensate. From the QCD point of view this study provides a non-trivial comparison, as the behavior of QCD in background magnetic fields close to the chiral cross-over temperature is well understood by now. We emphasize at this point once more the fact that we do not seek to employ the $(2 + 1)$ -dimensional GN as a realistic model that should reliably reproduce all QCD phenomenology without any sort of modifications. Rather, this study should be regarded as a first step into the direction of the long-term goal of approaching QCD from the perspective of simple model theories beyond the mean-field limit. The GN model, being the simplest 4FT, was chosen in order to assess the qualitative differences one should expect to arise when going beyond the mean-field limit in a generic theory of interacting fermions. However, it also allows us to better understand to which extent the qualitative differences between QCD and model theories are reflected on the level of observables.

In order to study the effects of a background magnetic field on the finite-temperature GN model, we plot phase diagrams in the (B, T) plane for different physical volumes in Fig. 6.15. These phase diagrams should be contrasted with the analogous infinite-volume mean-field result shown in Fig. 3.5a. We indicate the rough estimates for the critical temperature at $B = 0$ and $N_s = 16$, obtained previously via the chiral susceptibility and the Binder cumulant, respectively, as the gray bands in Fig. 6.15.

One observes that for all temperatures below T_c the magnetic field has a clear tendency to increase $\langle |\bar{\sigma}| \rangle$, apart from the aforementioned finite-size effects, which disappear on our largest lattice. This is in agreement with the mean-field picture, stating – in essence – that the competition between T and B is relatively uncomplicated: higher temperatures destroy the order via thermal fluctuations, while stronger magnetic fields restore the order via misaligning the spins of the fermions and anti-fermions comprising the chiral condensate. The interplay between the two control parameters T and B is thus very much straightforward and expected both in the mean-field limit and beyond.

Above the phase transition at $T = T_c$ the magnetic field ceases to have a noticeable effect on the order parameter. This is also consistent with the expectation, as it is no

6. Magnetic Catalysis

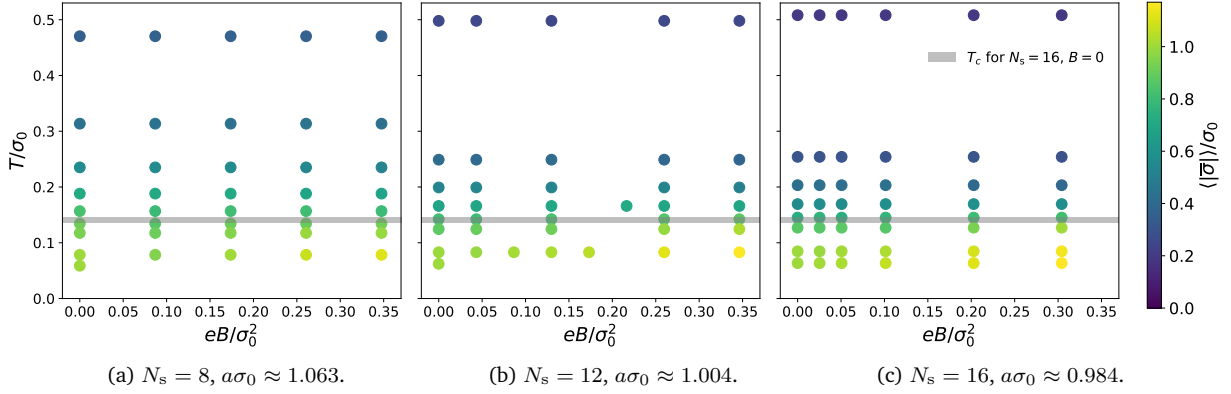


Figure 6.15: Phase diagram in the (B, T) plane for different physical volumes and constant lattice spacing. The gray bands indicate the critical temperature for $N_s = 16$ and $B = 0$, see the main text for details.

different in the mean-field limit. One might be tempted to think that, since $\langle |\bar{\sigma}| \rangle$ does not vanish beyond T_c , one should expect to observe magnetic catalysis in that region as well. However, what we really measure in the symmetric phase is the modulus of fluctuations of $\bar{\sigma}$ around zero. Such fluctuations should be less affected by the magnetic field and our data indeed support this picture. The critical temperature itself remains approximately constant as a function of B in all of Fig. 6.15.

Notice, however, that the magnetic fields we can consider in our setup for fixed a are rather weak. In order to study stronger fields (in units of σ_0^2), we approach smaller lattice spacings at a fixed physical volume in Fig. 6.16. The thick gray lines are a rough estimate for the B -dependence of the critical temperature, obtained here via the chiral susceptibility only. To be precise, we determine the peak of χ for every value of B considered and use the peak position as an estimate for T_c . If this is not possible unambiguously within errors we quote the mean value of the competing peak positions as the critical temperature instead. With this very crude estimate we find that the critical temperature increases slightly for the strongest magnetic fields considered. Comparing with Fig. 3.5a, where the critical temperature starts to increase noticeably at around $eB/\sigma_0^2 \approx 0.8$, our findings are in accordance with the mean-field results. Albeit being a relatively weak statement, this nonetheless once again suggests that the phase structure beyond the mean-field limit cannot simply be obtained from the large- N_f results via re-scaling them by some uniform N_f -dependent scaling factor. We have seen that one would, e.g., require different such factors for scaling T_c and μ_c , respectively.

Not taking into account the finite-size effects leading to a dip in $\langle |\bar{\sigma}| \rangle$ for $b = 1$, all of our data are consistent with the picture of magnetic catalysis beyond T_c , i.e., there do not appear to be any signs of inverse magnetic catalysis within the region of broken chiral symmetry. Beyond T_c , we once again find the condensate to be independent of B . These results show that the finite-temperature behavior of the $(2 + 1)$ -dimensional GN model in a magnetic field is qualitatively different from the analogous situation in QCD, where inverse magnetic catalysis governs the region around the chiral cross-over. This

6. Magnetic Catalysis

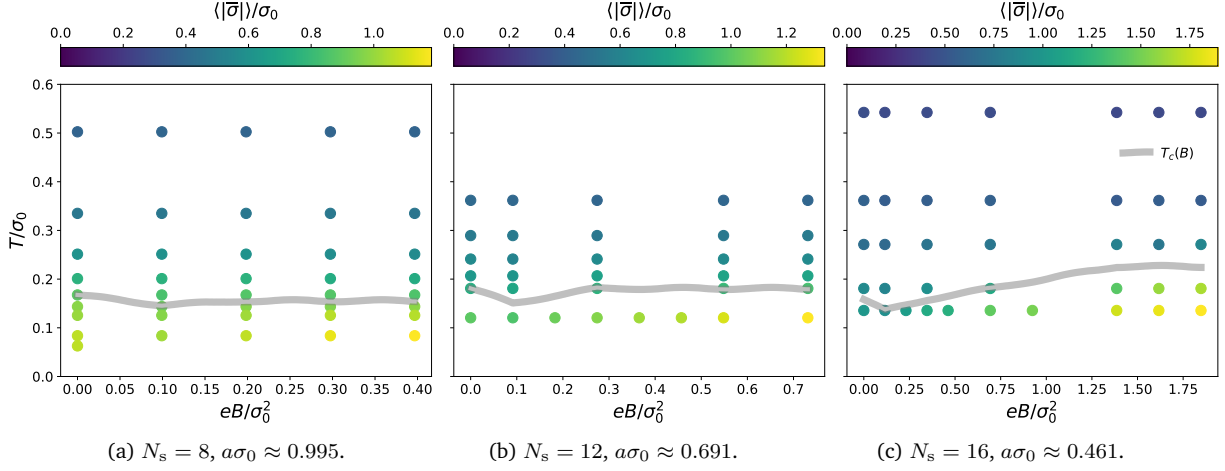


Figure 6.16: Phase diagram in the (B, T) plane for different lattice spacings and constant physical volume. The gray bands indicate a rough estimate for the critical temperature, see the main text for details. Notice the different x -axis and color map scales.

observation lends further evidence to the claim that inverse magnetic catalysis in QCD is a gluonic effect, caused by the back-reaction of quarks onto the gluon distribution [279].

We emphasize that, while *a priori* there was no reason to believe that allowing for quantum fluctuations in the GN model should give rise to inverse magnetic catalysis at finite temperature despite its absence in the mean-field limit, the finite- N_f behavior of the model is not fully understood yet, especially for non-vanishing magnetic fields. A situation where fluctuations, having the tendency to restore chiral symmetry, could lead to a non-trivial interplay between the temperature and the magnetic field, resulting in non-monotonic behavior of the order parameter or a decrease of the critical temperature with B , was not inconceivable.

6.6.3 Low temperature and non-vanishing chemical potential

Finally, we turn to the case of finite μ and B , which is the most interesting case from the QCD perspective, as this regime is not accessible in Monte-Carlo simulations based on importance sampling. We shall only consider cubic lattices, i.e., low temperatures, for the remainder of this section.

In Fig. 6.17 we show the μ -dependence of $\langle |\bar{\sigma} \rangle$ for different magnetic field strengths and increasing physical volumes at fixed a . Investigating the data for $N_s = 8$ first, one observes that the – by now familiar – finite-size effects are also present at finite μ . Once again, they become less prominent on larger volumes, as expected. By and large, the μ -dependence of the order parameter seems to change little on a qualitative level when the magnetic field is switched on, as chiral symmetry is spontaneously broken at $\mu = 0$ and becomes restored for larger μ for all values of the magnetic field. This is true for all lattice sizes considered.

All of our data are fully consistent with the picture of magnetic catalysis everywhere

6. Magnetic Catalysis

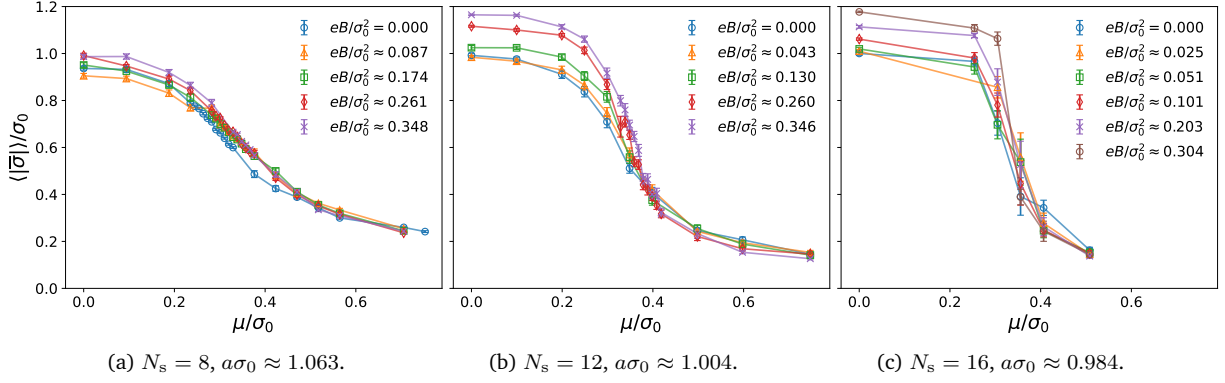


Figure 6.17: μ -dependence of the chiral condensate for different magnetic field strengths and physical volumes of cubic lattices ($N_s = N_t$) at constant lattice spacing.

below the phase transition at $\mu = \mu_c$. While some data points have overlapping error margins that would – in principle – also allow for the converse interpretation, we see no clear evidence for a decrease of the order parameter with B anywhere in our results. Making any precise statements on the largest lattice is less straightforward due to very limited statistics and the $N_s = 16$ results should rather be thought of as a rough consistency check. However, no clear evidence for inverse magnetic catalysis can be found there either. On the other hand, beyond the phase transition, where we again only measure the absolute value of fluctuations around $\bar{\sigma} = 0$, the magnetic field leaves the chiral condensate almost unaffected, which is expected and was also observed at the finite-temperature phase transition for $\mu = 0$ discussed above.

We have furthermore investigated the order of the phase transition in μ at finite B in analogy to Fig. 6.12. In Fig. 6.18 we show a comparison between the effective potential close to the phase transition in μ for different magnetic field strengths. The clear triple-minimum structure in V_{eff} is no longer observed at $B \neq 0$. While the data are consistent with the presence of a first-order transition for some values of B , at other points a strong second-order transition appears to be favored. From the point of view of the mean-field approach, this is not all that surprising. After all, there is a qualitative difference between $B = 0$ mean-field results on finite and infinite volumes,

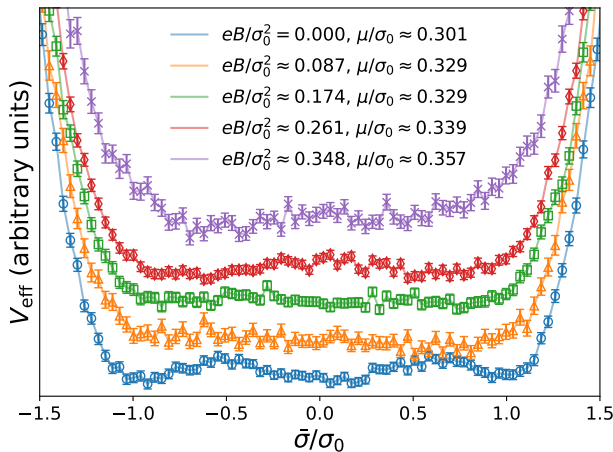


Figure 6.18: (Constraint) effective potential close to the phase transition in μ for different values of the magnetic field. The data are shifted vertically for visual clarity. $N_s = N_t = 8$, $a\sigma_0 \approx 1.063$, i.e., $T/\sigma_0 \approx 0.118$.

6. Magnetic Catalysis

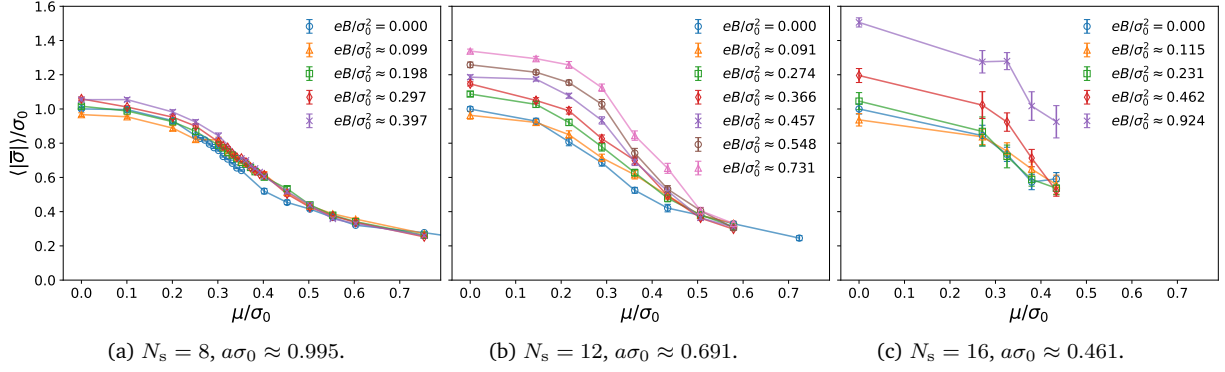


Figure 6.19: μ -dependence of the chiral condensate for different magnetic field strengths and lattice spacings at constant physical volume on cubic lattices ($N_s = N_t$).

see Section 3.6. On the contrary, the $B \neq 0$ effective potential is the same irrespective of the volume, the only distinction for different volumes being the different allowed values of B according to (3.4). By that, while one finds a first-order transition in mean-field for finite volumes and $B = 0$, switching on a sufficiently weak magnetic field could result in the phase transition being of strong second order instead. Our lattice results indicate that the transition indeed becomes weaker for non-vanishing B . As before, however, these investigations are really only conclusive on our smallest lattice for reasons of statistics.

We do not find any evidence for the presence of multiple phase transitions in μ , neither of first nor of second order. We emphasize, however, that our investigation cannot completely rule them out either. As we have mentioned earlier, the exact position of a phase transition is very difficult to estimate from the behavior of the order parameter alone and one should instead look for multiple minima of the effective potential. In particular, one should either search for signs of more than three simultaneous minima or for two non-adjacent values of μ which both exhibit three minima. While we do not find indications for either of these scenarios, our relatively coarse scan in μ might conceivably simply have missed them. After all, it is expected that multiple phase transitions – if present – happen in close succession.

Lastly, we once again consider smaller lattice spacings in order to study larger magnetic fields in units of σ_0^2 . The corresponding results are shown in Fig. 6.19. While finite-size effects are obviously more prominent here, all qualitative statements made above are still valid. There is no sign of inverse magnetic catalysis or of multiple phase transitions in μ . Instead, the magnetic field tends to enhance the breaking of chiral symmetry everywhere before it is restored in a (single) phase transition. Also note that the critical chemical potential increases with B , as can be seen from Fig. 6.18.

6.6.4 Search for inhomogeneities

While in $1 + 1$ dimensions inhomogeneous phases have been known to exist in 4FTs for a long time, see the discussion in Sections 5.1 and 5.2, the situation in $2 + 1$ dimensions

is less clear. It appears as if at $B = 0$ inhomogeneities can be found in the mean-field limit with certain lattice discretizations [122, 123]. These inhomogeneities, however, were shown to fully disappear once the cutoff is removed. There are no studies of inhomogeneities in the $(2 + 1)$ -dimensional GN model beyond the mean-field limit to be found to date, to the best of our knowledge. Moreover, there exist no studies, not even in the mean-field limit, on the question of whether a non-zero background magnetic field might induce such inhomogeneities in the model. We mention that, in spite of the assumption of the magnetic field to be homogeneous itself, this question is not necessarily obsolete. In fact, in some four-dimensional theories a non-zero magnetic field seems to favor inhomogeneous phases at finite density that would otherwise be disfavored [125–128].

The intuitive picture behind this is as follows: As we have discussed in Section 6.1, a strong enough magnetic field leads to a dimensional reduction of fermionic systems due to the LLL dominance. This means that a $(3 + 1)$ -dimensional theory in a strong magnetic field is to a certain degree equivalent to a $(1 + 1)$ -dimensional one at $B = 0$, where the remaining spatial direction, in which propagation is not suppressed, lies along the magnetic field. Now, as we have seen in detail in Chapter 5, fermionic theories in $1 + 1$ dimensions are prone to exhibit inhomogeneous structures, be it via perfect or quasi-long-range order. This means that one expects inhomogeneities to form along the magnetic field axis in $3 + 1$ dimensions, which is indeed the case according to [125–128].

In our $(2 + 1)$ -dimensional setup the interpretation is more difficult. Since the spatial motion of fermions only takes place in a two-dimensional plane perpendicular to the magnetic field, propagation along the magnetic field axis is prohibited altogether. For strong enough fields, the theory is then effectively $(0 + 1)$ -dimensional and the spatial propagation of fermions should be completely suppressed. It is not clear intuitively whether this situation could give rise to spatial (or, for that matter, temporal) inhomogeneities.

We now aim to fill this vacancy, thereby neatly bridging the gap between Chapter 5 and the present chapter. To this end, we employ the spatial correlation function $C_{\sigma\sigma}$ defined in (6.19). We have scanned our entire (B, T, μ) parameter space for possible traces of inhomogeneities, indicated by oscillating behavior of $C_{\sigma\sigma}$. Of course, the expectation is to find them at finite μ , if at all. In Fig. 6.20 we show the spatial correlation function for one exemplary data point at non-zero B and μ . One observes no sign for any inhomogeneous behavior and we have verified that this result is indeed representative for all parameter values we have considered in our simulations. This indicates that there are no inhomogeneities present in the GN model in $2 + 1$ dimensions at $N_f = 1$ even at finite lattice spacing, in contrast to earlier simulations at $B = 0$ using staggered fermions [333]. It would be interesting to study the mean-field limit of these results as well. Perhaps crystalline order can be found for large N_f and finite B and is only destroyed by bosonic quantum fluctuations.

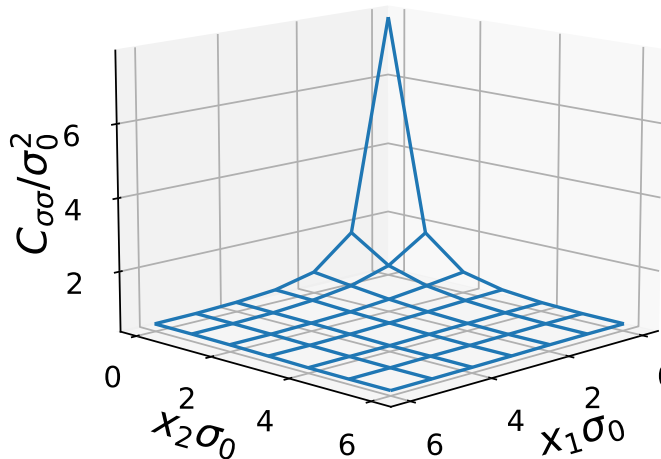


Figure 6.20: Spatial correlation function $C_{\sigma\sigma}(x_1, x_2)$ from (6.19) for $N_s = N_t = 12$, $T/\sigma_0 \approx 0.083$, $\mu/\sigma_0 \approx 0.349$, $eB/\sigma_0^2 \approx 0.346$ and $a\sigma_0 \approx 1.004$. Due to the lattice periodicity we only show half of each coordinate axis.

6.6.5 Comparison to the literature

Let us now compare what we have found in our $N_f = 1$ lattice simulations with the existing literature. We only know of one other work investigating the phase structure of the $(2 + 1)$ -dimensional magnetized GN model beyond the mean-limit, namely the OPT study [334]. There, it was found that the phase structure for finite flavor number is not so different from its mean-field counterpart, at least down to $N_f = 2$. In particular, multiple phase transitions in μ at finite B were found to still be present and inverse catalysis was even claimed to persist for arbitrarily strong magnetic fields beyond the large- N_f limit. Obviously, these results are at odds with ours.

In order to resolve this discrepancy, let us first make the following comments: To begin with, it seems questionable to us whether the leading-order OPT computation, giving corrections of $\mathcal{O}(N_f^{-1})$, is really reliable for $N_f = 2$. Assuming that it can indeed be trusted, there are a few important differences in the computation of [334] and the one presented here. For one, the OPT study is performed in the continuum and on an infinite volume, whereas we consider a lattice of finite extent. We see no reason to believe that the discretization should give rise to the discrepancy, as, after all, our continuum extrapolations seem rather stable. Finite-volume effects, on the other hand, are a different story, as they were shown in Section 3.6 to cause a qualitative difference in the mean-field theory, at least at $B = 0$. Still, for the aforementioned reasons finite-volume effects should play less of a role when the magnetic field is non-zero.

The fundamental difference we believe could be at the origin of the disagreement lies in the tacit assumption of homogeneity of σ , i.e., $\sigma(x) = \text{const.}$, in [334]. In our simulations, on the other hand, we allow for arbitrary fluctuations in σ on the level of individual configurations. While we do not observe inhomogeneities on the level of expectation values, the dynamics are clearly different when allowing for arbitrary bosonic quantum fluctuations and we believe that this crucial ingredient might explain the discrepancy between the OPT study and our results. More concretely, one may envision the following situation: We know from preliminary investigations discussed in

Section 6.2.1 that the overlap operator allows for a straightforward identification of the Landau level structure, at least in a theory of non-interacting fermions in two dimensions with periodic boundary conditions. Allowing for interactions introduces fluctuations in $\sigma(x)$ that will certainly wash out the well-separated Landau levels in Fig. 6.1a to a certain degree. If such fluctuations are strong enough, individual Landau levels might no longer be distinguishable at all. One may then conjecture that Landau-level-induced effects such as the multiple phase transition pattern can no longer be present once the separation between Landau levels tends to zero. Work in this direction is currently ongoing.

7 Conclusions & Outlook

In this thesis we have investigated two four-Fermi theories in low dimensions in detail, namely the chiral Gross-Neveu model (2.19) in $1 + 1$ dimensions and the Gross-Neveu model (2.20) in $2 + 1$ dimensions. It was the main goal of this thesis to perform lattice simulations at finite numbers of fermionic flavors in order to study the models beyond the mean-field limit, where they are understood best. Such a study is important due to the fact that realistic theories describing real physical systems most likely require a treatment that goes beyond the mean-field limit. Since in the latter one observes a plethora of non-trivial physical effects in the models studied here, a central goal of this thesis was to elucidate to which extent these effects are left intact by fluctuations.

In particular, it has been known for some time that two-dimensional 4FTs in the mean-field limit can develop inhomogeneous phases, where the chiral condensate (as an order parameter for chiral symmetry breaking) acquires a non-trivial space-dependence. We devoted Chapter 5 to a lattice study, using SLAC fermions, of the $(1 + 1)$ -dimensional χ GN model for low flavor numbers, $N_f = 2$ and $N_f = 8$. We find that, indeed, inhomogeneities are present in the system even beyond the mean-field limit and presumably persist when the lattice spacing approaches zero. We have emphasized that our results should not be interpreted as signs for the spontaneous breakdown of some continuous symmetry, be it chiral symmetry or translations. Rather, we believe that correlations in our setup decay to zero for large enough distances. For temperatures close to zero this decay is likely algebraic, in accordance with the existence of a BKT phase. Thus, our results are not in conflict with the CHMW theorem.

Moreover, we have mapped out the parameter space spanned by the temperature and the chemical potential to see how the existence or non-existence of inhomogeneities depends on these control parameters. We have found that for low temperatures and large enough μ inhomogeneities always exist on some length scale. For very small μ , on the other hand, the wave-length of chiral-spiral-like configurations exceeds the spatial extent, such that inhomogeneities cannot form. Despite bosonic fluctuations altering the mean-field picture quantitatively, we still observe remnants of the large- N_f phase structure in our results. One way of interpreting inhomogeneous structures is to investigate the constraint potential [328], whose flat regions have been linked to the presence of inhomogeneous field configurations [335], the constraint itself being enforced in $1 + 1$ dimensions by the CHMW theorem.

The main focus of this thesis, however, was the study of the $(2 + 1)$ -dimensional GN model exposed to a background electromagnetic field. In Chapter 3 we provided a detailed study of the model in the large- N_f limit, discussing the combined effects of

non-zero temperature, magnetic field and chemical potential on the chiral condensate. While for $\mu = 0$ the magnetic field causes an enhancement of chiral symmetry breaking, termed magnetic catalysis, the phase structure at finite chemical potential is highly non-trivial. Due to the emergent Landau-level structure, which becomes especially important for weak magnetic fields, one observes multiple phase transitions in μ . Moreover, one finds that the critical chemical potential, corresponding to the chiral phase transition, is non-monotonic in B . Similar results can be found when considering the model on a finite volume. In particular, the quantization of spatial momenta on finite volumes can induce first-order transitions in the system even at finite temperature, in close analogy to the effects induced by the Landau quantization.

We then proceeded to study the model on the lattice for $N_f = 1$ flavor of reducible fermions, using the overlap formalism, in Chapter 6. Our simulations were thus performed as far away from the mean-field limit as possible. We found that the GN model shows qualitatively different behavior beyond the mean-field limit. In particular, we did not find any traces of inverse magnetic catalysis or multiple phase transitions. On the contrary, within the region of spontaneously broken chiral symmetry, which increases in size with B , we found that the magnetic field only enhances chiral symmetry breaking. Moreover, finite-size effects were identified and their origins explained. For $B = 0$, on the other hand, we confirmed the existence of a first-order transition in μ at low non-vanishing temperature. We briefly investigated possible inhomogeneous structures in the model, with the conclusion that no such inhomogeneities can be found for any value of the magnetic field, chemical potential, temperature or volume considered.

Let us now briefly discuss how to possibly extend the work presented in this thesis. The ultimate goal that motivated our research was to study QCD from the point of view of fermionic model theories. One of the main reasons for this is the fact that QCD at finite density suffers from the infamous complex-action problem, prohibiting the application of conventional lattice field theory techniques. On the other hand, as we have shown, some model theories do not suffer from this problem, or only to a lesser extent. However, as has become especially clear in Chapter 6, the simple GN model in $2 + 1$ dimensions is still quite far away from the desired application in the study of QCD phenomenology. While this was expected from the beginning, we have gained important insights into which ingredients are necessary in any effective theory of QCD to reproduce the correct physics.

It appears to be necessary to not only include gluonic degrees of freedom, but also to somehow mimic the back-reaction of magnetized quarks onto their distribution. In a similar way as the sea quark contributions, responsible for inverse magnetic catalysis around the chiral cross-over in QCD, the four-Fermi coupling should run with the magnetic field. This incorporates an effective change in the gluon dynamics, which one integrates out, due to the magnetic field.

One may thus picture the following procedure of systematically approaching QCD,

starting from low-dimensional 4FTs: First of all, one should consider continuous chiral symmetries as in QCD, and therefore employ models of the NJL type. One should then endow the auxiliary scalar fields, introduced via Hubbard-Stratonovich transformation, with kinetic terms, resulting in quark-meson-like models. This allows for a proper interpretation of the low-energy degrees of freedom as dynamical pions. Notice, however, that the introduction of kinetic terms for scalar fields means that there is no pure four-Fermi analog for the theory anymore. On the other hand, it has the advantage that quark-meson models are renormalizable in four space-time dimensions, such that one no longer has to restrict to low dimensions in order to work with renormalizable theories. As a next step, one may couple the theories to the Polyakov loop, thereby introducing gauge degrees of freedom. Lastly, one should make the couplings run with the magnetic field. One sees from this discussion that the effort of going from simple low-dimensional fermionic theories to realistic effective theories that correctly reproduce QCD phenomenology can be considerable. Whether such modified theories still have significant computational advantages as compared to QCD itself remains to be seen.

As interesting directions for future research we mention the study of inhomogeneous magnetic fields [336], which better represent the physical situation during a particle collision, as well as that of QCD within electric fields [337], for which lattice simulations suffer from a complex-action problem. Moreover, it would be interesting to study the effect of background gravitational fields on 4FTs [338] beyond the mean-field limit.

Appendices

A Derivation of Landau levels

In this appendix we shall demonstrate how the spectrum of the Dirac operator in a magnetic field is given in terms of discrete Landau levels. For the discussion, we consider a $(2 + 1)$ -dimensional space-time, albeit in an irreducible representation of the Dirac algebra for simplicity. To conform with the literature, we denote the irreducible gamma matrices with the usual symbol γ_μ instead of the notation introduced in Section 2.2.4. For the discussion, we assume a finite space-time volume $V = \beta L^2$, on which the fermions obey their usual boundary conditions.

Consider the Dirac operator

$$D = \not{\nabla} + m , \quad (\text{A.1})$$

where the covariant derivative is given by

$$\nabla_\mu = \partial_\mu + ieA_\mu , \quad (\text{A.2})$$

e denotes the elementary electric charge and A_μ is a vector potential describing a constant and homogeneous magnetic field of magnitude B . With the usual definition of the field-strength tensor,

$$F_{\mu\nu} := \partial_\mu A_\nu - \partial_\nu A_\mu , \quad (\text{A.3})$$

we have $B = F_{12}$. Notice that we may also introduce a chemical potential into this Dirac operator in a straightforward way, namely as the imaginary part of A_0 .

In the following, we shall be interested in computing the spectrum of one-particle energies and their corresponding degeneracies. To this end, we separate the time-direction in D by multiplying with γ_0 , which gives

$$\gamma_0 D = \nabla_0 + h , \quad (\text{A.4})$$

where h is the Dirac Hamiltonian whose (squared) eigenvalues we want to compute. It is defined as

$$h = \gamma_0 m + \gamma_0 \gamma_i \nabla_i , \quad (\text{A.5})$$

such that

$$h^2 = m^2 - (\gamma_i \nabla_i)^2 . \quad (\text{A.6})$$

We have thus reduced the problem to the computation of the spectrum of $(\gamma_i \nabla_i)^2$.

Notice that $\gamma_i \nabla_i$ is precisely the massless Dirac operator in $2 + 0$ dimensions. In this two-dimensional theory the role of the matrix γ_* is simply played by γ_0 , as it anti-commutes with both γ_1 and γ_2 . Indeed, in the following we shall mostly use two-dimensional terminology, as we, for instance, refer to eigenfunctions of γ_0 with eigenvalue $+1$ and -1 as right-handed and left-handed, respectively. For the remainder of this section we closely follow [309].

Let us denote the zero modes of $i\gamma_i \nabla_i$ as ψ_p , where p is an index running from 1 to the total number n of zero modes. Non-zero eigenvalues of $i\gamma_i \nabla_i$ shall be denoted as $\lambda_q \neq 0$ and the corresponding eigenfunctions as ψ_q , where q runs from $n + 1$ to ∞ . Notice that $i\gamma_i \nabla_i$ is Hermitian, such that its eigenvalues are real. Since on the space of zero modes $i\gamma_i \nabla_i$ commutes with γ_0 , the ψ_p have definite chirality and we denote the numbers of right- and left-handed zero modes by n_+ and n_- , respectively, such that $n = n_+ + n_-$. Moreover, from the eigenvalue equation

$$i\gamma_i \nabla_i \psi_q = \lambda_q \psi_q \quad (\text{A.7})$$

it follows that

$$i\gamma_i \nabla_i (\gamma_0 \psi_q) = -\lambda_q (\gamma_0 \psi_q) , \quad (\text{A.8})$$

which means that for every non-zero eigenvalue its negative is also in the spectrum, while their corresponding eigenfunctions, ψ_q and $\gamma_0 \psi_q$, are orthogonal. From this one concludes that only the zero modes contribute to the so-called Witten index [339],

$$\text{tr} \left[\gamma_0 e^{t(\gamma_i \nabla_i)^2} \right] = \sum_{p=1}^n (\psi_p, \gamma_0 \psi_p) + \sum_{q=n+1}^{\infty} e^{-t\lambda_q^2} (\psi_q, \gamma_0 \psi_q) = \sum_{p=1}^n (\psi_p, \gamma_0 \psi_p) = n_+ - n_- , \quad (\text{A.9})$$

where we have expressed the trace as a sum over the eigenstates of $i\gamma_i \nabla_i$. Performing a heat-kernel expansion [340] to write the diagonal elements of $e^{t(\gamma_i \nabla_i)^2}$ as

$$\langle x | e^{t(\gamma_i \nabla_i)^2} | x \rangle = \frac{1}{4\pi t} (1 + \gamma_0 e F_{12} t + \mathcal{O}(t^2)) , \quad (\text{A.10})$$

leads back to (A.9) upon multiplication with γ_0 and integration over space. Since, as has been highlighted in [309], the Witten index is independent of the parameter t , one only needs to retain the second term in (A.10) and obtains

$$\text{tr} \left[\gamma_0 e^{t(\gamma_i \nabla_i)^2} \right] = \frac{e}{2\pi} \int d^2 x B , \quad (\text{A.11})$$

where we have used the definition of the magnetic field, $B = F_{12}$, and the fact that the identity matrix in Dirac space has a trace of 2. Combining this result with (A.9) and

introducing the magnetic flux $\Phi := e \int d^2x B$ we find the two-dimensional index theorem

$$\frac{\Phi}{2\pi} = n_+ - n_- , \quad (\text{A.12})$$

relating the index of $i\gamma_i\nabla_i$, i.e., the difference between the respective numbers of its right- and left-handed zero modes to the magnetic flux.

Since Φ is proportional to an integer, $\Phi = 2\pi b$, one also concludes that the magnetic flux through a torus is quantized. For a constant and homogeneous magnetic field B through a torus of area L^2 this quantization condition is reflected as

$$eB = \frac{2\pi}{L^2} b . \quad (\text{A.13})$$

Turning back to the computation of the spectrum of $i\gamma_i\nabla_i$, it is straightforward to show that

$$(\gamma_i\nabla_i)^2 = \nabla_i^2 + \frac{ie}{2}\gamma_i\gamma_j F_{ij} , \quad (\text{A.14})$$

where the second term on the right-hand side is the usual Pauli term. It follows that

$$- (\gamma_i\nabla_i)^2 = -\nabla_i^2 + \frac{\Phi}{L^2}\gamma_0 . \quad (\text{A.15})$$

Since ∇_i and $\gamma_i\nabla_i$ are both anti-Hermitian operators, their respective squares are negative semi-definite. Thus, for $\Phi > 0$ the operator $-(\gamma_i\nabla_i)^2$ can only have left-handed zero modes, while for $\Phi < 0$ they can only be right-handed. This fact is commonly referred to as the vanishing theorem. Only for vanishing magnetic flux can both left- and right-handed zero modes be present at the same time. This case, however, is not considered here, as the computation of the spectrum is straightforward for $\Phi = 0$.

Note that γ_0 commutes with $-(\gamma_i\nabla_i)^2$. From (A.7) and (A.8) it thus follows that $\frac{1}{2}(\mathbb{1} \pm \gamma_0)\psi_q$ are both eigenfunctions of $-(\gamma_i\nabla_i)^2$ with the same eigenvalue λ_q^2 , but come with opposite chirality. With the knowledge we have acquired so far, we may now derive the eigenvalues of $-(\gamma_i\nabla_i)^2$. Combining our last statement with the vanishing theorem and (A.15) we conclude that there are $\frac{|\Phi|}{2\pi}$ zero modes, all of them being either left- or right-handed, while the higher modes have a degeneracy of $\frac{|\Phi|}{\pi}$ each, but are split in half into both left- and right-handed ones. The eigenvalues of the latter are integer multiples of $\frac{2\Phi}{L^2}$.

In summary, we find the squared one-particle energies E_l^2 , i.e., the eigenvalues of the squared Dirac Hamiltonian h^2 (A.6) to be

$$E_l^2 = m^2 + 2|eB|l . \quad (\text{A.16})$$

These quantized energy levels, labeled by the non-negative integer l , are referred to as Landau levels and their degeneracy is given by $d_l = (2 - \delta_{l0})\frac{L^2}{2\pi}|eB|$.

B The chiral condensate from the density of states

Here we derive some relations that are used in the context of Chapter 3. To begin with, let us consider the dispersion relation (3.2) of $(2 + 1)$ -dimensional non-interacting fermions without a magnetic field. We shall work in an irreducible representation of the Dirac algebra with two-component spinors.

The density of states with an energy below some value ε , i.e., the integrated density of states, is given by

$$\rho_0(\varepsilon) = \frac{2}{L^2} \sum_{\mathbf{p}} \Theta(\varepsilon - E_{\mathbf{p}}) , \quad (\text{B.17})$$

where the factor of 2 takes into account the two-fold (spin) degeneracy. With (3.2) and the discretization of spatial momenta on a torus, (2.1), we thus find

$$\rho_0(\varepsilon) = \frac{2}{L^2} \sum_{\mathbf{n} \in \mathbb{Z}^2} \Theta \left(\varepsilon - \sqrt{m^2 + \frac{4\pi^2}{L^2} (n_1^2 + n_2^2)} \right) . \quad (\text{B.18})$$

Introducing the sum-of-squares function,

$$r_2(n) = |\{(n_1, n_2) \in \mathbb{Z}^2 | n_1^2 + n_2^2 = n\}| , \quad (\text{B.19})$$

counting the number of pairs of integers whose squares sum up to n , leads to

$$\rho_0(\varepsilon) = \frac{2}{L^2} \sum_{n=0}^{\infty} r_2(n) \Theta \left(\varepsilon - \sqrt{m^2 + \frac{4\pi^2}{L^2} n} \right) , \quad (\text{B.20})$$

Similarly, we find for the Landau levels (3.1) at $B \neq 0$ that

$$\rho_b(\varepsilon) = \frac{1}{L^2} \sum_{l=0}^{\infty} d_l \Theta(\varepsilon - E_l) = \frac{|eB|}{2\pi} \left[\Theta(\varepsilon - m) + 2 \sum_{l=1}^{\infty} \Theta \left(\varepsilon - \sqrt{m^2 + 2|eB|l} \right) \right] . \quad (\text{B.21})$$

where we have used the definition of the Landau-level degeneracy d_l (3.3). Now, with (3.4) and (3.1) we obtain

$$\rho_b(\varepsilon) = \frac{|b|}{L^2} \left[\Theta(\varepsilon - m) + 2 \sum_{l=1}^{\infty} \Theta \left(\varepsilon - \sqrt{m^2 + \frac{4\pi|b|}{L^2} l} \right) \right] . \quad (\text{B.22})$$

Let us now use these densities of states to compute the fermion condensate $\langle \bar{\psi}\psi \rangle$. Since in a massive free theory

$$\langle \bar{\psi}\psi \rangle = \frac{1}{Z} \int \mathcal{D}\bar{\psi} \mathcal{D}\psi e^{-\int d^3x \bar{\psi} i D \psi} \bar{\psi}\psi \quad (\text{B.23})$$

with $D = \not{\nabla} + m$ and

$$Z = \int \mathcal{D}\bar{\psi} \mathcal{D}\psi e^{-\int d^3x \bar{\psi} i D \psi} = \det D, \quad (\text{B.24})$$

the condensate can be computed from the Dirac operator D via

$$\langle \bar{\psi} \psi \rangle = -\frac{1}{V} \frac{\partial}{\partial m} \ln \det D = -\frac{1}{2V} \frac{\partial}{\partial m} \ln \det D^2, \quad (\text{B.25})$$

where the factor $\frac{1}{V}$ compensates for the space-time integration. Assuming that the determinant can be written as

$$\det(D^2) = \det(Q^2 + m^2), \quad (\text{B.26})$$

with some suitable operator Q^2 , and using $\ln \det D = \text{tr} \ln D$, the condensate becomes

$$\langle \bar{\psi} \psi \rangle = -\frac{m}{V} \text{tr} \frac{1}{Q^2 + m^2}. \quad (\text{B.27})$$

In the eigenbasis of Q^2 , the trace is simply a sum over its eigenvalues λ_Q^2 ,

$$\langle \bar{\psi} \psi \rangle = -\frac{m}{V} \sum_{\lambda_Q^2} \frac{1}{\lambda_Q^2 + m^2}, \quad (\text{B.28})$$

regularized in an appropriate way.

Let us first consider the Dirac operator for free fermions in $2 + 1$ dimensions and at $B = 0$, $D = \not{\partial} + m$. It is not hard to convince oneself that $\det(D^2) = \det(-\partial^2 + m^2)$, such that $Q^2 = -\partial^2$ in (B.26). The eigenvalues of $-\partial^2$ are the squared momenta p^2 with a two-fold degeneracy due to the spin structure and with p_i given in (2.1). For the Matsubara frequencies p_0 we introduce the more conventional symbol $\omega_n = \frac{2\pi}{\beta} (n + \frac{1}{2})$, such that, from (B.28), we find

$$\langle \bar{\psi} \psi \rangle_0 = -\frac{m}{V} \sum_{n=-\infty}^{\infty} \sum_{\mathbf{p}} \frac{2}{\omega_n^2 + \mathbf{p}^2 + m^2}. \quad (\text{B.29})$$

Introducing the density of energy states $g_0 = \frac{\partial}{\partial \varepsilon} \rho_0(\varepsilon)$ and using (B.17), whose derivative is a sum of Dirac deltas, as well as (3.2), we thus obtain

$$\langle \bar{\psi} \psi \rangle_0 = -\frac{m}{\beta} \sum_{n=-\infty}^{\infty} \int d\varepsilon \frac{1}{\omega_n^2 + \varepsilon^2} g_0(\varepsilon). \quad (\text{B.30})$$

Next, we turn to the case of non-zero magnetic field, where $D = \not{\partial} + ie\mathcal{A} + m$. We can use the decomposition (A.4) with $\nabla_0 = \partial_0$ since we do not consider a chemical potential here, to write

$$\det(D^2) = \det[(\gamma_0 D)^2] = \det[(\partial_0 + h)^2]. \quad (\text{B.31})$$

As ∂_0 , which has the eigenvalues $i\omega_n$, commutes with h , whose eigenvalues we denote as λ , the determinant is given by the regularized product

$$\det [(\partial_0 + h)^2] = \prod_{n,\lambda} (i\omega_n + \lambda)^2 = \prod_{n,\lambda} (\omega_n^2 + \lambda^2) = \det (-\partial_0^2 + h^2), \quad (\text{B.32})$$

where we have used that the product over n contains both ω_n and $-\omega_n$ for each n . Thus, using the definition of h^2 in (A.6), we find

$$\det (D^2) = \det (m^2 - \partial_0^2 - (\gamma_i \nabla_i)^2), \quad (\text{B.33})$$

i.e., $Q^2 = -\partial_0^2 - (\gamma_i \nabla_i)^2$ in (B.26). We have computed the eigenvalues of $(\gamma_i \nabla_i)^2$ and their degeneracies in Appendix A. In analogy to the $B = 0$ case above we introduce $g_b = \frac{\partial}{\partial \varepsilon} \rho_b(\varepsilon)$, such that, using (B.21) and (3.1), the condensate for non-zero magnetic field takes the form

$$\langle \bar{\psi} \psi \rangle_b = -\frac{m}{\beta} \sum_{n=-\infty}^{\infty} \int d\varepsilon \frac{1}{\omega_n^2 + \varepsilon^2} g_b(\varepsilon), \quad (\text{B.34})$$

reminiscent of (B.30).

C Zeta function regularization

We present a short account on the zeta function regularization and renormalization technique. We follow [130] but mention that earlier accounts can be found as well [341, 342]. Let A denote a self-adjoint second-order elliptic differential operator with eigenvalues λ_n , n being an integer enumerating the eigenvalues. The zeta function of A is defined as

$$\zeta_A(s) = \sum'_n \lambda_n^{-s}, \quad (\text{C.35})$$

where the prime indicates omission of all zero eigenvalues here and in what follows. The zero modes have to be projected out in a suitable way.

The sum in (C.35) converges for sufficiently large s and the zeta function defined in this way can then be analytically continued to a meromorphic function of s in a unique way [343]. One then finds, formally,

$$\left. \frac{d}{ds} \zeta_A(s) \right|_{s=0} = - \sum'_n \ln \lambda_n = - \ln \det' A, \quad (\text{C.36})$$

where we have used $\det A = \prod_n \lambda_n$. One then defines the determinant of A as

$$\det' A := \exp \left[- \left. \frac{d}{ds} \zeta_A(s) \right|_{s=0} \right]. \quad (\text{C.37})$$

For simple systems this expression for the determinant can be computed in closed form. The result is then both regularized and renormalized at the same time, which is possible due to the analytical continuation of $\zeta_A(s)$, in a similar fashion as in the more conventional dimensional regularization technique [344, 345].

One representation of the zeta function, which shall turn out to be particularly convenient for our computations, is given by the Mellin transform of the (trace of the) heat kernel of A , $K(t) = \text{tr}' [e^{-At}]$,

$$\zeta_A(s) = \frac{1}{\Gamma(s)} \int_0^\infty dt t^{s-1} K(t), \quad (\text{C.38})$$

which can be derived by using the definition of the gamma function,

$$\Gamma(s) := \int_0^\infty dt t^{s-1} e^{-t}, \quad (\text{C.39})$$

with an appropriate re-scaling of the integration variable.

D Derivation of the effective potential

In this appendix we derive the effective potential of the GN model in $2 + 1$ space-time dimensions in the mean-field limit, assuming σ to be homogeneous in space and time throughout. For the most part, we employ the zeta function technique introduced in Appendix C. See also [346, 347].

D.1 The vacuum case

To begin with, let us consider the GN model at vanishing temperature, chemical potential and magnetic field in the chiral limit. We consider a reducible representation of gamma matrices, where spinors are four-component objects. The corresponding effective potential from (3.16) and (3.18) is given by

$$V_{\text{eff}} = \frac{\sigma^2}{2g^2} - \frac{1}{V} \ln \det D, \quad (\text{D.40})$$

where we will later let the space-time volume V tend to infinity and the Dirac operator is given by $D = \not{\partial} + \sigma$. We compute $\ln \det D = \frac{1}{2} \ln \det D^2$ via the zeta function, i.e., using (C.37), which amounts to

$$\ln \det D = -\frac{1}{2} \zeta'_{D^2}(s) \Big|_{s=0}, \quad (\text{D.41})$$

where ζ_{D^2} is the zeta function corresponding to $A = D^2$ in (C.38). Thus,

$$\zeta_{D^2}(s) = \frac{4}{\Gamma(s)} \int_0^\infty dt t^{s-1} \sum_p e^{-t(p^2 + \sigma^2)}, \quad (\text{D.42})$$

where we have used the property $\det(D^2) = \det(-\partial^2 + \sigma^2)$ and we write the trace explicitly as a sum over the eigenvalues of $-\partial^2$. The factor 4 takes into account their spin degeneracy in the reducible representation.

Since we let the volume approach infinity, we may replace the sum over momenta by an integral with measure $d^3p = \frac{(2\pi)^3}{V}$. Evaluating this Gaussian momentum integral leaves us with

$$\zeta_{D^2}(s) = \frac{V}{2\pi^{3/2}} \frac{1}{\Gamma(s)} \int_0^\infty dt t^{s-5/2} e^{-t\sigma^2}. \quad (\text{D.43})$$

Using (C.39), we find

$$\zeta_{D^2}(s) = \frac{V}{2\pi^{3/2}} \frac{\Gamma(s - \frac{3}{2})}{\Gamma(s)} |\sigma|^{3-2s}. \quad (\text{D.44})$$

We need to compute the derivative of ζ_{D^2} at $s = 0$, see (D.41), for which we use the following useful properties:

$$\frac{1}{\Gamma(0)} = 0, \quad \left. \frac{\partial}{\partial s} \frac{1}{\Gamma(s)} \right|_{s=0} = 1, \quad \Gamma\left(-\frac{3}{2}\right) = \frac{4\sqrt{\pi}}{3}. \quad (\text{D.45})$$

We obtain

$$\zeta'_{D^2}(s)|_{s=0} = \frac{2V}{3\pi} |\sigma|^3. \quad (\text{D.46})$$

The effective potential (D.40) thus reads

$$V_{\text{eff}}(\sigma) = \frac{\sigma^2}{2g_R^2} + \frac{|\sigma|^3}{3\pi}, \quad (\text{D.47})$$

where we have introduced g_R^2 to indicate that the coupling is understood to be the renormalized one, which is implicit in the zeta function formalism. Indeed, the above expression for V_{eff} is already renormalized, i.e., finite.

The expectation value $\langle \sigma \rangle$ is given as the minimum position of V_{eff} , i.e., as the solution of the gap equation (3.19). We find

$$\frac{\partial}{\partial \sigma} V_{\text{eff}}(\sigma) = \frac{\sigma}{g_R^2} + \frac{\sigma|\sigma|}{\pi}. \quad (\text{D.48})$$

Hence, the trivial solution $\sigma = 0$ exists for all values of the coupling. However, if the renormalized coupling becomes negative, one additionally finds the non-trivial solutions

$$\sigma = \pm \frac{\pi}{g_R^2}, \quad (\text{D.49})$$

which both minimize V_{eff} . The situation where $g_R^2 < 0$ corresponds to the strong-coupling regime, where the bare coupling g^2 is larger than some critical value g_c^2 . On the other hand, the weak-coupling regime $g^2 < g_c^2$ implies $g_R^2 > 0$. Quite intuitively, a condensate can only be formed for sufficiently strong interactions.

Since the minimum position of V_{eff} corresponds to $\langle \sigma \rangle$, which is in turn proportional to the chiral condensate by virtue of (2.42), we conclude that in the strong-coupling regime chiral symmetry is spontaneously broken at vanishing temperature, chemical potential and magnetic field. In what follows we shall thus always assume strong couplings, such that we can use the positive non-trivial solution of (D.48) as a scale. We define

$$\sigma_0 := -\frac{\pi}{g_R^2} > 0. \quad (\text{D.50})$$

The following computations go along the same lines as the one presented here, albeit the calculation of the determinant becomes more involved.

D.2 Non-zero temperature and chemical potential

Let us now consider the case of non-zero temperature and chemical potential, restricting to vanishing magnetic field for the time being. The appropriate Dirac operator reads

$$D = \not{\partial} + \sigma + \mu\gamma_0, \quad (\text{D.51})$$

and we have $\det(D^2) = \det(\sigma^2 - (\partial_0 + \mu)^2 - (\gamma_i \partial_i)^2)$ from (B.33) with the trivial replacements $\partial_0 \rightarrow \nabla_0 = \partial_0 + \mu$, $\nabla_i \rightarrow \partial_i$ and $m \rightarrow \sigma$. Moreover, we consider a finite spatial volume L^2 for now, such that the momenta p_i are discretized according to (2.1). With this, the zeta function is given by

$$\zeta_{D^2}(s) = \frac{4}{\Gamma(s)} \int_0^\infty dt t^{s-1} \sum_{n=-\infty}^\infty \sum_{\mathbf{p}} e^{-t(\sigma^2 + (\omega_n + i\mu)^2 + \mathbf{p}^2)}, \quad (\text{D.52})$$

the factor 4 again arising due to the use of four-component spinors. We make use of the Poisson resummation formula,

$$\sum_{n=-\infty}^\infty e^{-t(\omega_n + i\mu)^2} = \frac{\beta}{2\sqrt{\pi}} \sum_{k=-\infty}^\infty \frac{(-1)^k}{\sqrt{t}} e^{-k\beta\mu - \frac{\beta^2 k^2}{4t}}, \quad (\text{D.53})$$

to obtain

$$\zeta_{D^2}(s) = \frac{2\beta}{\sqrt{\pi}} \frac{1}{\Gamma(s)} \sum_{k=-\infty}^\infty (-1)^k e^{-k\beta\mu} \int_0^\infty dt t^{s-3/2} \sum_{\mathbf{p}} e^{-t(\sigma^2 + \mathbf{p}^2) - \frac{\beta^2 k^2}{4t}}. \quad (\text{D.54})$$

In principle, one could use analogous Poisson resummation formulas of the form

$$\sum_{p_i=-\infty}^{\infty} e^{-tp_i^2} = \frac{L}{2\sqrt{\pi}} \sum_{k_i=-\infty}^{\infty} \frac{(-1)^{k_i}}{\sqrt{t}} e^{-\frac{L^2 k_i^2}{4t}} \quad (\text{D.55})$$

for the sums over the spatial momenta p_i as well. However, we refrain from doing so for the full zeta function.

Instead, we separate ζ_{D^2} into a vacuum contribution ($k = 0$) and thermal corrections ($k \neq 0$):

$$\zeta_{D^2}(s) = \zeta_0(s) + \zeta_T(s), \quad (\text{D.56})$$

where

$$\zeta_0(s) = \frac{2\beta}{\sqrt{\pi}} \frac{1}{\Gamma(s)} \int_0^\infty dt t^{s-3/2} \sum_{\mathbf{p}} e^{-t\varepsilon_{\mathbf{p}}^2} \quad (\text{D.57})$$

and

$$\zeta_T(s) = \frac{4\beta}{\sqrt{\pi}} \frac{1}{\Gamma(s)} \int_0^\infty dt t^{s-3/2} \sum_{k=1}^{\infty} (-1)^k \cosh(k\beta\mu) \sum_{\mathbf{p}} e^{-t\varepsilon_{\mathbf{p}}^2 - \frac{\beta^2 k^2}{4t}}. \quad (\text{D.58})$$

Here, we have introduced $\varepsilon_{\mathbf{p}} := \sqrt{\sigma^2 + \mathbf{p}^2}$. Only for ζ_0 do we apply (D.55), such that

$$\zeta_0(s) = \frac{V}{2\pi^{3/2}} \frac{1}{\Gamma(s)} \int_0^\infty dt t^{s-5/2} \sum_{\mathbf{k} \in \mathbb{Z}^2} e^{-t\sigma^2 - \frac{L^2 \mathbf{k}^2}{4t}}, \quad (\text{D.59})$$

To evaluate the integral over t , we split the sum over \mathbf{k} into a contribution from $\mathbf{k} = 0$ and the remaining terms, the latter of which we indicate by a prime in the sum. For the former, we use (C.39) and for the latter we make use of an identity for Mellin transforms (see, e.g., [348]), reading

$$\int_0^\infty dt t^{s-1} e^{-at - \frac{b}{t}} = 2 \left(\frac{b}{a}\right)^{s/2} K_s(2\sqrt{ab}), \quad (\text{D.60})$$

where $K_\nu(z) = K_{-\nu}(z)$ denotes the modified Bessel functions of the second kind. We end up with

$$\zeta_0(s) = \frac{V}{2\pi^{3/2}} \frac{\Gamma(s - \frac{3}{2})}{\Gamma(s)} |\sigma|^{3-2s} + \frac{V}{\pi^{3/2}} \frac{1}{\Gamma(s)} \left(\frac{2|\sigma|}{L}\right)^{3/2-s} \sum_{\mathbf{k}}' \frac{1}{|\mathbf{k}|^{3/2-s}} K_{\frac{3}{2}-s}(L|\sigma||\mathbf{k}|), \quad (\text{D.61})$$

where the first term comes from $\mathbf{k} = 0$ and corresponds to the vacuum zeta function in an infinite volume (D.44) and the second term gives finite-size corrections.

For the thermal term $\zeta_T(s)$ we also use (D.60) to evaluate the integral over t . We

obtain

$$\zeta_T(s) = \frac{8\beta}{\sqrt{\pi}} \frac{1}{\Gamma(s)} \sum_{k=1}^{\infty} (-1)^k \cosh(k\beta\mu) \sum_{\mathbf{p}} \left(\frac{2\varepsilon_{\mathbf{p}}}{\beta k} \right)^{1/2-s} K_{\frac{1}{2}-s}(\beta\varepsilon_{\mathbf{p}}k) . \quad (\text{D.62})$$

With the explicit forms

$$K_{1/2}(z) = \sqrt{\frac{\pi}{2z}} e^{-z} , \quad K_{3/2}(z) = \sqrt{\frac{\pi}{2z}} e^{-z} \left(1 + \frac{1}{z} \right) \quad (\text{D.63})$$

and using (D.45), the derivative of the full zeta function at $s = 0$ reads

$$\begin{aligned} \zeta_{D^2}(s)|_{s=0} &= \frac{2V}{3\pi} |\sigma|^3 + \frac{2V}{L^2\pi} |\sigma| \sum_{\mathbf{k}}' e^{-L|\sigma||\mathbf{k}|} \frac{1}{\mathbf{k}^2} \left(1 + \frac{1}{L|\sigma||\mathbf{k}|} \right) \\ &+ 8 \sum_{k=1}^{\infty} \frac{(-1)^k}{k} \cosh(k\beta\mu) \sum_{\mathbf{p}} e^{-\beta\varepsilon_{\mathbf{p}}k} . \end{aligned} \quad (\text{D.64})$$

Using the identity

$$\sum_{k=1}^{\infty} \frac{(-1)^k}{k} \cosh(k\beta\mu) e^{-k\beta\varepsilon} = -\frac{1}{2} \left[\ln(1 + e^{-\beta(\varepsilon+\mu)}) + \ln(1 + e^{-\beta(\varepsilon-\mu)}) \right] \quad (\text{D.65})$$

the sum over k can now be evaluated, giving the final result for the effective potential on a finite volume and with non-zero T and μ from (D.40) and (D.41),

$$\begin{aligned} V_{\text{eff}}^{(V)} &= \frac{\sigma^2}{2g_R^2} + \frac{|\sigma|^3}{3\pi} + \frac{1}{L^2\pi} |\sigma| \sum_{\mathbf{k}}' e^{-L|\sigma||\mathbf{k}|} \frac{1}{\mathbf{k}^2} \left(1 + \frac{1}{L|\sigma||\mathbf{k}|} \right) \\ &- \frac{2}{V} \sum_{\mathbf{p}} \left[\ln \left(1 + e^{-\beta(\sqrt{\sigma^2+\mathbf{p}^2}+\mu)} \right) + \ln \left(1 + e^{-\beta(\sqrt{\sigma^2+\mathbf{p}^2}-\mu)} \right) \right] . \end{aligned} \quad (\text{D.66})$$

Let us now take the limit $L \rightarrow \infty$. To this end, we go back to (D.54) and replace the sum over spatial momenta by an integral by introducing $d^2p = \frac{(2\pi)^2}{L^2}$. We may then perform the resulting Gaussian momentum integral to obtain

$$\zeta_{D^2}(s) = \frac{V}{2\pi^{3/2}} \frac{1}{\Gamma(s)} \sum_{k=-\infty}^{\infty} (-1)^k e^{-k\beta\mu} \int_0^{\infty} dt t^{s-5/2} e^{-t\sigma^2 - \frac{\beta^2 k^2}{4t}} . \quad (\text{D.67})$$

Once more splitting into contributions from $k =$ and $k \neq 0$, the first corresponding to the vacuum term, and using (D.60), we find

$$\begin{aligned} \zeta_{D^2}(s) &= \frac{V}{2\pi^{3/2}} \frac{\Gamma(s - \frac{3}{2})}{\Gamma(s)} |\sigma|^{3-2s} \\ &+ \frac{2V}{\pi^{3/2}} \frac{1}{\Gamma(s)} \left(\frac{2|\sigma|}{\beta} \right)^{3/2-s} \sum_{k=1}^{\infty} (-1)^k \cosh(k\beta\mu) \frac{1}{k^{3/2-s}} K_{\frac{3}{2}-s}(\beta|\sigma|k) . \end{aligned} \quad (\text{D.68})$$

Now, we again use (D.45) and (D.63), as well as the identities

$$\sum_{k=1}^{\infty} \frac{(-1)^k}{k^2} \cosh(k\beta\mu) e^{-k\beta|\sigma|} = \frac{1}{2} [\text{Li}_2(-e^{-\beta(|\sigma|+\mu)}) + \text{Li}_2(-e^{-\beta(|\sigma|-\mu)})] , \quad (\text{D.69})$$

$$\sum_{k=1}^{\infty} \frac{(-1)^k}{k^3} \cosh(k\beta\mu) e^{-k\beta|\sigma|} = \frac{1}{2} [\text{Li}_3(-e^{-\beta(|\sigma|+\mu)}) + \text{Li}_3(-e^{-\beta(|\sigma|-\mu)})] , \quad (\text{D.70})$$

where the $\text{Li}_\nu(z)$ are polylogarithms,

$$\text{Li}_\nu(z) = \sum_{n=1}^{\infty} \frac{z^n}{n^\nu} . \quad (\text{D.71})$$

For the effective potential (D.40) at finite temperature and chemical potential and in an infinite spatial volume we thus find

$$\begin{aligned} \lim_{L \rightarrow \infty} V_{\text{eff}}^{(B=0)} &= \frac{\sigma^2}{2g_R^2} + \frac{|\sigma|^3}{3\pi} + \frac{1}{\pi\beta^3} [\beta|\sigma| \text{Li}_2(-e^{-\beta(|\sigma|+\mu)}) + \text{Li}_3(-e^{-\beta(|\sigma|+\mu)})] \\ &\quad + \frac{1}{\pi\beta^3} [\beta|\sigma| \text{Li}_2(-e^{-\beta(|\sigma|-\mu)}) + \text{Li}_3(-e^{-\beta(|\sigma|-\mu)})] . \end{aligned} \quad (\text{D.72})$$

D.3 Non-zero temperature, chemical potential and magnetic field

Next, we compute the effective potential for the GN model in $2+1$ dimensions in a finite magnetic field, for non-zero temperature and chemical potential. The Dirac operator reads

$$D = \not{\partial} + ie\not{A} + \mu\gamma_0 . \quad (\text{D.73})$$

For the zeta function of D^2 we use $\det(D^2) = \det(\sigma^2 - (\partial_0 + \mu)^2 - (\gamma_i \nabla)^2)$ from (B.33). It reads

$$\zeta_{D^2} = \frac{2}{\Gamma(s)} \int_0^\infty dt t^{s-1} \sum_{n=-\infty}^{\infty} \sum_{l=0}^{\infty} e^{-t(\sigma^2 + (\omega_n + i\mu)^2 + 2eBl)} d_l , \quad (\text{D.74})$$

where we assume $eB > 0$. Inserting the definition of d_l and performing the Poisson resummation (D.53), we obtain

$$\zeta_{D^2} = \frac{eBV}{2\pi^{3/2}} \frac{1}{\Gamma(s)} \int_0^\infty dt t^{s-3/2} \sum_{k=-\infty}^{\infty} (-1)^k e^{-k\beta\mu} \sum_{l=0}^{\infty} e^{-t(\sigma^2 + 2eBl) - \frac{\beta^2 k^2}{4t}} \tilde{d}_l , \quad (\text{D.75})$$

where $\tilde{d}_l = (2 - \delta_{0l})$. We once again proceed by splitting the sum over k into a vacuum term $k = 0$ and the remaining summands. After a few lines of algebra, using (C.39) and

(D.60), we find

$$\zeta_{D^2} = \frac{eBV}{2\pi^{3/2}} \frac{1}{\Gamma(s)} \sum_{l=0}^{\infty} \tilde{d}_l \left[\Gamma\left(s - \frac{1}{2}\right) \varepsilon_l^{1-2s} \right. \quad (\text{D.76})$$

$$\left. + 2 \sum_{k=1}^{\infty} (-1)^k \cosh(k\beta\mu) \left(\frac{\beta k}{2\varepsilon_l}\right)^{s-1/2} K_{s-1/2}(\beta k \varepsilon_l) \right], \quad (\text{D.77})$$

where $\varepsilon_l = \sqrt{\sigma^2 + 2eBl}$. Using (D.45) as well as $\Gamma(-1/2) = -2\sqrt{\pi}$, we obtain for the derivative of ζ_{D^2} at zero

$$\zeta'_{D^2}(s)|_{s=0} = \frac{eBV}{2\pi^{3/2}} \sum_{l=0}^{\infty} \tilde{d}_l \left[-2\sqrt{\pi}\varepsilon_l + 2 \sum_{k=1}^{\infty} (-1)^k \cosh(k\beta\mu) \sqrt{\frac{2\varepsilon_l}{\beta k}} K_{1/2}(\beta k \varepsilon_l) \right]. \quad (\text{D.78})$$

Introducing the Hurwitz zeta function

$$\zeta_H(s, a) = \sum_{n=0}^{\infty} \frac{1}{(n+a)^s}, \quad (\text{D.79})$$

we obtain, after some algebra,

$$\zeta'_{D^2}(s)|_{s=0} = \frac{eBV}{2\pi} \sum_{l=0}^{\infty} \tilde{d}_l \left[-2\sqrt{2eB} \zeta_H\left(-\frac{1}{2}, \frac{\sigma^2}{2eB}\right) + 2|\sigma| \right. \quad (\text{D.80})$$

$$\left. + \frac{1}{\beta} \sum_{l=0}^{\infty} \tilde{d}_l \sum_{k=1}^{\infty} (-1)^k (e^{k\beta\mu} + e^{-k\beta\mu}) \frac{1}{k} e^{-\beta k \varepsilon_l} \right]. \quad (\text{D.81})$$

The sum over k may once more be computed using (D.69). After the dust has settled, we then obtain for the full effective potential the result

$$V_{\text{eff}}^{(B)} = \frac{\sigma^2}{2g_R^2} + \frac{|\sigma|eB}{2\pi} - \frac{(2eB)^{3/2}}{2\pi} \zeta_H\left(-\frac{1}{2}, \frac{\sigma^2}{2eB}\right) \quad (\text{D.82})$$

$$- \frac{eB}{2\pi\beta} \sum_{l=0}^{\infty} \tilde{d}_l \left[\ln(1 + e^{-\beta(\varepsilon_l + \mu)}) + \ln(1 + e^{-\beta(\varepsilon_l - \mu)}) \right].$$

E On the complex-action problem

We briefly discuss the (non-)realness of the lattice action (6.14) in our simulations of the $(2+1)$ -dimensional GN model in a magnetic field. Since QCD at finite chemical potential is plagued by the complex-action problem one might wonder whether this is the case for the GN model as well or if similar arguments as in the $(1+1)$ -dimensional χ GN model, mentioned in Section 5.3, hold.

First of all, it turns out that there is no complex-action problem at finite B as long as μ vanishes. This fact is intimately connected with the use of four-component spinors in our

study. To see this, we follow [105] by writing the gamma matrices in the block-diagonal form introduced in (2.25). The overlap Dirac (6.11) then also decomposes into a block form,

$$D = \begin{pmatrix} D_1 & 0 \\ 0 & D_2 \end{pmatrix}, \quad (\text{E.83})$$

where D_1 and D_2 are the overlap operators corresponding to each of the two inequivalent irreducible representations in three dimensions. More concretely, we find the two irreducible analogues of (6.11),

$$\begin{aligned} D_1(\mu, B) &= D_{\text{ov},1}(B) + (\sigma + \mu\tau_0) \left(\mathbb{1} - \frac{a}{2} D_{\text{ov},1}(B) \right), \\ D_2(\mu, B) &= D_{\text{ov},2}(B) + (\sigma - \mu\tau_0) \left(\mathbb{1} - \frac{a}{2} D_{\text{ov},2}(B) \right), \end{aligned} \quad (\text{E.84})$$

where we have made explicit the μ - and B -dependence of the operators. The irreducible components of the massless overlap operator (4.17) read (we omit the superscript (0) for better readability)

$$D_{\text{ov},i}(B) = \frac{1}{a} \left[1 + A_{\text{W},i}(B) \left(A_{\text{W},i}^\dagger(B) A_{\text{W},i}(B) \right)^{-1/2} \right], \quad (\text{E.85})$$

where $i = 1, 2$ and, in analogy to (4.18),

$$A_{\text{W},i}(B) = a \not{D}_{\text{W},i}(B) - \mathbb{1} a m_{\text{W}}. \quad (\text{E.86})$$

Finally, the irreducible components of the Wilson operator (4.7) are given by

$$\begin{aligned} \not{D}_{\text{W},1}(B) &= \frac{1}{2} \left[\tau_\mu (\nabla_\mu^* + \nabla_\mu) - a \nabla_\mu^* \nabla_\mu \right], \\ \not{D}_{\text{W},2}(B) &= \frac{1}{2} \left[-\tau_\mu (\nabla_\mu^* + \nabla_\mu) - a \nabla_\mu^* \nabla_\mu \right], \end{aligned} \quad (\text{E.87})$$

with the one-sided covariant difference operators ∇_μ and ∇_μ^* defined in (4.5). We emphasize that the expressions (E.84) are precisely what one would find when working in one of the irreducible representations of the Dirac algebra in $2 + 1$ dimensions.

Now, due to the fact that $\nabla_\mu^* + \nabla_\mu$ is anti-hermitian while $\nabla_\mu^* \nabla_\mu$ and τ_μ are hermitian for all μ , we find that $\not{D}_{\text{W},1}^\dagger(B) = \not{D}_{\text{W},2}(B)$. One can convince oneself that this, in turn, implies that $D_1^\dagger(0, B) = D_2(0, B)$, such that

$$\det D(0, B) = \det D_1(0, B) \det D_2(0, B) = |\det D_1(0, B)|^2 \geq 0, \quad (\text{E.88})$$

i.e., the fermion determinant is real and non-negative for vanishing chemical potential, such that there is no complex-action problem.

Let us now consider the case $B = 0$ and $\mu \neq 0$, where the above procedure no longer works due to the chemical potential appearing with different signs in D_1 and D_2 ,

respectively. Instead, we use the fact that for zero magnetic field the covariant difference operators ∇_μ^* and ∇_μ reduce to ordinary one-sided difference operators, which are real. Then, one finds $\not{D}_{W,1}(0)^* = \tau_2 \not{D}_{W,2}(0) \tau_2$, where the right-hand side amounts to a charge conjugation of $\not{D}_{W,2}(0)$ [108]. Similarly, one shows that $D_1(\mu, 0)^* = \tau_2 D_2(\mu, 0) \tau_2$, such that, as above,

$$\det D(\mu, 0) = |\det D_1(\mu, 0)|^2 \geq 0, \quad (\text{E.89})$$

and there is no complex-action problem.

For the combined case where both B and μ are non-vanishing, however, neither the realness of the difference operators nor the properties of the reducible representation can be used. Indeed, it turns out that the fermion determinant has a non-vanishing imaginary part in general. However, as was discussed in [106], for certain observables \mathcal{O} one may still obtain reliable estimates despite this fact. To see this, consider the expectation value of \mathcal{O} with respect to a complex Euclidean action $S = S_R + iS_I$ with real and imaginary parts S_R and S_I , respectively. We have

$$\langle \mathcal{O} \rangle = \frac{\int \mathcal{D}\sigma e^{-S_R - iS_I} \mathcal{O}[\sigma]}{\int \mathcal{D}\sigma e^{-S_R - iS_I}} \quad (\text{E.90})$$

and we may – in principle – interpret the complex phase of the action, e^{-iS_I} , as part of the observable by writing

$$\langle \mathcal{O} \rangle = \frac{\langle e^{-iS_I} \mathcal{O} \rangle_R}{\langle e^{-iS_I} \rangle_R}, \quad (\text{E.91})$$

where $\langle \cdot \rangle_R$ denotes the expectation value with respect to the real part of S only:

$$\langle \mathcal{O} \rangle_R = \frac{\int \mathcal{D}\sigma e^{-S_R} \mathcal{O}[\sigma]}{\int \mathcal{D}\sigma e^{-S_R}}. \quad (\text{E.92})$$

This is the standard re-weighting approach. On paper, $\langle e^{-iS_I} \mathcal{O} \rangle_R$ and $\langle e^{-iS_I} \rangle_R$ may both be evaluated in a Monte Carlo simulation as the Boltzmann factor now has a proper probabilistic interpretation. However, it is well known that the re-weighting technique in general does not solve the sign problem [39].

We proceed by introducing the covariance of two observables \mathcal{O} and \mathcal{O}' with respect to e^{-S_R} as

$$\text{cov}_R(\mathcal{O}, \mathcal{O}') = \langle \mathcal{O} \mathcal{O}' \rangle_R - \langle \mathcal{O} \rangle_R \langle \mathcal{O}' \rangle_R. \quad (\text{E.93})$$

This allows for an exact re-writing of (E.91) as

$$\langle \mathcal{O} \rangle = \langle \mathcal{O} \rangle_R + \frac{\text{cov}_R(e^{-iS_I}, \mathcal{O})}{\langle e^{-iS_I} \rangle_R}. \quad (\text{E.94})$$

If the complex-action problem was severe, the average phase $\langle e^{-iS_I} \rangle_R$ would be close to zero, complicating the evaluation of the right-hand side of (E.94). In our simulations of

the magnetized GN model in $2 + 1$ dimensions, however, this seems not to be the case and the average phase instead takes values close to unity [106]. Moreover, as we have demonstrated in [106], the covariance between the complex phase and our primary observable of interest, $\mathcal{O}[\sigma] = |\bar{\sigma}|$, approximately vanishes.

We know of no analytical argument why $|\bar{\sigma}|$ and e^{-iS_I} should be uncorrelated and, thus, why the fact that S_I is non-zero should not play a role in the computation of $\langle |\bar{\sigma}| \rangle$. Nonetheless, the numerical results presented in [106] suggest that the imaginary part of the action may simply be ignored. As the ratio between $\text{cov}(e^{-iS_I}, \bar{\sigma})_R$ and $\langle e^{-iS_I} \rangle_R$ is close to zero in our simulations, such that $\langle |\bar{\sigma}| \rangle \approx \langle |\bar{\sigma}| \rangle_R$, we thus merely compute the expectation value with respect to e^{-S_R} . We emphasize, however, that these observations likely only hold for the small lattice volumes we consider here. There is no guarantee that the complex-action problem is unproblematic for larger volumes as well. Moreover, one should keep in mind that the above statement was only made for the case $\mathcal{O} = |\bar{\sigma}|$. For general observables it might no longer be true and one should expect a more severe complex-action problem.

References

- [1] F. Wilczek, *QCD in Extreme Conditions*, *CRM Series in Mathematical Physics*, **567** (2002), arXiv: [hep-ph/0003183](#) (cit. on p. 3)
- [2] K. Fukushima, *QCD matter in extreme environments*, *J. Phys. G* **39**, 013101 (2012), arXiv: [1108.2939 \[hep-ph\]](#) (cit. on p. 3)
- [3] V. A. Miransky and I. A. Shovkovy, *Quantum field theory in a magnetic field: From quantum chromodynamics to graphene and Dirac semimetals*, *Phys. Rep.* **576**, 1 (2015), arXiv: [1503.00732 \[hep-ph\]](#) (cit. on pp. 3, 4)
- [4] J. O. Andersen, W. R. Naylor, and A. Tranberg, *Phase diagram of QCD in a magnetic field*, *Rev. Mod. Phys.* **88**, 025001 (2016), arXiv: [1411.7176 \[hep-ph\]](#) (cit. on p. 3)
- [5] J. Rafelski and B. Müller, *Magnetic Splitting of Quasimolecular Electronic States in Strong Fields*, *Phys. Rev. Lett.* **36**, 517 (1976) (cit. on p. 3)
- [6] V. V. Skokov, A. Yu. Illarionov, and V. D. Toneev, *Estimate of the magnetic field strength in heavy-ion collisions*, *Int. J. Mod. Phys. A* **24**, 5925 (2009), arXiv: [0907.1396 \[nucl-th\]](#) (cit. on p. 3)
- [7] V. Voronyuk et al., *Electromagnetic field evolution in relativistic heavy-ion collisions*, *Phys. Rev. C* **83**, 054911 (2011), arXiv: [1103.4239 \[nucl-th\]](#) (cit. on p. 3)
- [8] A. Bzdak and V. Skokov, *Event-by-event fluctuations of magnetic and electric fields in heavy ion collisions*, *Phys. Lett. B* **710**, 171 (2012), arXiv: [1111.1949 \[hep-ph\]](#) (cit. on p. 3)
- [9] W.-T. Deng and X.-G. Huang, *Event-by-event generation of electromagnetic fields in heavy-ion collisions*, *Phys. Rev. C* **85**, 044907 (2012), arXiv: [1201.5108 \[nucl-th\]](#) (cit. on p. 3)
- [10] K. Tuchin, *Particle Production in Strong Electromagnetic Fields in Relativistic Heavy-Ion Collisions*, *Adv. High Energy Phys.* **2013** (2013), arXiv: [1301.0099 \[hep-ph\]](#) (cit. on p. 3)
- [11] I. Danhoni and F. S. Navarra, *Magnetic field in relativistic heavy-ion collisions: Testing the classical approximation*, *Phys. Rev. C* **103**, 024902 (2021), arXiv: [2011.00726 \[hep-ph\]](#) (cit. on p. 3)
- [12] T. Gezhagn and A. K. Chaubey, *Electromagnetic Field Evolution in Relativistic Heavy Ion Collisions and Its Effects of Flow of Partices*, *Front. Phys.* **9**, 791108 (2022), arXiv: [2107.01467 \[nucl-th\]](#) (cit. on p. 3)

-
- [13] D. E. Kharzeev, L. D. McLerran, and H. J. Warringa, *The effects of topological charge change in heavy ion collisions: "Event by event \mathcal{P} and \mathcal{CP} violation"*, *Nucl. Phys. A* **803**, 227 (2008), arXiv: 0711.0950 [hep-ph] (cit. on p. 3)
- [14] K. Fukushima, D. E. Kharzeev, and H. J. Warringa, *Chiral magnetic effect*, *Phys. Rev. D* **78**, 074033 (2008), arXiv: 0808.3382 [hep-ph] (cit. on p. 3)
- [15] B. I. Abelev et al. (STAR collaboration), *Azimuthal Charged-Particle Correlations and Possible Local Strong Parity Violation*, *Phys. Rev. Lett.* **103**, 251601 (2009), arXiv: 0909.1739 [nucl-ex] (cit. on p. 3)
- [16] R. Belmont (for the ALICE collaboration), *Charge-dependent anisotropic flow studies and the search for the Chiral Magnetic Wave in ALICE*, *Nucl. Phys. A* **931**, 981 (2014), arXiv: 1408.1043 [nucl-ex] (cit. on p. 3)
- [17] M. A. Metlitski and A. R. Zhitnitsky, *Anomalous axion interactions and topological currents in dense matter*, *Phys. Rev. D* **72**, 045011 (2005), arXiv: hep-ph/0505072 (cit. on p. 4)
- [18] D. E. Kharzeev and H.-U. Yee, *Chiral magnetic wave*, *Phys. Rev. D* **83**, 085007 (2011), arXiv: 1012.6026 [hep-th] (cit. on p. 4)
- [19] K. Fukushima, *Chiral symmetry and heavy-ion collisions*, *J. Phys. G* **35**, 104020 (2008), arXiv: 0806.0292 [hep-ph] (cit. on p. 4)
- [20] P. V. Buividovich, M. I. Polikarpov, and O. V. Teryaev, *Lattice Studies of Magnetic Phenomena in Heavy-Ion Collisions*, *Lect. Notes Phys.* **871**, 377 (2013), arXiv: 1211.3014 [hep-ph] (cit. on p. 4)
- [21] K. Fukushima, *Views of the Chiral Magnetic Effect*, *Lect. Notes Phys.* **871**, 241 (2013), arXiv: 1209.5064 [hep-ph] (cit. on p. 4)
- [22] D. E. Kharzeev, *Topology, Magnetic Field, and Strongly Interacting Matter*, *Annu. Rev. Nucl. Part. Sci.* **65**, 193 (2015), arXiv: 1501.01336 [hep-ph] (cit. on p. 4)
- [23] R. C. Duncan and C. Thompson, *Formation of Very Strongly Magnetized Neutron Stars: Implications for Gamma-Ray Bursts*, *Astrophys. J. Lett.* **392**, L9 (1992) (cit. on p. 4)
- [24] D. Lai and S. L. Shapiro, *Cold Equation of State in a Strong Magnetic Field: Effects of Inverse β -Decay*, *Astrophys. J.* **383**, 745 (1991) (cit. on p. 4)
- [25] C. Thompson and R. C. Duncan, *Neutron Star Dynamos and the Origins of Pulsar Magnetism*, *Astrophys. J.* **408**, 194 (1993) (cit. on p. 4)
- [26] A. K. Harding and D. Lai, *Physics of strongly magnetized neutron stars*, *Rep. Prog. Phys.* **69**, 2631 (2006), arXiv: astro-ph/0606674 (cit. on p. 4)
- [27] E. J. Ferrer and V. de la Incera, *Magnetism in Dense Quark Matter*, *Lect. Notes Phys.* **871**, 399 (2013), arXiv: 1208.5179 [nucl-th] (cit. on p. 4)

-
- [28] A. P. Igoshev, S. B. Popov, and R. Hollerbach, *Evolution of Neutron Star Magnetic Fields*, *Universe* **7**, 351 (2021), arXiv: 2109.05584 [astro-ph] (cit. on p. 4)
- [29] M. Bocquet et al., *Rotating neutron star models with a magnetic field*, *Astron. Astrophys.* **301**, 757 (1995), arXiv: gr-qc/9503044 (cit. on p. 4)
- [30] E. V. Gorbar, V. A. Miranskyy, and I. A. Shovkova, *Chiral asymmetry of the Fermi surface in dense relativistic matter in a magnetic field*, *Phys. Rev. C* **80**, 032801(R) (2009), arXiv: 0904.2164 [hep-ph] (cit. on p. 4)
- [31] T. Vachaspati, *Magnetic fields from cosmological phase transitions*, *Phys. Lett. B* **265**, 258 (1991) (cit. on p. 4)
- [32] K. Enqvist and P. Olesen, *On primordial magnetic fields of electroweak origin*, *Phys. Lett. B* **319**, 178 (1993), arXiv: hep-ph/9308270 (cit. on p. 4)
- [33] G. Baym, D. Bödeker, and L. McLerran, *Magnetic fields produced by phase transition bubbles in the electroweak phase transition*, *Phys. Rev. D* **53**, 662 (1996), arXiv: hep-ph/9507429 (cit. on p. 4)
- [34] M. Hindmarsh and A. Everett, *Magnetic fields from phase transitions*, *Phys. Rev. D* **58**, 103505 (1998), arXiv: astro-ph/9708004 (cit. on p. 4)
- [35] D. Grasso and H. R. Rubinstein, *Magnetic fields in the early Universe*, *Phys. Rep.* **348**, 163 (2001), arXiv: 0911.4771 [astro-ph] (cit. on p. 4)
- [36] K. Subramanian, *Magnetic fields in the early Universe*, *Astron. Nachr.* **331**, 110 (2010), arXiv: 0911.4771 [astro-ph] (cit. on p. 4)
- [37] Chernodub. M. N., *Superconductivity of QCD vacuum in strong magnetic field*, *Phys. Rev. D* **82**, 085011 (2010), arXiv: 1008.1055 [hep-ph] (cit. on p. 4)
- [38] J. N. Guenther, *Overview of the QCD phase diagram – Recent progress from the lattice*, (2020), arXiv: 2010.15503 [hep-lat] (cit. on p. 4)
- [39] M. Troyer and U.-J. Wiese, *Computational Complexity and Fundamental Limitations to Fermionic Quantum Monte Carlo Simulations*, *Phys. Rev. Lett.* **94**, 170201 (2005), arXiv: cond-mat/0408370 (cit. on pp. 4, 34, 115)
- [40] C. Gattringer and K. Langfeld, *Approaches to the sign problem in lattice field theory*, *Int. J. Mod. Phys. A* **31**, 1643007 (2016), arXiv: 1603.09517 [hep-lat] (cit. on p. 4)
- [41] C. E. Berger et al., *Complex Langevin and other approaches to the sign problem in quantum many-body physics*, *Phys. Rep.* **892**, 1 (2021), arXiv: 1907.10183 [cond-mat] (cit. on p. 4)
- [42] S. Muroya et al., *Lattice QCD at Finite Density: An Introductory Review*, *Prog. Theor. Phys.* **110**, 615 (2003), arXiv: hep-lat/0306031 (cit. on p. 4)

- [43] P. de Forcrand, *Simulating QCD at finite density*, *PoS (LAT2009)*, 010 (2010), arXiv: 1005.0539 [hep-lat] (cit. on pp. 4, 34)
- [44] S. Scherer, *Introduction to Chiral Perturbation Theory*, *Adv. Nucl. Phys.* **27**, 277 (2003), arXiv: hep-ph/0210398 (cit. on p. 4)
- [45] E. Fermi, *Versuch einer Theorie der β -Strahlen. I*, *Z. Phys.* **88**, 161 (1934) (cit. on p. 4)
- [46] U. Vogl and W. Weise, *The Nambu and Jona-Lasinio Model: Its Implications for Hadrons and Nuclei*, *Prog. Part. Nucl. Phys.* **27**, 195 (1991) (cit. on p. 5)
- [47] S. P. Klevansky, *The Nambu–Jona-Lasinio model of quantum chromodynamics*, *Rev. Mod. Phys.* **64**, 649 (1992) (cit. on p. 5)
- [48] K.-I. Kondo, *Toward a first-principle derivation of confinement and chiral-symmetry-breaking crossover transitions in QCD*, *Phys. Rev. D* **82**, 065024 (2010), arXiv: 1005.0314 [hep-th] (cit. on p. 5)
- [49] B. Rosenstein, B. J. Warr, and S. H. Park, *Dynamical symmetry breaking in four-fermion interaction models*, *Phys. Rep.* **205**, 59 (1991) (cit. on p. 5)
- [50] D. J. Gross and A. Neveu, *Dynamical symmetry breaking in asymptotically free field theories*, *Phys. Rev. D* **10**, 3235 (1974) (cit. on pp. 5, 13, 14)
- [51] B. Rosenstein, B. J. Warr, and S. H. Park, *Four-Fermion Theory is Renormalizable in 2+1 dimensions*, *Phys. Rev. Lett.* **62**, 1433 (1989) (cit. on p. 5)
- [52] Y. Nambu and G. Jona-Lasinio, *Dynamical Model of Elementary Particles Based on an Analogy with Superconductivity. I*, *Phys. Rev.* **122**, 345 (1961) (cit. on pp. 5, 13)
- [53] Y. Nambu and G. Jona-Lasinio, *Dynamical Model of Elementary Particles Based on an Analogy with Superconductivity. II*, *Phys. Rev.* **124**, 246 (1961) (cit. on pp. 5, 13)
- [54] A. Chodos and H. Minakata, *The Gross-Neveu model as an effective theory for polyacetylene*, *Phys. Lett. A* **191**, 39 (1994) (cit. on p. 5)
- [55] H. Caldas, *An effective field theory model for one-dimensional CH chains: effects at finite chemical potential, temperature and external Zeeman magnetic field*, *J. Stat. Mech.* **2011**, P10005 (2011), arXiv: 1106.0948 [cond-mat] (cit. on p. 5)
- [56] F. Moraes et al., *First-order transition to a novel metallic state in $[\text{Na}_y^+(\text{CH})^{-y}]_x$: In situ electron spin resonance during chemical and electrochemical doping*, *Synth. Metals* **11**, 271 (1985) (cit. on p. 5)
- [57] K. Krishana et al., *Plateaus Observed in the Field Profile of Thermal Conductivity in the Superconductor $\text{Bi}_2\text{Sr}_2\text{CaCu}_2\text{O}_8$* , *Science* **277**, 83 (1997) (cit. on p. 5)

- [58] W. V. Liu, *Parity breaking and phase transition induced by a magnetic field in high T_c superconductors*, *Nucl. Phys. B* **556**, 563 (1999), arXiv: [cond-mat/9808134](#) (cit. on p. 5)
- [59] V. Ch. Zhukovskii et al., *Magnetic Catalysis of P -Parity Breakdown in a Massive Gross–Neveu Model and High- T_c Superconductivity*, *JETP Lett.* **73**, 121 (2001), arXiv: [hep-th/0012256](#) (cit. on p. 5)
- [60] A. N. Kalinkin and V. M. Skorikov, *Phase Transitions in Four-Fermion Models*, *Inorg. Mater.* **39**, 765 (2003) (cit. on p. 5)
- [61] J. E. Drut and D. T. Son, *Renormalization group flow of quartic perturbations in graphene: Strong coupling and large- N limits*, *Phys. Rev. B* **77**, 075115 (2008), arXiv: [0710.1315 \[cond-mat\]](#) (cit. on p. 5)
- [62] I. F. Herbut, V. Juričić, and B. Roy, *Theory of interacting electrons on the honeycomb lattice*, *Phys. Rev. B* **79**, 085116 (2009), arXiv: [0811.0610 \[cond-mat\]](#) (cit. on p. 5)
- [63] D. Ebert et al., *Phase transitions in hexagonal, graphene-like lattice sheets and nanotubes under the influence of external conditions*, *Ann. Phys.* **371**, 254 (2016), arXiv: [1509.08093 \[cond-mat\]](#) (cit. on p. 5)
- [64] D. Ebert and D. Blaschke, *Thermodynamics of a generalized graphene-motivated $(2+1)D$ Gross–Neveu model beyond the mean field within the Beth–Uhlenbeck approach*, *Prog. Theor. Exp. Phys.* **2019**, 123I01 (2019), arXiv: [1811.07109 \[cond-mat\]](#) (cit. on p. 5)
- [65] R. Jackiw and J. R. Schrieffer, *Solitons with fermion number $\frac{1}{2}$ in condensed matter and relativistic field theories*, *Nucl. Phys. B* **190**, 253 (1981) (cit. on p. 5)
- [66] D. K. Campbell and A. R. Bishop, *Solitons in polyacetylene and relativistic-field-theory models*, *Phys. Rev. B* **24**, 4859(R) (1981) (cit. on p. 5)
- [67] D. K. Campbell and A. R. Bishop, *Soliton excitations in polyacetylene and relativistic field theory models*, *Nucl. Phys. B* **200**, 297 (1982) (cit. on p. 5)
- [68] M. J. Rice et al., *Solitons, polarons, and phonons in the infinite polyynes chain*, *Phys. Rev. B* **34**, 4139 (1986) (cit. on p. 5)
- [69] A. Saxena and A. R. Bishop, *Multipolaron solutions of the Gross-Neveu field theory: Toda potential and doped polymers*, *Phys. Rev. A* **44**, R2251(R) (1991) (cit. on p. 5)
- [70] D. K. Campbell, *Conducting polymers and relativistic field theories*, *Synth. Metals* **125**, 117 (2002) (cit. on p. 5)
- [71] J. Hofmann, *Dimensional reduction in quantum field theories at finite temperature and density*, *Phys. Rev. D* **82**, 125027 (2010), arXiv: [1009.4071 \[hep-th\]](#) (cit. on p. 5)

- [72] M. Thies, *From relativistic quantum fields to condensed matter and back again: updating the Gross-Neveu phase diagram*, *J. Phys. A* **39**, 12707 (2006), arXiv: [hep-th/0601049](#) (cit. on pp. 5, 23, 50)
- [73] R. F. Dashen, S.-k. Ma, and R. Rajaraman, *Finite-temperature behavior of a relativistic field theory with dynamical symmetry breaking*, *Phys. Rev. D* **11**, 1499 (1975) (cit. on p. 5)
- [74] W. Dittrich and B.-G. Englert, *One-loop thermal corrections in the Gross-Neveu model*, *Nucl. Phys. B* **179**, 85 (1981) (cit. on p. 5)
- [75] K. G. Klimenko, *Phase structure of generalized Gross-Neveu models*, *Z. Phys. C* **37**, 457 (1988) (cit. on p. 5)
- [76] T. F. Trembl, *Dynamical mass generation in the Gross-Neveu model at finite temperature and density*, *Phys. Rev. D* **39**, 679 (1989) (cit. on p. 5)
- [77] B. Rosenstein, B. J. Warr, and Park. S. H., *Thermodynamics of (2+1)-dimensional four-fermion models*, *Phys. Rev. D* **39**, 3088 (1989) (cit. on p. 5)
- [78] R. Pausch, M. Thies, and V. L. Dolman, *Solving the Gross-Neveu model with relativistic many-body methods*, *Z. Phys. A* **338**, 441 (1991) (cit. on p. 5)
- [79] H. Yamamoto and I. Ichinose, *Phase structure of quasi (2+1)-dimensional four-Fermi theory with global chiral $U(1)$ symmetry*, *Nucl. Phys. B* **370**, 695 (1992) (cit. on p. 5)
- [80] T. Inagaki, T. Kouno, and T. Muta, *Phase Structure of Four-Fermion Theories at Finite Temperature and Chemical Potential in Arbitrary Dimensions*, *Int. J. Mod. Phys. A* **10**, 2241 (1995), arXiv: [hep-ph/9409413](#) (cit. on p. 5)
- [81] Y. Cohen, S. Elitzur, and E. Rabinovici, *A Monte Carlo study of the Gross-Neveu model*, *Nucl. Phys. B* **220**, 102 (1983) (cit. on p. 5)
- [82] S. Hands, A. Kocić, and J. B. Kogut, *Four-Fermi Theories in Fewer Than Four Dimensions*, *Ann. Phys.* **224**, 29 (1993), arXiv: [hep-lat/9208022](#) (cit. on p. 5)
- [83] S. Hands, *Four Fermion Models at Non-Zero Density*, *Nucl. Phys. A.* **642**, 228c (1998), arXiv: [hep-lat/9806022](#) (cit. on p. 5)
- [84] S. J. Hands, J.B. Kogut, and C. G. Strouthos, *The (2+1)-dimensional Gross-Neveu model with a $U(1)$ chiral symmetry at nonzero temperature*, *Phys. Lett. B* **515**, 407 (2001), arXiv: [hep-lat/0107004](#) (cit. on p. 5)
- [85] S. Hands, B. Lucini, and S. Morrison, *Numerical portrait of a relativistic thin film BCS superfluid*, *Phys. Rev. D* **65**, 036004 (2002), arXiv: [hep-lat/0109001](#) (cit. on p. 5)
- [86] C. G. Strouthos, *Phase diagram of the three-dimensional NJL model*, *Eur. Phys. J. A* **18**, 211 (2003), arXiv: [hep-lat/0209143](#) (cit. on p. 5)

-
- [87] C. G. Strouthos and D. N. Walters, *Mass generation without phase coherence at nonzero temperature*, *Phys. Rev. D* **67**, 034505 (2003), arXiv: [hep-lat/0212002](#) (cit. on p. 5)
- [88] S. Christofi and C. Strouthos, *Three dimensional four-fermion models – A Monte Carlo study*, *JHEP* **2007**, 088 (2007), arXiv: [hep-lat/0612031](#) (cit. on p. 5)
- [89] S. Hands, *Towards critical physics in $2 + 1d$ with $U(2N)$ -invariant fermions*, *JHEP* **2016**, 15 (2016), arXiv: [1610.04394 \[hep-lat\]](#) (cit. on p. 5)
- [90] V. Schön and M. Thies, *Emergence of the Skyrme crystal in Gross-Neveu and 't Hooft models at finite density*, *Phys. Rev. D* **62**, 096002 (2000), arXiv: [hep-th/0003195](#) (cit. on pp. 6, 23, 50)
- [91] V. Schön and M. Thies, *2d Model Field Theories at Finite Temperature and Density, At the Frontier of Particle Physics, 1945* (2001), arXiv: [hep-th/0008175](#) (cit. on pp. 6, 23, 50)
- [92] J. Bardeen, L. N. Cooper, and J. R. Schrieffer, *Theory of Superconductivity*, *Phys. Rev.* **108**, 1175 (1957) (cit. on p. 6)
- [93] P. Fulde and R. A. Ferrell, *Superconductivity in a Strong Spin-Exchange Field*, *Phys. Rev.* **135**, A550 (1964) (cit. on p. 6)
- [94] A. I. Larkin and Yu. N. Ovchinnikov, *Nonuniform state of superconductors*, *Zh. Eksp. Teor. Fiz.* **47**, 1136 (1964) (cit. on p. 6)
- [95] J. J. Kinnunen et al., *The Fulde-Ferrell-Larkin-Ovchinnikov state for ultracold fermions in lattice and harmonic potentials: a review*, *Rep. Prog. Phys.* **81**, 046401 (2018), arXiv: [1706.07076 \[cond-mat\]](#) (cit. on p. 6)
- [96] D. Müller, M. Buballa, and J. Wambach, *Dyson–Schwinger study of chiral density waves in QCD*, *Phys. Lett. B* **727**, 240 (2013), arXiv: [1308.4303 \[hep-ph\]](#) (cit. on p. 6)
- [97] W.-j. Fu, J. M. Pawłowski, and F. Rennecke, *QCD phase structure at finite temperature and density*, *Phys. Rev. D* **101**, 054032 (2020), arXiv: [1909.02991 \[hep-ph\]](#) (cit. on p. 6)
- [98] M. Alford, J. A. Bowers, and K. Rajagopal, *Crystalline color superconductivity*, *Phys. Rev. D* **63**, 074016 (2001), arXiv: [hep-ph/0008208 \[hep-ph\]](#) (cit. on p. 6)
- [99] R. D. Pisarski and F. Rennecke, *Signatures of Moat Regimes in Heavy-Ion Collisions*, *Phys. Rev. Lett* **127**, 152302 (2021), arXiv: [2103.06890 \[hep-ph\]](#) (cit. on p. 6)
- [100] M. Buballa and S. Carignano, *Inhomogeneous chiral condensates*, *Prog. Part. Nucl. Phys.* **81**, 39 (2015), arXiv: [1406.1367 \[hep-ph\]](#) (cit. on p. 6)

- [101] A. S. Vshivtsev, K. G. Klimenko, and B. V. Magnitsky, *Vacuum structure of the $(\bar{\psi}\psi)_3^2$ -model, accounting for the magnetic field and chemical potential*, *Theor. Math. Phys.* **106**, 319 (1996) (cit. on p. 6)
- [102] J. J. Lenz and M. Mandl, *Remnants of large- N_f inhomogeneities in the 2-flavor chiral Gross-Neveu model*, *PoS (LATTICE2021)* (2022), arXiv: 2110.12757 [hep-lat] (cit. on pp. 8, 57)
- [103] M. Mandl, J. J. Lenz, and A. Wipf, *Magnetic catalysis in the 1-flavor Gross-Neveu model in $2 + 1$ dimensions*, *PoS (LATTICE2022)* (2023), arXiv: 2211.10333 [hep-lat] (cit. on p. 8)
- [104] J. J. Lenz, M. Mandl, and A. Wipf, *Inhomogeneities in the two-flavor chiral Gross-Neveu model*, *Phys. Rev. D* **105**, 034512 (2022), arXiv: 2109.05525 [hep-lat] (cit. on pp. 8, 53, 56–58, 62, 64)
- [105] J. J. Lenz, M. Mandl, and A. Wipf, *Magnetic catalysis in the $(2 + 1)$ -dimensional Gross-Neveu model*, *Phys. Rev. D* **107**, 094505 (2023), arXiv: 2302.05279 [hep-lat] (cit. on pp. 8, 40, 78, 80, 114)
- [106] J. J. Lenz, M. Mandl, and A. Wipf, *The magnetized $(2+1)$ -dimensional Gross-Neveu model at finite density*, (2023), arXiv: 2304.14812 [hep-lat] (cit. on pp. 8, 78, 115, 116)
- [107] L. Dolan and R. Jackiw, *Symmetry behavior at finite temperature*, *Phys. Rev. D* **9**, 3320 (1974) (cit. on p. 9)
- [108] A. Wipf, *Statistical Approach to Quantum Field Theory, An Introduction*, 2nd edition, *Lecture Notes in Physics Vol. 992* (2021), Springer Cham, ISBN: 978-3-030-83262-9 (cit. on pp. 10, 11, 53, 115)
- [109] C. Wetterich, *Spinors in euclidean field theory, complex structures and discrete symmetries*, *Nucl. Phys. B* **852**, 174 (2011), arXiv: 1002.3556 [hep-th] (cit. on pp. 11, 12)
- [110] F. Gehring, H. Gies, and L. Janssen, *Fixed-point structure of low-dimensional relativistic fermion field theories: Universality classes and emergent symmetry*, *Phys. Rev. D* **92**, 085046 (2015), arXiv: 1506.07570 [hep-th] (cit. on p. 11)
- [111] W. E. Thirring, *A Soluble Relativistic Field Theory*, *Ann. Phys.* **3**, 91 (1958) (cit. on p. 14)
- [112] R. D. Pisarski, *Chiral-symmetry breaking in three-dimensional electrodynamics*, *Phys. Rev. D* **29**, 2423(R) (1984) (cit. on p. 14)
- [113] G. W. Semenoff, *Condensed-Matter Simulation of a Three-Dimensional Anomaly*, *Phys. Rev. Lett.* **53**, 2449 (1984) (cit. on p. 14)
- [114] S. Hands, *Domain wall fermions for planar physics*, *JHEP* **2015**, 47 (2015), arXiv: 1507.07717 [hep-lat] (cit. on pp. 15, 77)

- [115] R. L. Stratonovich, *On a Method of Calculating Quantum Distribution Functions*, *Sov. Phys. Dokl.* **2**, 416 (1957) (cit. on p. 16)
- [116] J. Hubbard, *Calculation of partition functions*, *Phys. Lett. B* **3**, 77 (1959) (cit. on p. 16)
- [117] L. Landau, *Diamagnetismus der Metalle*, *Z. Physik* **64**, 629 (1930) (cit. on p. 19)
- [118] G. 't Hooft, *Some Twisted Self-Dual Solutions for the Yang-Mills Equations on a Hypertorus*, *Commun. Math. Phys.* **81**, 267 (1981) (cit. on p. 20)
- [119] M. H. Al-Hashimi and U.-J. Wiese, *Discrete accidental symmetry for a particle in a constant magnetic field on a torus*, *Ann. Phys.* **324**, 343 (2009), arXiv: 0807.0630 [quant-ph] (cit. on p. 20)
- [120] I. S. Gradshteyn and I. M. Ryzhik, *Table of Integrals, Series, and Products*, 7th edition, (2007), Academic Press, ISBN: 978-0-12-373637-6 (cit. on p. 21)
- [121] M. Thies and K. Urlichs, *Revised phase diagram of the Gross-Neveu model*, *Phys. Rev. D* **67**, 125015 (2003), arXiv: hep-th/0302092 (cit. on pp. 23, 50)
- [122] M. Buballa et al., *Regulator dependence of inhomogeneous phases in the $(2 + 1)$ -dimensional Gross-Neveu model*, *Phys. Rev. D* **103**, 034503 (2021), arXiv: 2012.09588 [hep-lat] (cit. on pp. 23, 95)
- [123] L. Pannullo, M. Wagner, and M. Winstel, *Inhomogeneous Phases in the Chirally Imbalanced $2 + 1$ -Dimensional Gross-Neveu Model and Their Absence in the Continuum Limit*, *Symmetry* **14**, 265 (2022), arXiv: 2112.11183 [hep-lat] (cit. on pp. 23, 95)
- [124] L. Pannullo and M. Winstel, *Absence of inhomogeneous chiral phases in $(2 + 1)$ -dimensional four-fermion and Yukawa models*, (2023), arXiv: 2305.09444 [hep-ph] (cit. on p. 23)
- [125] G. Başar, G. V. Dunne, and D. E. Kharzeev, *Chiral Magnetic Spirals*, *Phys. Rev. Lett.* **104**, 232301 (2010), arXiv: 1003.3464 [hep-ph] (cit. on pp. 23, 95)
- [126] I. E. Frolov, V. Ch. Zhukovsky, and K. G. Klimenko, *Chiral density waves in quark matter within the Nambu–Jona-Lasinio model in an external magnetic field*, *Phys. Rev. D* **82**, 076002 (2010), arXiv: 1007.2984 [hep-ph] (cit. on pp. 23, 95)
- [127] T. Tatsumi, K. Nishiyama, and S. Karasawa, *Novel Lifshitz point for chiral transition in the magnetic field*, *Phys. Lett. B* **743**, 66 (2015), arXiv: 1405.2155 [hep-ph] (cit. on pp. 23, 95)
- [128] M. Buballa and S. Carignano, *Inhomogeneous chiral symmetry breaking in dense neutron-star matter*, *Eur. Phys. J. A* **52**, 57 (2016), arXiv: 1508.04361 [nucl-th] (cit. on pp. 23, 95)

-
- [129] M. Moshe and J. Zinn-Justin, *Quantum field theory in the large N limit: a review*, *Phys. Rep.* **385**, 69 (2003), arXiv: [hep-th/0306133](#) (cit. on p. 23)
- [130] S. W. Hawking, *Zeta Function Regularization of Path Integrals in Curved Spacetime*, *Commun. Math. Phys.* **55**, 133 (1977) (cit. on pp. 24, 106)
- [131] S. P. Klevansky and R. H. Lemmer, *Chiral-symmetry restoration in the Nambu–Jona-Lasinio model with a constant electromagnetic field*, *Phys. Rev. D* **39**, 3478 (1989) (cit. on pp. 25, 66)
- [132] K. G. Klimenko, *Three-dimensional Gross-Neveu model in an external magnetic field. I*, *Theor. Math. Phys.* **89**, 1161 (1991) (cit. on pp. 25, 27, 66, 67)
- [133] K. G. Klimenko, *Three-dimensional Gross-Neveu model at nonzero temperature and in an external magnetic field*, *Theor. Math. Phys.* **90**, 1 (1992) (cit. on pp. 25, 67)
- [134] K. G. Klimenko, *Three-dimensional Gross-Neveu model at nonzero temperature and in the presence of an external electromagnetic field*, *Z. Phys. C* **54**, 323 (1992) (cit. on pp. 25, 67)
- [135] J. K. Boomsma and D. Boer, *Influence of strong magnetic fields and instantons on the phase structure of the two-flavor Nambu–Jona-Lasinio model*, *Phys. Rev. D* **81**, 074005 (2010), arXiv: [0911.2164 \[hep-ph\]](#) (cit. on p. 26)
- [136] Sh. Fayazbakhsh and N. Sadooghi, *Phase diagram of hot magnetized two-flavor color-superconducting quark matter*, *Phys. Rev. D* **83**, 025026 (2011), arXiv: [1009.6125 \[hep-ph\]](#) (cit. on p. 26)
- [137] B. Chatterjee, H. Mishra, and A. Mishra, *Vacuum structure and chiral symmetry breaking in strong magnetic fields for hot and dense quark matter*, *Phys. Rev. D* **84**, 014016 (2011), arXiv: [1101.0498 \[hep-ph\]](#) (cit. on p. 26)
- [138] S. S. Avancini et al., *QCD critical end point under strong magnetic fields*, *Phys. Rev. D* **85**, 091901(R) (2012), arXiv: [1202.5641 \[hep-ph\]](#) (cit. on p. 26)
- [139] G. N. Ferrari, A. F. Garcia, and M. B. Pinto, *Chiral transition within effective quark models under magnetic fields*, *Phys. Rev. D* **86**, 096005 (2012), arXiv: [1207.3714 \[hep-ph\]](#) (cit. on p. 26)
- [140] P. G. Allen and N. N. Scoccola, *Quark matter under strong magnetic fields in $SU(2)$ NJL-type models: Parameter dependence of the cold dense matter phase diagram*, *Phys. Rev. D* **88**, 094005 (2013), arXiv: [1309.2258 \[hep-ph\]](#) (cit. on p. 26)
- [141] R. Z. Denke and M. B. Pinto, *Influence of a repulsive vector coupling in magnetized quark matter*, *Phys. Rev. D* **88**, 056008 (2013), arXiv: [1306.6246 \[hep-ph\]](#) (cit. on p. 26)
- [142] A. G. Grunfeld et al., *Phase structure of cold magnetized quark matter within the $SU(3)$ NJL model*, *Phys. Rev. D* **90**, 044024 (2014), arXiv: [1402.4731 \[hep-ph\]](#) (cit. on p. 26)

- [143] G. Cao, L. He, and P. Zhuang, *Collective modes and Kosterlitz-Thouless transition in a magnetic field in the planar Nambu–Jona-Lasinio model*, *Phys. Rev. D* **90**, 056005 (2014), arXiv: 1408.5364 [hep-ph] (cit. on p. 26)
- [144] M. Ferreira, P. Costa, and C. Providência, *Multiple critical endpoints in magnetized three flavor quark matter*, *Phys. Rev. D* **97**, 014014 (2018), arXiv: 1712.08378 [hep-ph] (cit. on p. 26)
- [145] F. Preis, A. Rebhan, and A. Schmitt, *Inverse magnetic catalysis in dense holographic matter*, *JHEP* **2011**, 33 (2011), arXiv: 1012.4785 [hep-th] (cit. on pp. 26, 27)
- [146] F. Preis, A. Rebhan, and A. Schmitt, *Inverse Magnetic Catalysis in Field Theory and Gauge-Gravity Duality*, *Lect. Notes Phys.* **871**, 51 (2013), arXiv: 1208.0536 [hep-ph] (cit. on pp. 26, 68)
- [147] T. D. Cohen, *Functional Integrals for QCD at Nonzero Chemical Potential and Zero Density*, *Phys. Rev. Lett.* **91**, 222001 (2003), arXiv: hep-ph/0307089 (cit. on p. 30)
- [148] W. J. de Haas and P. M. van Alphen, *The dependence of the susceptibility of diamagnetic metals upon the field*, *Proc. Acad. Sci. Amst.* **33**, 1106 (1930) (cit. on p. 30)
- [149] L. Schubnikov and W. J. de Haas, *A New Phenomenon in the Change of Resistance in a Magnetic Field of Single Crystals of Bismuth*, *Nature* **126**, 500 (1930) (cit. on p. 30)
- [150] D. Ebert et al., *Magnetic oscillations in dense cold quark matter with four-fermion interactions*, *Phys. Rev. D* **61**, 025005 (1999), arXiv: hep-ph/9905253 (cit. on p. 30)
- [151] T. Inagaki, Y. Matsuo, and H. Shimoji, *Precise phase structure in a four-fermion interaction model on a torus*, *Prog. Theor. Exp. Phys.* **2022**, 013B09 (2022), arXiv: 2108.03583 [hep-ph] (cit. on p. 32)
- [152] I. Horváth, A. D. Kennedy, and S. Sint, *A New Exact Method for Dynamical Fermion Computations with Non-Local Actions*, *Nucl. Phys. B (Proc. Suppl.)* **73**, 834 (1999), arXiv: hep-lat/9809092 (cit. on pp. 34, 53)
- [153] B. H. Wellegehausen, *Phase diagrams of exceptional and supersymmetric lattice gauge theories*, PhD thesis, Friedrich-Schiller Universität Jena, 2012 (cit. on p. 34).
- [154] K. G. Wilson, *Confinement of quarks*, *Phys. Rev. D* **10**, 2445 (1974) (cit. on p. 35)
- [155] J. Kogut and L. Susskind, *Hamiltonian formulation of Wilson’s lattice gauge theories*, *Phys. Rev. D* **11**, 395 (1975) (cit. on p. 35)
- [156] I.-O. Stamatescu and T. T. Wu, *Lattice Fermion Formulation with One-Sided Derivatives*, *Nucl. Phys. B (Proc. Suppl.)* **32**, 838 (1995) (cit. on p. 36)

- [157] K. Osterwalder and R. Schrader, *Axioms for Euclidean Green's Functions II*, *Commun. Math. Phys.* **42**, 281 (1975) (cit. on p. 36)
- [158] N. Sadooghi and H. J. Rothe, *Continuum behavior of lattice QED, discretized with one-sided lattice differences in one-loop order*, *Phys. Rev. D* **55**, 6749 (1997), arXiv: [hep-lat/9610001](#) (cit. on p. 36)
- [159] K. G. Wilson, *Quarks and Strings on a Lattice*, *New Phenomena in Subnuclear Physics* **13**, 69 (1977) (cit. on p. 36)
- [160] S. Chandrasekharan and U.-J. Wiese, *An introduction to chiral symmetry on the lattice*, *Prog. Part. Nucl. Phys.* **53**, 373 (2004), arXiv: [hep-lat/0405024](#) (cit. on p. 36)
- [161] S. Aoki and K. Higashijima, *The Recovery of the Chiral Symmetry in Lattice Gross-Neveu Model*, *Prog. Theor. Phys.* **76**, 521 (1986) (cit. on p. 36)
- [162] H. B. Nielsen and M. Ninomiya, *Absence of neutrinos on a lattice: (I). Proof by homotopy theory*, *Nucl. Phys. B* **185**, 20 (1981) (cit. on p. 36)
- [163] H. B. Nielsen and M. Ninomiya, *Absence of neutrinos on a lattice: (II). Intuitive topological proof*, *Nucl. Phys. B* **193**, 173 (1981) (cit. on p. 36)
- [164] H. B. Nielsen and M. Ninomiya, *A no-go theorem for regularizing chiral fermions*, *Phys. Lett. B* **105**, 219 (1981) (cit. on p. 36)
- [165] D. Friedan, *A proof of the Nielsen-Ninomiya theorem*, *Comm. Math. Phys.* **85**, 481 (1982) (cit. on p. 36)
- [166] S. D. Drell, M. Weinstein, and S. Yankielowicz, *Strong-coupling field theory. I. Variational approach to ϕ^4 theory*, *Phys. Rev. D* **14**, 487 (1976) (cit. on p. 36)
- [167] S. D. Drell, M. Weinstein, and S. Yankielowicz, *Strong-coupling field theories. II. Fermions and gauge fields on a lattice*, *Phys. Rev. D* **14**, 1627 (1976) (cit. on pp. 36, 37)
- [168] A. Kirchberg, J. D. Länge, and A. Wipf, *From the Dirac operator to Wess-Zumino models on spatial lattices*, *Ann. Phys.* **316**, 357 (2005), arXiv: [hep-th/0407207](#) (cit. on p. 37)
- [169] C. Wozar and A. Wipf, *Supersymmetry breaking in low dimensional models*, *Ann. Phys.* **327**, 774 (2012), arXiv: [1107.3324 \[hep-lat\]](#) (cit. on p. 37)
- [170] L. H. Karsten and J. Smit, *Axial symmetry in lattice theories*, *Nucl. Phys. B* **144**, 536 (1978) (cit. on pp. 37, 40, 41)
- [171] L. H. Karsten and J. Smit, *The vacuum polarization with SLAC lattice fermions*, *Phys. Lett. B* **85**, 100 (1979) (cit. on p. 37)
- [172] G. Bergner et al., *Low-dimensional supersymmetric lattice models*, *Ann. Phys.* **323**, 946 (2008), arXiv: [0705.2212 \[hep-lat\]](#) (cit. on p. 37)

-
- [173] T. Kästner et al., *Two-dimensional Wess-Zumino models at intermediate couplings*, *Phys. Rev. D* **78**, 095001 (2008), arXiv: 0807.1905 [hep-lat] (cit. on p. 37)
- [174] B. H. Wellegehausen, D. Schmidt, and A. Wipf, *Critical flavor number of the Thirring model in three dimensions*, *Phys. Rev. D* **96**, 094504 (2017), arXiv: 1708.01160 [hep-lat] (cit. on p. 37)
- [175] J. J. Lenz, B. H. Wellegehausen, and A. Wipf, *Absence of chiral symmetry breaking in Thirring models in 1 + 2 dimensions*, *Phys. Rev. D* **100**, 054501 (2019), arXiv: 1905.00137 [hep-lat] (cit. on p. 37)
- [176] P. H. Ginsparg and K. G. Wilson, *A remnant of chiral symmetry on the lattice*, *Phys. Rev. D* **25**, 2649 (1982) (cit. on p. 37)
- [177] M. Lüscher, *Exact chiral symmetry on the lattice and the Ginsparg-Wilson relation*, *Phys. Lett. B* **428**, 342 (1998), arXiv: hep-lat/9802011 (cit. on p. 38)
- [178] S. Chandrasekharan, *Lattice QCD with Ginsparg-Wilson fermions*, *Phys. Rev. D* **60**, 074503 (1999), arXiv: hep-lat/9805015 (cit. on p. 38)
- [179] W. Bietenholz, *Solutions of the Ginsparg-Wilson relation and improved domain wall fermions*, *Eur. Phys. J. C* **6**, 537 (1999), arXiv: hep-lat/9803023 (cit. on p. 38)
- [180] R. Narayanan and H. Neuberger, *Infinitely many regulator fields for chiral fermions*, *Phys. Lett. B* **302**, 62 (1993), arXiv: hep-lat/9212019 (cit. on p. 38)
- [181] R. Narayanan and H. Neuberger, *Chiral Fermions on the Lattice*, *Phys. Rev. Lett.* **71**, 3251 (1993), arXiv: hep-lat/9308011 (cit. on p. 38)
- [182] R. Narayanan and H. Neuberger, *Chiral determinant as an overlap of two vacua*, *Nucl. Phys. B* **412**, 574 (1994), arXiv: hep-lat/9307006 (cit. on p. 38)
- [183] R. Narayanan and H. Neuberger, *A construction of lattice chiral gauge theories*, *Nucl. Phys. B* **443**, 305 (1995), arXiv: hep-th/9411108 (cit. on p. 38)
- [184] H. Neuberger, *More about exactly massless quarks on the lattice*, *Phys. Lett. B* **427**, 353 (1998), arXiv: hep-lat/9801031 (cit. on p. 38)
- [185] H. Neuberger, *Exactly massless quarks on the lattice*, *Phys. Lett. B* **417**, 141 (1998), arXiv: hep-lat/9707022 (cit. on p. 38)
- [186] Y. Kikukawa and H. Neuberger, *Overlap in odd dimensions*, *Nucl. Phys. B* **513**, 735 (1998), arXiv: hep-lat/9707016 (cit. on p. 39)
- [187] W. Bietenholz and J. Nishimura, *Ginsparg-Wilson fermions in odd dimensions*, *JHEP* **2001**, 015 (2001), arXiv: hep-lat/0012020 (cit. on pp. 39, 77)
- [188] P. Hernández, K. Jansen, and M. Lüscher, *Locality properties of Neuberger's lattice Dirac operator*, *Nucl. Phys. B* **552**, 363 (1999), arXiv: hep-lat/9808010 (cit. on p. 39)

-
- [189] I. Horváth, *Ginsparg-Wilson Relation and Ultralocality*, *Phys. Rev. Lett.* **81**, 4063 (1998), arXiv: [hep-lat/9808002](#) (cit. on p. 39)
- [190] P. Hasenfratz and F. Karsch, *Chemical potential on the lattice*, *Phys. Lett. B* **125**, 308 (1983) (cit. on pp. 39, 43)
- [191] J. Bloch and T. Wettig, *Overlap Dirac Operator at Nonzero Chemical Potential and Random Matrix Theory*, *Phys. Rev. Lett.* **97**, 012003 (2006), arXiv: [hep-lat/0604020](#) [[hep-lat](#)] (cit. on p. 39)
- [192] D. Banerjee, R. V. Gavai, and S. Sharma, *Thermodynamics of the ideal overlap quarks on the lattice*, *Phys. Rev. D* **78**, 014506 (2008), arXiv: [0803.3925](#) [[hep-lat](#)] (cit. on p. 39)
- [193] R. V. Gavai and S. Sharma, *Anomalies at finite density and chiral fermions*, *Phys. Rev. D* **81**, 034501 (2010), arXiv: [0906.5188](#) [[hep-lat](#)] (cit. on p. 39)
- [194] R. V. Gavai and S. Sharma, *Exact chiral invariance at finite density on the lattice*, *Phys. Lett. B* **716**, 446 (2012), arXiv: [1111.5944](#) [[hep-lat](#)] (cit. on pp. 39, 77)
- [195] R. V. Gavai and S. Sharma, *Divergences in the quark number susceptibility: The origin and a cure*, *Phys. Lett. B* **749**, 8 (2015), arXiv: [1406.0474](#) [[hep-lat](#)] (cit. on p. 39)
- [196] D. S. Roberts et al., *Wave functions of the proton ground state in the presence of a uniform background magnetic field in lattice QCD*, *Phys. Rev. D* **83**, 094504 (2011), arXiv: [1011.1975](#) [[hep-lat](#)] (cit. on p. 40)
- [197] M. D'Elia and F. Negro, *Chiral properties of strong interactions in a magnetic background*, *Phys. Rev. D* **83**, 114028 (2011), arXiv: [1103.2080](#) [[hep-lat](#)] (cit. on pp. 40, 68, 83)
- [198] F. Bruckmann and G. Endrődi, *Dressed Wilson loops as dual condensates in response to magnetic and electric fields*, *Phys. Rev. D* **84**, 074506 (2011), arXiv: [1104.5664](#) [[hep-lat](#)] (cit. on pp. 40, 83)
- [199] H. Ikeda and S. Hashimoto, *$O(a^2)$ improvement of the overlap-Dirac operator*, *PoS (LAT2009)* (2010), arXiv: [0912.4119](#) [[hep-lat](#)] (cit. on p. 48)
- [200] Y.-G. Cho et al., *Improved lattice fermion action for heavy quarks*, *JHEP* **2015**, 72 (2010), arXiv: [1504.01630](#) [[hep-lat](#)] (cit. on p. 48)
- [201] U. Wolff, *The phase diagram of the infinite- N Gross-Neveu model at finite temperature and chemical potential*, *Phys. Lett. B* **157**, 303 (1985) (cit. on pp. 49, 50)
- [202] A. Barducci et al., *Thermodynamics of the massive Gross-Neveu model*, *Phys. Rev. D* **51**, 3042 (1995), arXiv: [hep-th/9406117](#) (cit. on pp. 49, 51)

- [203] A. Brzoska and M. Thies, *No first-order phase transition in the Gross-Neveu model?*, *Phys. Rev. D* **65**, 125001 (2002), arXiv: [hep-th/0112105](#) (cit. on p. 50)
- [204] M. Thies, *Analytical solution of the Gross-Neveu model at finite density*, *Phys. Rev. D* **69**, 067703 (2004), arXiv: [hep-th/0308164](#) (cit. on p. 50)
- [205] O. Schnetz, M. Thies, and K. Urlichs, *Phase diagram of the Gross-Neveu model: exact results and condensed matter precursors*, *Ann. Phys.* **314**, 425 (2004), arXiv: [hep-th/0402014](#) (cit. on p. 50)
- [206] P. de Forcrand and U. Wenger, *New baryon matter in the lattice Gross-Neveu model*, *PoS (LAT2006)*, 152 (2006), arXiv: [hep-lat/0610117](#) (cit. on p. 50)
- [207] R. Narayanan, *Phase diagram of the large N Gross-Neveu model in a finite periodic box*, *Phys. Rev. D* **101**, 096001 (2020), arXiv: [2001.09200 \[hep-th\]](#) (cit. on p. 50)
- [208] M. Thies and K. Urlichs, *From nondegenerate conducting polymers to dense matter in the massive Gross-Neveu model*, *Phys. Rev. D* **72**, 105008 (2005), arXiv: [hep-th/0505024](#) (cit. on p. 50)
- [209] G. Başar and G. V. Dunne, *Self-Consistent Crystalline Condensate in Chiral Gross-Neveu and Bogoliubov–de Gennes Systems*, *Phys. Rev. Lett.* **100**, 200404 (2008), arXiv: [0803.1501 \[hep-th\]](#) (cit. on p. 50)
- [210] G. Başar and G. V. Dunne, *Twisted kink crystal in the chiral Gross-Neveu model*, *Phys. Rev. D* **78**, 065002 (2008), arXiv: [0806.2659 \[hep-th\]](#) (cit. on p. 50)
- [211] G. Başar, G. V. Dunne, and M. Thies, *Inhomogeneous condensates in the thermodynamics of the chiral NJL_2 model*, *Phys. Rev. D* **79**, 105012 (2009), arXiv: [0903.1868 \[hep-th\]](#) (cit. on pp. 50, 60)
- [212] K. Ohwa, *Crystalline ground state in chiral Gross-Neveu and Cooper pair models at finite densities*, *Phys. Rev. D* **65**, 085040 (2002), arXiv: [hep-ph/0111074](#) (cit. on p. 50)
- [213] D. Nickel, *Inhomogeneous phases in the Nambu–Jona-Lasinio and quark-meson model*, *Phys. Rev. D* **80**, 074025 (2009), arXiv: [0906.5295 \[hep-ph\]](#) (cit. on p. 50)
- [214] D. Nickel, *How Many Phases Meet at the Chiral Critical Point?*, *Phys. Rev. Lett.* **103**, 072301 (2009), arXiv: [0902.1778 \[hep-ph\]](#) (cit. on p. 50)
- [215] C. Boehmer, M. Thies, and K. Urlichs, *Tricritical behavior of the massive chiral Gross-Neveu model*, *Phys. Rev. D* **75**, 105017 (2007), arXiv: [hep-th/0702201](#) (cit. on p. 50)
- [216] T. Kojo et al., *Quarkyonic chiral spirals*, *Nucl. Phys. A* **843**, 37 (2010), arXiv: [0912.3800 \[hep-ph\]](#) (cit. on p. 51)

- [217] R. E. Peierls, *Quantum Theory of Solids*, (1955), Clarendon Press (cit. on p. 51)
- [218] N. D. Mermin and H. Wagner, *Absence of Ferromagnetism or Antiferromagnetism in One- or Two-Dimensional Isotropic Heisenberg Models*, *Phys. Rev. Lett.* **17**, 1133 (1966) (cit. on p. 51)
- [219] N. D. Mermin, *Crystalline Order in Two Dimensions*, *Phys. Rev.* **176**, 250 (1968) [Erratum: *Phys. Rev. B* **20**, 4762 (1979)] (cit. on p. 51)
- [220] P. C. Hohenberg, *Existence of Long-Range Order in One and Two Dimensions*, *Phys. Rev.* **158**, 383 (1967) (cit. on p. 51)
- [221] S. Coleman, *There are no Goldstone Bosons in Two Dimensions*, *Commun. Math. Phys.* **31**, 259 (1973) (cit. on p. 51)
- [222] V. L. Berezinskii, *Destruction of long-range order in one-dimensional and two-dimensional systems having a continuous symmetry group I. Classical systems*, *Sov. Phys. JETP* **32**, 493 (1971) (cit. on p. 52)
- [223] V. L. Berezinskii, *Destruction of long-range order in one-dimensional and two-dimensional systems having a continuous symmetry group II. Quantum systems*, *Sov. Phys. JETP* **34**, 610 (1972) (cit. on p. 52)
- [224] J. M. Kosterlitz and D. J. Thouless, *Ordering metastability and phase transitions in two-dimensional systems*, *J. Phys. C* **6**, 1181 (1973) (cit. on p. 52)
- [225] S. T. Bramwell and P. C. W. Holdsworth, *Magnetization: A characteristic of the Kosterlitz-Thouless-Berezinskii transition*, *Phys. Rev. B* **49**, 8811 (1994) (cit. on p. 52)
- [226] E. Witten, *Chiral symmetry, the $1/N$ expansion and the $SU(N)$ Thirring model*, *Nucl. Phys. B* **145**, 110 (1978) (cit. on pp. 52, 59)
- [227] Y. Nambu, *Quasi-Particles and Gauge Invariance in the Theory of Superconductivity*, *Phys. Rev.* **117**, 648 (1960) (cit. on p. 52)
- [228] J. Goldstone, *Field Theories with «Superconductor» Solutions*, *Nuovo Cim.* **19**, 154 (1961) (cit. on p. 52)
- [229] J. Goldstone, A. Salam, and S. Weinberg, *Broken Symmetries*, *Phys. Rev.* **127**, 965 (1962) (cit. on p. 52)
- [230] J. O. Andersen, *Phase fluctuations in low-dimensional Gross-Neveu models*, (2005), arXiv: [hep-th/0506261](https://arxiv.org/abs/hep-th/0506261) (cit. on pp. 52, 64)
- [231] E. Babaev, *Mass generation without symmetry breakdown in the chiral Gross-Neveu model at finite temperature and finite N in $2+1$ dimensions*, *Phys. Lett. B* **497**, 323 (2001), arXiv: [hep-th/9907089](https://arxiv.org/abs/hep-th/9907089) (cit. on p. 52)
- [232] F. Karsch, J. Kogut, and H. W. Wyld, *The Gross-Neveu model at finite temperature and density*, *Nucl. Phys. B* **280**, 289 (1987) (cit. on p. 53)

- [233] J. Lenz et al., *Inhomogeneous phases in the Gross-Neveu model in $1 + 1$ dimensions at finite number of flavors*, *Phys. Rev. D* **101**, 094512 (2020), arXiv: 2004.00295 [hep-lat] (cit. on pp. 53, 55–57)
- [234] J. Lenz et al., *Baryons in the Gross-Neveu model in $1 + 1$ dimensions at finite number of flavors*, *Phys. Rev. D* **102**, 114501 (2020), arXiv: 2007.08382 [hep-lat] (cit. on p. 53)
- [235] K. Horie and C. Nonaka, *Inhomogeneous Phases in the Chiral Gross-Neveu Model on the Lattice*, *PoS (LATTICE2021)*, 150 (2021), arXiv: 2112.02261 [hep-lat] (cit. on p. 59)
- [236] R. Ciccone, L. Di Pietro, and M. Serone, *Inhomogeneous Phase of the Chiral Gross-Neveu Model*, *Phys. Rev. Lett.* **129**, 071603 (2022), arXiv: 2203.07451 [hep-th] (cit. on pp. 59, 65)
- [237] V. P. Gusynin, V. A. Miransky, and I. A. Shovkovy, *Catalysis of Dynamical Flavor Symmetry Breaking by a Magnetic Field in $2 + 1$ Dimensions*, *Phys. Rev. Lett.* **73**, 3499 (1994) [Erratum: *Phys. Rev. Lett.* **76**, 1005 (1996)], arXiv: hep-ph/9405262 (cit. on pp. 66, 67)
- [238] B. J. Harrington, S. Y. Park, and A. Yildiz, *External-field-induced phase transition in the N -component Thirring model*, *Phys. Rev. D* **11**, 1472 (1975) (cit. on p. 66)
- [239] K. G. Klimenko, *Three-dimensional Gross-Neveu model in an external electric field. II*, *Theor. Math. Phys.* **89**, 1287 (1991) (cit. on p. 66)
- [240] I. V. Krive and S. A. Naftulin, *Dynamical symmetry breaking and phase transitions in a three-dimensional Gross-Neveu model in a strong magnetic field*, *Phys. Rev. D* **46**, 2737 (1992) (cit. on p. 66)
- [241] V. P. Gusynin, V. A. Miransky, and I. A. Shovkovy, *Dynamical flavor symmetry breaking by a magnetic field in $2 + 1$ dimensions*, *Phys. Rev. D* **52**, 4718 (1995), arXiv: hep-th/9407168 (cit. on pp. 67, 68)
- [242] V. P. Gusynin, V. A. Miransky, and I. A. Shovkovy, *Dimensional reduction and dynamical chiral symmetry breaking by a magnetic field in $3 + 1$ dimensions*, *Phys. Lett. B* **349**, 477 (1995), arXiv: hep-ph/9412257 (cit. on p. 67)
- [243] V. P. Gusynin, V. A. Miransky, and I. A. Shovkovy, *Dimensional reduction and catalysis of dynamical symmetry breaking by a magnetic field*, *Nucl. Phys. B* **462**, 249 (1996), arXiv: hep-ph/9509320 (cit. on p. 67)
- [244] I. A. Shovkovy, *Magnetic Catalysis: A Review*, *Lect. Notes Phys.* **871**, 13 (2013), arXiv: 1207.5081 [hep-ph] (cit. on p. 67)
- [245] P. A. Lee and S. R. Shenoy, *Effective Dimensionality Change of Fluctuations in Superconductors in a Magnetic Field*, *Phys. Rev. Lett.* **28**, 1025 (1972) (cit. on p. 67)

- [246] A. Chodos, K. Everding, and D. A. Owen, *QED with a chemical potential: The case of a constant magnetic field*, *Phys. Rev. D* **42**, 2881 (1990) (cit. on p. 67)
- [247] D. D. Scherer and H. Gies, *Renormalization group study of magnetic catalysis in the 3d Gross-Neveu model*, *Phys. Rev. B* **85**, 195417 (2012), arXiv: 1201.3746 [cond-mat] (cit. on p. 67)
- [248] K. Fukushima and J. M. Pawłowski, *Magnetic catalysis in hot and dense quark matter and quantum fluctuations*, *Phys. Rev. D* **86**, 076013 (2012), arXiv: 1203.4330 [hep-ph] (cit. on p. 67)
- [249] N. Mueller and J. M. Pawłowski, *Magnetic catalysis and inverse magnetic catalysis in QCD*, *Phys. Rev. D* **91**, 116010 (2015), arXiv: 1502.08011 [hep-ph] (cit. on p. 67)
- [250] L. D. Landau and E. M. Lifshitz, *Statistical Physics*, 3rd edition, *Course of Theoretical Physics Vol. 5* (1980), Butterworth-Heinemann Oxford, ISBN: 978-0-08-057046-4 (cit. on p. 68)
- [251] S Kanemura, H.-T. Sato, and H. Tochimura, *Thermodynamic Gross-Neveu model in a constant electromagnetic fields*, *Nucl. Phys. B* **517**, 567 (1998), arXiv: hep-ph/9707285 (cit. on p. 68)
- [252] T. Inagaki, D. Kimura, and T. Murata, *Four-Fermion Interaction Model in a Constant Magnetic Field at Finite Temperature and Chemical Potential*, *Prog. Theor. Phys.* **111**, 371 (2004), arXiv: hep-ph/0312005 (cit. on p. 68)
- [253] E. S. Fraga and A. J. Mizher, *Chiral transition in a strong magnetic background*, *Phys. Rev. D* **78**, 025016 (2008), arXiv: 0804.1452 [hep-ph] (cit. on p. 68)
- [254] K. Fukushima, *Phase diagrams in the three-flavor Nambu–Jona-Lasinio model with the Polyakov loop*, *Phys. Rev. D* **77**, 114028 (2008) [Erratum: *Phys. Rev. D* **78**, 039902 (2008)], arXiv: 0803.3318 [hep-ph] (cit. on p. 68)
- [255] A. J. Mizher, M. N. Chernodub, and E. S. Fraga, *Phase diagram of hot QCD in an external magnetic field: Possible splitting of deconfinement and chiral transitions*, *Phys. Rev. D* **82**, 105016 (2010), arXiv: 1004.2712 [hep-ph] (cit. on p. 68)
- [256] J. O. Andersen and R. Khan, *Chiral transition in a magnetic field and at finite baryon density*, *Phys. Rev. D* **85**, 065026 (2012), arXiv: 1105.1290 [hep-ph] (cit. on p. 68)
- [257] J. O. Andersen, W. R. Naylor, and A. Tranberg, *Inverse magnetic catalysis and regularization in the quark-meson model*, *JHEP* **2015**, 42 (2015), arXiv: 1410.5247 [hep-ph] (cit. on p. 68)
- [258] G. W. Semenoff, I. A. Shovkovy, and L. C. R. Wijewardhana, *Phase transition induced by a magnetic field*, *Mod. Phys. Lett. A* **13**, 1143 (1998), arXiv: hep-ph/9803371v2 (cit. on p. 68)

- [259] E. V. Gorbar et al., *Magnetic field driven metal-insulator phase transition in planar systems*, *Phys. Rev. B* **66**, 045108 (2002), arXiv: cond-mat/0202422 (cit. on p. 68)
- [260] V. P. Gusynin et al., *Excitonic gap, phase transition, and quantum Hall effect in graphene*, *Phys. Rev. B* **74**, 195429 (2006), arXiv: cond-mat/0605348 (cit. on p. 68)
- [261] B. Roy and I. F. Herbut, *Inhomogeneous magnetic catalysis on graphene's honeycomb lattice*, *Phys. Rev. B* **83**, 195422 (2011), arXiv: 1102.3481 [cond-mat] (cit. on p. 68)
- [262] C. DeTar, C. Winterowd, and S. Zafeiropoulos, *Magnetic Catalysis in Graphene Effective Field Theory*, *Phys. Rev. Lett.* **117**, 266802 (2016), arXiv: 1607.03137 [hep-lat] (cit. on p. 68)
- [263] C. DeTar, C. Winterowd, and S. Zafeiropoulos, *Lattice field theory study of magnetic catalysis in graphene*, *Phys. Rev. B* **95**, 165442 (2017), arXiv: 1608.00666 [hep-lat] (cit. on p. 68)
- [264] H. Chen et al., *Interacting quantum Hall states in a finite graphene flake and at finite temperature*, *Phys. Rev. B* **102**, 205401 (2020), arXiv: 2006.02473 [cond-mat] (cit. on p. 68)
- [265] E. S. Fraga and L. F. Palhares, *Deconfinement in the presence of a strong magnetic background: An exercise within the MIT bag model*, *Phys. Rev. D* **86**, 016008 (2012), arXiv: 1201.5881 [hep-ph] (cit. on p. 68)
- [266] A. Chodos et al., *New extended model of hadrons*, *Phys. Rev. D* **9**, 3471 (1974) (cit. on p. 68)
- [267] E. S. Fraga, *Thermal Chiral and Deconfining Transitions in the Presence of a Magnetic Background*, *Lect. Notes Phys.* **871**, 121 (2013), arXiv: 1208.0917 [hep-ph] (cit. on p. 68)
- [268] V. A. Miransky and I. A. Shovkovy, *Magnetic catalysis and anisotropic confinement in QCD*, *Phys. Rev. D* **66**, 045006 (2002), arXiv: hep-ph/0205348 (cit. on pp. 68, 69)
- [269] G. Martinelli et al., *The proton and neutron magnetic moments in lattice QCD*, *Phys. Lett. B* **116**, 434 (1982) (cit. on p. 68)
- [270] C. Bernard et al., *Lattice Quantum Chromodynamics Calculation of Some Baryon Magnetic Moments*, *Phys. Rev. Lett.* **49**, 1076 (1982) (cit. on p. 68)
- [271] M. D'Elia, S. Mukherjee, and F. Sanfilippo, *QCD phase transition in a strong magnetic background*, *Phys. Rev. D* **82**, 051501(R) (2010), arXiv: 1005.5365 [hep-lat] (cit. on p. 68)

-
- [272] M. D’Elia, *Lattice QCD Simulations in External Background Fields*, *Lect. Notes Phys.* **871**, 181 (2013), arXiv: 1209.0374 [hep-lat] (cit. on p. 68)
- [273] G. S. Bali et al., *The QCD phase diagram for external magnetic fields*, *JHEP* **2012**, 44 (2012), arXiv: 1111.4956 [hep-lat] (cit. on pp. 68, 69)
- [274] G. S. Bali et al., *QCD quark condensate in external magnetic fields*, *Phys. Rev. D* **86**, 071502(R) (2012), arXiv: 1206.4205 [hep-lat] (cit. on pp. 68, 69)
- [275] G. Endrődi, *Critical point in the QCD phase diagram for extremely strong background magnetic fields*, *JHEP* **2015**, 173 (2015), arXiv: 1504.08280 [hep-lat] (cit. on p. 68)
- [276] M. D’Elia et al., *QCD phase diagram in a magnetic background for different values of the pion mass*, *Phys. Rev. D* **98**, 054509 (2018), arXiv: 1808.07008 [hep-lat] (cit. on p. 68)
- [277] G. Endrődi et al., *Magnetic catalysis and inverse catalysis for heavy pions*, *JHEP* **2019**, 7 (2019), arXiv: 1904.10296 [hep-lat] (cit. on p. 68)
- [278] M. D’Elia et al., *Phase diagram of QCD in a magnetic background*, *Phys. Rev. D* **105**, 034511 (2022), arXiv: 2111.11237 [hep-lat] (cit. on p. 68)
- [279] F. Bruckmann, G. Endrődi, and T. G. Kovács, *Inverse magnetic catalysis and the Polyakov loop*, *JHEP* **2013**, 112 (2013), arXiv: 1303.3972 [hep-lat] (cit. on pp. 68, 69, 92)
- [280] T. Banks and A. Casher, *Chiral symmetry breaking in confining theories*, *Nucl. Phys. B* **169**, 103 (1980) (cit. on pp. 69, 75)
- [281] K. Fukushima and Y. Hidaka, *Magnetic Catalysis Versus Magnetic Inhibition*, *Phys. Rev. Lett.* **110**, 031601 (2013), arXiv: 1209.1319 [hep-ph] (cit. on p. 69)
- [282] P. N. Meisinger and M. C. Ogilvie, *Chiral symmetry restoration and \mathbb{Z}_N symmetry*, *Phys. Lett. B* **379**, 163 (1996), arXiv: hep-lat/9512011 (cit. on p. 69)
- [283] K. Fukushima, M. Ruggieri, and R. Gatto, *Chiral magnetic effect in the Polyakov–Nambu–Jona-Lasinio model*, *Phys. Rev. D* **81**, 114031 (2010), arXiv: 1003.0047 [hep-ph] (cit. on p. 69)
- [284] R. Gatto and M. Ruggieri, *Dressed Polyakov loop and phase diagram of hot quark matter in a magnetic field*, *Phys. Rev. D* **82**, 054027 (2010), arXiv: 1007.0790 [hep-ph] (cit. on p. 69)
- [285] R. Gatto and M. Ruggieri, *Deconfinement and chiral symmetry restoration in a strong magnetic background*, *Phys. Rev. D* **83**, 034016 (2011), arXiv: 1012.1291 [hep-ph] (cit. on p. 69)

- [286] K. Kashiwa, *Entanglement between chiral and deconfinement transitions under strong uniform magnetic background field*, *Phys. Rev. D* **83**, 117901 (2011), arXiv: [1104.5167 \[hep-ph\]](#) (cit. on p. 69)
- [287] E.S. Fraga, B. W. Mintz, and J. Schaffner-Bielich, *A search for inverse magnetic catalysis in thermal quark-meson models*, *Phys. Lett. B* **731**, 154 (2014), arXiv: [1311.3964 \[hep-ph\]](#) (cit. on p. 69)
- [288] P. Costa et al., *Phase transition and critical end point driven by an external magnetic field in asymmetric quark matter*, *Phys. Rev. D* **89**, 056013 (2014), arXiv: [1307.7894 \[hep-ph\]](#) (cit. on p. 69)
- [289] R. Gatto and M. Ruggieri, *Quark Matter in a Strong Magnetic Background*, *Lect. Notes Phys.* **871**, 87 (2013), arXiv: [1207.3190 \[hep-ph\]](#) (cit. on p. 69)
- [290] R. L. S. Farias et al., *Importance of asymptotic freedom for the pseudocritical temperature in magnetized quark matter*, *Phys. Rev. C* **90**, 025203 (2014), arXiv: [1404.3931 \[hep-ph\]](#) (cit. on p. 69)
- [291] M. Ferreira et al., *Deconfinement and chiral restoration within the $SU(3)$ Polyakov–Nambu–Jona-Lasinio and entangled Polyakov–Nambu–Jona-Lasinio models in an external magnetic field*, *Phys. Rev. D* **89**, 016002 (2014) [Erratum: *Phys. Rev. D* **89**, 019902 (2014)], arXiv: [1305.4751 \[hep-ph\]](#) (cit. on p. 69)
- [292] M. Ferreira et al., *Inverse magnetic catalysis in the $(2 + 1)$ -flavor Nambu–Jona-Lasinio and Polyakov–Nambu–Jona-Lasinio models*, *Phys. Rev. D* **89**, 116011 (2014), arXiv: [1404.5577 \[hep-ph\]](#) (cit. on p. 69)
- [293] A. Ayala, M. Loewe, and R. Zamora, *Inverse magnetic catalysis in the linear sigma model with quarks*, *Phys. Rev. D* **91**, 016002 (2015), arXiv: [1406.7408 \[hep-ph\]](#) (cit. on p. 69)
- [294] A. Ayala et al., *Magnetized effective QCD phase diagram*, *Phys. Rev. D* **92**, 096011 (2015) [Erratum: *Phys. Rev. D* **92**, 119905 (2015)], arXiv: [1509.03345 \[hep-ph\]](#) (cit. on p. 69)
- [295] A. Ahmad and A. Raya, *Inverse magnetic catalysis and confinement within a contact interaction model for quarks*, *J. Phys. G* **43**, 065002 (2016), arXiv: [1602.06448 \[hep-ph\]](#) (cit. on p. 69)
- [296] W. R. Tavares et al., *Nambu–Jona-Lasinio $SU(3)$ model constrained by lattice QCD: thermomagnetic effects in the magnetization*, *Eur. Phys. J. A* **57**, 278 (2021), arXiv: [2104.11117 \[hep-ph\]](#) (cit. on p. 69)
- [297] S. S. Avancini et al., *Light pseudoscalar meson masses under strong magnetic fields within the $SU(3)$ Nambu–Jona-Lasinio model*, *Phys. Rev. D* **104**, 094040 (2021), arXiv: [2109.01911 \[hep-ph\]](#) (cit. on p. 69)

- [298] G. Endrődi and G. Markó, *Magnetized baryons and the QCD phase diagram: NJL model meets the lattice*, *JHEP* **2019**, 36 (2019), arXiv: 1905.02103 [hep-lat] (cit. on p. 69)
- [299] A. Bandyopadhyay and R. L. S. Farias, *Inverse magnetic catalysis: how much do we know about?*, *Eur. Phys. J. Spec. Top.* **230**, 719 (2021), arXiv: 2003.11054 [hep-ph] (cit. on p. 69)
- [300] A. Ayala et al., *QCD phase diagram in a magnetized medium from the chiral symmetry perspective: the linear sigma model with quarks and the Nambu–Jona-Lasinio model effective descriptions*, *Eur. Phys. J. A* **57**, 234 (2021), arXiv: 2104.05854 [hep-ph] (cit. on p. 69)
- [301] J. O. Andersen, *QCD phase diagram in a constant magnetic background. Inverse magnetic catalysis: where models meet the lattice*, *Eur. Phys. J. A* **57**, 189 (2021), arXiv: 2102.13165 [hep-ph] (cit. on p. 69)
- [302] D. Gómez Dumm, J. P. Carlomagno, and N. N. Scoccola, *Strong-Interaction Matter under Extreme Conditions from Chiral Quark Models with Nonlocal Separable Interactions*, *Symmetry* **13**, 11 (2021), arXiv: 2101.09574 [hep-ph] (cit. on p. 69)
- [303] M. A. Halasz et al., *Phase diagram of QCD*, *Phys. Rev. D* **58**, 096007 (1998), arXiv: hep-ph/9804290 (cit. on p. 70)
- [304] K. Fukushima and T. Hatsuda, *The phase diagram of dense QCD*, *Rep. Prog. Phys.* **74**, 014001 (2011), arXiv: 1005.4814 [hep-ph] (cit. on p. 70)
- [305] D. R. Hofstadter, *Energy levels and wave functions of Bloch electrons in rational and irrational magnetic fields*, *Phys. Rev. B* **14**, 2239 (1976) (cit. on p. 71)
- [306] G. Endrődi, *QCD in magnetic fields: from Hofstadter’s butterfly to the phase diagram*, *PoS (LATTICE2014)* (2015), arXiv: 1410.8028 [hep-lat] (cit. on p. 71)
- [307] F. Bruckmann et al., *Landau levels in QCD*, *Phys. Rev. D* **96**, 074506 (2017), arXiv: 1705.10210 [hep-lat] (cit. on p. 71)
- [308] M. F. Atiyah and I. M. Singer, *The Index of Elliptic Operators: V*, *Ann. Math.* **93**, 139 (1971) (cit. on p. 72)
- [309] I. Sachs and A. Wipf, *Finite Temperature Schwinger Model*, *Helv. Phys. Acta* **65**, 652 (1992), arXiv: 1005.1822 [hep-th] (cit. on pp. 72, 102)
- [310] P. Hasenfratz, V. Laliena, and F. Niedermayer, *The index theorem in QCD with a finite cut-off*, *Phys. Lett. B* **427**, 125 (1998), arXiv: hep-lat/9801021 (cit. on p. 72)
- [311] T.-W. Chiu, *Topological phases in the Neuberger-Dirac operator*, *Phys. Rev. D* **60**, 114510 (1999), arXiv: hep-lat/9810002 (cit. on pp. 72, 74)

- [312] J. Smit and J. C. Vink, *Remnants of the index theorem on the lattice*, *Nucl. Phys. B* **286**, 485 (1987) (cit. on p. 72)
- [313] R. Narayanan and P. Vranas, *A numerical test of the continuum index theorem on the lattice*, *Nucl. Phys. B* **506**, 373 (1997), arXiv: [hep-lat/9702005](#) (cit. on p. 72)
- [314] T.-W. Chiu, *Topological charge and the spectrum of exactly massless fermions on the lattice*, *Phys. Rev. D* **58**, 074511 (1998), arXiv: [hep-lat/9804016](#) (cit. on p. 72)
- [315] C. Gattringer and I. Hip, *On the spectrum of the Wilson-Dirac lattice operator in topologically non-trivial background configurations*, *Nucl. Phys. B* **536**, 363 (1998), arXiv: [hep-lat/9712015](#) (cit. on p. 72)
- [316] F. Farchioni et al., *Eigenvalue spectrum of massless Dirac operators on the lattice*, *Nucl. Phys. B* **549**, 364 (1999), arXiv: [hep-lat/9812018](#) (cit. on p. 72)
- [317] P. Bicudo, *Criterion for the index theorem on the lattice*, (2002), arXiv: [hep-lat/9912015](#) (cit. on p. 72)
- [318] S. Chandrasekharan, *Ginsparg-Wilson fermions: A study in the Schwinger model*, *Phys. Rev. D* **59**, 094502 (1999), arXiv: [hep-lat/9810007](#) (cit. on p. 74)
- [319] C. Gattringer and C. B. Lang, *Quantum Chromodynamics on the Lattice, An Introductory Presentation*, 1st edition, *Lecture Notes in Physics Vol. 788* (2010), Springer Berlin, Heidelberg, ISBN: 978-3-642-01849-7 (cit. on pp. 74, 75)
- [320] R. G. Edwards, U. M. Heller, and R. Narayanan, *Study of chiral symmetry in quenched QCD using the overlap Dirac operator*, *Phys. Rev. D* **59**, 094510 (1999), arXiv: [hep-lat/9811030](#) (cit. on p. 75)
- [321] P. Vranas, I. Tziligakis, and J. Kogut, *Fermion-scalar interactions with domain wall fermions*, *Phys. Rev. D* **62**, 054507 (2000), arXiv: [hep-lat/9905018](#) (cit. on p. 77)
- [322] D. B. Kaplan, *A method for simulating chiral fermions on the lattice*, *Phys. Lett. B* **288**, 342 (1992) (cit. on p. 77)
- [323] Y. Igarashi, H. So, and N. Ukita, *Ginsparg–Wilson relation and lattice chiral symmetry in fermionic interacting theories*, *Phys. Lett. B* **535**, 363 (2002), arXiv: [hep-lat/0203019](#) (cit. on p. 77)
- [324] I. Ichinose and K. Nagao, *Gross-Neveu model with overlap fermions*, *Mod. Phys. Lett. A* **15**, 857 (2000), arXiv: [hep-lat/9909035](#) (cit. on p. 77)
- [325] J. van den Eshof et al., *Numerical methods for the QCDd overlap operator. I. Sign-function and error bounds*, *Comput. Phys. Commun.* **146**, 203 (2002), arXiv: [hep-lat/0202025](#) (cit. on p. 77)

- [326] K. Binder, *Finite Size Scaling Analysis of Ising Model Block Distribution Functions*, *Z. Phys. B* **43**, 119 (1981) (cit. on p. 79)
- [327] D. Schmidt, *Three-Dimensional Four-Fermion Theories with Exact Chiral Symmetry on the Lattice*, PhD thesis, Friedrich-Schiller Universität Jena, 2017 (cit. on p. 82).
- [328] L. O’Raifeartaigh, A. Wipf, and H. Yoneyama, *The constraint effective potential*, *Nucl. Phys. B* **271**, 653 (1986) (cit. on pp. 87, 98)
- [329] J. B. Kogut and C. G. Strouthos, *Chiral symmetry restoration in the three-dimensional four-fermion model at nonzero temperature and density*, *Phys. Rev. D* **63**, 054502 (2001), arXiv: [hep-lat/9904008](#) (cit. on p. 88)
- [330] P. M. Stevenson, *Optimized perturbation theory*, *Phys. Rev. D* **23**, 2916 (1981) (cit. on p. 88)
- [331] J.-L. Kneur et al., *Emergence of tricritical point and liquid-gas phase in the massless $2 + 1$ dimensional Gross-Neveu model*, *Phys. Rev. D* **76**, 045020 (2007), arXiv: [0705.0676 \[hep-th\]](#) (cit. on p. 88)
- [332] J.-L. Kneur et al., *Updating the phase diagram of the Gross-Neveu model in $2+1$ dimensions*, *Phys. Lett. B* **657**, 136 (2007), arXiv: [0705.0673 \[hep-ph\]](#) (cit. on p. 88)
- [333] S. Hands et al., *Fermi surface phenomena in the $(2 + 1)D$ four-Fermi model*, *Phys. Rev. D* **68**, 016005 (2003), arXiv: [hep-lat/0302021](#) (cit. on p. 95)
- [334] J.-L. Kneur, M. B. Pinto, and R. O. Ramos, *Phase diagram of the magnetized planar Gross-Neveu model beyond the large- N approximation*, *Phys. Rev. D* **88**, 045005 (2013), arXiv: [1306.2933 \[hep-ph\]](#) (cit. on p. 96)
- [335] G. Endrődi, T. G. Kovács, and G. Markó, *Spontaneous Symmetry Breaking via Inhomogeneities and the Differential Surface Tension*, *Phys. Rev. Lett.* **127**, 232002 (2021), arXiv: [2109.03668 \[hep-lat\]](#) (cit. on p. 98)
- [336] B. B. Brandt et al., *Thermal QCD in a non-uniform magnetic background*, (2023), arXiv: [2305.19029 \[hep-lat\]](#) (cit. on p. 100)
- [337] G. Endrődi and G. Markó, *On electric fields in hot QCD: perturbation theory*, *JHEP* **2022**, 15 (2022), arXiv: [2208.14306 \[hep-ph\]](#) (cit. on p. 100)
- [338] H. Gies and Salek A. S., *Curvature bound from gravitational catalysis in thermal backgrounds*, *Phys. Rev. D* **103**, 125027 (2021), arXiv: [2103.05542 \[hep-th\]](#) (cit. on p. 100)
- [339] E. Witten, *Constraints on supersymmetry breaking*, *Nucl. Phys. B* **202**, 253 (1982) (cit. on p. 102)
- [340] D. V. Vassilevich, *Heat kernel expansion: user’s manual*, *Phys. Rep.* **388**, 279 (2003), arXiv: [hep-th/0306138](#) (cit. on p. 102)

References

- [341] D. B. Ray and I. M. Singer, *R-Torsion and the Laplacian on Riemannian Manifolds*, *Adv. Math.* **7**, 145 (1971) (cit. on p. 106)
- [342] J. S. Dowker and R. Critchley, *Effective Lagrangian and energy-momentum tensor in de Sitter space*, *Phys. Rev. D* **13**, 3224 (1976) (cit. on p. 106)
- [343] E. Elizalde, *Zeta-function regularization is uniquely defined and well*, *J. Phys. A: Math. Gen.* **27**, L299 (1994), arXiv: [hep-th/9308028](#) (cit. on p. 106)
- [344] C. G. Bollini and J. J. Giambiagi, *Dimensional Renormalization: The Number of Dimensions as a Regularizing Parameter*, *Nuovo Cim.* **12B**, 21 (1972) (cit. on p. 107)
- [345] G. 't Hooft and M. Veltman, *Regularization and renormalization of gauge fields*, *Nucl. Phys. B* **44**, 189 (1972) (cit. on p. 107)
- [346] S. K. Blau, M. Visser, and A. Wipf, *Determinants, Dirac Operators, and One-loop Physics*, *Int. J. Mod. Phys. A* **4**, 1467 (1989) (cit. on p. 107)
- [347] S. K. Blau, M. Visser, and A. Wipf, *Analytic results for the effective action*, *Int. J. Mod. Phys. A* **6**, 5409 (1991), arXiv: [0906.2851 \[hep-th\]](#) (cit. on p. 107)
- [348] A. Erdelyi et al., *Tables of Integral Transforms, vol. I*, (1954), McGraw-Hill New York, ISBN: 07-019549-8 (cit. on p. 110)

Acronyms

4FT	four-Fermi theory
BCS	Bardeen-Cooper-Schrieffer
BKT	Berezinskii-Kosterlitz-Thouless
CERN	Conseil européen pour la recherche nucléaire (European Organization for Nuclear Research)
χ GN	chiral Gross-Neveu
CHMW	Coleman-Hohenberg-Mermin-Wagner
DSE	Dyson-Schwinger equation
FFLO	Fulde-Ferrell-Larkin-Ovchinnikov
GN	Gross-Neveu
GS	Gvai and Sharma
LHC	Large Hadron Collider
LLL	lowest Landau level
MIT	Massachusetts Institute of Technology
NJL	Nambu–Jona-Lasinio
OPT	optimized perturbation theory
PNJL	Polyakov-loop-extended NJL
PQM	Polyakov-loop-extended quark-meson
QCD	quantum chromodynamics
rHMC	rational hybrid Monte-Carlo
SLAC	Stanford linear accelerator complex

Acknowledgments

First and foremost, I thank Prof. Andreas Wipf for allowing me to join and perform research in his group as well as for supervising me during my time as a Ph.D. student. I am grateful for the countless discussions we had that enabled me to profit from his experience. Secondly, I thank Julian Lenz for essentially acting as my secondary supervisor, sharing much of his knowledge with me during our collaborations and never getting tired of my endless questions.

This work would not have been possible without our secretaries Katrin Kanter and Lisann Schmidt, who were exceptional at making sure that all sorts of bureaucracy involved were always being properly taken care of. I also thank Nicole Ullrich and Dr. Angela Unkroth from the dean's office for their support in the late stages of my Ph.D., especially with regards to the doctoral examination regulations. I acknowledge André Sternbeck as a representative for the team of the URZ Jena, as well as for the internal IT team of the TPI, for helping me out with any IT-related questions.

I profited greatly from discussions and correspondence with Gergely Endrődi, Christof Gattringer, Tamás Kovács, Laurin Pannullo, Markus Schröfl, José Simão, Ivan Soler, Marc Wagner and Marc Winstel and I am indebted to Christof Gattringer, Marc Wagner and Andreas Wipf for writing letters of recommendation for my postdoc applications.

I am particularly grateful for Katrin Hölbling, Julian Lenz, José Simão and Ivan Soler for proofreading this thesis and pointing out numerous errors. Furthermore, I want to acknowledge all of the B.Sc., M.Sc. and Ph.D. students who I met during my time in Jena (and who are too numerous to be listed here explicitly) for valuable discussions and conversations, both in a work-related context as well as in a private one. Regarding the latter I also appreciate my bandmates for providing much needed relief in my free time.

Most importantly, I wish to thank my girlfriend Katrin Hölbling for her unending support and patience during almost four years of me living abroad.

This work, as well as all of my conference fees and travel expenses, have been funded by the Deutsche Forschungsgemeinschaft (DFG) under Grant No 406116891 within the Research Training Group RTG 2522/1.

Ehrenwörtliche Erklärung

Hiermit erkläre ich ehrenwörtlich,

- 1.1 dass mir die geltende Promotionsordnung bekannt ist;
- 1.2 dass ich die Dissertation selbst angefertigt habe, keine Textabschnitte eines Dritten oder eigener Prüfungsarbeiten ohne Kennzeichen übernommen und alle von mir benutzten Hilfsmittel, persönlichen Mitteilungen und Quellen in meiner Arbeit angegeben habe;
- 1.3 dass bei der Auswahl und Auswertung des hier präsentierten Materials mich die nachstehen aufgeführten Personen in der jeweils beschriebenen Weise unterstützt haben:
 - Andreas Wipf: Betreuung der Arbeit über die gesamte Dauer der Promotion als betreuender Hochschullehrer;
 - Julian Lenz: enge Kooperation über die gesamte Dauer der Promotion, insbesondere bei den Arbeiten zu Kapiteln 5 und 6;
- 1.4 dass die Hilfe einer kommerziellen Promotionsvermittlerin/eines kommerziellen Promotionsvermittlers nicht in Anspruch genommen wurde und dass Dritte weder unmittelbar noch mittelbar geldwerte Leistungen für Arbeiten erhalten haben, die im Zusammenhang mit dem Inhalt der vorgelegten Dissertation stehen;
- 1.5 dass die Dissertation noch nicht als Prüfungsarbeit für eine staatliche oder andere wissenschaftliche Prüfung eingereicht wurde;
- 1.6 dass eine gleiche, eine in wesentlichen Teilen ähnliche oder eine andere Abhandlung nicht bei einer anderen Hochschule als Dissertation eingereicht wurde.

Ort, Datum

Unterschrift des Verfassers